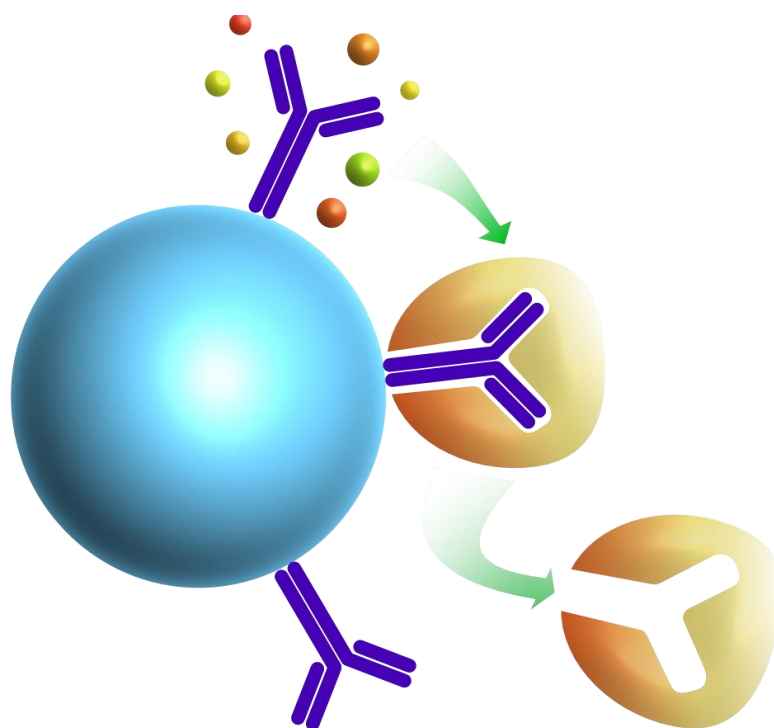




**UNIVERSITÀ
DI TORINO**

Doctoral School of the University of Torino
PhD Program in Chemical and Materials Sciences 35th cycle

The solid phase polymerization synthesis approach for the molecularly imprinted polymers



Matteo Chiarello

Supervisor:
Prof. **Claudio Baggiani**



**UNIVERSITÀ
DI TORINO**

Doctoral School of the University of Torino
PhD Program in Chemical and Materials Sciences 35th cycle

The solid phase polymerization synthesis approach for the molecularly imprinted polymers

Candidate: **Matteo Chiarello**

Supervisor: Prof. **Claudio Baggiani**

Jury Members: Prof. **Laura Anfossi**

Università di Torino
Dipartimento di Chimica

Prof. **Maria Minunni**

Università degli studi di Firenze
Dipartimento di Chimica "Ugo Schiff"

Prof. **Stefano Cinti**

Università degli studi di Napoli "Federico II"
Dipartimento di Farmacia

Head of the Doctoral School: Prof. Eleonora Bonifacio

PhD Program Coordinator: Prof. Bartolomeo Civalleri

Torino, 1° Giugno 2023

TABLE OF CONTENTS

TABLE OF CONTENTS	5
1 INTRODUCTION	7
1.1 <i>The Molecular imprinting strategy</i>	7
1.2 <i>The nanoimprinting approach</i>	12
1.3 <i>The solid phase polymerization technique</i>	16
1.4 <i>Characterization of the MIP</i>	25
1.5 <i>Conclusions and aim of the work</i>	29
1.6 <i>Bibliography</i>	30
2 EFFECT OF DIFFERENT EXPERIMENTAL CONDITIONS ON THE BINDING ABILITIES OF CIPROFLOXACIN NANOMIPS	41
2.1 <i>Introduction</i>	41
2.2 <i>Experimental</i>	43
2.3 <i>Results and discussions</i>	48
2.4 <i>Conclusions</i>	58
2.5 <i>Bibliography</i>	59
3 AN EXPERIMENTAL DESIGN ON THE MONOMERIC FORMULATION FOR THE WATER SYNTHESIS NANOMIPS	63
3.1 <i>Introduction</i>	63
3.2 <i>Experimental</i>	65
3.3 <i>Results and discussions</i>	70
3.4 <i>Conclusions</i>	73
3.5 <i>Bibliography</i>	74
4 EFFECT OF POLYMERIZATION TIME ON THE BINDING PROPERTIES OF CIPROFLOXACIN NANOMIPS	75
4.1 <i>Introduction</i>	75
4.2 <i>Experimental</i>	76
4.3 <i>Results and discussions</i>	81
4.4 <i>Conclusions</i>	91
4.5 <i>Bibliography</i>	92
5 RABBIT IGG-IMPRINTED NANOMIPS: EFFECT OF THE CROSS-LINKER ON AFFINITY AND SELECTIVITY	93
5.1 <i>Introduction</i>	93

5.2	<i>Experimental</i>	95
5.3	<i>Results and discussions</i>	99
5.4	<i>Conclusions</i>	108
5.5	<i>Bibliography</i>	109
6	THE USE OF THE MIMIC TEMPLATE IN THE SOLID-PHASE SYNTHESIS: THE EXAMPLE OF AN OCHRATOXIN A-IMPRINTED NANOMIP	115
6.1	<i>Introduction</i>	115
6.2	<i>Experimental</i>	117
6.3	<i>Results and discussions</i>	121
6.4	<i>Conclusions</i>	124
6.5	<i>Bibliography</i>	125
7	THE EFFECT OF THE PRESENCE OF AN ENANTIOMERIC TEMPLATE: THE EXAMPLE OF LEVOTHYROXINE NANOMIPS	127
7.1	<i>Introduction</i>	127
7.2	<i>Experimental</i>	129
7.3	<i>Results and discussion</i>	135
7.4	<i>Conclusions</i>	138
7.5	<i>Bibliography</i>	139
8	NANOMIP-BASED SOLID PHASE EXTRACTION OF FLUOROQUINOLONES FROM HUMAN URINE	141
8.1	<i>Introduction</i>	141
8.2	<i>Experimental</i>	143
8.3	<i>Results and discussions</i>	148
8.4	<i>Conclusions</i>	154
8.5	<i>Bibliography</i>	155
9	GENERAL CONCLUSIONS	159
10	APPENDICES	163
10.1	<i>Additional work outside the scope of the thesis</i>	163
10.2	<i>Publications</i>	171
10.3	<i>Activity during the PhD</i>	173
10.4	<i>Abbreviation used in the text</i>	175
10.5	<i>Buffers preparation</i>	177

1 INTRODUCTION

1.1 THE MOLECULAR IMPRINTING STRATEGY

1.1.1 Why?

The ability to recognise and bind a specific target molecule is a fundamental process in nature and in the living organisms. This ability is the foundation of every biological response system based on a receptor-ligand interaction. For example, some living organisms communicate to each other via pheromone systems [1], or the vertebrate neural system, which is based on receptors and neurotransmitters [2]. However, one of the most famous and important biological recognition-bond system is the antigen-antibody one.

The ability of animals to create, select, optimise, and produce antibodies against external threats, and to memorise them to reuse over the time is impressive, as result of an evolution process lasted millions of years. Animals are able to produce antibodies against a very high number of classes of substances [3]. The only limit to obtain an immune response in a living organism is the biocompatibility of the substances. The properties that must be considered are: water solubility, toxicity (*i.e.*, substances should not be lethal before antibodies are developed) and dimension of the molecules.

For their characteristics, natural antibodies find application in a wide variety of fields, such as therapeutic processes [4], diagnostic systems [5], and sensors [6]. Actually, it is very difficult overcome the use of animals to produce synthetic substances with similar properties.

In the last decades, researchers have tried to replicate this very efficient system with the aim of creating the ideal “artificial antibody” [7]. The most promising way to reach it is the Molecularly Imprinted Polymers (MIPs), which are the subject of this PhD thesis. 50 years have passed since the early studies of Wulff and Shea; 40 years since the first MIP with non-covalent interactions [8], and 75 from the first intuitions and study of Pauling [9]. Over the years, the technology beyond MIPs has evolved to obtain better polymer particles. In this works we will not focus on the past, *i.e.* the classical polymerization approaches, but we will discuss the state-of-the-art of the nanoimprinting techniques.

1.1.2 Fundamentals of the technique

MIPs are micro or nano sized objects with the ability to selectively bind a target molecule. The high selectivity is obtained through the “construction of the MIP” in the presence of the target molecule, that takes the name of “template molecule” or,

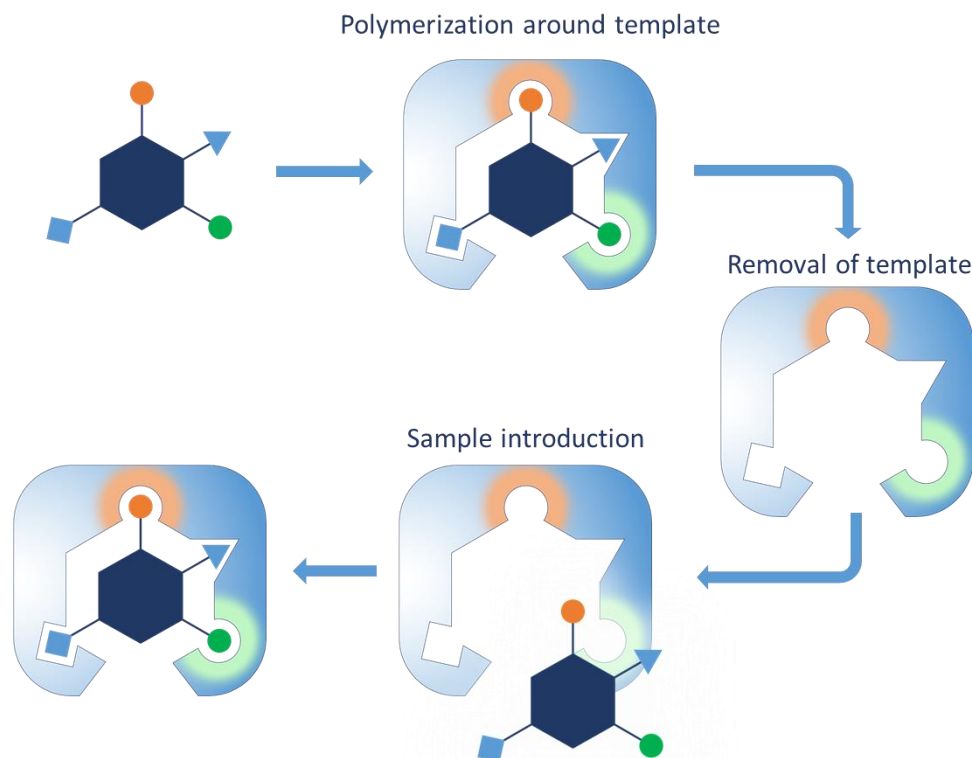


Figure 1-1 - General working mechanism of MIPs

more simply, “template”, which give a memory effect with the creation of a specific binding site. This is possible since the creation of the MIP occurs through the use of functional building blocks. The monomers, with different functional moieties, are able to establish intermolecular interactions with the template molecule by organising themselves around it. The monomers present double bonds, or equivalent functionalities, which make them able to react with each other, creating a polymer lattice. With the polymerization step the “interaction sphere” is freeze in an exact conformation. The removal of the template molecule causes neither collapse of the system nor a variation in the geometrical configuration of the “interaction sphere”, which then takes the name of “imprinted site” or “binding site”. The imprinted site has the ability to rebind again the template molecule, keeping a chemical memory of it [10].

The recognition of the template molecule is a combination of chemical and geometric-steric factors. The chemical factors are the presence of functional groups which can interact with complementary moieties of the template molecule. Possible interactions are Van der Waals forces, ligand exchange or hydrogen bonds (H-bonds). On the other hand, the geometric-steric factors are given by the polymeric structure, that keeps the functional moieties of the monomer and of the template in the correct reciprocal positions, acting like a skeleton.

It is natural to wonder how much these objects can be similar to natural antibodies, and what are the differences; the main characteristics of both are summarised in Table 1.1 In the last decades, MIPs have evolved and, also thank to the most recent techniques like the solid phase polymerization synthesis (SPPS)

[11], we can obtain objects with the desired characteristics which, in some cases, could be able to replace natural antibodies. In particular, nanoMIPs (MIPs with dimension in the order of hundreds of nanometers [12]) are suitable for immunoassays [13] or sensors [14]. The affinity constants of MIPs obtained with the SPPS are very high, in the order of $10^6 - 10^9 \text{ M}^{-1}$, while in the case of natural antibodies these values are in the order of 10^7 or more. In the table 1-1 are summarized the principal characteristics of both the systems.

One of the main limits in using antibodies is that producing them against small molecules is quite challenging. This process is possible with the use of an immunogenic carrier like a protein [15], but in this way the antibodies recognize not only the small molecule but also part of the protein carrier covalently bound to it. On the other hand, not only are MIPs able to overcome this limit, but small rigid molecules with several functional groups represent the perfect templates. In the recent years, new synthesis techniques, like the SPPS, allowed also the imprinting of proteins and other biological macromolecules [12]. Another important advantage of MIPs is that they are inexpensive. Apart from the possible cost of the template molecules, reagents and material used for the synthesis of the MIPs have a very low price.

Table 1-1. Main differences between natural antibodies and MIPs.

		Natural antibodies	MIP
Dimension of the immunogen/template molecules	<5 kDa	Yes, but using immunogenic carrier	Yes, except for poorly functionalised templates
	>5 kDa	Yes	Yes
Binding mechanism		Well known	Known, but some aspects are under debate
Mean affinity constant		$10^7 - 10^9 \text{ M}^{-1}$	$10^4 - 10^6 \text{ M}^{-1}$ ($10^6 - 10^9$ for nanoMIPs)
Binding site density		Low, μM	Depends on the polymerisation method
Binding kinetics		Fast association, slow dissociation	Slow association and dissociation
Binding selectivity		High	High to medium, in some cases it is difficult to discriminate similar substances
Reproducibility		Limited to batch-to-batch	High
Non-specific binding		Negligible	Not negligible
Resistance to extreme experimental condition (pH, temperature, vibration, organic solvents)		No	Yes, depends on the system
Reusability		No, can be yes in immunosensors	Yes, with some limitations
Cost for single batch		Low for polyclonals, from medium to high for monoclonals	Very low
Health risks		Not significant	Particles can be dangerous if inhaled. Some reagents are toxic

1.1.3 The principal building elements

All the advantages discussed above are due to the features of the “building elements” used to make MIPs. The most common system is the use of acrylamide and metylacrilamide derivate monomers with the free radical polymerization, but also it is possible the use of other polymerization system like the living/controlled radical polymerization [10]. In general, the monomers have the capability to both interact with the template molecules through intermolecular bonds, and react with other monomer molecules to create a polymer lattice. These two capabilities are obtained with different features present in different parts of the monomers. The cross-linking capabilities, in the most of cases, is obtained by the presence of carbon double bonds, that in the radical process they break to single bonds linking other molecules. The functional moiety is a group that can do intermolecular bonds like H-bonds, van der Waals force, ionic or metal complexation [10]. The choice of monomers is a fundamental step in the development of MIPs, and different templates interact better with different monomers. Theoretically, for each template should be tried and evaluated different monomers and the ratio between these in the monomer’s mixture, to identify the best building blocks for every template.

If we polymerize only the functionalized monomers, each one with a single double carbon bond, we don’t obtain a polymer lattice but a linear structure. To create a three-dimensional lattice, we must employ molecules that can do more than two bonds with the other monomers. This type of monomers takes the name of cross-linkers, and they have not the capability to interacts with the template. The amount of cross-linker regulates the rigidity of the MIPs particle.

Historically, also the porogen agent also is important. It promotes the formation of a sponge-like porous structure in the MIPs. However, with the nanoMIPs approach (see the next chapter) the importance of porogens diminished.

The last building block is the environment of reaction, which represented also one of the biggest limits of the traditional MIPs. Indeed, only organic solvents could be employed, making the use of instable or not soluble templates (e.g. proteins) impossible. The recent introduction of new techniques like the emulsion polymerization (see below) or the SPPS overcomes this limit and make it possible the use of a water polymerization environment.

The environment of reaction influences the mechanism of polymerization, and in water the most common system is the use of the free radical process [10, 11]. The proper radical activators are chosen according to the selected type of polimerization.

1.2 THE NANOIMPRINTING APPROACH

1.2.1 Overcoming the limits of the classical approach

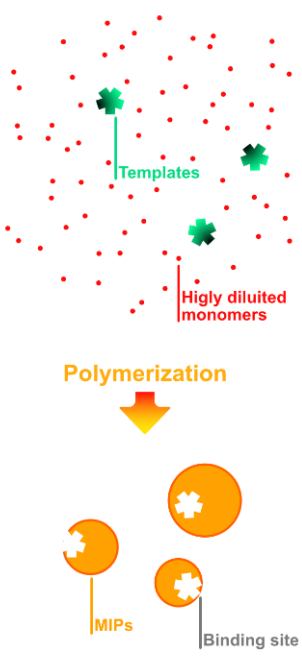
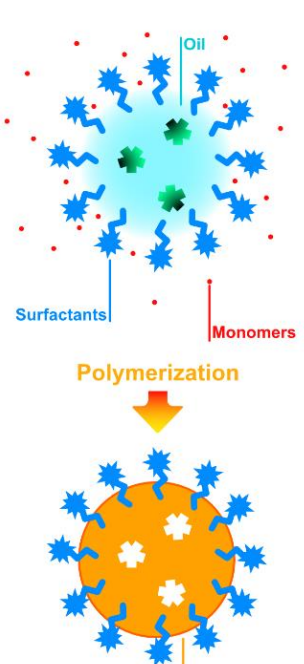
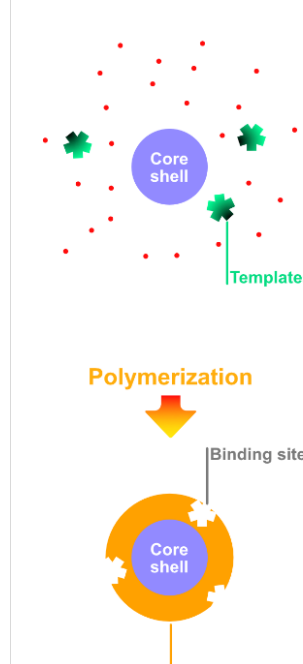
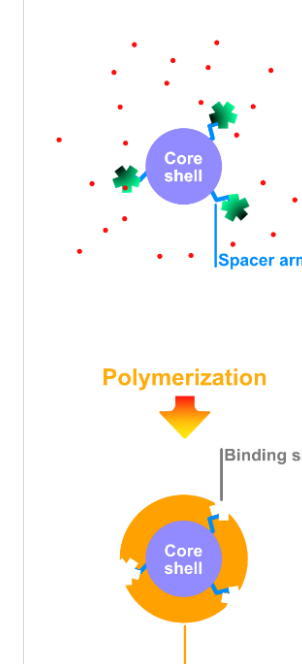
The classical approaches to make MIPs present several problems and limits, which led researchers to develop new methods to overcome them. One of the most effective has been the directly obtaining of the nanoparticles of polymers. Using the classical approach, the particles of MIPs are obtained through grinding of the polymeric bulk mass. This step produces particles with non-homogeneous shape and dimension, a polymeric powder hardly usable in several applications. Furthermore, the grinding step destroys a relevant part of the binding sites in the core of the bulk polymer, enhancing the heterogeneity in shapes and binding constants. Moreover, parts of the imprinted sites remain in the core of the particles, hindering the immediate release of the template molecules trapped inside the polymer bulk, which can be released over the time, during the analytical use of MIP, leading to the phenomenon called “bleeding” [16, 17].

To directly obtain sub-micrometric imprinted particles, several methods were developed in the last thirty years. These methods are based on the introduction of a factor that prevent the formation of big particles and the fusion of different polymerization sites, preferring that many radical polymerization sites remain separate. In this way, the obtained nanoparticles present regular shapes and homogeneous dimensions. In some cases, the polymerization in water environment is also possible.

The most common nanoimprinting methods are the precipitation and the emulsion polymerizations. A particular type of nanoMIPs are the core shell MIPs. In this case, the polymer does not grow free in solution, but it grows on the surface of nanoparticles of other materials with properties like fluorescence, magnetism, ecc. The surface imprinting MIPs are a derivation of these polymers.

The characteristics of the four principal MIP synthetic approaches are summarized in Table 1-2.

Table 1-2 - The four main nanoimprinting techniques

Precipitation	Emulsion	Core shell	Surface imprinting
			
Use of solvents - surfactants			
In some cases	Yes	No	No
Control of the binding site orientation			
No	No	No	Yes
Core shell			
No	No	Yes	Yes
Bleeding phenomena			
Yes	Yes	Possible	No
Difficult to make			
Low	Medium	High	High

1.2.2 Precipitation polymerization

In the precipitation polymerization, monodisperse spherical polymer particles are synthesized with high purity. This method of synthesis was applied for the first time in 1999 for nanoMIPs imprinted against 17β -estradiol and theophylline [18]. The precipitation polymerization is carried out with a highly diluted monomer solution (2% v/v) containing the template molecules. When the growing particles

exceed a critical molecular weight, these precipitate in spherical MIPs with diameters of a few μm or less [19].

There are different methods that can be applied to obtain MIPs by precipitation. The first involves a post-dilution polymerization, where the pre-polymerized particles are diluted after an initial polymerization time and continuing the polymerization to obtain nanogels [20]. Another approach induces polymerization in concentrated monomer solutions and stopping it before the gelation point, through the dilution of the reaction environment [21]. For nanoparticles formation, a small amount of pre-polymer is added to a poor solubilizer solvent for the polymer [22] (typical ratio 1:100; in this case the bulk polymerization process is terminated early leading to nanoparticles). Another method is to perform precipitation polymerization in aqueous media containing the surfactant in a very low concentration to avoid the use of organic solvents. In this way is possible to imprint peptide nanoMIPs [23]. The obtained nanoMIPs are then separated by centrifugation and washing.

The particle size is influenced by several parameters such as the type of solvent [24, 25] and cross-linker [26], the monomeric formulation and the ratio between different monomers, the type of template [27] and temperature. Generally, agitation during polymerization leads to more monodisperse particles.

NanoMIPs obtained via precipitation exhibits a uniform size distribution and higher yield [19]. Moreover, as no surfactants are necessary, the imprinting of biomolecular templates is also possible [28]. One drawback of precipitated nanoMIPs, in comparison to classical MIPs, is that if the polymerization is carried out in highly diluted monomer solutions, this can negatively affect the interaction between the functional monomer and the template, thus decreasing the sensitivity and the selectivity [29]. This limitation, however, is overcompensated by the significantly higher surface-to-volume ratio of nanoparticles compared to classical synthesis. A further general advantage of precipitation polymerization compared to other nanoMIPs synthesis, such as emulsion polymerization, is the relatively low consumption of reagents during polymerization and the increased purity of the resulting nanoparticles.

1.2.3 Emulsion polymerization

The emulsion polymerization approaches mix organic cross-linker and monomers with the template and emulsify them in an aqueous phase containing a surfactant. The most common system is the oil-in-water emulsion (O/W). The emulsion is obtained by vigorous stirring or sonication [30]. It is possible to obtain nanoMIPs with this technique employing co-surfactant and/or co-stabilizer, *e.g.* sodium dodecyl sulphate (SDS), in the disperse phase. The surfactant suppresses diffusion processes in the continuous phase, and consequently a stable emulsion with homogeneous droplet size is obtained. In this case the system takes the name of mini- or micro-emulsion polymerization [31]. Further stabilizers are used to generate particles in the dispersed phase with sizes of around 50–1000 nm. [32].

Some applications of this technique to proteins, like the lysozyme [33-35], are reported in the literature. Very important is the selection of the correct stabilizers and surfactants, that some of the most used molecules can denature the protein templates or destabilize their structures [28]. In the case of hydrophilic peptides as templates, it is possible to functionalize them with fatty-acid chains, because they can act as surfactants themselves. During the polymerization, the modified peptide is situated between the two phases, with its hydrophobic head in the oil layer and the hydrophilic tail at the surface of the aqueous media containing the monomers [36].

Mini-emulsion MIPs show high sensitivity and selectivity. Furthermore, the resulting MIPs exhibit imprinted surfaces with improved binding site homogeneity and accessibility if compared to classical MIPs. In general, one drawback of emulsion polymerization compared to precipitation polymerization is that the first usually requires the use of a larger number of chemicals, including surfactants, buffer components and stabilizers. These chemicals must be removed after the synthesis of MIPs nanoparticles, leading to more sophisticated washing procedures and sometimes lower purity of the material.

1.2.4 Surface imprinting and core shell MIPs

In literature, there are two other important methods to obtain nanoMIPs: the core-shell technique and the surface imprinting.

The core-shell MIPs are nanoparticles where only the surface layer consists of the polymer with imprinted sites, while the core of the particles consists of other materials, *e.g.* magnetic materials like iron oxide, quantum dots or catalytic groups [10, 37]. The synthesis of core-shell MIPs is divided into two steps. The first is the creation of the solid core with different methods, according to the desired functionalities. The second step is the synthesis of the MIP layer around the previously synthesized core. The most common way to do that is the grafting of a thin layer of MIPs, but it is also possible to use other nanoMIPs synthesis methods, like the emulsion or the precipitation polymerization. Anyhow, the radical activator needs to be nearby to the core shell surface, even better if grafted. In addition, it is possible to use the same methods to functionalize the nanoparticles with anchoring groups or fluorescent groups after the synthesis.

Derived from the core-shell MIPs, the surface imprinting is based on the same two synthetic steps, but with the presence of a non-polymeric core [38]. The template molecules are grafted on the non-polymeric core with spacer arms. The most common core is a silica nanoparticle. The following polymerization step creates a thin layer of MIP around this complex, incorporating the template molecules. The layer of MIP is very thin, in the order of few nm. After the polymerization, the spacer arms are broken, and the template molecules are removed. The resulted nanoMIPs exhibit very regular shape and dimension and the binding sites are present only on the surface of the nanoparticles.

1.3 THE SOLID PHASE POLYMERIZATION TECHNIQUE

The continuous search to obtain MIPs with smaller dimension, more regular binding sites and higher binding constants led to the development of different methods and techniques. The methods analyzed so far have improved the general characteristics of MIPs compared to the traditional ones, but all these methods present several limits like the use of organic solvents and surfactants. The solid phase polymerization synthesis (SPPS) is the most recent method to obtain nanoMIPs, which have considerably overcome many of these limits.

1.3.1 Fundamentals

The SPPS is a revolutionary approach to produce nanoMIPs based on a paradigm shift, which is the status of the template molecules in the reaction environment. Developed by Piletsky *et al.* in 2013 [39], SPPS is an evolution of the precipitation polymerization, where the template molecules are not free in solution but immobilized on a surface. This causes the elimination of the “bleeding effect” and provides the possibility to use the template molecules for more than one synthesis. The common immobilization surface consists of glass beads with a diameter of 50-110 μm . The glass beads are completely inert in the polymerization process. Furthermore, the condition of high dilution of the monomers makes it possible to carry out the reaction in a water solution, without the use of organic solvents. The formation of MIPs nanoparticles takes place near the surface of the glass beads, while the polymers formed in the solution, far away from the glass beads, do not exhibit imprinted sites. The sub-sequent collection of the imprinted nanoMIPs is easy.

The use of grafted template, where the molecules have the same orientation, leads to a dramatic improvement of the quality of the binding sites and to a good accessibility of these. The binding sites are only on the surface of MIPs nanoparticle, but not in their bulk, which maintains a constant shape. From the point of view of the experimental data, this means that the equilibrium constants are never lower than 10^6 M^{-1} .

The obtained nanoMIPs are spheres with very homogeneous dimension, in the order of 100-250 nm [40]. The nanoMIPs can aggregate in solution and present low ζ potential.

1.3.2 Synthesis process

The synthesis protocol was developed and extensively explained by Piletsky *et al.* [11], successfully adopted also by other research groups. The protocol is summarized in Figure 1-2.

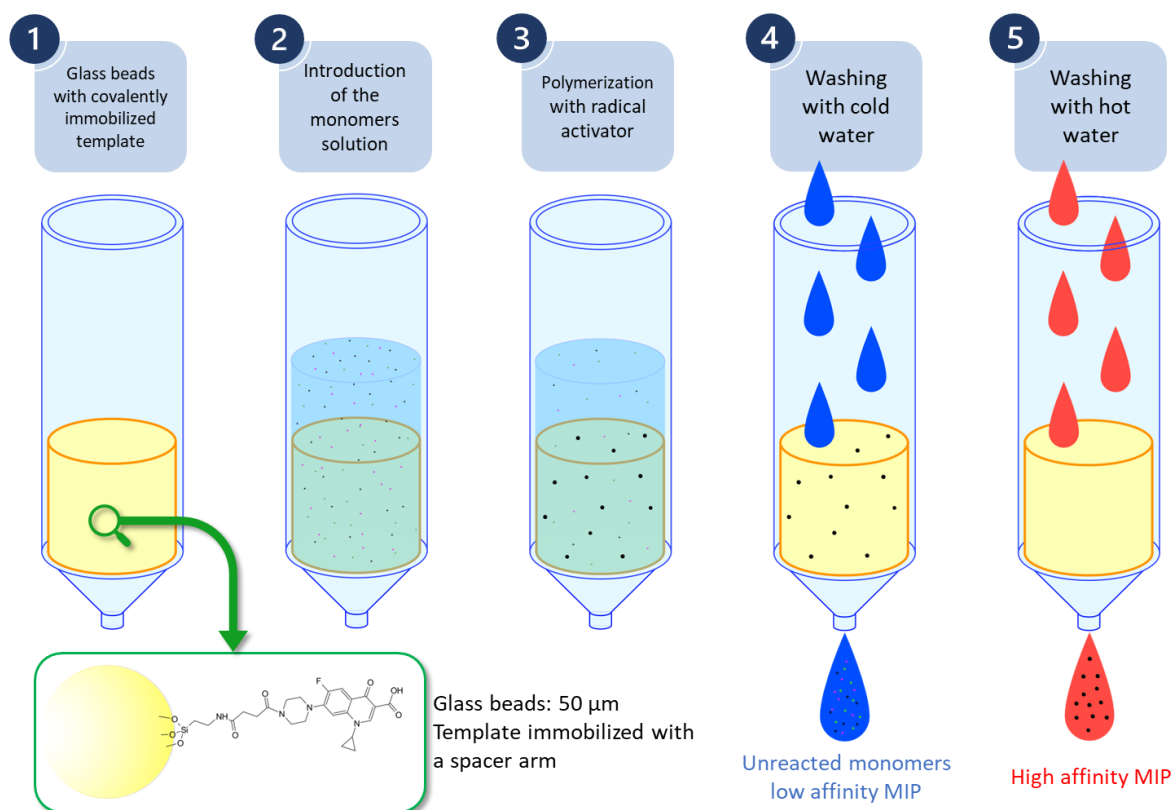


Figure 1-2 – The solid phase synthesis process in water environment

The synthesis consists of three steps: template-glass beads complex preparation, synthesis of nanoMIPs and separation of the latter.

- Template-glass beads complex preparation

Glass beads are the most common solid phase support with a diameter of 50-100 μm . Their surface must be treated to allow the covalent grafting of the template molecules. The activation of the surface silanols is achieved by boiling in NaOH solution. After this treatment, the silanols react with functionalized silane *e.g.* amino propyl trimethoxy silane, which functionalizes the glass beads with groups like amines, carboxylic acids or thiols. These groups are able to bond the template molecules and their functional groups. It is possible to add a spacer arm between the template molecule and the functional groups on the glass beads. The length of the spacer arm affects the binding capability of the nanoMIPs [41]. The environment and the type of addition reaction depend on the classical organic reactions used for the grafting.

- Synthesis of the nanoMIPs

The polymerization can take place in an organic or water environment. The choice is based on the type of template and matters related to the green chemistry question. If for peptides and proteins templates the use of water synthesis

environments is mandatory, it is not for the small organic molecules. However, the water synthesis is usable in almost all cases with good results.

The choice of monomers and polymerization reaction is different for the two reactions environment. The most used monomers in water are summarized in the Figure 1-3.

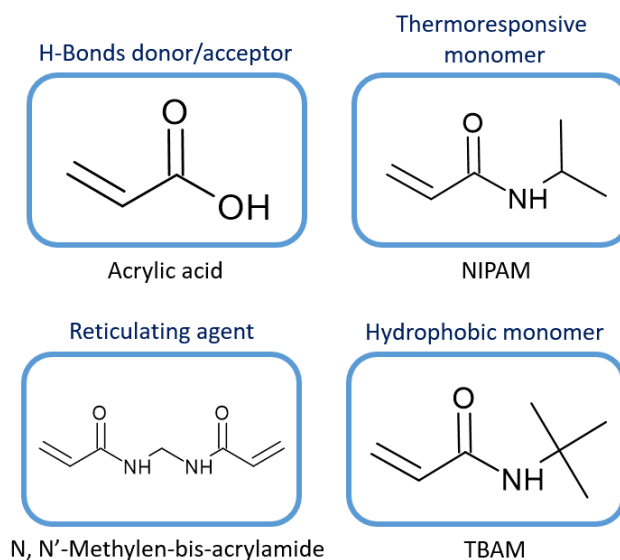


Figure 1-3 - Most common monomers for water environment synthesis

Each monomer has a specific function. In the water environment, which was the most explored during my PhD, the acrylic acid has the capability to make hydrogen bonds, n-isopropylacrylamide (NIPAm) has the thermoresponsive behavior, tert-butylacrylamide (TBAm) has the hydrophobic moiety. The N,N'-methylene-bis-acrylamide is the most used cross-linker, but it is also possible to use other cross-linkers affecting the binding properties of the nanoMIPs [40]. The polymerization system is a free radical reaction activated via chemicals activator. The monomers mixture is put in a cartridge with several grams of template-functionalized glass beads. The suspension is degassed with a constant flow of N₂ to erase oxygen traces, and the polymerization starts after the addition of the radical activators. The reaction can last from few minutes to several hours.

The process in an organic environment is the same, with different monomers dissolved in acetonitrile. In literature, the methacrylic acid is the most used for his H-bond donor/acceptor capability, while ethylene glycol dimethacrylate (EDMA) and trimethylolpropane trimethacrylate (TRIM) are commonly employed as cross linkers. The radical process is catalyzed by temperature or UV rays.

- Separation of nanoMIPs

In the water environment synthesis, the separation of the polymerized nanoMIPs is based on the thermoresponsive behaviour of the nanoparticles given by NIPAM. First, a washing with cold water put out the non-imprinted particles, the unreacted monomers and the low-affinity nanoMIPs, which are imprinted nanoparticles with very low affinity for the template. After this washing step, the nanoMIPs are

collected with some hot water washings. The nanoMIPs can be concentrated with different methods, like the ultrafiltration, freeze-drying or rotavapor.

1.3.3 Mechanism of polymerization

The exact mechanism of reaction is not fully understood due to the impossibility to observe the polymerization process, but through the analysis of experimental data and some rational considerations we can build a model probably very close to the real one [42].

After the addition of radical initiators, the polymerization starts to create bonds between the functionalized monomers. The position of the monomers is crucial because this translates to the capability to selectively bind the template molecules. The position of the functionalized monomers in the solution or bond to the template molecules is established by the energy saving with the complex template-monomers or template-water and monomers-water. Theoretically, the energy saving is positive, and the monomers bind the template molecules, but it is very difficult to measure this energy. The starting point of the polymerization is a probabilistic event, but if most of the monomers are close to the template molecules, most of the events happen there, like in a nucleation site. In the first step of the polymerization, a lot of oligomers are created with very high affinity but low selectivity for the template [43], because their structure is very flexible and adaptable to the template structure. At this point oligomers formed in solution can bind the template molecules, meanwhile other oligomers formed around the template molecules move away from these. This equilibrium is broken during the polymerization, as long as the binding site conformation can readapt itself. The nanoparticles grow in the first two hours of the reaction [43], as long as monomers are present in solution. In the figure 1-4 is schematized this process.

After the polymerization, unreacted monomers, non-imprinted polymers and low affinity MIP nanoparticles are washed away with a cold solvent. The imprinted nanoparticles stay tied to the template molecules, because the only cold solvent washing doesn't break the bonds. The following wash with hot solvent, instead, acts on the physics properties of the materials. The nanoparticles present a thermoresponsive behavior due to the presence of the NIPAM residues inside. In literature it is reported that the NIPAM gel particles change their hydrodynamic diameter, shrinking over a precise temperature called Volume Phase Transition Temperature (VPTT) [44]. This temperature is around 34° C for pure NIPAM nanoparticles. Upon this temperature, the nanoparticles collapse with a temporary modification of the binding sites and the consequent break of the bond with the template molecules.

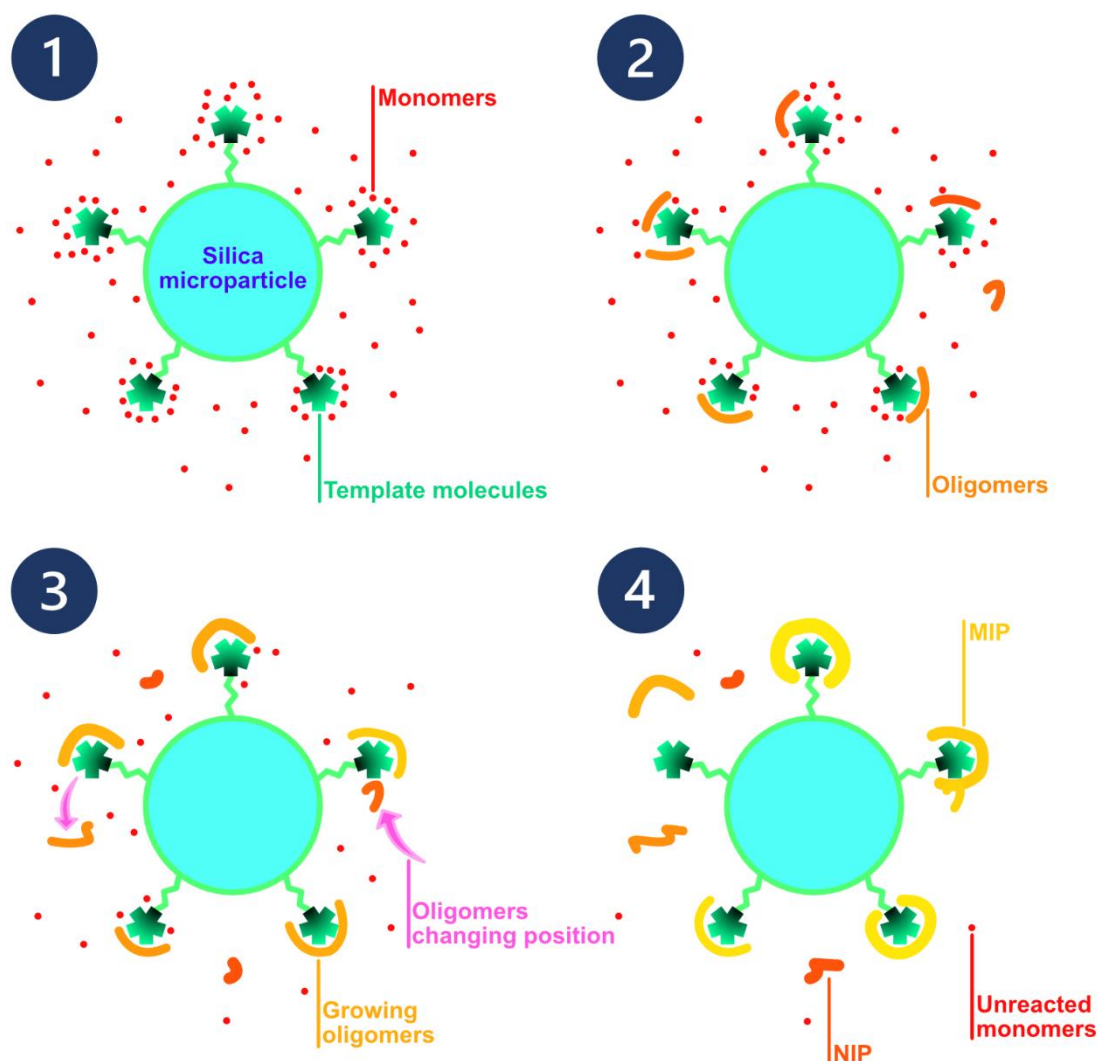


Figure 1-4 - mechanism of nanoMIPs formation

1.3.4 The non-imprinting problem

One of the most complex limits of the solid-phase nanoMIPs is how to get non-imprinted nanoparticles (nanoNIPs). Producing non-imprinted polymers is fundamental to evaluate how many of the binding with the target molecule is for the imprinting sites and not for a general nonspecific binding on the surface of the nanoparticles, since the surface of the nanoparticles presents the same functional groups of the monomers of the imprinted site. The difference between the two types of binds is not the chemistry of the nanoparticles surface, but the geometrical conformation of these functional groups around the template molecules in the binding site.

The difference between MIPs and NIPs is only the presence and the absence, respectively, of template molecules during the polymerization step. The MIP and

the corresponding NIP must have the same monomers formulation. Due to the identical chemical composition and behavior of the nanoparticles, good MIPs will have corresponding NIPs that bond well the target molecules [45].

In the other nanoMIPs synthesis techniques it is easy to get NIPs because the template molecules are in the same physical state of the polymerization environment. For this characteristic the absence of the template does not cause a change in the morphology of the nanoparticles. Instead, in the SPPS the absence of template-grafted glass makes impossible to get the same morphology, because we imprint only the glass spheres, while we lost the “merging of monomers” around the template molecule like a “nucleation site”. In the figure 1-5 is pictured this problem.

This means that we can not use NIPs obtained by the SPPS. In this case, the options are two, both with negative aspects: use the NIPs obtained with a different polymerization method or use nanoMIPs from the SPPS but imprinted against a completely different template. In the first case we use a real non-imprinted polymer, without any imprinted binding sites and with the only capability to establish non-specific bonds. But these NIPs have not the same shape and morphology of the MIPs obtained with the SPPS. This is a very important problem since we compare the binding properties of two similar but different objects.

The only way to use the solid phase to obtain NIPs is to imprint for very different template molecules. For example, a MIP imprinted for a protein is usable as NIP for a little molecule, and *vice versa*. The major limit of this method is that we make the empirical assumption that very different binding sites have not cross recognition for the template molecules. In the case of the MIP imprinted for little molecules and used as NIP for proteins, we can be quite certain that the dimension of the imprinted site is too small to accommodate a big object like a protein. In the opposite case, there is no assurance that no portion of the protein binding site can have a partial specific binding with the little molecule, which can surely enter the site. In this case it is theoretically preferable to use another MIP imprinted for a little, but very different molecule, to minimize the probabilities that the target molecule enters in the binding site.

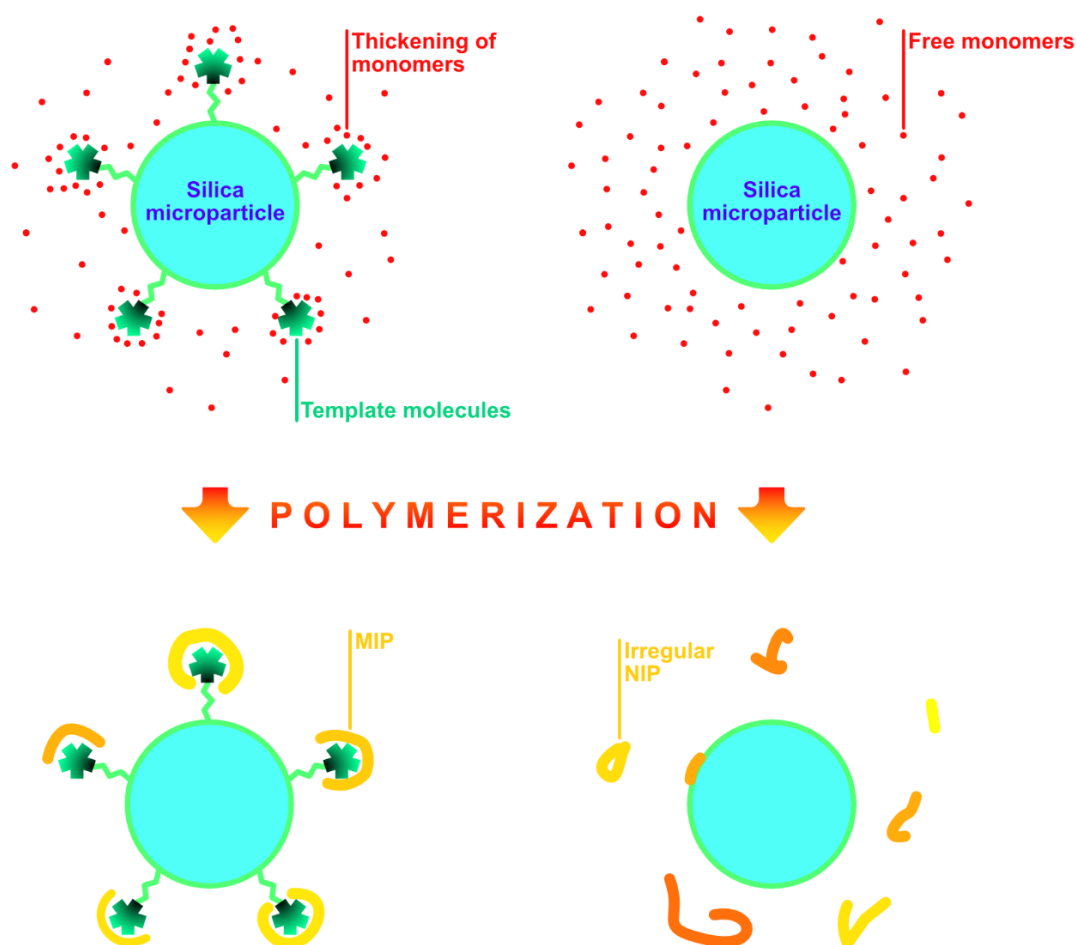


Figure 1-5 - The non-imprinting problem in the SPPS method

None of these methods is perfect, and further studies on this issue are necessary to overcome this limit and establish a scientifically shared methodology.

1.3.5 Literature example

The solid phase polymerization is a relatively recent technique. The first article about it appeared in the literature in the 2013, reporting a MIP for the melamine [39]. In this work by Piletsky *et al.*, previous ideas and systems [46, 47] are combined and improved into this new synthesis method. In this and in many of the earlier works [48], the polymerization happens in an automatic reactor, but in general in the later article this system disappeared on behalf of the simpler batch synthesis.

The vast majority of the papers published between 2013 and 2022 reporting of the application of the SPPS are listed in Table 1-3.^a

In those years the SPPS technique was applied to many types of substances with an enormous interest in the biochemistry field. We can divide the works in two periods. In the first one, from the early studies of Piletsky in 2013 to around 2017/2018, the research was driven by the curiosity to apply this innovative technique to several different types of template substances. Several works were about proof-of-concept molecules, trying to obtain MIPs for classes of substances for which the classical synthesis methods were not feasible. Included in this category there are many papers about the trypsin [48–59] - a very inexpensive protein, and the vancomycin [13, 14, 39, 55, 60]. Unsuprisingly, some of the applications were not investigated in further studies, like the one to whole viruses [60, 61].

In the second period, started in 2017/2018, the SPPS had a major breakthrough, with an increase in publications and imprinted substances, in particular proteins and small biomolecules, and the application of these nanoMIPs in several analytical fields. One of the most promising is the application to sensors.

^a The articles were searched on Scopus on September 7th 2022 with the use of the following keywords: “solid phase polymerization”, “solid phase synthesis”, “solid-phase synthesis” AND “Mip”

Table 1-3 - Literature works about the solid phase polymerization synthesis application

Type of target	Target	Year	Reference
Small molecules	Melamine	2013	[39]
	Cocaine	2015, 2017	[62-64]
	Diclofenac	2015	[14]
	Metoprolol	2016	[65]
	Fumonisin B2	2016	[66]
	Glucosamine	2016	[66]
	L-thyroxine	2016	[66]
	Biotin	2016, 2018, 2021	[55, 66, 67]
	4-ethylphenol	2016	[68]
	Indole-3-butyric acid	2017	[69]
	Adenosine monophosphate	2017	[70]
	THC	2018	[54]
	Histamine	2018	[71]
	N-L-hexanoyl homoserine lactone (C6-AHL)	2019	[72]
	Ochratoxin A	2019	[73]
	Fumonisin B1	2019	[74]
	N-hexanoyl-L-homoserine lactone	2020	[75]
Paracetamol	2021	[76]	
Doxorubicin	2022	[77]	
Proteins	Trypsin	2014 - 2021	[48 - 59]
	Pepsin	2014, 2021	[48, 78]
	α -amylase	2014, 2019	[48, 53]
	Kallikrein	2016	[50]
	RNase	2016	[50]
	β -lactoglobulin	2016	[79]
	Albumin	2019, 2021	[53, 80]
	Heart-fatty acid binding protein	2019	[81]
	ST2 protein	2019	[81]
	IgG Fc epitope	2019	[82]
	Epidermal growth factor receptor epitope (EGFR)	2020, 2022	[57, 83]
	β -lactoglobulin	2021	[84]
	Cadherin	2022	[77]
	Angiogenin	2022	[77]
Short peptides and glycopeptides	Vancomycin	2013 - 2018	[13, 14, 39, 55, 60]
	Generic peptide	2019	[53]
	HIV peptide	2019	[85]
	Insulin	2021	[86]
	CB-1 receptor peptide	2021	[87]
	Surface cell proteins	2021	[88]
Oxytocin	2022	[89]	
Macromolecules	12 nucleic bases	2016	[90]
	Hyaluronic acid	2019, 2022	[77, 91]
Viruses	Bacteriophage MS2	2015	[60, 61]
	Adenovirus	2015	[60]

1.4 CHARACTERIZATION OF MIP

The characterization of the synthesized material is fundamental to determine the quality of the synthesis and its properties. In particular, for the MIP nanoparticles, different properties must be evaluated, starting from the physical ones, like the morphology and the shape. This step can be skipped if a previously standardized protocols of synthesis is being used, since we can assume that nanoMIPs synthesized with the same protocols but for different substances are similar. Anyhow, the most important thing is the evaluation of the binding properties, because they depend on the template.

1.4.1 Binding properties

In every recognition system, it is essential to know how well the system is able to bind the target molecule and discriminate between other similar molecules. In chemistry, these abilities are described by two parameters: the affinity and the selectivity. While the affinity is an absolute value, the selectivity is a relative parameter between two or more different substances, where one of these is the target molecule. For MIPs, other important binding parameters are the imprinting factor (or IF), the kinetic of binding and the number of binding sites (or B_{\max}).

All these parameters are expressed like numerical values. To obtain these values from the experiments, rigid experimental protocols and mathematics models are required, to elaborate the experimental data into the values of the binding constants.

In a dynamic equilibrium, where it is very difficult to measure the direct interaction between the MIP binding site and the target molecules, the easiest way is to evaluate the macroscopic effect of these interactions. Two main methods are reported in the literature: the batch rebinding, also used in this work, and the frontal chromatography [92]. In the work of my PhD I have used the batch rebinding system.

Knowing the exact amount of MIP nanoparticles and putting these solutions in contact with a known quantity of the target molecules, after an equilibration time we can quantify the bond and the free fractions of the target molecules through analytical procedures like HPLC-Fluorescence [41], Surface Plasmon Resonance spectroscopy (SPR) [65] or the Bradford assay [40]. It is also possible to use the Quartz Crystal Microbalance (QCM) gravimetric sensing to directly measure the bond fraction [28]. From these data, we can calculate the equilibrium constants and the number of binding sites with the use of isotherm equations. These mathematical models describe the binding system with a well level of precision but with some theoretical assumptions. Several models of isotherm are available to calculate the binding properties of MIPs, with a variable number of parameters and typology of binding sites. In most of the cases, the results obtained from different mathematical models are very similar; if so, the best strategy is to choose

the simplest model: the Langmuir one. This isotherm is based on three assumptions:

- (a) the number of adsorption layers is only one;
- (b) all surface binding sites are equivalent;
- (c) there is no cooperation effect between close adsorbed molecules that may affect the binding constant.

A basic assumption of the Langmuir theory is that the sorption takes place in specific homogeneous sites within the target molecule. It is then assumed that once a template molecule occupies a site, no further adsorption can occur in that site.

The equation of the Langmuir model is:

$$B = \frac{B_{max}K_{eq}F}{1 + K_{eq}F}$$

Where: B = Bond fraction of the molecules

B_{max} = Maximum bond fraction or number of binding sites

F = Free fraction of the molecules

K_{eq} = Equilibrium constant of the system

From the Langmuir model two important parameters can be obtained: the number of binding sites (B_{max}) and the equilibrium constant of the binding between the MIP and the target molecule. This equilibrium constant expresses the strength of the binding, *i.e.* the affinity.

If we compare constants for the same MIP against various target molecules, but different from the template, we can evaluate the selectivity of the MIP. In particular, it is important to evaluate and compare the affinity for the template molecule and molecules of the same family, to understand the capability of the MIP to discriminate between similar but different molecules. The equation to calculate the selectivity (α) is:

$$\alpha = \frac{K_{eq} \text{ other substance}}{K_{eq} \text{ template}}$$

The number of binding sites does not depend only on the really imprinted sites on the MIP. In fact, there is the paradox that substances with lower affinity than the template molecules have higher B_{max} than the template molecule. The reason is that the “binding sites” are not only the “imprinted sites”, but every portion of the

MIP surface that can bind the molecules. In the case of the template molecule, the number of “binding sites” match the number of “imprinted sites”, and so B_{max} . In the case of low-affinity molecules, these are not only bonded to the imprinted sites, but also to a lot of portions of the MIP surface. In these cases, the values of B_{max} are higher.

The imprinting factor is one of the most used parameters in literature to evaluate the quality of the MIP. This factor is the ratio between the affinity constant of the target molecule with the MIP and with the respective NIP. This factor represents the difference between the specific bond and the non-specific bond of the molecules with the nanoparticle. The formula to calculate the imprinting factor (IF) is:

$$IF = \frac{K_{eq} \text{ MIP}}{K_{eq} \text{ NIP}}$$

At last, the evaluation of the bond kinetic is important to study how fast the MIP bonds the target molecules, to compare it with other systems and to apply it to other approaches like immunochemistry assays or sensor [93, 94].

1.4.2 Morphological properties

To study the dimensions and the shapes of the nanoparticles, there are two different types of techniques: the ones which directly see the nanoparticles or the ones which only measure their dimension.

In the first category there are the electronic microscopy and atomic force microscopy. The electronic microscopy, in particular SEM, is the most used technique to study the morphology of the nanoMIPs. To observe MIP nanoparticles with this technique, it is fundamental treat the polymer nanoparticles to make them conductive. One of the possible methods is a treatment with osmium tetroxide (OsO_4) [20]. In some cases, also the transmission electron microscopy is used [48, 55]. The measurement of the dimensions with electron microscopy is done manually on the collected images using a vector graphics editor.

Another used microscopy technique is the atomic force microscopy (AFM). In this technique a cantilever scans the surface measuring the attraction force of the atoms, creating a 3D map of these. The advantage of the AFM is that it is possible to observe MIP nanoparticles without a conductive treatment, but only with an immobilization on the analytical surface [40].

The other category of techniques is not based on the direct observation via images of the sample but only on the measurement of a physical property. The most commons are the dynamic light scattering (DLS) and the nanoparticles tracking analysis (NTA). The DLS is a technique based on the capability of the particles

suspension to scatter the laser-generated light [95]. NanoMIPs are insoluble in water and, in this solvent, make a suspension usable for DLS analysis. This technique is fast and not destructive for the sample. The sonication is used to break the nanoparticles aggregates. It is largely applied to nanoMIPs, to measure the hydrodynamic diameter, the zeta potential and the polydispersity index [43, 55, 58, 76]. The NTA technique is similar to DLS but in this case the scattering of the laser-generated light is used only to illuminate the suspended nanoparticles. The Brownian motions of the nanoparticles are followed by a camera, and the instrument uses these data to determine the nanoparticles dimensions [95]. In the recent years, NTA has joined DLS as techniques to measure nanoMIPs properties [40].

1.4.3 Spectroscopic properties

Other two techniques are sometimes used to study the properties of the nanoMIPs. To obtain information about the monomeric formulation and the presence of functional groups the infrared spectroscopy can be useful. In particular, this technique is not helpful to study the formulation of a self-produced polymer, but to evaluate the quality of the polymerization [89].

NMR is helpful to study the interaction between the monomers, the polymers and the template molecules. In particular, measuring the chemical shifts of the template in the presence of an increasing concentration of different types of monomers gives us information about the best monomer for the template [89]. It is a univariate information and the effective interaction in the monomers mixture can be different.

1.5 CONCLUSIONS AND AIM OF THE WORK

The SPPS is the most promising technique to make nanoMIPs. Since its introduction, the technique has had a big impact on the MIPs field, and a lot of works have explored new applications and templates. Nevertheless, like every new technology that involves several parameters, a lot of optimization steps and experimental trials are required to find the best experimental conditions. In this case, the ones which allow obtaining nanoMIPs with the highest affinity and selectivity for the target molecule, and better morphological properties. Some of the experimental parameters involved are: the monomers formulation, the ratio between monomers, the time of polymerization, the presence of a waiting time between the start of polymerization and the insertion of the template molecules in the reaction environment, the type of crosslinker, the environment of polymerization and the length of the spacer arm.

In my PhD project, I explored some of these parameters, with two proof-of concept templates, ciprofloxacin and rabbit immunoglobulins, described in the to which the first part of this thesis (chapters 2-5).

In the second chapter, three conditions are evaluated: the type of reaction environment (organic or water), the pH of the rebinding experiment environment, and the length of the spacer arm, combined in an experimental design.

In the third chapter, a second experimental design is discussed, to pinpoint the best monomeric ratio for the nanoMIPs imprinted in water. In the fourth chapter, the effect of the polymerization time in both synthesis environments is described, trying to better understand the mechanism of polymerization in addition to finding the best polymerization conditions.

Finally, in the fifth chapter the effect of the change of the crosslinker on the binding properties of the nanoMIPs, keeping unchanged the monomers molar ratio, is discussed, exploring the influence of the rigidity of the polymeric lattice on the binding.

The second part of this thesis is dedicated to the development of SPPS nanoMIPs for different substances and their analytical applications.

In chapters 6 and 7, the study of nanoMIPs imprinted for the ochratoxin A and the L-Thyroxine, respectively, are reported. For the former, the employment of the mimic template was explored, while for the latter also the importance of the grafted template orientation was evaluated.

Finally, in chapter 8, the application of the optimized nanoMIP for ciprofloxacin in a solid phase extraction (SPE) device is described.

1.6 BIBLIOGRAPHY

- [1] M. Sun, Y. Liu, W. Walker, C. Liu, S. Gu, Y. Zhang, J. Zhou, G. Wang. Identification and characterization of pheromone receptors and interplay between receptors and pheromone binding proteins in the diamondback moth, *plutella xylostella*. *PLoS One*, **2013**, *8*, e62098, doi: 10.1371/journal.pone.0062098.
- [2] V. Ralevic, G. Burnstock. Receptors for purines and pyrimidines. *Pharmacol. Rev.* **1998**, *50*, 413–92, Pubmed: 9755289.
- [3] E. Harlow, D. Lane. *Antibodies: A Laboratory Manual*. Cold Spring Harbor Press, Laurel Hollow, USA, 1988.
- [4] A. Casadevall, L.A. Pirofski, M.J. Joyner. The principles of antibody therapy for infectious diseases with relevance for covid-19. *mBio*, vol. 12, no. 2, pp. 1–13, 2021, doi: 10.1128/MBIO.03372-20.
- [5] L. Anfossi, C. Baggiani, C. Giovannoli, G. D’Arco, G. Giraudi. Lateral-flow immunoassays for mycotoxins and phycotoxins: A review. *Anal. Bioanal. Chem.* **2013**, *405*, 467–480, doi: 10.1007/S00216-012-6033-4.
- [6] J. Homola. Surface plasmon resonance sensors for detection of chemical and biological species. *Chem. Rev.* **2008**, *108*, 462–493, doi: 10.1021/CR068107D.
- [7] Y. Hoshino, K.J. Shea. The evolution of plastic antibodies. *J. Mater. Chem.*, **2011**, *21*, 3517 – 3521, doi: 10.1039/CoJM03122D.
- [8] G. Wulff. Forty years of molecular imprinting in synthetic polymers: Origin, features and perspectives. *Microchim. Acta*, **2013**, *180*, 1359–1370, doi: 10.1007/s00604-013-0992-9.
- [9] L. Pauling. Nature of forces between large molecules of biological interest. *Nature*, **1948**, *161*, 707–709, doi: 10.1038/161707a0.
- [10] L. Chen, X. Wang, W. Lu, X. Wu, J. Li. Molecular imprinting: Perspectives and applications. *Chem Soc Rev*, **2016**, *45*, 2137–2211, doi: 10.1039/c6cs00061d.
- [11] F. Canfarotta, A. Poma, A. Guerreiro, S. Piletsky. Solid-phase synthesis of molecularly imprinted nanoparticles. *Nature Protoc.*, **2016**, *11*, 443–455, doi: 10.1038/nprot.2016.030.
- [12] D. Refaat, M. Aggour, A. Farghali, R. Mahajan, J. Wiklander, I. Nicholls, S. Piletsky. Strategies for molecular imprinting and the evolution of MIP

- nanoparticles as plastic antibodies—synthesis and applications. *Int J Mol Sci*, **2019**, *20*, 6304, doi: 10.3390/IJMS20246304.
- [13] R. v. Shutov, A. Guerreiro, E. Moczko, I. Perz de Vargas-Sansalvador, I. Chianella, M. J. Whitcombe, S. Piletsky. Introducing MINA - the molecularly imprinted nanoparticle assay. *Small*, **2014**, *10*, 1086–1089, doi: 10.1002/sml.201301996.
- [14] Z. Altintas, A. Guerreiro, S. A. Piletsky, I. E. Tothill. NanoMIP based optical sensor for pharmaceuticals monitoring. *Sens Actuators B*, **2015**, *213*, 305–313, doi: 10.1016/j.snb.2015.02.043.
- [15] I. Chipinda, J. M. Hettick, P. D. Siegel. Haptentation: chemical reactivity and protein binding. *J Allergy (Cairo)*, **2011**, *2011*, 1–11, doi: 10.1155/2011/839682.
- [16] L. Chen, S. Xu, J. Li. Recent advances in molecular imprinting technology: current status, challenges and highlighted applications. *Chem Soc Rev*, **2011**, *40*, 2922–2942, doi: 10.1039/c0cs00084a.
- [17] Å. Zander, P. Findlay, T. Renner, B. Sellergren, A. Swietlow. analysis of nicotine and its oxidation products in nicotine chewing gum by a molecularly imprinted solid-phase extraction. *Anal Chem*, **1998**, *70*, 3304–3314, doi: 10.1021/ac971272w.
- [18] L. Ye, P.A.G. Cormack, K. Mosbach. Molecularly imprinted monodisperse microspheres for competitive radioassay. *Anal Commun*, **1999**, *36*, 35–38. doi: 10.1039/a809014i.
- [19] F. G. Tamayo, M. M. Titirici, A. Martin-Esteban, B. Sellergren. Synthesis and evaluation of new propazine-imprinted polymer formats for use as stationary phases in liquid chromatography. *Anal Chim Acta*, **2005**, *542*, 38–46, doi: 10.1016/j.aca.2004.12.063.
- [20] S. Subrahmanyam, A. Guerreiro, A. Poma, E. Moczko, E. Piletska, S. Piletsky. Optimisation of experimental conditions for synthesis of high affinity MIP nanoparticles. *Eur Polym J*, **2013**, *49*, 100–105, doi: 10.1016/j.eurpolymj.2012.09.022.
- [21] P. Lieberzeit, A. Afzal, A. Rehman, F. Dickert. Nanoparticles for detecting pollutants and degradation processes with mass-sensitive sensors. *Sens Actuators B*, **2007**, *127*, 132–136, doi: 10.1016/j.snb.2007.07.020.
- [22] R. Schirhagl, U. Latif, F. L. Dickert. Atrazine detection based on antibody replicas. *J Mater Chem*, **2011**, *21*, 14594, doi: 10.1039/c1jm11576f.

- [23] Y. Hoshino, T. Kodama, Y. Okahata, K. J. Shea. Peptide imprinted polymer nanoparticles: a plastic antibody. *J Am Chem Soc*, **2008**, *130*, 15242–15243, doi: 10.1021/ja8062875.
- [24] S. Pardeshi, R. Dhodapkar, A. Kumar. Molecularly imprinted microspheres and nanoparticles prepared using precipitation polymerisation method for selective extraction of gallic acid from *Emblica officinalis*. *Food Chem*, **2014**, *146*, 385–393, doi: 10.1016/j.foodchem.2013.09.084.
- [25] W.H. Li, H.D.H. Stöver. Porous monodisperse poly(divinylbenzene) microspheres by precipitation polymerization. *J. Polym. Sci. A* **1998**, *36*, 1543–1551, doi: 10.1002/(SICI)1099-0518(19980730)36:10<1543::AID-POLA7>3.0.CO;2-R
- [26] K. Yoshimatsu, K. Reimhult, A. Krozer, K. Mosbach, K. Sode, L. Ye. Uniform molecularly imprinted microspheres and nanoparticles prepared by precipitation polymerization: the control of particle size suitable for different analytical applications. *Anal Chim Acta*, **2007**, *584*, 112–121, doi: 10.1016/j.aca.2006.11.004.
- [27] Z. Chen, L. Ye. Controlling size and uniformity of molecularly imprinted nanoparticles using auxiliary template. *J Mol Recogn*. **2012**, *25*, 370–376, doi: 10.1002/jmr.2161.
- [28] R. Schirhagl, P.A. Lieberzeit, F.L. Dickert. Chemosensors for viruses based on artificial immunoglobulin copies. *Adv Mater*, **2009**, *22*, 2078–2081, Dec. 2009, doi: 10.1002/adma.200903517.
- [29] A. Poma, A. P. F. Turner, and S. A. Piletsky, ‘Advances in the manufacture of MIP nanoparticles’, *Trends Biotechnol*, vol. 28, no. 12, pp. 629–637, Dec. 2010, doi: 10.1016/j.tibtech.2010.08.006.
- [30] J. Wackerlig, P. A. Lieberzeit. Molecularly imprinted polymer nanoparticles in chemical sensing – synthesis, characterisation and application. *Sens Actuators B*, **2015**, *207*, 144–157, doi: 10.1016/j.snb.2014.09.094.
- [31] D. Vaihinger, K. Landfester, I. Kräuter, H. Brunner, G.E.M. Tovar. Molecularly imprinted polymer nanospheres as synthetic affinity receptors obtained by miniemulsion polymerisation. *Macromol Chem Phys*, **2003**, *203*, 1965–1973, doi: 10.1002/1521-3935(200209)203:13<1965::AID-MACP1965>3.0.CO;2-C
- [32] S. Slomkowski, J. V. Alemán, R. G. Gilbert, M. Hess, K. Horie, R. G. Jones, P. Kubisa, I. Meisel, W. Mormann, S. Penczek, R.F.T. Stepto. Terminology of polymers and polymerization processes in dispersed systems (IUPAC Recommendations 2011). *Pure Appl Chem*, **2011**, *83*, 2229–2259, doi: 10.1351/PAC-REC-10-06-03

- [33] G. Sener, E. Ozgur, E. Yilmaz, L. Uzun, R. Say, A. Denizli. Quartz crystal microbalance based nanosensor for lysozyme detection with lysozyme imprinted nanoparticles. *Biosens Bioelectron*, **2010**, *26*, 815–821, doi: 10.1016/j.bios.2010.06.003.
- [34] G. Sener, L. Uzun, R. Say, A. Denizli. Use of molecular imprinted nanoparticles as biorecognition element on surface plasmon resonance sensor. *Sens Actuators B*, **2011**, *160*, 791–799, doi: 10.1016/j.snb.2011.08.064.
- [35] M.E. Çorman, S. Akgöl. Preparation of molecular imprinted hydrophobic polymeric nanoparticles having structural memories for lysozyme recognition. *Artif Cells Blood Subst Biotechnol*, **2012**, *40*, 245–255, doi: 10.3109/10731199.2012.657204.
- [36] Z. Zeng, Y. Hoshino, A. Rodriguez, H. Yoo, K.J. Shea. Synthetic polymer nanoparticles with antibody-like affinity for a hydrophilic peptide. *ACS Nano*, **2010**, *4*, 199–204, doi: 10.1021/nn901256s.
- [37] D. Refaat, M.G. Aggour, A.A. Farghali, R. Mahajan, J.G. Wiklander, I.A. Nicholls, S.A. Piletsky. Strategies for molecular imprinting and the evolution of MIP nanoparticles as plastic antibodies—Synthesis and applications. *Int J Mol Sci*, **2019**, *20*, 6304, doi: 10.3390/IJMS20246304.
- [38] X. Ding, P.A. Heiden. Recent developments in molecularly imprinted nanoparticles by surface imprinting techniques. *Macromol Mater Eng*, **2014**, *299*, 268–282, doi: 10.1002/mame.201300160.
- [39] A. Poma, A. Guerreiro, M.J. Whitcombe, E.v. Piletska, A.P.F. Turner, S.A. Piletsky. Solid-phase synthesis of molecularly imprinted polymer nanoparticles with a reusable template—“Plastic antibodies”. *Adv Funct Mater*, **2013**, *23*, 2821–2827, doi: 10.1002/adfm.201202397.
- [40] M. Chiarello, L. Anfossi, S. Cavalera, F. di Nardo, T. Serra, F. Sordello, C. Baggiani. Rabbit IgG-imprinted nanoMIPs by solid phase synthesis: the effect of cross-linkers on their affinity and selectivity. *J Mater Chem B*, **2022**, *10*, 6724–6731. 2022. <https://doi.org/10.1039/D2TB00245K>.
- [41] S. Cavalera, M. Chiarello, F. di Nardo, L. Anfossi, C. Baggiani. Effect of experimental conditions on the binding abilities of ciprofloxacin-imprinted nanoparticles prepared by solid-phase synthesis. *React Funct Polym*, **2021**, *163*, 104893, doi: 10.1016/j.reactfunctpolym.2021.104893.
- [42] T. Cowen, E. Stefanucci, E. Piletska, G. Marrazza, F. Canfarotta, S.A. Piletsky. Synthetic mechanism of molecular imprinting at the solid phase.

- Macromolecules*, **2020**, *53*, 1435–1442, doi: 10.1021/acs.macromol.9b01913.
- [43] M. Chiarello, L. Anfossi, S. Cavalera, F. di Nardo, F. Artusio, R. Pisano, C. Baggiani. Effect of polymerization time on the binding properties of ciprofloxacin-imprinted nanomips prepared by Solid-Phase Synthesis. *Polymers*, **2021**, *13*, 2656, doi: 10.3390/polym13162656.
- [44] R. Mohsen, G.J. Vine, N. Majcen, B.D. Alexander, M.J. Snowden. Characterization of thermo and pH responsive NIPAM based microgels and their membrane blocking potential. *Colloids Surf A*, **2013**, *428*, 53–59, doi: 10.1016/j.colsurfa.2013.03.031.
- [45] C. Baggiani, C. Giovannoli, L. Anfossi, C. Passini, P. Baravalle, G. Giraudi. A connection between the binding properties of imprinted and nonimprinted polymers: a change of perspective in molecular imprinting. *J Am Chem Soc*, **2012**, *134*, 1513–1518, doi: 10.1021/ja205632t.
- [46] X. Shen, L. Ye. Interfacial molecular imprinting in nanoparticle-stabilized emulsions. *Macromolecules*, **2011**, *44*, 5631–5637, doi: 10.1021/ma200837n.
- [47] A.R. Guerreiro, I. Chianella, E. Piletska, M.J. Whitcombe, S.A. Piletsky. Selection of imprinted nanoparticles by affinity chromatography. *Biosens Bioelectron*, **2009**, *24*, 2740–2743, doi: 10.1016/j.bios.2009.01.013.
- [48] A. Poma, A. Guerreiro, S. Caygill, E. Moczko, S. Piletsky. Automatic reactor for solid-phase synthesis of molecularly imprinted polymeric nanoparticles (MIP NPs) in water. *RSC Adv*, **2014**, *4*, 4203–4206, doi: 10.1039/C3RA46838K.
- [49] A. Poma, H. Brahmabhatt, H.M. Pendergraff, J.K. Watts, N.W. Turner. Generation of novel hybrid aptamer-molecularly imprinted polymeric nanoparticles. *Adv Mater*, **2015**, *27*, 750–758, doi: 10.1002/adma.201404235.
- [50] Y. Garcia, K. Smolinska-Kempisty, E. Pereira, E. Piletska, S. Piletsky. Development of competitive ‘pseudo’-ELISA assay for measurement of cocaine and its metabolites using molecularly imprinted polymer nanoparticles. *Anal Methods*, **2017**, *9*, 4592–4598, doi: 10.1039/C7AY01523B.
- [51] K. Smolinska-Kempisty, O.S. Ahmad, A. Guerreiro, K. Karim, E. Piletska, S. Piletsky. New potentiometric sensor based on molecularly imprinted nanoparticles for cocaine detection. *Biosens Bioelectron*, **2017**, *96*, 49–54, doi: 10.1016/j.bios.2017.04.034.

- [52] Z. Altintas, B. France, J.O. Ortiz, I.E. Tothill. Computationally modelled receptors for drug monitoring using an optical based biomimetic SPR sensor. *Sens Actuators B*, **2016**, *224*, 726–737, doi: 10.1016/j.snb.2015.10.075.
- [53] K. Smolinska-Kempisty, A. Guerreiro, F. Canfarotta, C. Cáceres, M.J. Whitcombe, S. Piletsky. A comparison of the performance of molecularly imprinted polymer nanoparticles for small molecule targets and antibodies in the ELISA format. *Sci Rep*, **2016**, *6*, 37638, doi: 10.1038/srep37638.
- [54] F. Canfarotta, J. Czulak, K. Betlem, A. Sachdeva, K. Eersels, B. van Grinsven, T.J. Cleij, M. Peeters. A novel thermal detection method based on molecularly imprinted nanoparticles as recognition elements. *Nanoscale*, **2018**, *10*, 2081–2089, doi: 10.1039/C7NR07785H.
- [55] B. Abbott, T.S. Bedwell, F. Grillo, S. Piletsky, M.J. Whitcombe, E. Piletska, A. Garcia-Cruz, T. Cowen, S.A. Piletsky. Use of polymeric solid phase in synthesis of MIP nanoparticles for biotin. *React Funct Polym*, **2022**, *170*, 105109, doi: 10.1016/j.reactfunctpolym.2021.105109.
- [56] D. Garcia-Mutio, A. Gomez-Caballero, A. Guerreiro, S. Piletsky, M.A. Goicolea, R.J. Barrio. Solid-phase synthesis of imprinted nanoparticles grafted on gold substrates for voltammetric sensing of 4-ethylphenol. *Sens Actuators B Chem*, **2016**, *236*, 839–848, doi: 10.1016/j.snb.2016.02.018.
- [57] L. Chen, T. Muhammad, B. Yakup, S.A. Piletsky. New immobilisation protocol for the template used in solid-phase synthesis of MIP nanoparticles. *Appl Surf Sci*, **2017**, *406*, 115–121, doi: 10.1016/j.apsusc.2017.02.105.
- [58] C.A. Mourão, F. Bokeloh, J. Xu, E. Prost, L. Duma, F. Merlier, S.M. Bueno, K. Haupt, B. Tse Sum Bui. Dual-Oriented Solid-Phase Molecular Imprinting: Toward Selective Artificial Receptors for Recognition of Nucleotides in Water. *Macromolecules*, **2017**, *50*, 7484–7490, doi: 10.1021/acs.macromol.7b01782.
- [59] F. Canfarotta, J. Czulak, A. Guerreiro, A.G. Cruz, S. Piletsky, G.E. Bergdahl, M. Hedström, B. Mattiasson. A novel capacitive sensor based on molecularly imprinted nanoparticles as recognition elements. *Biosensors and Bioelectronics*, **2018**, *120*, 108–114, doi: 10.1016/j.bios.2018.07.070.
- [60] X. Feng, J. Ashley, T. Zhou, A. Halder, Y. Sun. A facile molecularly imprinted polymer-based fluorometric assay for detection of histamine. *RSC Adv*, **2018**, *8*, 2365–2372, doi: 10.1039/C7RA11507E.
- [61] J. Garcia Lopez, E. Piletska, M.J. Whitcombe, J. Czulak, S.A. Piletsky. Application of molecularly imprinted polymer nanoparticles for degradation

- of the bacterial autoinducer *N*-hexanoyl homoserine lactone. *Chemical Communications*, **2019**, *55*, 2664–2667, doi: 10.1039/C8CC07685E.
- [62] D. López-Puertollano, T. Cowen, A. García-Cruz, E. Piletska, A. Abad-Somovilla, A. Abad-Fuentes, S. Piletsky. Study of Epitope Imprinting for Small Templates: Preparation of NanoMIPs for Ochratoxin A. *ChemNanoMat*, **2019**, *5*, 651–657, doi: 10.1002/cnma.201900050.
- [63] H. Munawar, A. Garcia-Cruz, M. Majewska, K. Karim, W. Kutner, S.A. Piletsky. Electrochemical determination of fumonisin B1 using a chemosensor with a recognition unit comprising molecularly imprinted polymer nanoparticles. *Sens Actuators B Chem*, **2020**, *321*, 128552, doi: 10.1016/j.snb.2020.128552.
- [64] A. Guha, O.S. Ahmad, A. Guerreiro, K. Karim, N. Sandström, V.P. Ostanin, W. van der Wijngaart, S.A. Piletsky, S.K. Ghosh. Direct detection of small molecules using a nano-molecular imprinted polymer receptor and a quartz crystal resonator driven at a fixed frequency and amplitude. *Biosensors and Bioelectronics*, **2020**, *158*, 112176, doi: 10.1016/j.bios.2020.112176.
- [65] K. Alanazi, A. Garcia Cruz, S. di Masi, A. Voorhaar, O.S. Ahmad, T. Cowen, E. Piletska, N. Langford, T.J. Coats, M.R. Sims, S.A. Piletsky. Disposable paracetamol sensor based on electroactive molecularly imprinted polymer nanoparticles for plasma monitoring. *Sensors and Actuators B: Chemical*, **2021**, *329*, 129128, doi: 10.1016/j.snb.2020.129128.
- [66] B. Tse Sum Bui, K. Haupt. Molecularly imprinted polymer hydrogel nanoparticles: synthetic antibodies for cancer diagnosis and therapy. *ChemBioChem*, **2022**, *23*, e202100598, doi: 10.1002/cbic.202100598.
- [67] S. Ambrosini, S. Beyazit, K. Haupt, B. Tse Sum Bui. Solid-phase synthesis of molecularly imprinted nanoparticles for protein recognition. *Chemical Communications*, **2013**, *49*, 6746, doi: 10.1039/c3cc41701h.
- [68] J. Xu, S. Ambrosini, E. Tamahkar, C. Rossi, K. Haupt, B. Tse Sum Bui. Toward a universal method for preparing molecularly imprinted polymer nanoparticles with antibody-like affinity for proteins. *Biomacromolecules*, **2016**, *17*, 345–353, doi: 10.1021/acs.biomac.5b01454.
- [69] J. Ashley, X. Feng, A. Halder, T. Zhou, Y. Sun. Dispersive solid-phase imprinting of proteins for the production of plastic antibodies. *Chemical Communications*, **2018**, *54*, 3355–3358, doi: 10.1039/C8CC00343B.
- [70] J. Xu, K. Haupt, B. Tse Sum Bui. Core–shell molecularly imprinted polymer nanoparticles as synthetic antibodies in a sandwich fluoroimmunoassay for trypsin determination in human serum. *ACS Appl Mater Interfaces*, **2017**, *9*, 24476–24483, doi: 10.1021/acsami.7b05844.

- [71] T.S. Bedwell, N. Anjum, Y. Ma, J. Czulak, A. Poma, E. Piletska, M.J. Whitcombe, S.A. Piletsky. New protocol for optimisation of polymer composition for imprinting of peptides and proteins. *RSC Advances*, **2019**, *9*, 27849–27855. doi: 10.1039/C9RA05009D.
- [72] J. Xu, E. Prost, K. Haupt, B. Tse Sum Bui. Direct and sensitive determination of trypsin in human urine using a water-soluble signaling fluorescent molecularly imprinted polymer nanoprobe. *Sens Actuators B Chem*, 2018, *258*, 10–17, doi: 10.1016/j.snb.2017.11.077.
- [73] K. Betlem, F. Canfarotta, R. Raumbault, C.E. Banks, K. Eersels, B. van Grinsven, T.J. Cleij, R. Crapnell, A. Hudson, M. Peeters. Thermistors coated with molecularly imprinted nanoparticles for the electrical detection of peptides and proteins. *Analyst*, **2020**, *145*, 5419–5424, doi: 10.1039/DOAN01046D.
- [74] M.v. Sullivan, O. Clay, M.P. Moazami, J.K. Watts, N.W. Turner. Hybrid aptamer-molecularly imprinted polymer (aptaMIP) nanoparticles from protein recognition—a trypsin model. *Macromol Biosci*, **2021**, *21*, 2100002, doi: 10.1002/mabi.202100002.
- [75] C. Cáceres, E. Moczko, I. Basozabal, A. Guerreiro, S. Piletsky. Molecularly imprinted nanoparticles (nanomips) selective for proteins: optimization of a protocol for solid-phase synthesis using automatic chemical reactor. *Polymers (Basel)*, **2021**, *13*, 314, doi: 10.3390/polym13030314.
- [76] Y. García, J. Czulak, E.D. Pereira, S.A. Piletsky, E. Piletska. A magnetic molecularly imprinted nanoparticle assay (MINA) for detection of pepsin. *React Funct Polym*, **2022**, *170*, 105133, doi: 10.1016/j.reactfunctpolym.2021.105133.
- [77] J. Ashley, Y. Shukor, I.E. Tothill. The use of differential scanning fluorimetry in the rational design of plastic antibodies for protein targets. *Analyst*, **2016**, *141*, 6463–6470, doi: 10.1039/C6AN01155A.
- [78] W.A.A. Sudjarwo, M.T. Dobler, P.A. Lieberzeit. QCM-based assay designs for human serum albumin. *Anal Bioanal Chem*, **2022**, *414*, 731–741, doi: 10.1007/s00216-021-03771-0.
- [79] R.D. Crapnell, F. Canfarotta, J. Czulak, R. Johnson, K. Betlem, F. Mecozzi, M.P. Down, K. Eersels, B. van Grinsven, T.J. Cleij, R. Law, C.E. Banks, M. Peeters. Thermal detection of cardiac biomarkers heart-fatty acid binding protein and ST2 using a molecularly imprinted nanoparticle-based multiplex sensor platform. *ACS Sensors*, **2019**, *4*, 2838–2845, doi: 10.1021/acssensors.9b01666.

- [80] E. Moczko, A. Guerreiro, C. Cáceres, E. Piletska, B. Sellergren, and S.A. Piletsky. Epitope approach in molecular imprinting of antibodies. *Journal of Chromatography B*, **2019**, *1124*, 1–6, doi: 10.1016/j.jchromb.2019.05.024.
- [81] S.S. Piletsky, A. Garcia Cruz, E. Piletska, S.A. Piletsky, E.O. Aboagye, A. C. Spivey. Iodo silanes as superior substrates for the solid phase synthesis of molecularly imprinted polymer nanoparticles. *Polymers (Basel)*, **2022**, *14*, 1595, doi: 10.3390/polym14081595.
- [82] R. D'Aurelio, J. Ashley, T. Rodgers, L. Trinh, J. Temblay, M. Pleasants, I. Tothill. Development of a nanoMIPs-SPR-based sensor for β -Lactoglobulin detection. *Chemosensors*, **2020**, *8*, 94, doi: 10.3390/chemosensors8040094
- [83] Z. Altintas, J. Pocock, K.A. Thompson, I.E. Tothill. Comparative investigations for adenovirus recognition and quantification: Plastic or natural antibodies? *Biosens Bioelectron*, **2015**, *74*, 996–1004, doi: 10.1016/j.bios.2015.07.076.
- [84] J. Xu, F. Merlier, B. Avasse, V. Vieillard, P. Debré, K. Haupt, B. Tse Sum Bui. Molecularly imprinted polymer nanoparticles as potential synthetic antibodies for immunoprotection against HIV. *ACS Applied Materials & Interfaces*, **2019**, *11*, 9824–9831, doi: 10.1021/acsami.8b22732.
- [85] A. Garcia Cruz, I. Haq, T. Cowen, S. di Masi, S. Trivedi, K. Alanazi, E. Piletska, A. Mujahid, S.A. Piletsky. Design and fabrication of a smart sensor using in silico epitope mapping and electro-responsive imprinted polymer nanoparticles for determination of insulin levels in human plasma. *Biosensors and Bioelectronics*, **2020**, *169*, 112536, doi: 10.1016/j.bios.2020.112536.
- [86] A. Gómez-Caballero, A. Elejaga-Jimeno, G. García del Caño, N. Unceta, A. Guerreiro, M. Saumell-Esnaola, J. Sallés, M.A. Goicolea, R.J. Barrio. Solid-phase synthesis of imprinted nanoparticles as artificial antibodies against the C-terminus of the cannabinoid CB₁ receptor: exploring a viable alternative for bioanalysis. *Microchimica Acta*, **2021**, *188*, 368, doi: 10.1007/s00604-021-05029-z.
- [87] S.S. Piletsky, E. Piletska, M. Poblocka, S. Macip, D.J.L. Jones, M. Braga, T.H. Cao, R. Singh, A.C. Spivey, E.O. Aboagye, S.A. Piletsky. Snapshot imprinting: rapid identification of cancer cell surface proteins and epitopes using molecularly imprinted polymers. *Nano Today*, **2021**, *41*, 101304, doi: 10.1016/j.nantod.2021.101304.

- [88] R. Mahajan, S. Suriyanarayanan, G.D. Olsson, J.G. Wiklander, T. Aastrup, B. Sellergren, I.A. Nicholls. Oxytocin-selective nanogel antibody mimics. *Int J of Mol Sci*, **2022**, *23*, 2534, doi: 10.3390/ijms23052534.
- [89] H. Brahmabhatt, A. Poma, H. M. Pendergraff, J. K. Watts, N. W. Turner. Improvement of DNA recognition through molecular imprinting: hybrid oligomer imprinted polymeric nanoparticles (oligoMIP NPs). *Biomater Sci*, **2016**, *4*, 281–287, doi: 10.1039/C5BM00341E.
- [90] P.X. Medina Rangel, S. Laclef, J. Xu, M. Panagiotopoulou, J. Kovensky, B. Tse Sum Bui, K. Haupt. Solid-phase synthesis of molecularly imprinted polymer nanolabels: affinity tools for cellular bioimaging of glycans. *Scientific Reports*, **2019**, *9*, 1–9, doi: 10.1038/s41598-019-40348-5.
- [91] Z. Altintas, M. Gittens, A. Guerreiro, K.A. Thompson, J. Walker, S. Piletsky, I.E. Tothill. Detection of waterborne viruses using high affinity molecularly imprinted polymers. *Anal Chem*, **2015**, *87*, 6801–6807, doi: 10.1021/acs.analchem.5b00989.
- [92] J.A. García-Calzón, M.E. Díaz-García. Characterization of binding sites in molecularly imprinted polymers. *Sens Actuators B Chem*, 2007, *123*, 1180–1194, doi: 10.1016/j.snb.2006.10.068.
- [93] D. Lakshmi, A. Bossi, M.J. Whitcombe, I. Chianella, S.A. Fowler, S. Subrahmanyam, E. Piletska, S.A. Piletsky. Electrochemical sensor for catechol and dopamine based on a catalytic molecularly imprinted polymer-conducting polymer hybrid recognition element. *Analytical Chemistry*, **2009**, *81*, 3576–3584, doi: 10.1021/ac802536p.
- [94] J. Foote, H.N. Eisen. Kinetic and affinity limits on antibodies produced during immune responses. *Proceedings of the National Academy of Sciences*, **1995**, *92*, 1254–1256, doi: 10.1073/pnas.92.5.1254.
- [95] V. Filipe, A. Hawe, and W. Jiskoot. Critical evaluation of nanoparticle tracking analysis (NTA) by nanosight for the measurement of nanoparticles and protein aggregates. *Pharm Res*, **2010**, *27*, 796–810, doi: 10.1007/s11095-010-0073-2.

2 EFFECT OF DIFFERENT EXPERIMENTAL CONDITIONS ON THE BINDING ABILITIES OF CIPROFLOXACIN NANOMIPs

2.1 INTRODUCTION

In recent years, as previously shown, the solid-phase synthesis was applied to a lot of different template molecules. In general, most of the applications are based on the synthesis protocol published by Piletsky *et al.* [1] without modifications except for some cases [2]. In most of the examples reported in the introduction of this thesis, nanoMIPs are prepared in an aqueous medium, using N,N'-methylene-bis-acrylamide as a cross-linker and ammonium persulfate as a radical initiator. It is also possible to find several examples of nanoMIPs prepared in polar organic solvents, using ethylene dimethacrylate or trimethylolpropane trimethacrylate as a cross-linker [3-7].

Empirically, every synthesis parameter can have an influence on the binding capability of the nanoMIPs, and the influence may be, eventually, template-dependent. Due to the impossibility to set each parameter for each template unless a long experimental work, it is important to understand the MIP general behavior and responses to create a scheme of the most important parameters to be considered in their synthesis.

With the introduction of the SPPS technique, the synthesis in water environment started to have a unprecedented key role in the MIP history. It is important to evaluate how this more flexible synthesis can overcome the organic synthesis and produce nanoMIPs with better binding properties. Furthermore, new parameters were introduced with the SPPS technique, like the spacer arm that binds the template molecules and the glass beads. In general, several factors will need to be completely understood before considering this technique to be mature.

2.1.1 Aim of the work and objectives

The preparation of nanoMIPs by solid-phase synthesis seems to be a very versatile method, where the experimental conditions can be changed according to the current needs. Thus, to get more insights about the actual versatility of this innovative approach, the goal of this work is to directly compare the binding properties of nanoMIPs prepared with the same template but in different experimental conditions.

In this work we selected and tested two different levels of two synthesis parameters, as reported in Table 2-1: the length of the spacer arm that tie the template molecules to the glass beads and the synthesis environment. Finally, the

binding properties were assessed by measuring adsorption isotherms and binding kinetics of the resulting nanoMIPs in aqueous medium at three different pHs.

Table 2-1 – Classification of the produced MIPs according to the experimental design (d = 2, n = 4) by varying the spacer arm and synthesis environment conditions

		Spacer arm	
		Long chain (LC)	Short chain (SC)
Synthesis environment	Acetonitrile (acn)	acn LC-MIPs	acn SC-MIPs
	Water (w)	w LC-MIPs	w SC-MIPs

For this purpose, a fluoroquinolone antibiotic was chosen as template, the ciprofloxacin, whose molecular imprinting has been widely described in the literature [8-10], but none nanoMIPs preparation has not been described so far, through the solid-phase synthesis technique. Ciprofloxacin was covalently bond to glass beads, provided or not with a glutaraldehyde-based spacer arm ("long chain" / "short chain" beads) and nanoMIPs were synthesized in polymerization mixtures based on different solvents (water vs. acetonitrile). The different type of synthesis environment means the production of not identical nanoMIPs, because monomers and radical initiators work differently in water and in organic solvent. Summarizing, different radical initiators (ammonium persulfate vs. AIBN), cross-linking agents (methylen-bis-acrylamide vs. EDMA / TRIM) and functional monomers (acrylic acid / N-tert-butylacrylamide / isopropylacrylamide vs. methacrylic acid) were used.

2.2 EXPERIMENTAL

2.2.1 Materials

Glass beads were Spheringlass-2429 70-100 μm average particle size (Potters, UK). Ciprofloxacin was purchased by Supelco (Milan, Italy).

Acrylic acid (AA), 3-(aminopropyl)trimethoxysilane (APTMS), ammonium persulphate (APS), azo-bis-isobutyronitrile (AIBN), 1-ethyl-3-(3-dimethylaminopropyl)carbodiimide (EDC), ethylenediamine, ethylene dimethacrylate (EDMA), glutaraldehyde (50% aqueous solution), hexamethyldisilazane (HMDS), N-hydroxysuccinimide (NHS), N-isopropylacrylamide (NIPAm), methacrylic acid (MAA), N,N'-methylene-bis-acrylamide (BIS), morpholinethansulphonic acid (sodium salt, MES), sodium borohydride, N-tert-butylacrylamide (TBAm), N,N,N',N'-tetramethylethylenediamine (TEMED), N,N'-diisopropylcarbodiimide (DIC), and trimethylolpropane trimethacrylate (TRIM) were purchased by Sigma-Merck (Milan, Italy).

Solvents and all other chemicals were purchased from Sigma-Merck (Milan, Italy). All the solvents were of HPLC grade, whereas all chemicals were of analytical grade.

The water used was ultra-purified in Purelab Prima System from Elga (Marlow, UK). Polymerization inhibitors in the monomers were removed by filtration through activated basic alumina.

Antibiotic stock solutions were prepared by dissolving 10 mg of the substance in 25 mL of methanol/acetic acid 95/5 (v/v) then stored in the dark at $-20\text{ }^{\circ}\text{C}$.

2.2.2 Glass beads amination

In a 100-mL round-bottomed flask, 25 g of glass beads in 50 mL of 1 M aqueous NaOH and boiled for 1 h. Then, they were diluted with 50 mL of ultrapure water and filtered on a 0.22 μm nylon membrane. The glass beads were washed with 100 mL of 1 M aqueous HCl and with ultrapure water till neutrality. Then they were rinsed twice with acetone and dried at $60\text{ }^{\circ}\text{C}$ overnight.

The dried glass beads were transferred in a 1-L round-bottomed flask and dispersed in 50 mL of toluene, removing water by azeotropic distillation. Then, the flask was cooled to room temperature, 10 mL of APTMS were added, and the mixture let to react overnight. The glass beads were filtered on a 0.22 μm nylon membrane and washed with 3x50 mL of toluene.

To end-cap the residual silanols, the glass beads were transferred in a 250-mL round-bottomed flask and dispersed in 50 mL of toluene, removing water by azeotropic distillation. Then, the flask was cooled to room temperature, 1 mL of HMDS was added to the dispersion and the mixture let to react overnight. The

end-capped glass beads, named “short-chain beads” (SC-beads) were filtered on a 0.22 μm nylon membrane, rinsed twice with acetone and dried at 60 $^{\circ}\text{C}$ overnight. After silanization, the amino groups available on the silanized glass beads surface were determined by Kaiser’s method [11] as 1,1 $\mu\text{mol/g}$.

To introduce the glutaraldehyde-based spacer arm, 10 g of SC-glass beads were transferred in a 25-mL glass vial, dispersed in 10 mL of a freshly prepared 5% (v/v) glutaraldehyde solution in phosphate buffer (10 mM, pH 7.4) and incubated at 25 $^{\circ}\text{C}$ for 2 h. Then, 0.5 mL of freshly distilled ethylenediamine was added and the flask was incubated at 25 $^{\circ}\text{C}$ for 2 hours. The pH of the mixture was adjusted to pH 10, 20 mg of sodium borohydride were added and after 1 h the glass beads, named “long-chain beads” (LC-beads) were filtered on a 0.22 μm nylon membrane, washed with ultrapure water, rinsed twice with acetone and dried at 60 $^{\circ}\text{C}$ overnight.

2.2.3 Template immobilization

In 25-mL glass vials 20 mg of ciprofloxacin (0.06 mmol) were dissolved in 20 mL of MES buffer (10 mM, pH 4.7), 104 mg of NHS (0.9 mmol) and 140 mg of EDC (0.6 mmol) were added and the solutions incubated at 4 $^{\circ}\text{C}$ for 60 min. Then, they were transferred in 100-mL flasks containing 10 g of aminated glass beads (SC or LC). The suspensions were incubated at room temperature overnight, filtered on a 0.22 μm nylon membrane, washed with ultrapure water, rinsed twice with acetone, dried under vacuum at room temperature and stored in the dark at 4 $^{\circ}\text{C}$.

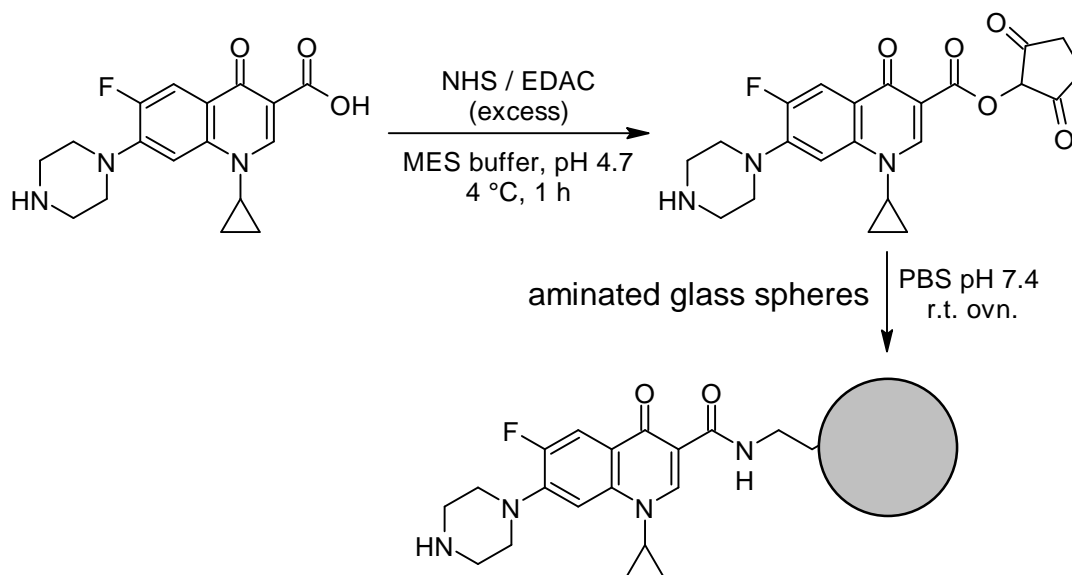


Figure 2-1 - Covalent conjugation of ciprofloxacin on aminated glass beads

2.2.4 Synthesis of nanoMIPs

The polymerization mixtures were prepared in according with the literature [1], with minor modifications and adjusting the dilution of monomers to avoid formation of unwanted lumps of polymer.

For nanoMIPs prepared in acetonitrile (acnSC-MIP and acnLC-MIP), 0.946 mL of MAA (11.15 mmol), 1.027 mL of EDMA (5.45 mmol), 1.019 mL of TRIM (3.19 mmol) and 50 mg of AIBN (0.30 mmol) were dissolved in 20 mL of acetonitrile. Then, 5 mL of mixture were added to 25-mL polypropylene SPE cartridges containing 2.5 g of SC- or LC-glass beads. The cartridges were purged with nitrogen for 5 min, sealed and left to polymerize at 60 °C for 1 h in a roller-equipped incubator. The supernatant was drained by vacuum aspiration, the dry cartridges were cooled to 4 °C and polymerization by-products and low-affinity nanoMIPs were washed with 5x2 mL of ice-cold acetonitrile. High affinity nanoMIPs were collected by eluting the cartridges with 5x2 mL of methanol - acetic acid 9+1 (v/v). The eluate was evaporated in a rotovap, weighted, and stored at 4 °C.

For nanoMIPs prepared in water (wSC-MIP and wLC-MIP), 20 mg of NIPAm (0.177 mmol), 33 mg of TBAm (0.259 mmol, previously dissolved in 1 mL of ethanol), 11 µL of AA (0.160 mmol) and 1 mg of BIS (0.0065 mmol) were dissolved in 50 mL of ultrapure water. Then, 5 mL of mixture were added to 25-mL polypropylene SPE cartridges containing 2.5 g of SC- or LC-glass beads. The cartridges were purged with nitrogen for 5 min, 3 µL of TEMED and 100 µL of 30 mg mL⁻¹ aqueous solution of APS were added and the polymerization was carried out at room temperature for 1 h in a roller-equipped incubator. The supernatant was drained by vacuum aspiration, the dry cartridges were cooled to 4 °C and polymerization by-products and low-affinity nanoMIPs were washed with 5x2 mL of ice-cold water. High affinity nanoMIPs were collected by eluting the cartridges with 5x2 mL of hot water. The eluate was lyophilized, weighted, and stored at 4 °C.

Not-imprinted polymers (NIPs) were prepared by precipitation polymerization in the same experimental conditions in terms of composition of the polymerization mixture, quantity of solvent and polymerization time, but without the presence of functionalized glass beads. After the polymerization, the slightly opalescent solution was filtered on 0.22 µm nylon membranes to eliminate larger polymers, dried (synthesis in acetonitrile) or lyophilized (synthesis in water), weighted, and stored at 4 °C.

2.2.5 Coupling of nanoMIPs to glass beads

In 4-mL glass vials 1 mg of nanoMIPs were dissolved under sonication in 1 mL of MES buffer (50 mM, pH 4.7), 8 mg of NHS (0.069 mmol) and 21.5 mg of EDC (0.138 mmol) were added and the solutions incubated at room temperature for 60 min. Then, they were transferred in 10-mL flasks containing 1 g of LC-glass beads. The suspensions were incubated at room temperature overnight, filtered on 0.22

μm nylon membranes, washed with ultrapure water, rinsed twice with acetone, dried under vacuum at room temperature and stored in the dark at 4 °C.

2.2.6 HPLC method

Reverse phase HPLC analysis was used for fluoroquinolones determination. The HPLC apparatus (Merck-Hitachi, Milan, Italy) was a LaChrom Elite system composed of a programmable binary pump L-2130, an auto-sampler L-2200, a fluorescence detector L-2480, provided with EZChrom Elite software for the instrumental programming, data acquisition and data processing. The column used was a 100 mm \times 4.6 mm Chromolith RP-18 (Merck, Milan, Italy). The mobile phase was water/acetonitrile 85+15, formic acid 0.5% (v/v). Elution was performed in isocratic conditions at a flow rate of 0.7 mL/min. The sample volume injected was 5 μL , and the fluorescence wavelength were $\lambda_{\text{ex}}=280/\lambda_{\text{em}}=440$ nm. Ciprofloxacin solutions between 25 and 400 ng/mL were prepared in the eluent immediately before use. The solutions were analyzed in triplicate and mean peak areas were plotted against ciprofloxacin concentration. The calibration plot was drawn by using a weighted linear regression (weight = 1/conc).

2.2.7 Determination of binding properties

To measure binding isotherms, about 40 mg of glass beads supporting nanoMIPs were exactly weighed in 4 mL flat bottom amber glass vials. Then, 1.0 mL of solutions containing increasing amounts of ciprofloxacin ranging from 25 to 400 ng was added. The vials were incubated for 2 hours at room temperature under continuous agitation on a horizontal rocking table. Then, the solutions were filtered on 0.22 μm nylon membranes and the free amounts of ciprofloxacin were measured by HPLC analysis. Each experimental point was assessed as the average of two repeated measures.

To measure binding kinetics, about 40 mg of glass beads supporting nanoMIPs were exactly weighed in 4 mL flat bottom amber glass vials. Then, 1.0 mL of solutions containing 50 ng of ciprofloxacin were added and the vials were incubated for time intervals between 0.5 and 8 minutes at room temperature under continuous agitation on a horizontal rocking table. Then, the solutions were immediately filtered on 0.22 μm nylon membranes, and the free amounts of ciprofloxacin were measured by HPLC analysis. Each experimental point was assessed as the average of two repeated measures.

Binding parameters were calculated by using SigmaPlot 12 (Systat Software Inc., Richmond, CA, USA). Non-linear least square fitting was applied to the averaged experimental data. Binding isotherm parameters were calculated by using a Langmuir binding isotherm model.

Binding kinetics parameters were calculated by using a 1st order kinetic model:

$$B = B_{eq}[1 - \exp(-k_{ass}t)]$$

where B is the ligand bond to the nanoMIP at time t, B_{eq} the ligand bond to the polymer at equilibrium and k_{ass} the association kinetic constant.

To assure robust results, weighted (1/y) Pearson VII limit minimization was chosen as the minimization method. To avoid being trapped in local minima, which would give incorrect results, minimizations were carried out several times by using different initial guess values for the binding parameters.

2.3 RESULTS AND DISCUSSIONS

2.3.1 Size and dimension of the nanoparticles

Under all the experimental conditions considered, the solid-phase synthesis produced nanoMIPs fully soluble in water, resulting in transparent and colourless solutions, without any perceivable turbidity. Yields calculated respect to the amount of monomers in the polymerization mixtures were: 5.4 mg (2.5%) for acnLC-MIP, 5.0 mg (2.3%) for acnSC-MIP, 1.9 mg (29%) for wLC-MIP, and 1.5 mg (23%) for wSC-MIP. Dynamic light scattering measurements performed on nanoMIPs are reported in Figure 2-2. They show particles with diameters on the order of magnitude of hundreds of nanometres (acnLC-MIP: 166 ± 87 , acnSC-MIP: 147 ± 96 , wLC-MIP: 255 ± 147 , wSC-MIP: 198 ± 73).

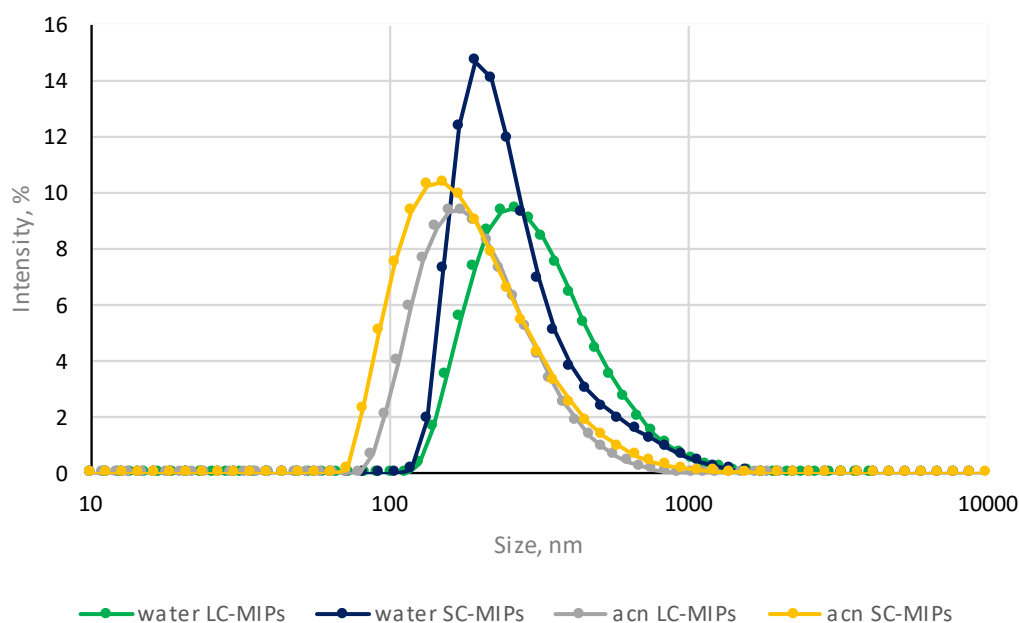


Figure 2-2 - DLS of the four prepared nanoMIPs

2.3.2 Binding properties

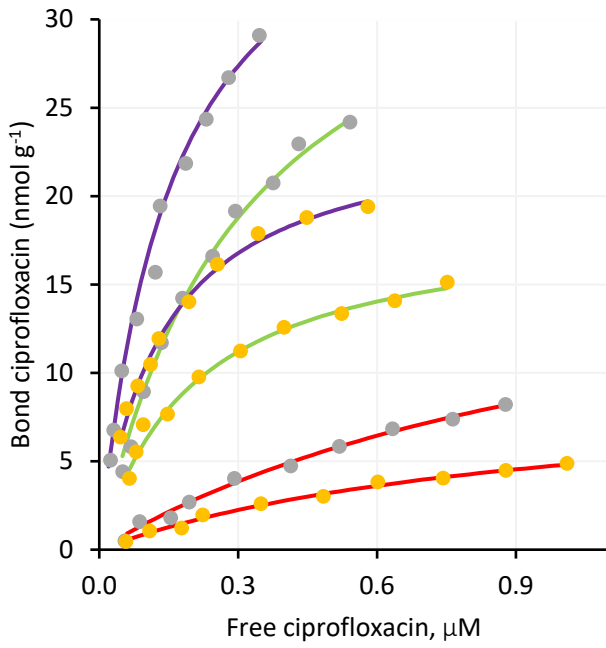
As the binding properties of nanoMIPs towards ciprofloxacin can be obtained from the analysis of their equilibrium binding isotherms, an efficient separation between free and bound ligand is mandatory. So, we had to devise an experimental approach that made this separation simple and fast, as slow methods like ultrafiltration or dialysis did not represent a viable way. We have therefore chosen to support the nanoMIPs on the same glass beads used for their synthesis in order to easily separate by filtration the grafted beads – carrying the bound ligand – from the solution which contains the free ligand.

Preliminary experiments showed that bare glass beads, HDMS-silanized beads, and beads functionalized with a spacer arm based on aminated glutaraldehyde (LC-beads) were unable to bind ciprofloxacin in an aqueous medium in a pH range between 4 and 8, while LC-beads grafted with NIPs showed a limited binding, with calculated equilibrium binding constants in the order of magnitude of 10^4 M^{-1} at pH 6 (synthesis in water: $K_{\text{eq}} = 2.3 \pm 1.1 \times 10^4 \text{ M}^{-1}$; synthesis in acetonitrile: $K_{\text{eq}} = 8.9 \pm 1.1 \times 10^4 \text{ M}^{-1}$).

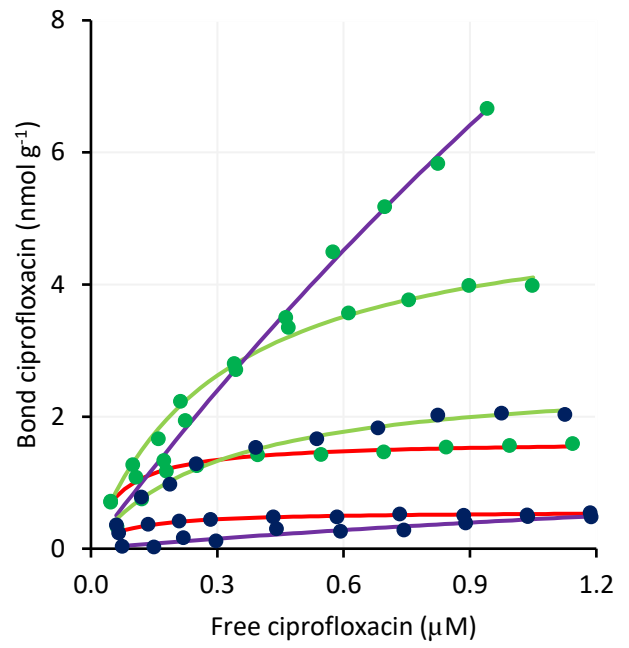
As seen in the introduction, it is obviously not possible to prepare a “nanoNIP” strictly following the solid-phase polymerization. In this work we have chosen to use NIPs prepared by precipitation polymerization with the same formulation used for the preparation of nanoMIPs. In the literature there are examples of MIPs which show unexpected molecular recognition properties towards molecules completely unrelated to the template [12-14]. For precaution, on the assumption that different polymerization methods have only limited effects on the binding properties of NIPs [15-16]. Therefore, it is plausible that whatever observed absorption of ciprofloxacin by the grafted beads is attributable mainly to the interaction of the antibiotic molecules with nanoMIPs, thus excluding the presence of any other non-specific binding.

The binding parameters obtained from binding isotherm and association kinetics plots (Figures 2-3 a-d) are reported in Tables 2-2 and 2-3. They confirm the versatility of the solid-phase synthesis approach as, regardless of the polymerization conditions, nanoMIPs strongly bind ciprofloxacin in buffered water, with equilibrium binding constants (K_{eq}) ranging from 10^5 to 10^7 M^{-1} . It is noteworthy that these values are about 100-1000 times higher than those reported in the literature for ciprofloxacin-imprinted polymers prepared by bulk polymerization [17-18], and they approach the average affinity values reported in the literature for natural antibodies directed towards small organic molecules [19]. The increased affinity for ciprofloxacin can be explained on the basis that the solid-phase polymerization technique allows to easily separate low affinity nanoMIPs from higher affinity ones by simply washing the glass beads once the polymerization is finished.

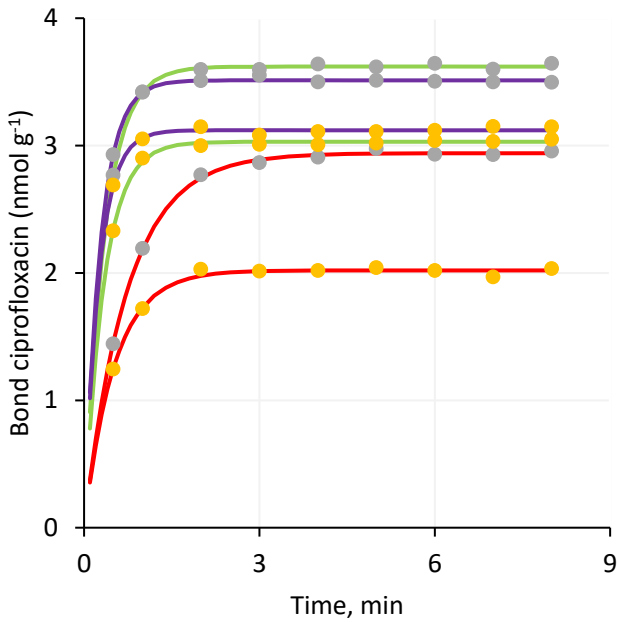
Effect of different experimental conditions on the binding abilities of ciprofloxacin nanoMIPs



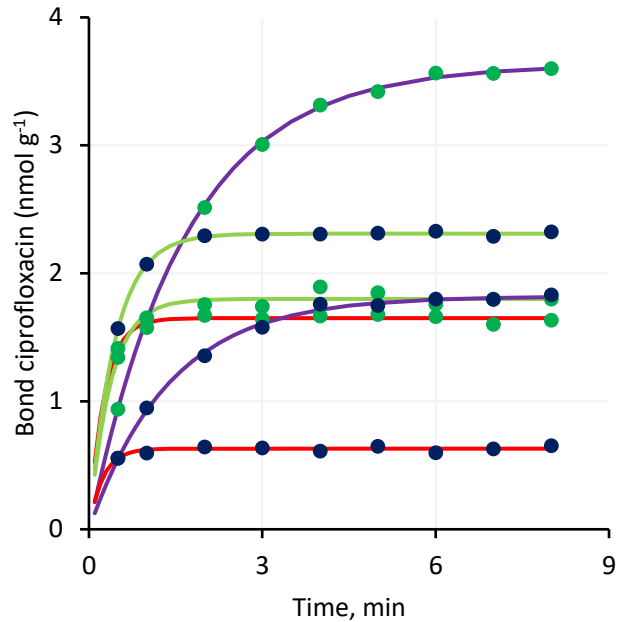
A



B



C



D

Figure 2-1 – Plot of the isotherms and kinetics of all the experimental conditions. To simplify it is adopted an unify color code for the MIPs and the pH. a) binding isotherm plots for nanoMIPs prepared in a) acetonitrile and b) water, and association kinetics plots for nanoMIPs prepared in c) acetonitrile and d) water.

The dot identifies the type of nanoMIP, and the code is:

YELLOW: acn LC-MIP, **GREY:** acn SC-MIP, **GREEN:** w LC-MIP, **BLUE:** w SC-MIP

The line identifies the buffer pH of the rebinding experiment, and the code is:

RED LINE: pH 4, **GREEN LINE:** pH 6, **PURPLE LINE:** pH 8

Table 2-2 - calculated binding equilibrium parameters (\pm standard error) for ciprofloxacin measured on nanoMIPs at pH 4, 6, and 8.

polymer	buffer pH	K_{eq} , $\times 10^{-6} M^{-1}$	B_{max} , nmol/g
acn LC-MIP	4	0.82 ± 0.15	2.94 ± 0.01
	6	3.20 ± 0.35	3.62 ± 0.01
	8	6.35 ± 0.83	3.51 ± 0.01
acn SC-MIP	4	1.05 ± 0.17	2.02 ± 0.01
	6	4.91 ± 0.52	3.03 ± 0.01
	8	7.49 ± 0.38	3.12 ± 0.09
w LC-MIP	4	15.40 ± 1.26	1.65 ± 0.01
	6	3.25 ± 0.24	5.31 ± 0.02
	8	0.21 ± 0.07	40.2 ± 0.05
w SC-MIP	4	12.16 ± 1.23	0.63 ± 0.01
	6	3.33 ± 0.31	2.31 ± 0.00
	8	0.27 ± 0.18	1.82 ± 0.01

Table 2-3 - Calculated association and dissociation rate parameters (\pm standard error) for ciprofloxacin measured on nanoMIPs at pH 4, 6, and 8.

polymer	buffer pH	k_{ass} , $\times 10^{-6} M^{-1} min^{-1}$	k_{dis} , min^{-1}
acn LC-MIP	4	1.36 ± 0.21	1.66 ± 0.41
	6	2.89 ± 0.44	0.90 ± 0.17
	8	3.60 ± 0.55	0.57 ± 0.11
acn SC-MIP	4	1.93 ± 0.60	1.84 ± 0.64
	6	2.97 ± 0.52	0.61 ± 0.12
	8	3.94 ± 0.11	0.53 ± 0.03
w LC-MIP	4	3.81 ± 0.23	0.25 ± 0.03
	6	2.70 ± 0.20	0.83 ± 0.09
	8	0.60 ± 0.08	2.83 ± 1.01
w SC-MIP	4	4.24 ± 0.54	0.35 ± 0.06
	6	2.26 ± 0.29	0.68 ± 0.11
	8	0.71 ± 0.20	2.62 ± 1.87

Equilibrium binding constants (K_{eq}) can be dissected into the association (k_{ass}) and dissociation (k_{dis}) kinetic rate constants, such that $K_{eq}=k_{ass}/k_{dis}$. It may therefore be interesting to examine the values of these rate constants in the case of nanoMIPs. As reported in figure 2-4, it is possible to observe a marked inverse proportionality between the values of k_{ass} and k_{dis} , where the values of k_{dis} decreases compared to the values of k_{ass} .

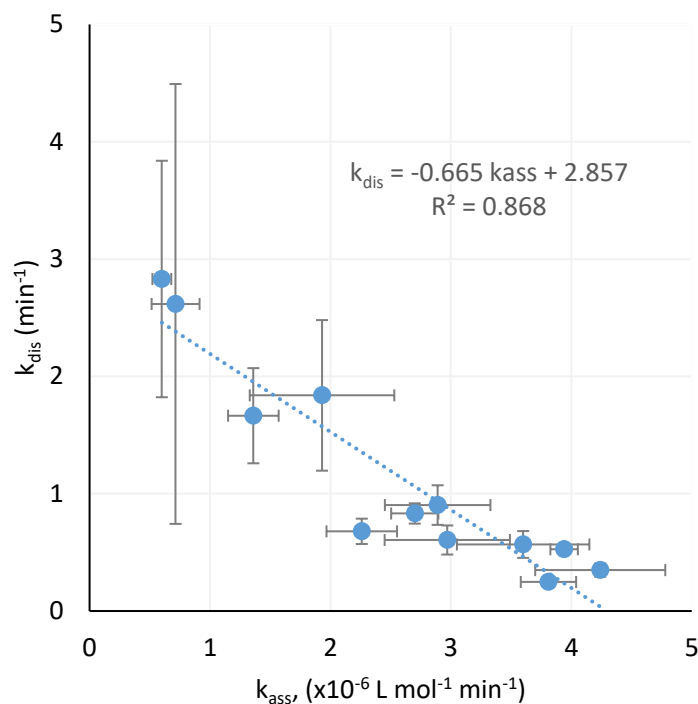


Figure 2-4 – Plot of the constants of dissociation k_{dis} vs constants of association k_{ass} . Error bars indicate 1 std. error unit

It follows that the resulting value of K_{eq} depends simultaneously on both the association and dissociation rate constants. The k_{ass} values are in the order of magnitude of $10^6 \text{ M}^{-1} \text{ min}^{-1}$ (0.60-4.24), comparable to those reported in the literature for antibodies directed towards organic molecules (10^6 - $10^7 \text{ M}^{-1} \text{ min}^{-1}$) [20]. This is not surprising, as it means that ciprofloxacin associates to the binding sites with kinetic rates comparable to natural antibodies, indicating the same diffusion-controlled process. On the contrary, nanoMIPs dissociate faster than natural antibodies, with k_{dis} values located in a range from 0.07 to 1.26 min^{-1} , markedly differing from the average value of 0.01-0.1 min^{-1} reported in the literature for natural antibodies [20].

2.3.3 Effect of spacer arm on ciprofloxacin binding

In analogy with the solid-phase peptide synthesis techniques [21], the presence/absence of a spacer arm between the surface of the glass beads and the covalently grafted template may influence the growth of the nanoMIP structure through steric hindrance effects. For this reason, we decided to covalently bind ciprofloxacin to aminated glass beads provided or not with a glutaraldehyde-based spacer arm ("long chain" / "short chain" beads). Concentrated aqueous solutions of glutaraldehyde are known to spontaneously polymerize to form mixtures of linear polymers of varying length [22]. Thus, glutaraldehyde-grafted glass beads ensure that the template is placed sufficiently far from the glass surface to minimize steric hindrance effects.

The comparison of equilibrium binding constants for pairs of nanoMIPs synthesized onto SC- or LC-beads shows small but systematic differences. NanoMIPs prepared in acetonitrile onto LC-beads (acnLC-MIP) have less affinity than nanoMIPs prepared in acetonitrile onto SC-beads (acnSC-MIP), while nanoMIPs prepared in water onto LC-beads (wLC-MIP) have greater affinity than nanoMIPs prepared in water onto SC-beads (wSC-MIP). However, a more in-depth analysis that takes into account the uncertainty on the calculated value of the constants shows no statistically relevant differences (t-test: $\alpha=0.05$, $n=10$, $t=0.13-1.72$) between pairs. Therefore, it is not possible to say with certainty that the presence of a spacer arm on the glass beads has an influence on the affinity of the resulting nanoMIPs. The same can be observed comparing the association rate constants of nanoMIPs synthesized onto SC- or LC-beads, as no statistically relevant differences (t-test: $\alpha=0.05$, $n=8$, $t=0.24-2.02$) between pairs can be observed. It indicates that the presence of a spacer arm on the glass beads has not an influence on the velocity of association of the resulting nanoMIPs.

On the contrary, the comparison of binding site density (B_{\max}) for pairs of nanoMIPs synthesized onto SC- or LC-beads shows large and systematic differences confirmed by statistical analysis (t-test: $\alpha=0.05$, $n=10$, $t=2.46-25.25$). NanoMIPs prepared in acetonitrile or water onto LC-beads (acnLC-MIP, wLC-MIP) have higher binding site density than nanoMIPs prepared in acetonitrile or water onto SC-beads (acnSC-MIP, wSC-MIP). The grafting protocol on glass beads is identical for all the nanoMIPs considered, so it is reasonable to assume that the quantity of nanoMIPs grafted is the same. Consequently, different B_{\max} values must depend on the experimental conditions of nanoMIP preparation. Since it does not seem to be a significant difference between nanoMIP prepared in water and acetonitrile (see section 2.3.4), it can be concluded that it is the presence of the spacer arm to control the density of the binding sites, probably through a steric hindrance effect between the growing polymer and the glass surface.

2.3.4 Effect of polymerization conditions on ciprofloxacin binding

As stated in the introduction, nanoMIPs can be obtained by solid-phase synthesis using very different polymerization mixtures. Polymerization in aqueous environment typically involves the use of polar functional monomers, N,N'-methylene-bis-acrylamide as a cross-linker and ammonium persulphate as a radical initiator. On the contrary, polymerization in an organic environment – typically acetonitrile – involves the use of less polar functional monomers, using ethylene dimethacrylate or trimethylolpropane trimethacrylate as cross-linkers and radical initiators such as AIBN or RAFT agents. It is therefore possible that nanoMIPs produced from significantly different polymerization mixtures can exhibit different binding properties towards the same ligand.

The comparison of binding parameters for nanoMIPs synthesized in acetonitrile (acnLC-MIP/acnSC-MIP) or water (wLC-MIP/wSC-MIP) shows a strong dependence from the pH of the rebinding buffer. This dependence can be traced back to the solvent in which the nanoMIPs are prepared and the protonation state of template and functional monomers. In fact, in both the polymerization mixtures it is present a pH-sensitive functional monomer (methacrylic acid in acetonitrile-based mixtures, acrylic acid in water-based mixtures) and ciprofloxacin presents two substituents subject to acid-base equilibria: a secondary nitrogen on the piperazinyll ring ($pK_a=8.74$) and a carboxylic group on the quinolone structure ($pK_a=6.09$) [23].

About equilibrium binding constants, as reported in Figure 2-5, when the pH of the buffer increases, the values are decreasing for nanoMIPs prepared in water, while they increase for those prepared in acetonitrile. Concerning the first one, the concentration of acrylic acid is 3.2 mM, corresponding to a calculated pH of about 3.4. In these conditions, the protonated form of the acid prevails, ruling out ionic interactions with the protonated secondary nitrogen but not hydrogen bond-based interactions with the grafted template. Thus, when nanoMIPs prepared in water rebind ciprofloxacin, binding is strongest at pH 4, where carboxyls in the polymer structure are fully protonated and hydrogen bonding is possible, but it decreases at higher pHs, where carboxyls deprotonate progressively, losing the ability to establish hydrogen bonds.

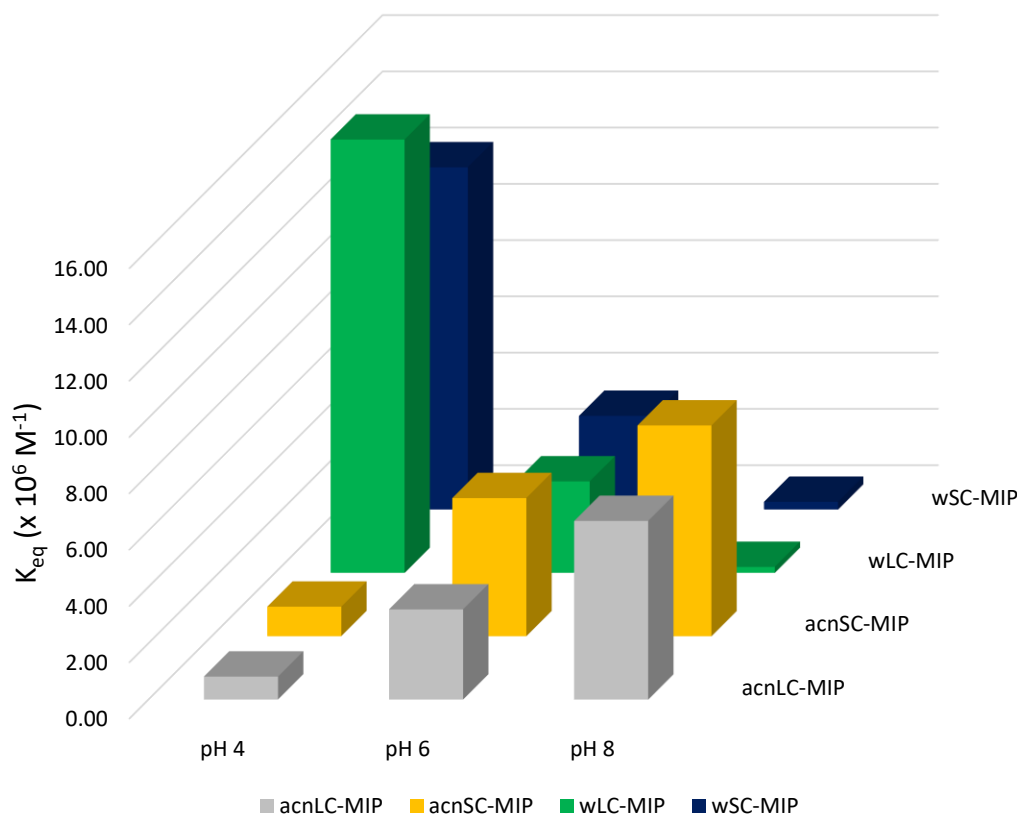


Figure 2-5 - Effect of buffer pH on the equilibrium binding constants (K_{eq})

Concerning the synthesis in acetonitrile, grafted template and methacrylic acid are in their neutral forms, but an ion pair could form anyway between the acid and the secondary nitrogen. Thus, when nanoMIPs prepared in acetonitrile rebind ciprofloxacin, an acidic buffer suppresses the ion pair interaction (methacrylic acid is protonated and neutral, secondary nitrogen on ciprofloxacin is positively charged), while neutral or basic buffers stabilizes the ion pair interaction (methacrylic acid is deprotonated and negatively charged, secondary nitrogen on ciprofloxacin is yet positively charged), thus increasing the binding affinity.

About the association rate constants, as reported in Figure 2-6, the values show the same trend as the equilibrium binding constants, decreasing when pH increases in the case of nanoMIPs prepared in water, and increasing when pH increases in the case of nanoMIPs prepared in acetonitrile. These trends can be explained in the light of what has been said in the case of the equilibrium constant: nanoMIPs show an increasing loss of binding ability due to the progressive deprotonation of polymeric carboxyls (nanoMIPs prepared in water) or the suppression of ion-pairs (nanoMIPs prepared in acetonitrile), causing a slowing of the association and an acceleration of the dissociation processes. It is presumably due to the progressive deformation of the binding site, which becomes less tight and therefore less able to bind and retain the ciprofloxacin molecule.

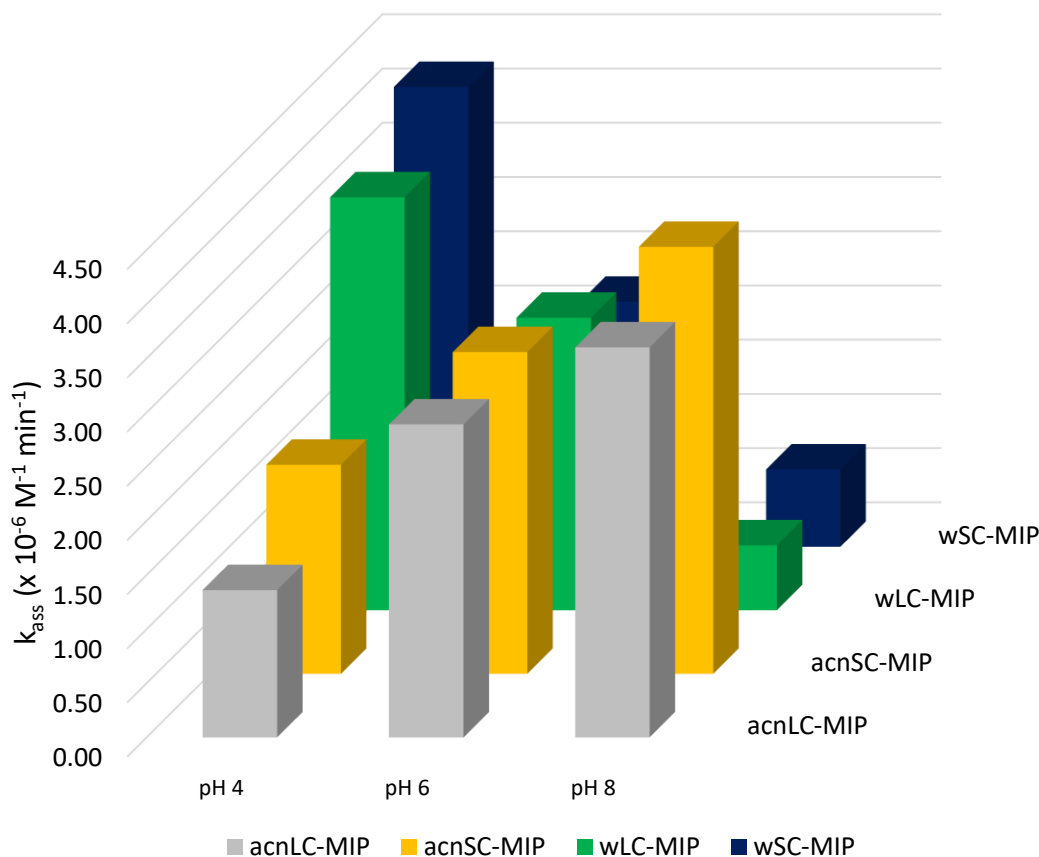


Figure 2-6 - Effect of buffer pH on the association rate binding constants (K_{ass})

The effect of the formulation of the polymerization mixture on the density of binding sites is reported in Figure 2-7.

A statistically significant increase in values passing from pH 4 to pH 6 is observed for all nanoMIPs (t-test: $\alpha=0.05$, $n=10$, $t=3.64-15.5$), while a further increase from pH 6 to pH 8 – although observable – is not significant (t-test: $\alpha=0.05$, $n=10$, $t=0.25-2.08$). This increase therefore occurs when the nanoMIPs are in a non-acidic environment. A possible explanation consists in the establishment of electrostatic repulsion between deprotonated carboxyls, which could cause an expansion of the polymer structure, with consequent greater accessibility of binding sites otherwise hidden.

Effect of different experimental conditions on the binding abilities of ciprofloxacin nanoMIPs

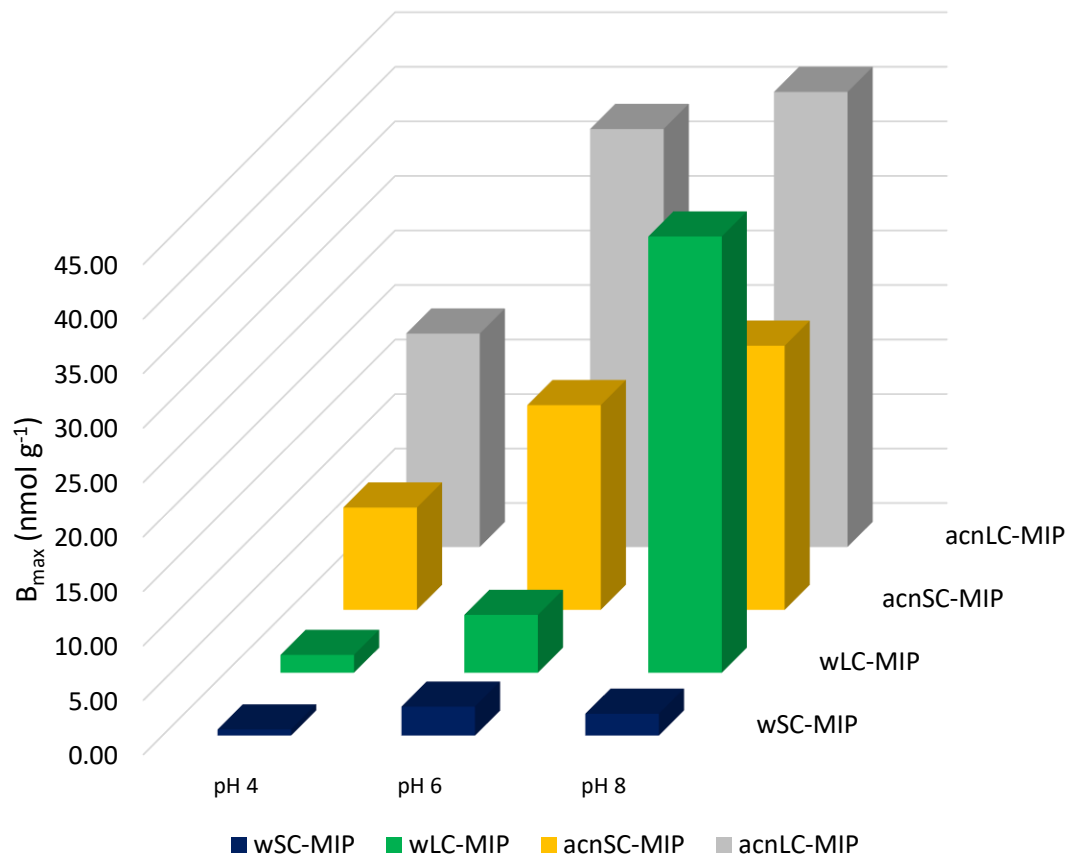


Figure 2-7 - Effect of buffer pH on the binding site density (B_{max})

2.4 CONCLUSIONS

The experimental results reported here confirm that the solid phase synthesis of molecularly imprinted polymers is a very flexible approach, where the experimental conditions such the nature of the polymerization mixture (N,N'-methylene-bis-acrylamide vs. ethylene dimethacrylate / trimethylolpropane trimethacrylate) or the polymerization environment (water vs. acetonitrile) are decisive in defining the binding properties of the resulting nanoMIPs through different non-covalent interactions that can be established between the polymer in formation and the immobilized template during the polymerization process. Moreover, these results show also that the solid phase synthesis approach is a powerful technique to easily prepare nanoMIPs fully compatible with the aqueous environment, with reduced non specific binding ($<10^3 \text{ M}^{-1}$), high equilibrium binding constants ($10^5\text{-}10^7 \text{ M}^{-1}$) and fast association rate constants ($\approx 10^6 \text{ M}^{-1}\text{min}^{-1}$), values which are comparable to those of natural antibodies.

The water polymerization is not secondary than the acetonitrile one, and nanoMIPs with the same properties or even better were obtained. We found out that the spacer arm length has more significant effect on the binding site density than on the binding constants. The latter parameter was not further investigated. We also shed light on the importance of the pH of the rebinding experiment environment a crucial parameter – not involved in the imprinting process – that it has an enormous influence on the binding properties. A study that does not consider this parameter could turn into a failure even if in the presence of a good nanoMIP.

In conclusion, if compared to traditional imprinted polymers, the enhanced binding properties of nanoMIPs prepared by solid-phase synthesis make these nanomaterials very promising recognition elements for applications in fields where aqueous compatibility, low non specific binding, high affinity and fast binding kinetics are basic requirements.

2.5 BIBLIOGRAPHY

- [1] F. Canfarotta, A. Poma, A. Guerreiro, S.A. Piletsky. Solid-phase synthesis of molecularly imprinted nanoparticles. *Nat. Protocols*, **2016**, *11*, 443-455, doi: 10.1038/nprot.2016.030.
- [2] D. López-Puertollano, T. Cowen, A. García-Cruz, E. Piletska, A. Abad-Somovilla, A. Abad-Fuentes, S. Piletsky. Study of epitope imprinting for small templates: preparation of nanoMIPs for ochratoxin A. *ChemNanoMat*, **2019**, *5*, 651–657, doi:10.1002/cnma.201900050.
- [3] A. Poma, A. Guerreiro, M.J. Whitcombe, E. Piletska, A.P.F. Turner, S.A. Piletsky. Solid-phase synthesis of molecularly imprinted polymer nanoparticles with a reusable template – “plastic antibodies”. *Adv. Funct. Mater*, **2013**, *23*, 2821-2827, doi: 10.1002/adfm.201202397.
- [4] E. Moczko, A. Guerreiro, E. Piletska, S. Piletsky. PEG-stabilized core–shell surface-imprinted nanoparticles. *Langmuir*, **2013**, *29*, 9891-9896, doi: 10.1021/la401891f.
- [5] Z. Altintas, A. Guerreiro, S.A. Piletsky, I.E. Tothill. NanoMIP based optical sensor for pharmaceuticals monitoring. *Sens Actuat B*, **2015**, *213*, 305-313: doi: 10.1016/j.snb.2015.02.043.
- [6] Z. Altintas. Surface plasmon resonance-based sensor for the detection of glycopeptide antibiotics in milk using rationally designed nanoMIPs. *Sci Reports*, **2018**, *8*, 11222, doi: 10.1038/s41598-018-29585-2.
- [7] Y. Yoshimi, D. Oino, H. Ohira, H. Muguruma, E. Moczko, S.A. Piletsky. Size of heparin-imprinted nanoparticles reflects the matched interactions with the target molecule. *Sensors*, **2019**, *19*, 2415, doi: 10.3390/s19102415.
- [8] M. Roberto Gama, C.B. Grespan Bottoli. Molecularly imprinted polymers for bioanalytical sample preparation. *J Chromatogr B*, **2017**, *1043*, 107-121, doi: 10.1016/j.jchromb.2016.09.045.
- [9] I.S. Ibarra, J.M. Miranda, I. Perez-Silva, C. Jardineza, G. Islas. Sample treatment based on molecularly imprinted polymers for the analysis of veterinary drugs in food samples: a review. *Anal Methods*, **2020**, *12*, 2958-2977, doi: 10.1039/d0ay00533a.
- [10] H. Santos, R.O. Martins, D.A. Soares, A.R. Chaves. Molecularly imprinted polymers for miniaturized sample preparation techniques: strategies for

- chromatographic and mass spectrometry methods. *Anal Methods*, **2020**, *12*, doi: 894-911. 10.1039/c9ay02227a.
- [11] E. Poli, V. Chaleix, C. Damia, Z. Hjezi, E. Champion, V. Sol. Efficient quantification of primary amine functions grafted onto apatite ceramics by using two UV-Vis spectrophotometric methods. *Anal Methods*, **2014**, *6*, 9622-9627, doi: 10.1039/c4ay02012j.
- [12] P.D. Martin, T.D. Wilson, I.D. Wilson, G.R. Jones. An unexpected selectivity of a propranolol-derived molecular imprint for tamoxifen. *Analyst*, **2001**, *126*, 757-759, doi: 10.1039/b102424h.
- [13] S.N. Zhou, E.P.C. Lai. N-phenylacrylamide functional polymer with high affinity for Ochratoxin A. *React Funct Polym*, **2004**, *58*, 35-42, doi: 10.1016/j.reactfunctpolym.2003.11.005.
- [14] L. Anfossi, C. Baggiani, P. Baravalle, C. Giovannoli, L. Guzzella, F. Pozzoni. Molecular recognition of the fungicide Carbendazim by a molecular imprinted polymer obtained through a mimic template approach. *Anal Lett*, **2009**, *342*, 807-820, doi: 10.1080/00032710802677183.
- [15] S.A. Mohajeri, G. Karimi, J. Aghamohammadian, M.R. Khansari. Clozapine recognition via molecularly imprinted polymers; bulk polymerization versus precipitation method. *J Appl Polym Sci*, **2011**, *121*, doi: 3590-3595. 10.1002/app.34147.
- [16] N. Phutthawong, M. Pattarawarapan. Synthesis of highly selective spherical caffeine imprinted polymers via ultrasound-assisted precipitation polymerization. *J Appl Polym Sci*, **2013**, *128*, 3893-3899, doi: 10.1002/APP.38596.
- [17] A.H. Kamel, W.H. Mahmouda, M.S. Mostafa. Biomimetic ciprofloxacin sensors made of molecularly imprinted network receptors for potential measurements. *Anal Methods*, **2011**, *3*, 957-964, doi: 10.1039/coay00706d.
- [18] G. Zhu, G. Cheng, P. Wang, W. Li, Y. Wang, J. Fan. Water compatible imprinted polymer prepared in water for selective solid phase extraction and determination of ciprofloxacin in real samples. *Talanta*, **2019**, *200*, 307-315, doi: 10.1016/j.talanta.2019.03.070.
- [19] K.N. Houk, A.G. Leach, S.P. Kim, X. Zhang. Binding affinities of host-guest, protein-ligand, and protein-transition-state complexes. *Angew Chem Int Ed*, **2003**, *42*, 4872-4897, doi: 10.1002/anie.200200565.

- [20] J. Foote, H.N. Eisent. Kinetic and affinity limits on antibodies produced during immune responses. *Proc Natl Acad Sci USA*, **1995**, *92*, 1254-1256, doi: 10.1073/pnas.92.5.1254.
- [21] I. Sucholeiki. Selection of supports for solid-phase organic synthesis. In: W.H. Moos, M.R. Pavia, B.K. Kay, A.D. Ellington (eds). Annual reports in combinatorial chemistry and molecular diversity. **1997**, vol 1, Springer, Dordrecht, doi: 10.1007/978-0-306-46904-6_5.
- [22] P.M. Hardy, A.C. Nicholls, H.N. Rydon. The nature of glutaraldehyde in aqueous solution. *J Chem Soc D*, **1969**, *10*, 565-566, doi: 10.1039/C29690000565.
- [23] K. Tornainen, S. Tammilehto, V. Ulvi. The effect of pH, buffer type and drug concentration on the photodegradation of ciprofloxacin. *Int J Pharm*, **1996**, *132*, 53-61, doi: 10.1016/0378-5173(95)04332-2.

3 AN EXPERIMENTAL DESIGN ON THE MONOMERIC FORMULATION FOR THE WATER SYNTHESIS NANOMIPs

3.1 INTRODUCTION

While the synthesis in organic environment and the monomers used for this have been subject of study in the last forty years, the water synthesis is an almost virgin field. Except some previous applications with the precipitation MIP [1], the water synthesis has become a leading actor with the solid phase synthesis. The previous chapter was investigated on the influence of the spacer arm length and the pH rebinding condition in this environment, without exploring the effect of different monomers or the change in ratio of these. The use of a very uncommon crosslinker like the N,N'-methylene-bis-acrylamide in a so little amount is also a source of questions. Also, it is very important exploring the role on the binding capability of all the used monomers in a multivariate approach. For these purposes, it is possible to investigate several types of monomers, and the molar ratio between them, for each template to individuate the bests. But, in the case of the ciprofloxacin template, there is yet a starting formulation from the previous works. For this, it is possible to focus only on the study of the effect of a modification of the monomeric molar ratio.

3.1.1 Aim of the work and objectives

In the formulation for the water synthesis nanoMIPs for the ciprofloxacin there are four functional monomers [2]: the acrylic acid, with the capability to make hydrogen bonds; the TBAm, with the capability to establish hydrophobic interactions; the NIPAm, that give the thermoresponsive behaviour to the nanoparticles and the BIS that is the crosslinker agent. To explore the effect of each monomer on the binding capability, and the multivariate effect of the combination of these, a two-factor central composite ($d = 2$, $n = 9$) experimental design was employed, by varying the relative quantity of the cross-linker (1–5 mol%) and the H-bond donor/acceptor monomer (acrylic acid, 10–50 mol%) in the polymerization mixtures. It was chosen to keep unchanged the amount of thermoresponsive monomer NIPAm, to maintain constant this behaviour and eliminate a possible change in the amount of recovered nanoMIPs from the synthesis. To choose the relative quantities of monomers, we started from the previously used monomer mixture, and we varied the amount of acrylic acid and BIS in three levels. The quantity of TBAm is dependent from the other two varied monomers. To study the nine nanoMIPs obtained, we evaluated the binding properties including the affinity to the ciprofloxacin and the selectivity to the

levofloxacin. The influence of the monomeric mixtures on these properties was determined through the use of a multilinear regression model.

3.2 EXPERIMENTAL

3.2.1 Materials

Glass beads were Spherglass-2429 70-100 μm average particle size (Potters, UK). Ciprofloxacin was purchased from Supelco (Milan, Italy).

Acrylic acid (AA), 3-(aminopropyl)trimethoxysilane (APTMS), ammonium persulphate (APS), azo-bis-isobutyronitrile (AIBN), 1-ethyl-3-(3-dimethylaminopropyl)carbodiimide (EDC), hexamethyldisilazane (HMDS), N-hydroxysuccinimide (NHS), N-isopropylacrylamide (NIPAm), N,N'-methylene-bis-acrylamide (BIS), morpholinethansulphonic acid (sodium salt, MES), sodium borohydride, N-tert-butylacrylamide (TBAm), N,N,N',N'-tetramethylethylenediamine (TEMED), ciprofloxacin (CPX), levofloxacin (LVX), N,N-dimethylaminopyridine (DMAP), N,N'-diisopropylcarbodiimide (DIC), succinic anhydride were purchased from Sigma-Merck (Milan, Italy).

Solvents and all other chemicals were purchased from Sigma-Merck (Milan, Italy). All the solvents were of HPLC grade, whereas all chemicals were of analytical grade.

The water used was ultra-purified in Purelab Prima System from Elga (Marlow, UK). Polymerisation inhibitors in the monomers were removed by filtration through activated basic alumina.

Antibiotic stock solutions were prepared by dissolving 10 mg of the substance in 25 mL of methanol/acetic acid 95/5 (v/v) then stored in the dark at $-20\text{ }^{\circ}\text{C}$.

3.2.2 Glass beads amination

In a 100-mL round-bottomed flask, 25 g of glass beads in 50 mL of 1 M aqueous NaOH and boiled for 1 h. Then, they were diluted with 50 mL of ultrapure water and filtered on a 0.22 μm nylon membrane. The glass beads were washed with 100 mL of 1 M aqueous HCl and with ultrapure water till neutrality. Then they were rinsed twice with acetone and dried at $60\text{ }^{\circ}\text{C}$ overnight.

The dried glass beads were transferred in a 1-L round-bottomed flask and dispersed in 50 mL of toluene, removing water by azeotropic distillation. Then, the flask was cooled to room temperature, 10 mL of APTMS were added, and the mixture let to react overnight. The glass beads were filtered on a 0.22 μm nylon membrane and washed with 3x50 mL of toluene.

To end-cap the residual silanols, the glass beads were transferred in a 250-mL round-bottomed flask and dispersed in 50 mL of toluene, removing water by azeotropic distillation. Then, the flask was cooled to room temperature, 1 mL of HMDS was added to the dispersion and the mixture let to react overnight. The end-capped glass beads, named "short-chain beads" (SC-beads) were filtered on a 0.22 μm nylon membrane, rinsed twice with acetone and dried at $60\text{ }^{\circ}\text{C}$ overnight.

After silanization, the amino groups available on the silanized glass beads surface were determined by Kaiser's method as 1,1 $\mu\text{mol/g}$.

3.2.3 Synthesis of ciprofloxacin hemisuccinamide

The template molecule, ciprofloxacin hemisuccinamide (Figure 3-1), was synthesized according to a modification of the procedure given by Noël *et al.* [3]. Succinic anhydride (100 mg, 1 mmol) was added to a suspension of CPX (331 mg, 1 mmol) in DMSO (2.0 mL) containing a catalytical amount of DMAP. The reaction mixture was stirred under nitrogen overnight at 95 °C and cooled down to room temperature. The resulting precipitate was filtered, washed successively with water and diethylether, and dried under reduced pressure. The expected hemisuccinamide was isolated as a fluffy white powder (98 mg, yield 75%), deemed pure by MS-HPLC (ESI: m/z 431.1 [MH⁺]).

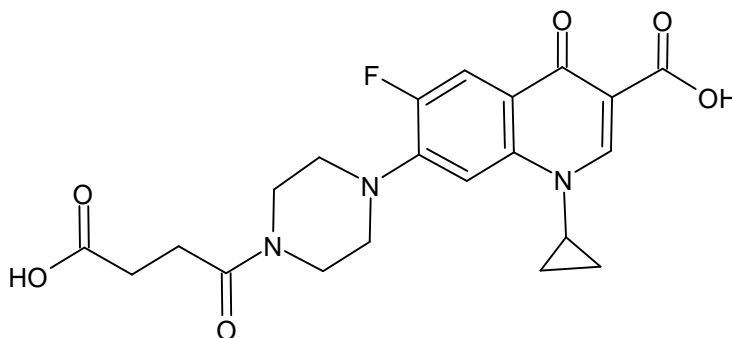


Figure 3-1 - Ciprofloxacin hemisuccinamide

3.2.4 Template immobilization

In 25-mL glass vials 10 mg of hemisuccinade ciprofloxacin (0.231 mmol) were dissolved in 10 mL of DMF, 26.7 mg of NHS (0.232 mmol) and 29.3 mg of DIC (0.232 mmol) were added and the solutions incubated for 60 min. Then, they were transferred in 25-mL flasks containing 5 g of aminated glass beads. The suspensions were incubated at room temperature overnight, filtered on a 0.22 μm nylon membrane, washed with DMF, rinsed twice with acetone, dried under vacuum at room temperature and stored in the dark at 4 °C.

3.2.5 Synthesis of nanoMIPs

For the nanoMIPs synthesized in water, the polymerization mixtures were prepared in according with the literature [4], with minor modifications. Nine pre-polymerization mixture were prepared with the same monomers but in different

molar ratio as reported in Table 3-1. The pre-polymerization mixtures were prepared in 25 mL of ultrapure water by mixing under sonication.

Table 3-1 - Formulation of the nine polymers. For each monomer are reported the molar ratio in the monomer mixtures, the mmol and the mass dissolved in 25 ml of ultrapure water. For the Acrylic acid is reported the volume instead of mass.

Polymer	Bis	AAC	TBA _m	NIPAm	
A	3	50	17	30	%
	0.00975	0.1625	0.05525	0.0975	mmol
	0.0015	11.14	0.0070	0.0110	g or μ l
B	2	40	28	30	%
	0.0065	0.13	0.091	0.0975	mmol
	0.0010	8.91	0.0116	0.0110	g or μ l
C	4	40	26	30	%
	0.013	0.13	0.0845	0.0975	mmol
	0.0020	8.91	0.0107	0.0110	g or μ l
D	1	30	39	30	%
	0.00325	0.0975	0.12675	0.0975	mmol
	0.0005	6.68	0.0161	0.0110	g or μ l
E	3	30	37	30	%
	0.00975	0.0975	0.12025	0.0975	mmol
	0.0015	6.68	0.0153	0.0110	g or μ l
F	5	30	35	30	%
	0.01625	0.0975	0.11375	0.0975	mmol
	0.0025	6.68	0.0145	0.0110	g or μ l
G	2	20	48	30	%
	0.0065	0.065	0.156	0.0975	mmol
	0.0010	4.46	0.0198	0.0110	g or μ l
H	4	20	46	30	%
	0.013	0.065	0.1495	0.0975	mmol
	0.0020	4.46	0.0190	0.0110	g or μ l
I	3	10	57	30	%
	0.00975	0.0325	0.18525	0.0975	mmol
	0.0015	2.23	0.0236	0.0110	g or μ l

Then, 5 mL of mixture was added to 50-mL polypropylene SPE cartridge containing 2.5 g of template functionalized glass beads. The cartridges were purged with nitrogen for 5 min. 3 μ L of TEMED and 100 μ L of 30 mg mL⁻¹ aqueous solution of APS were added and the polymerization was carried out at room temperature for 1 hour in a roller-equipped incubator. The supernatant was drained by vacuum aspiration, the dry cartridges were cooled to 4 °C and polymerization by-products and low-affinity nanoMIPs were washed with 10 \times 2 mL of ice-cold water. High affinity nanoMIPs were collected by eluting the

cartridges at room temperature with 5×3 mL hot water and 5×1 mL of 90% methanol/10% acetic acid v/v. The eluates were purified by gel-filtration in ultrapure water onto a 26 x 250 mm Sephadex G25 column. The nanoMIPs were isolated by centrifugation at 14000 x g, dried by lyophilisation and stored at 4 °C.

3.2.6 Coupling of nanoMIPs to glass beads

In 4-mL glass vials 1 mg of nanoMIPs was dissolved under sonication in 1 mL of MES buffer (50 mM, pH 4.7); 8 mg of NHS (0.069 mmol) and 21.5 mg of EDC (0.138 mmol) were added and the solutions incubated at room temperature for 60 min. Then, they were transferred in 10-mL flasks containing 1 g of amminated glass beads. The suspensions were incubated at room temperature overnight, filtered on 0.22 µm nylon membranes, washed with ultrapure water, rinsed twice with acetone, dried under vacuum at room temperature and stored in the dark at 4 °C.

3.2.7 HPLC method

Reverse phase HPLC analysis was used for fluoroquinolones determination. The HPLC apparatus (Merck-Hitachi, Milan, Italy) was a LaChrom Elite system composed of a programmable binary pump L-2130, an auto-sampler L-2200, a fluorescence detector L-2480, provided with EZChrom Elite software for the instrumental programming, data acquisition and data processing. The column used was a 100 mm × 4.6 mm Chromolith RP-18 (Merck, Milan, Italy). The mobile phase was water/acetonitrile 85+15, formic acid 0.5% (v/v). Elution was performed in isocratic conditions at a flow rate of 0.7 mL/min. The sample volume injected was 5 µL, and the fluorescence wavelength were $\lambda_{\text{ex}}=280/\lambda_{\text{em}}=440$ nm for the ciprofloxacin, and $\lambda_{\text{ex}}=280/\lambda_{\text{em}}=540$ nm for the levofloxacin. Ciprofloxacin solutions between 0.5 and 50 ng/mL were prepared in the eluent immediately before use. The solutions were analyzed twice and mean peak areas were plotted against fluoroquinolone concentration. The calibration plot was drawn by using a weighted linear regression (weight = 1/conc).

3.2.8 Determination of binding properties

To measure binding isotherms, about 40 mg of glass beads supporting nanoMIPs were exactly weighed in 4 mL flat bottom amber glass vials. Then, 1.0 mL of phosphate buffer (20 mM, pH 6) containing increasing amounts of fluoroquinolone ranging from 0.5 to 25 µg was added. The vials were incubated for 2 hours at room temperature under continuous agitation on a horizontal rocking table. Then, the solutions were filtered on 0.22 µm nylon membranes and the free

amounts of ciprofloxacin were measured by HPLC-fluorescence analysis. Each experimental point was assessed as the average of two repeated measures.

Binding parameters were calculated by using SigmaPlot 12 (Systat Software Inc., Richmond, CA, USA). Non-linear least square fitting was applied to the averaged experimental data. Binding isotherm parameters were calculated by using a Langmuir binding isotherm model.

The binding selectivity, α , was calculated as:

$$\alpha = \frac{K_{eq\text{levofloxacin}}}{K_{eq\text{ciprofloxacin}}}$$

where $K_{eq\text{ciprofloxacin}}$ and $K_{eq\text{levofloxacin}}$ are the equilibrium binding constants calculated for ciprofloxacin and levofloxacin, respectively.

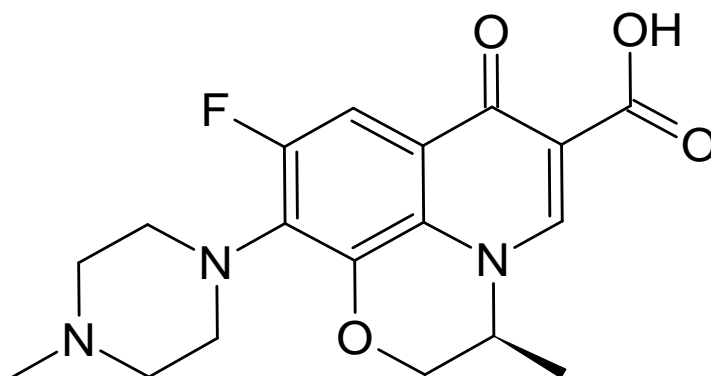


Figure 3-2 - Structure of the levofloxacin

3.3 RESULTS AND DISCUSSIONS

The binding affinities for ciprofloxacin calculated with Langmuirian binding models (the results of which are reported in Table 3-2) were fitted against the molar percentages of AA and TBAm by using a six-parameter polynomial model ($z = a_0 + a_1(\text{BIS}) + a_2(\text{AA}) + a_3(\text{AA} \cdot \text{BIS}) + a_4(\text{BIS})^2 + a_5(\text{AA})^2$). The mathematical levels used for the experimental design elaboration are reported in the Table 3-3. The six-parameters polynomial model was applied for both the substances used in the rebinding experiments: the ciprofloxacin, to calculate the nanoMIP affinity for the template molecule, and the levofloxacin, to evaluate the selectivity of the binding sites for a template-homologue molecule.

Table 3-2 - Binding proprieties values for the ciprofloxacin and the levofloxacin. The values are reported with ± 1 standard deviation.

Polymer	CIPROFLOXACIN		LEVOFLOXACIN		Selectivity
	K_{eq} (10^6 M^{-1})	B_{max} (nmol g^{-1})	K_{eq} (10^6 M^{-1})	B_{max} (nmol g^{-1})	
A	2.05 ± 1.12	8.3 ± 2.1	<0.01	2 ± 5	<0.01
B	2.44 ± 0.68	7.6 ± 1.1	<0.01	2 ± 5	<0.01
C	4.01 ± 0.62	8.8 ± 0.7	<0.01	2 ± 5	<0.01
D	3.99 ± 0.57	5.4 ± 0.3	3.57 ± 1.50	2.73 ± 0.81	0.90
E	1.39 ± 0.27	10.7 ± 1.4	1.15 ± 0.43	5.10 ± 2.80	0.83
F	3.00 ± 0.75	18.8 ± 2.9	5.01 ± 2.85	1.34 ± 0.43	1.67
G	3.08 ± 0.83	9.5 ± 1.4	3.37 ± 1.67	1.98 ± 0.64	1.09
H	0.63 ± 0.76	19.8 ± 20.8	3.09 ± 1.64	2.51 ± 0.90	4.90
I	0.37 ± 0.73	43.8 ± 77.8	2.99 ± 1.63	5.30 ± 2.16	8.08

Table 3-3 - Experimental design levels for the variables

Polymer	Acrylic acid		BIS	
	% mol	exp. design level	% mol	exp. design level
A	50	2	3	0
B	40	1	2	-1
C	40	1	4	1
D	30	0	1	-2
E	30	0	3	0
F	30	0	5	2
G	20	-1	2	-1
H	20	-1	4	1
I	10	-2	3	0

In the figure Figure 3-3 and Table 3-4 are reported the MLR responding surface and the mathematical coefficient for the K_{eq} of the ciprofloxacin. The response surface fits quite well with the experimental design points used, with a r^2 of 0.8164 and a fit standard error of 0.146. As the employed polynomial model provides an interaction term between the independent variables (parameter a_3), the resulting surface shows an obvious saddle shape, with two distinct regions where the binding affinities are higher (low cross-linker amount – low acrylic acid amount and high cross-linker amount – high acrylic acid amount) and an intermediate region with a saddle-centered maximum where the binding affinities are the lowest in condition of high cross-linker amount – low acrylic acid amount. It should be noted that the formulation of the polymerization mixture previously used [1] corresponds to a response surface region characterized by high binding constants. For these reasons, several polymers with very different molar composition were potentially suitable for this characteristic: Polymers C and F on one side, polymers D and G on the opposite.

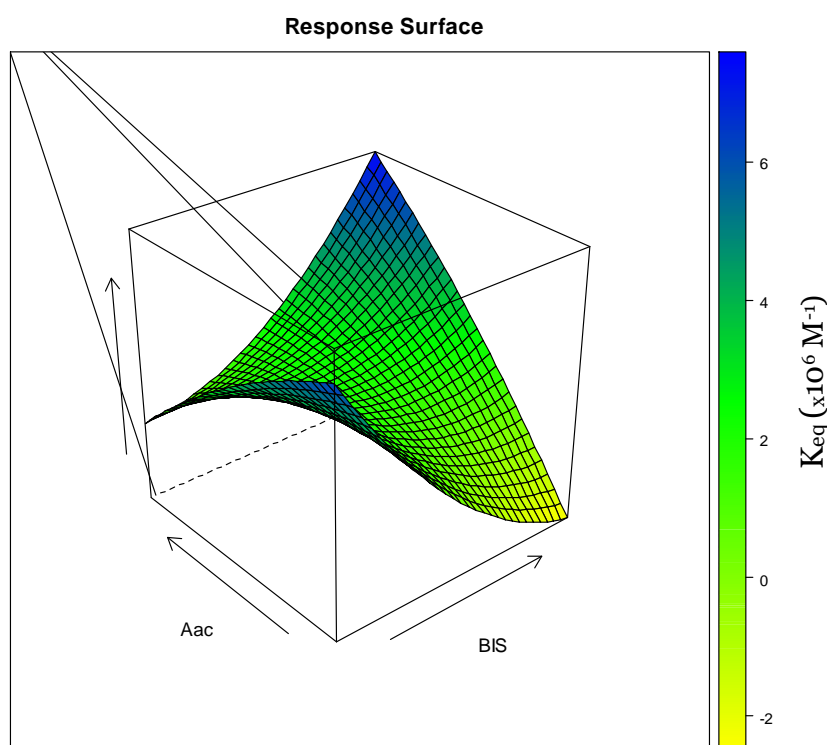


Figure 3-3 - Responding surface of the MLR for the ciprofloxacin bindings K_{eq}

Table 3-4 - Non linear fitting of 6-parameters polynomial model for the two-factor central composite ($d=2, n=9$) experimental design for the ciprofloxacin binding

Parameters	value \pm 1 s.e.
a₀	1.9844 \pm 0.4270
a₁	-0.2383 \pm 0.1654
a₂	0.5083 \pm 0.1654
a₃	1.0050 \pm 0.2864
a₄	0.4148 \pm 0.1601
a₅	-0.1565 \pm 0.1601

The MLR responding surface and the mathematical coefficient for the K_{eq} of the levofloxacin are reported in Figure 3-4 and Table 3-5. The response surface fits worse the experimental design points than the ciprofloxacin, with a r^2 of 0.7357 and a fit standard error of 0.148. The shape is different from the previous, with a half pipe shape. The interaction term between the independent variables is much smaller (0,07 vs 1), and there are high K_{eq} for low acrylic acid amount MIPs and for extreme BIS amount MIPs. Also, for the polymer A, B and C it was very difficult to calculate the binding properties because the binding recognition is very bad, and, in general, the B_{max} for the levofloxacin are much lower than for the ciprofloxacin. The polymers with medium amount of acrylic acid – low cross-linker amount have a very bad selectivity. In general, the area around the polymer C presents high affinity and high selectivity.

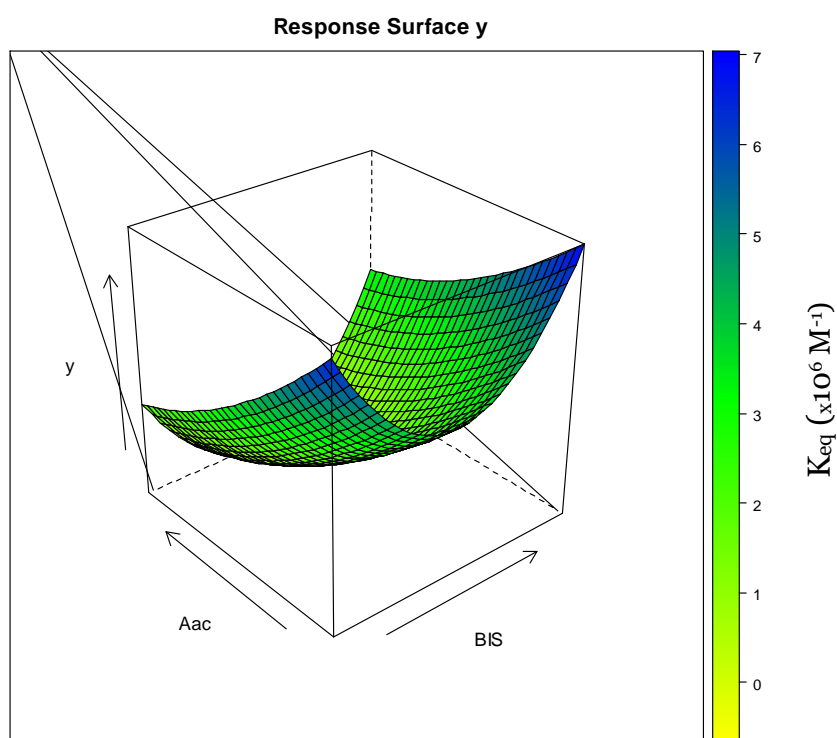


Figure 3-4 - Responding surface of the MLR for the K_{eq} of the levofloxacin

Table 3-5 - Non linear fitting of 6-parameters polynomial model for the two-factor central composite ($d=2, n=9$) experimental design for the levofloxacin binding

Parameters	value \pm 1 s.e.
a₀	0.7922 \pm 0.7170
a₁	0.2167 \pm 0.2777
a₂	-1.0333 \pm 0.2777
a₃	0.0700 \pm 0.4810
a₄	0.8521 \pm 0.2689
a₅	0.1546 \pm 0.2689

3.4 CONCLUSIONS

In this work, it was demonstrated that the optimization of the monomeric mixtures is a crucial step in the development of a good nanoMIP, and also a little modification can produce very different affinity properties. Furthermore, it was demonstrated that the effect of a change in the monomeric ratio is a multivariate phenomenon, and it is impossible to consider a variation of an only single element to improve the binding capability. Also, good experimental conditions to make a nanoMIP were individuated, in particular for the ciprofloxacin. The polymers C and G present excellent affinities for the template molecule (K_{eq} in order of 10^6 M^{-1}) and good selectivity. In general, the synthesis in water environment produces nanoMIPs with good affinity capability in every tried condition.

3.5 BIBLIOGRAPHY

- [1] X. Ding, P.A. Heiden. Recent Developments in molecularly imprinted nanoparticles by surface imprinting techniques. *Macromolecular Materials and Engineering*, **2014**, 299, 268–282, doi: 10.1002/mame.201300160.
- [2] S. Cavalera, M. Chiarello, F. di Nardo, L. Anfossi, C. Baggiani. Effect of experimental conditions on the binding abilities of ciprofloxacin-imprinted nanoparticles prepared by solid-phase synthesis. *Reactive and Functional Polymers*, **2021**, 163, 104893, doi: 10.1016/j.reactfunctpolym.2021.104893.
- [3] S. Noël, V. Gasser, B. Pesset, F. Hoegy, D. Rognan, I.J. Schalka, G.L.A. Mislin. Synthesis and biological properties of conjugates between fluoroquinolones and a N3"-functionalized pyochelin. *Org. Biomol. Chem.* **2011**, 9, 8288–8300, doi: 10.1039/C1OB06250F.
- [4] F. Canfarotta, A. Poma, A. Guerreiro, S.A. Piletsky. Solid-phase synthesis of molecularly imprinted nanoparticles. *Nature Protocols*, **2016**, 11, 443–455, doi: 10.1038/nprot.2016.030.

4 EFFECT OF POLYMERIZATION TIME ON THE BINDING PROPERTIES OF CIPROFLOXACIN NANOMIPs

4.1 INTRODUCTION

In the solid phase polymerization synthesis, the polymerization proceeds like in a precipitation polymerization, but in presence of the grafted template molecule on the glass beads. As mentioned in the introduction, the exact mechanism of formation of the nanoparticles is not actually known but only hypothesized [1]. It is possible that the polymerization process starts anywhere in the reaction environment, but it is probably favoured around the template molecules. This seems to be confirmed by the experiment reported in chapter 2, where a lower yield of imprinted MIPs was obtained with respect to the starting amount of monomers. One of the possible parameters that can be investigated to better understand this mechanism is the time of polymerization, which may also influence the binding properties of the nanoMIPs. Currently, only few published data on this topic are available [1-4]. In fact, available experimental protocols provide for very short reaction times – from few seconds to tens of minutes – when using the UV-initiated polymerization, or longer times when using the persulfate / TEMED initiator system. However, it is necessary to keep in mind that such polymerization times are intended as reasonable temporal intervals for the polymerization to occur, but there is still no formation of precipitated particles. Consequently, it could be interesting to check if the polymerization time has an effect on the binding properties of nanoMIPs.

4.1.1 Aim of the work and objectives

Here is presented an explorative study about the effect of different polymerization times on the binding properties of ciprofloxacin-imprinted nanoMIPs. The nanoMIPs were produced in both the synthesis environment, water and acetonitrile, at different time, between 10 minutes and 5 hours. The previously optimized synthesis conditions were used, *i.e.* monomeric formulation (formulation G in water – see chapter 3), spacer arm and rebinding buffer condition (see chapter 2). The binding properties were studied by partition equilibrium and rebinding kinetic experiments to measure the binding affinity and the kinetic rate constants. Furthermore, selectivity and non-specific binding were valued by measuring the rebinding of levofloxacin onto ciprofloxacin-imprinted nanoMIPs, and ciprofloxacin onto diclofenac-imprinted nanoMIPs, respectively. The morphology properties of the nanoparticles were also studied, using a dynamic light scattering instrument to measure the nanoMIPs hydrodynamic dimensions.

4.2 EXPERIMENTAL

4.2.1 Materials

Glass beads were Spheringlass-2429 70-100 μm average particle size (Potters, UK). Ciprofloxacin was purchased from Supelco (Milan, Italy).

Acrylic acid (AA), 3-(aminopropyl)trimethoxysilane (APTMS), ammonium persulphate (APS), azo-bis-isobutyronitrile (AIBN), 1-ethyl-3-(3-dimethylaminopropyl)carbodiimide (EDC), ethylenediamine, ethylene dimethacrylate (EDMA), hexamethyldisilazane (HMDS), N-hydroxysuccinimide (NHS), N-isopropylacrylamide (NIPAm), methacrylic acid (MAA), N,N'-methylene-bis-acrylamide (BIS), morpholinethansulphonic acid (sodium salt, MES), sodium borohydride, N-tert-butylacrylamide (TBAm), N,N,N',N'-tetramethylethylenediamine (TEMED), ciprofloxacin (CPX), levofloxacin (LVX), N,N-dimethylaminopyridine (DMAP), N,N'-diisopropylcarbodiimide (DIC), succinic anhydride and trimethylolpropane trimethacrylate (TRIM) were purchased from Sigma-Merck (Milan, Italy).

Solvents and all other chemicals were purchased from Sigma-Merck (Milan, Italy). All the solvents were of HPLC grade, whereas all chemicals were of analytical grade.

The water used was ultra-purified in Purelab Prima System from Elga (Marlow, UK). Polymerisation inhibitors in the monomers were removed by filtration through activated basic alumina.

Antibiotic stock solutions were prepared by dissolving 10 mg of the substance in 25 mL of methanol/acetic acid 95/5 (v/v) then stored in the dark at $-20\text{ }^{\circ}\text{C}$.

4.2.2 Glass beads amination

In a 100-mL round-bottomed flask, 25 g of glass beads in 50 mL of 1 M aqueous NaOH and boiled for 1 h. Then, they were diluted with 50 mL of ultrapure water and filtered on a 0.22 μm nylon membrane. The glass beads were washed with 100 mL of 1 M aqueous HCl and with ultrapure water till neutrality. Then they were rinsed twice with acetone and dried at $60\text{ }^{\circ}\text{C}$ overnight.

The dried glass beads were transferred in a 1-L round-bottomed flask and dispersed in 50 mL of toluene, removing water by azeotropic distillation. Then, the flask was cooled to room temperature, 10 mL of APTMS were added, and the mixture let to react overnight. The glass beads were filtered on a 0.22 μm nylon membrane and washed with 3x50 mL of toluene.

To end-cap the residual silanols, the glass beads were transferred in a 250-mL round-bottomed flask and dispersed in 50 mL of toluene, removing water by azeotropic distillation. Then, the flask was cooled to room temperature, 1 mL of HMDS was added to the dispersion and the mixture let to react overnight. The

end-capped glass beads, named “short-chain beads” (SC-beads) were filtered on a 0.22 μm nylon membrane, rinsed twice with acetone and dried at 60 °C overnight. After silanization, the amino groups available on the silanized glass beads surface were determined by Kaiser’s method as 1,1 $\mu\text{mol/g}$.

4.2.3 Synthesis of ciprofloxacin hemisuccinamide

The template molecule, ciprofloxacin hemisuccinamide (CPX-HS), was synthesized according to a modification of the procedure given by Noël et al. [5]. Succinic anhydride (100 mg, 1 mmol) was added to a suspension of CPX (331 mg, 1 mmol) in DMSO (2.0 mL) containing a catalytical amount of DMAP. The reaction mixture was stirred under nitrogen overnight at 95 °C and cooled down to room temperature. The resulting precipitate was filtered, washed successively with water and diethylether, and dried under reduced pressure. The expected hemisuccinamide was isolated as a fluffy white powder (98 mg, yield 75%), deemed pure by MS-HPLC (ESI: m/z 431.1 [MH⁺]).

4.2.4 Template immobilization

In 25-mL glass vials 10 mg of hemisuccinade ciprofloxacin (0.231 mmol) were dissolved in 10 mL of DMF, 26.7 mg of NHS (0.232 mmol) and 29.3 mg of DIC (0.232 mmol) were added and the solutions incubated for 60 min. Then, they were transferred in 25-mL flasks containing 5 g of aminated glass beads. The suspensions were incubated at room temperature overnight, filtered on a 0.22 μm nylon membrane, washed with DMF, rinsed twice with acetone, dried under vacuum at room temperature and stored in the dark at 4 °C.

4.2.5 Synthesis of nanoMIPs

For the nanoMIPs prepared in water, the polymerization mixtures were prepared in according with the literature [6]. A pre-polymerization mixture (Formulation G, molar ratio BIS : AA : NIPAm : TBAm = 2 : 20 : 30 : 48) was made in 25 mL of ultrapure water by mixing under sonication 0.0065 mmol of cross-linker (BIS: 1 mg), 4.7 mg of AA (0.065 mmol), 11 mg of NIPAm (0.097 mmol) and 19.8 mg of TBAm (0.156 mmol, dissolved in 0.5 mL of ethanol). Then, 5 mL of mixture was added to 50-mL polypropylene SPE cartridges containing 2.5 g of template functionalized glass beads. The cartridges were purged with nitrogen for 5 min. 3 μL of TEMED and 100 μL of 30 mg mL^{-1} aqueous solution of APS were added and the polymerization was carried out at room temperature for a time between 5 min and 2 hours in a roller-equipped incubator. The supernatant was drained by vacuum aspiration, the dry cartridges were cooled to 4 °C and polymerization by-products and low-affinity nanoMIPs were washed with 10 \times 2 mL of ice-cold water.

High affinity nanoMIPs were collected by eluting the cartridges at room temperature with 5×3 mL hot water and 5×1 mL of 90% methanol/10% acetic acid v/v. The eluates were purified by gel-filtration in ultrapure water onto a 26 x 250 mm Sephadex G25 column. The nanoMIPs were isolated by centrifugation at 14000 x g, dried by lyophilisation and stored at 4 °C.

For nanoMIPs prepared in acetonitrile, 118 µL of MAA (1.11 mmol), 128 µL of EDMA (0.54 mmol), 127 µL of TRIM (0.32 mmol) and 6.25 mg of AIBN (0.03 mmol) were dissolved in 25 mL of acetonitrile (molar ratio MAA : EDMA : TRIM = 56 : 28 : 16). Then, 5 mL of mixture were added to 25-mL polypropylene SPE cartridges containing 2.5 g of template functionalized glass beads. The cartridges were purged with nitrogen for 5 min, sealed and left to polymerize at 60 °C for a time between 10 minutes and 1 hour in a roller-equipped incubator. The supernatant was drained by vacuum aspiration, the dry cartridges were cooled to 4 °C and polymerization by-products and low-affinity nanoMIPs were washed with 5×2 mL of ice-cold acetonitrile. High affinity nanoMIPs were collected by eluting the cartridges with 5×2 mL of methanol - acetic acid 9+1 (v/v). The eluate was evaporated in a rotavap, weighted, and stored at 4 °C.

Not-imprinted polymers (nanoNIPs) were prepared in the same experimental conditions in terms of composition of the polymerization mixture and polymerization time but using glass-beads functionalized with diclofenac as solid phase.

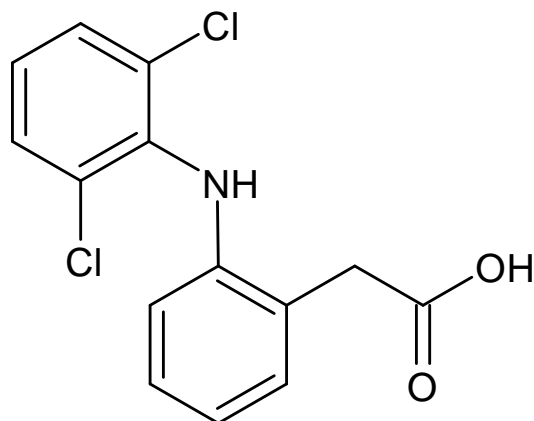


Figure 4-1 - Structure of the diclofenac

4.2.6 Coupling of nanoMIPs to glass beads

In 4-mL glass vials 1 mg of nanoMIPs were dissolved under sonication in 1 mL of MES buffer (50 mM, pH 4.7), 8 mg of NHS (0.069 mmol) and 21.5 mg of EDC (0.138 mmol) were added and the solutions incubated at room temperature for 60 min. Then, they were transferred in 10-mL flasks containing 1 g of aminated glass beads. The suspensions were incubated at room temperature overnight, filtered on 0.22 µm nylon membranes, washed with ultrapure water, rinsed twice

with acetone, dried under vacuum at room temperature and stored in the dark at 4 °C.

4.2.7 HPLC method

Reverse phase HPLC analysis was used for fluoroquinolones determination. The HPLC apparatus (Merck-Hitachi, Milan, Italy) was a LaChrom Elite system composed of a programmable binary pump L-2130, an auto-sampler L-2200, a fluorescence detector L-2480, provided with EZChrom Elite software for the instrumental programming, data acquisition and data processing. The column used was a 100 mm × 4.6 mm Chromolith RP-18 (Merck, Milan, Italy). The mobile phase was water/acetonitrile 85+15, acetic acid 1% (v/v). Elution was performed in isocratic conditions at a flow rate of 0.7 mL/min. The sample volume injected was 5 µL, and the fluorescence wavelength were $\lambda_{ex}=280/\lambda_{em}=440$ nm for the ciprofloxacin, and $\lambda_{ex}=278/\lambda_{em}=540$ nm for the levofloxacin. Ciprofloxacin solutions between 0.5 and 50 ng/mL were prepared in the eluent immediately before use. The solutions were analyzed in triplicate and mean peak areas were plotted against fluoroquinolone concentration. The calibration plot was drawn by using a weighted linear regression (weight = 1/conc).

4.2.8 Determination of binding properties

To measure binding isotherms, about 40 mg of glass beads supporting nanoMIPs were exactly weighed in 4 mL flat bottom amber glass vials. Then, 1.0 mL of phosphate buffer (20 mM, pH 6) containing increasing amounts of fluoroquinolone ranging from 0.5 to 50 µg was added. The vials were incubated for 2 hours at room temperature under continuous agitation on a horizontal rocking table. Then, the solutions were filtered on 0.22 µm nylon membranes and the free amounts of ciprofloxacin were measured by HPLC-fluorescence analysis. Each experimental point was assessed as the average of two repeated measures.

Binding parameters were calculated by using SigmaPlot 12 (Systat Software Inc., Richmond, CA, USA). Non-linear least square fitting was applied to the averaged experimental data. Binding isotherm parameters were calculated by using a Langmuir binding isotherm model.

Binding kinetics parameters were calculated by using a 1st order kinetic model:

$$B = B_{eq}[1 - \exp(-k_{ass}t)]$$

where B is the ligand bond to the nanoMIP at time t, B_{eq} the ligand bond to the polymer at equilibrium and k_{ass} the association kinetic constant.

To assure robust results, weighted (1/y) Pearson VII limit minimization was chosen as the minimization method. To avoid being trapped in local minima, which would give incorrect results, minimizations were carried out several times by using different initial guess values for the binding parameters.

The binding selectivity, α , was calculated as:

$$\alpha = \frac{K_{eq} \text{levofloxacin}}{K_{eq} \text{ciprofloxacin}}$$

where K_{eq} ciprofloxacin and K_{eq} levofloxacin are the equilibrium binding constants calculated for ciprofloxacin and levofloxacin, respectively.

4.2.9 Dynamic light scattering analysis

The hydrodynamic diameter distribution of the suspensions prepared was evaluated using a Zetasizer instrument (Zetasizer Nano-ZS, Malvern Instruments, U.K.). The measurements were performed after checking that the automatic attenuator was between 6 and 9. The results were expressed as hydrodynamic diameter distribution in intensity (average of mean values of 5 measurements).

4.3 RESULTS AND DISCUSSIONS

To study the effect of the duration of the polymerization process, both reaction environment were considered: the synthesis in water with the monomeric mixture optimized in the previous chapter, and the synthesis in acetonitrile. For the synthesis in water, they were considered polymerization times ranging from 15 minutes to 5 hours. For the synthesis in acetonitrile, we have considered polymerization times ranging from 10 minutes to 60 minutes. For the importance of the synthesis in water, we dedicated more attention and experiments on this than the acetonitrile nanoMIPs.

Under all the experimental conditions the solid-phase synthesis produced nanoMIPs fully suspensible in water, resulting in transparent and colourless solutions, without any perceivable turbidity. For the water synthesis, yields calculated respect to the amount of monomers in the polymerization mixtures were: 1.0 mg (15%) for 15 min, 1.4 mg (21%) for 30 min, 1.1 mg (17%) for 45 min, 1.8 mg (28%) for 1 h, 4.0 mg (61%) for 2 h, 1.2 mg (18%) for 3 h, and 3.5 mg (54%) for 5 h, respectively.

4.3.1 Size of water nanoMIPs

The measuring of the hydrodynamic dimensions of the nanoparticles was performed only for the nanoMIPs synthesized in water. Dynamic light scattering measurements performed on nanoMIPs are reported in Table 4-1. NanoMIPs prepared with a polymerization time of 15 min are characterized by a very small mean diameter (12 ± 5 nm) and a relatively high polydispersity index of 0.44. Instead, nanoMIPs prepared with longer polymerization times show particles whose diameters are of the order of magnitude of hundreds of nanometers and values for the polydispersity index slightly lower and substantially constant. A progressive increase in the average diameter is observed with the polymerization time, indicating that for times greater than 15 minutes the formation process of the nanoparticles is plausibly independent of the polymerization time. After two hours of polymerization, we don't observe a significant increase of the nanoparticles dimension. In the figure 4-2 they are graphical reported the size values in function of the polymerization times. It is possible to observe a rapid increase of the dimension between 0 to 1 hour follow by a very little increasing.

Table 4-1 - Dynamic light scattering results for ciprofloxacin-imprinted water nanoMIPs.

Polymerization time	Diameter (nm)	Polydispersity index
15 min	12 ± 5	0.44
30 min	120 ± 41	0.34
45 min	165 ± 42	0.26
1 h	154 ± 37	0.24
2 h	234 ± 84	0.36
3 h	236 ± 87	0.37
5 h	268 ± 94	0.35

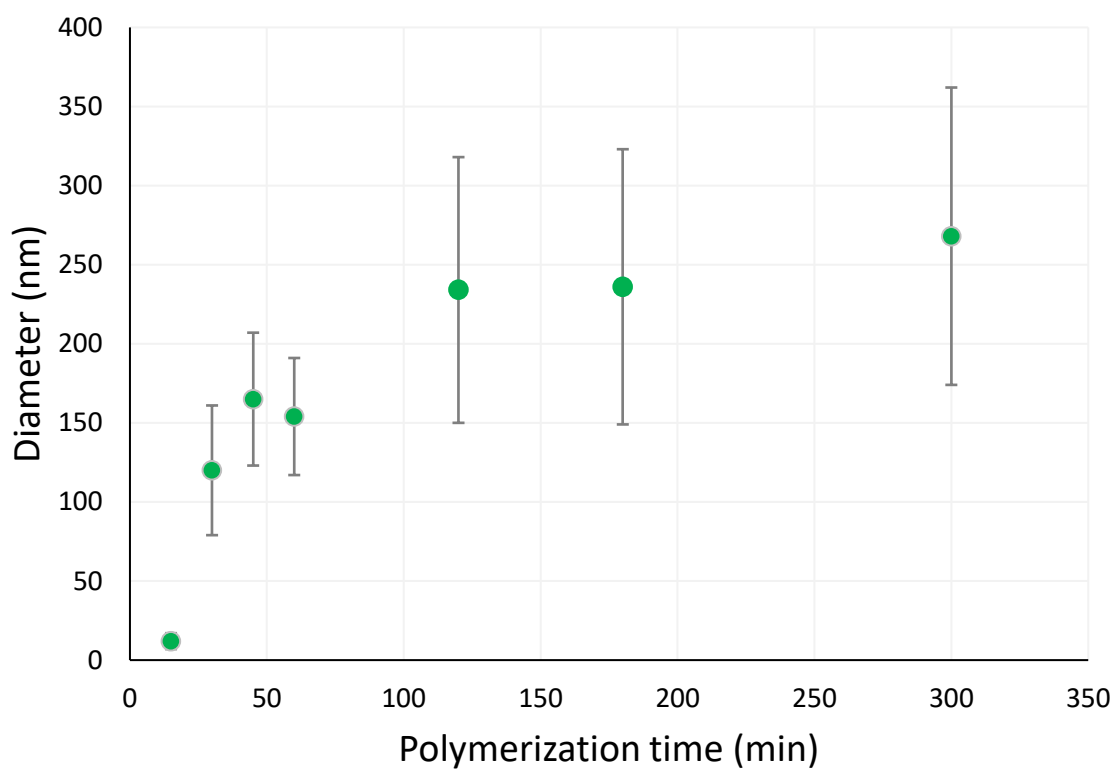


Figure 4-2 – Dimension of the ciprofloxacin-imprinted water nanoMIPs in function of the polymerization time. Error bars indicate 1 standard error unit.

4.3.2 Binding properties of the water nanoMIPs

To correctly evaluate the binding properties of nanoMIPs towards ciprofloxacin, the measurements of equilibrium binding isotherms and association kinetics require fast separation between free and bound ligand. As ultrafiltration or dialysis are quite slow, we chosen to support the nanoMIPs on the same glass beads used for their synthesis in order to easily separate by filtration the grafted beads – carrying the bound ligand – from the solution which contains the free ligand. Preliminary experiments showed that bare glass beads and HDMS-silanized beads were unable to bind ciprofloxacin in water, therefore it is reasonable to assume that the existence of a binding between ciprofloxacin and solid phase can be attributed to the interaction with nanoMIPs.

Table 4-2 - Equilibrium binding constants (± 1 standard error unit) measured for ciprofloxacin and levofloxacin on ciprofloxacin-imprinted water nanoMIPs and ciprofloxacin on diclofenac-imprinted nanoMIPs (nanoNIPs).

Polymerization time	CPX on nanoMIPs ($M^{-1} \times 10^6$)	LEV on nanoMIPs ($M^{-1} \times 10^6$)	CPX on nanoNIPs ($M^{-1} \times 10^6$)
15 min	15.39 \pm 2.14	13.54 \pm 0.95	1.96 \pm 0.38
30 min	8.48 \pm 0.81	2.12 \pm 0.86	2.25 \pm 0.68
45 min	8.44 \pm 1.75	1.32 \pm 0.44	0.57 \pm 0.22
1 h	8.84 \pm 1.65	0.78 \pm 0.30	0.82 \pm 0.44
2 h	4.30 \pm 0.60	0.77 \pm 0.50	1.14 \pm 0.21
3 h	1.74 \pm 0.87	0.58 \pm 0.65	1.21 \pm 0.86
5 h	0.82 \pm 0.33	0.60 \pm 0.28	NV

The binding parameters obtained from binding isotherm measured for ciprofloxacin and levofloxacin (Figure 4-3) are reported in Table 4-2. They confirm that nanoMIPs prepared by solid phase synthesis strongly bind the template ciprofloxacin and, in a lesser extent, the related fluoroquinolone levofloxacin with equilibrium binding constants (K_{eq}) in the range $10^6 - 10^7 M^{-1}$, with values progressively decreasing when polymerization time increases, and after 30 minutes it is indistinguishable to the non-specific binding. In contrast, the binding of ciprofloxacin to diclofenac-imprinted nanoMIPs (Figure 4-3) – which can then be regarded as a measure of non-specific binding – is always low and essentially constant. A statistical comparison (t-test: $\alpha = 0.05$, $n = 10$, $t < 2.101$) of the equilibrium binding constants for ciprofloxacin between nanoMIPs and nanoNIPs show that when nanoMIPs are polymerized for times longer than 2 hours there is no difference respect to nanoNIPs.

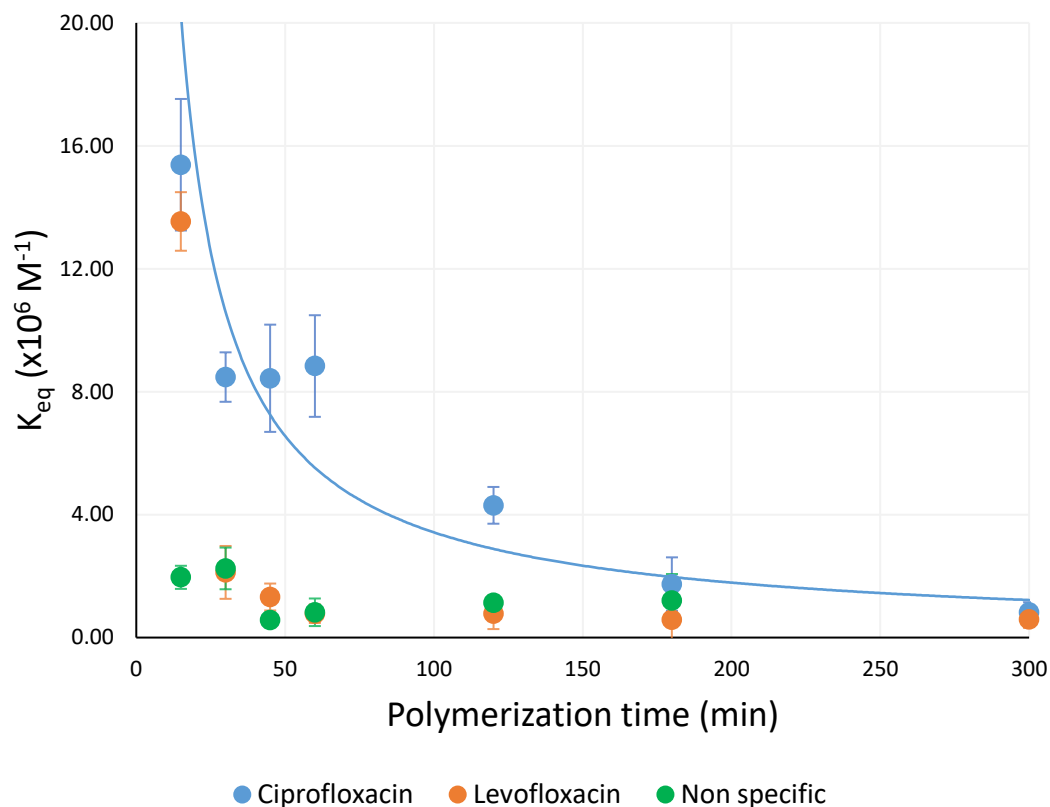


Figure 4-3 – Binding constant values for the ciprofloxacin, levofloxacin and the non-specific binding (ciprofloxacin binding measured on nanoNIPs) in function of the polymerization time for the water nanoMIPs. Error bars indicate 1 standard error unit.

Concerning selectivity, as reported in Figure 4-4, nanoMIPs polymerized for very short times are not able to discriminate between ciprofloxacin and levofloxacin, with a complete lack of selectivity. As the polymerization time increases, the selectivity improves markedly, reaching $\alpha \approx 0.1$ at 1 hour and then worsening again for longer polymerization times. To evaluate properly this trend, it is necessary to consider that for short polymerization times the values of the equilibrium binding constants for both ligands are high but statistically indistinguishable, therefore their numerical relationship must be unitary. On the contrary, for longer polymerization times, these values are markedly different between ciprofloxacin and levofloxacin. Indeed, those for levofloxacin cannot be distinguished by non-specific binding, while those for ciprofloxacin become so only for long polymerization times. Consequently, for intermediate times, a significant selectivity with α values much less than 1 but with a progressive tendency to rise comes out, while for longer time the lack of selectivity is a consequence of a binding behaviour of nanoMIPs indistinguishable from nanoNIPs for both the ligands.

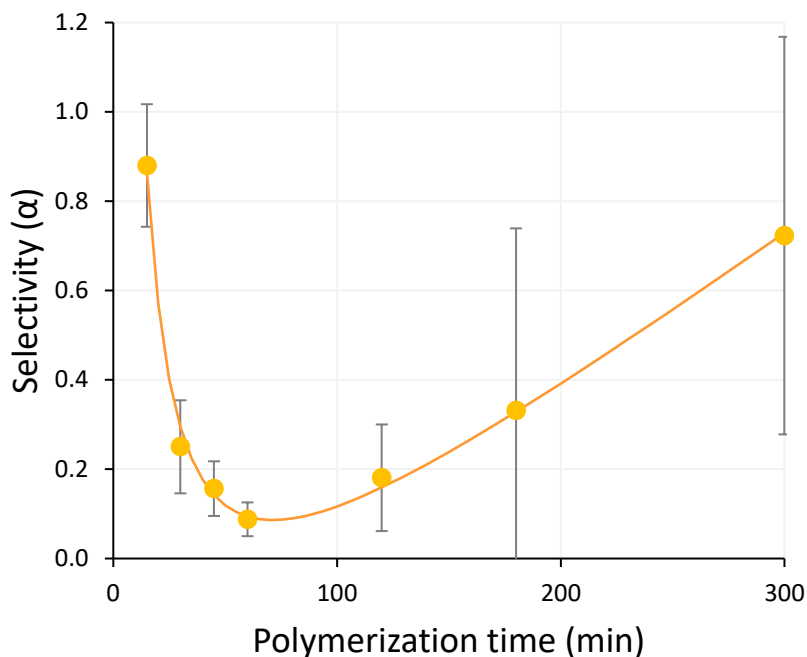


Figure 4-4 - Selectivity calculated on the levofloxacin/ciprofloxacin binding constant ratio for the water nanoMIPs in function of the polymerization time. Error bars indicate 1 standard error unit.

4.3.3 Binding kinetics of the water nanoMIPs

Equilibrium binding constants (K_{eq}) measured for ciprofloxacin water synthesis nanoMIPs can be broken down into dissociation (k_{dis}) and association (k_{ass}) kinetic rate constants, measuring k_{ass} (Figure 4-5) and calculating k_{dis} from the relationship $K_{eq} = k_{ass}/k_{dis}$. It may therefore be interesting to examine the values of these rate constants, reported in Table 4-3, in relation to the polymerization times.

Table 4-3 - Association and dissociation rate constants (± 1 standard error unit) measured for ciprofloxacin on ciprofloxacin-imprinted water nanoMIPs.

Polymerization time	k_{ass} (L mol ⁻¹ min ⁻¹ x 10 ⁻⁶)	k_{dis} (min ⁻¹)
15 min	2.88 ± 0.67	0.19 ± 0.07
30 min	1.68 ± 0.25	0.20 ± 0.03
45 min	1.80 ± 0.41	0.21 ± 0.09
1 h	1.75 ± 0.47	0.20 ± 0.08
2 h	1.34 ± 0.20	0.31 ± 0.05
3 h	0.80 ± 0.23	0.46 ± 0.24
5 h	0.75 ± 0.04	0.91 ± 0.13

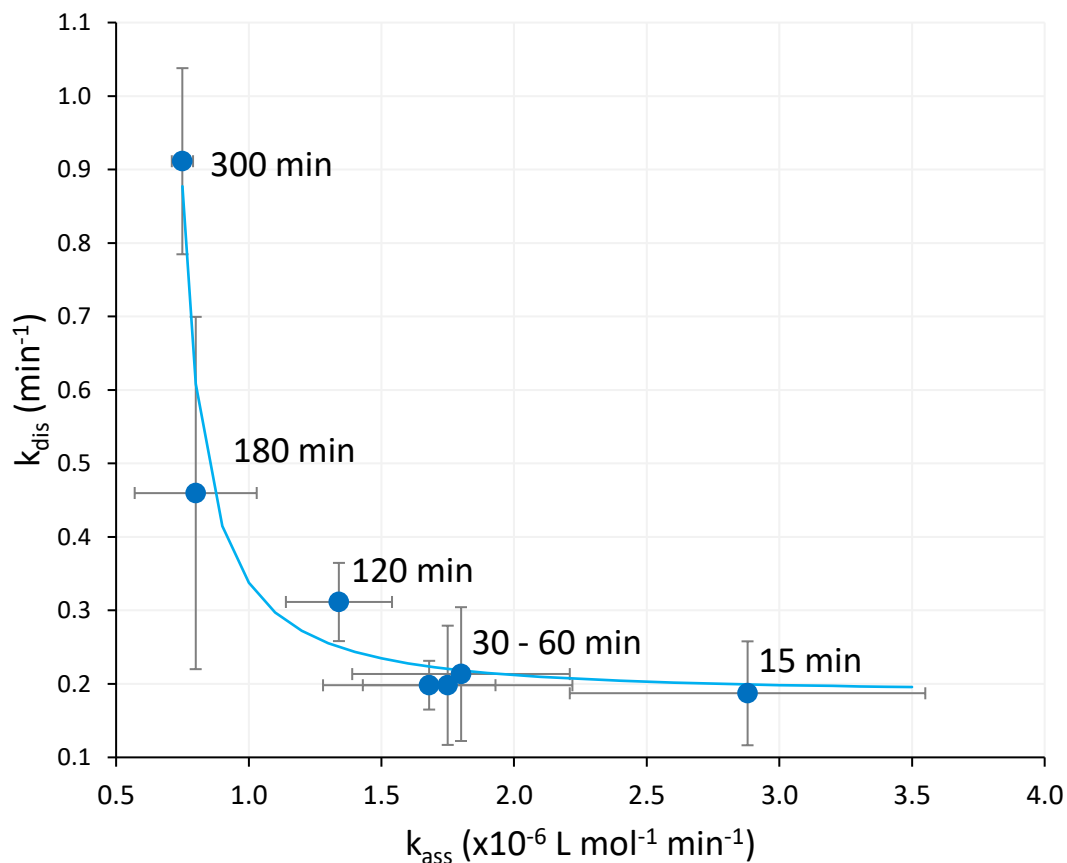


Figure 4-5 - Dissociation rate constants (k_{dis}) vs. association rate constants (k_{ass}) plot for ciprofloxacin on ciprofloxacin-nanoMIPs. Error bars indicate 1 standard error unit.

As reported in Figure 4-5, in the whole range of polymerization times considered in this work both dissociation and association rate constants change in a limited range (k_{dis} : 0.19-0.91 min $^{-1}$; k_{ass} : 0.75-2.88 $\times 10^6$ L mol $^{-1}$ min $^{-1}$), but considering only the nanoMIPs that show a greater affinity for ciprofloxacin (15 min – 1 h) it can be observed that the dissociation rate constant remains practically unchanged with a mean value of 0.2 min $^{-1}$. It follows that the affinity of ciprofloxacin for the imprinted binding sites mainly depends on the values of association rate constant, values which gradually decrease as the polymerization time increases. On the contrary, poorly binding nanoMIPs obtained with longer polymerization times show kinetic behaviours totally different. In fact, while association rate constants are low and substantially constant, dissociation rate constants are high and proportional to the polymerization time.

4.3.4 Binding properties of the acetonitrile nanoMIPs

Compared to the water synthesized nanoMIPs, for ciprofloxacin imprinted nanoMIPs in organic environment only a reduced number of experiments was carried out, focusing on the investigation of the binding properties.

In Table 4-4 are reported the values of the binding constants calculated for the ciprofloxacin, the levofloxacin and for the ciprofloxacin on nanoMIPs imprinted for the diclofenac (nanoNIPs).

Table 4-4 - Equilibrium binding constants (± 1 standard error unit) measured for ciprofloxacin and levofloxacin on ciprofloxacin-imprinted acn nanoMIPs and ciprofloxacin on diclofenac-imprinted nanoMIPs (nanoNIPs).

Polymerization time	CPXon nanoMIPs ($M^{-1} \times 10^6$)	LEV on nanoMIPs ($M^{-1} \times 10^6$)	CPX on nanoNIPs ($M^{-1} \times 10^6$)
10 min	2.23 ± 0.76	2.91 ± 0.47	0.60 ± 0.16
15 min	3.76 ± 0.70	1.31 ± 0.17	0.54 ± 0.11
30 min	4.10 ± 1.72	0.99 ± 0.17	0.62 ± 0.23
1 h	4.02 ± 0.76	0.99 ± 0.17	0.60 ± 0.16

In the organic environment, a different behaviour of the affinity for the ciprofloxacin was observed. As shown in Figure 4-6, the affinity increases over time from 10 to 60 minutes, and does not decrease. The values are smaller for the same times ($8-16 M^{-1} \times 10^6$ water nanoMIPs vs $2-4 M^{-1} \times 10^6$ ACN nanoMIPs), while the affinity for the levofloxacin decreases. At 10 minutes, the levofloxacin binding is better than for the ciprofloxacin, and after this time it decreases but without merging with the nonspecific binding. Like the in-water synthesis, the nonspecific binding remains constant at all polymerization times.

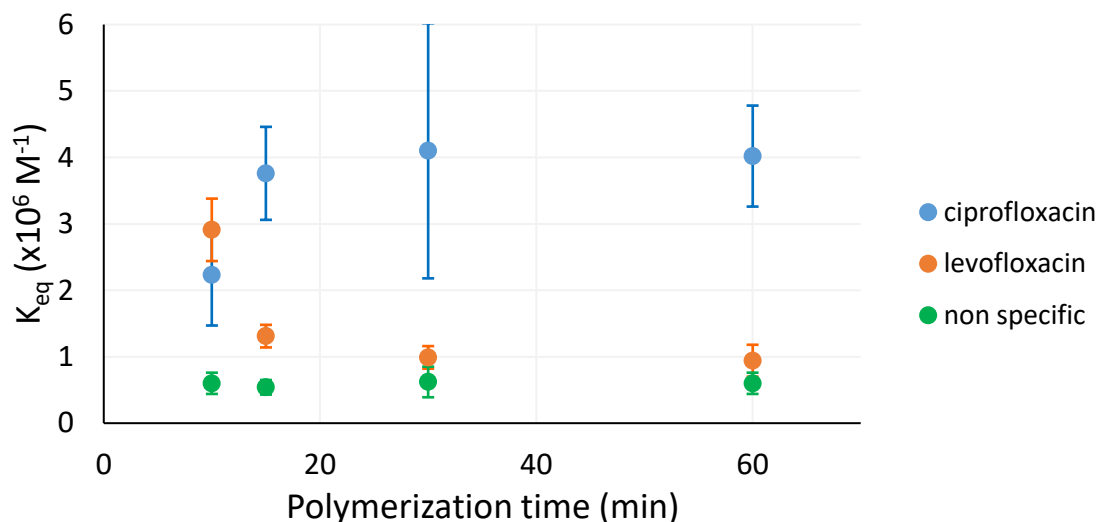


Figure 4-6 - Binding constant values for the ciprofloxacin, levofloxacin and the non-specific binding (ciprofloxacin binding measured on nanoMIPs) in function of the polymerization time for the acn nanoMIPs. Error bars indicate 1 standard error unit.

In the range 0- 60 minutes, the selectivity (Figure 4-7) has the same trend as that of water nanoMIPs. The selectivity grows up to α values of about 0.20, higher than the water nanoMIPs. After 60 minutes, there is not sufficient data to state whether α values grow like in the other system or not.

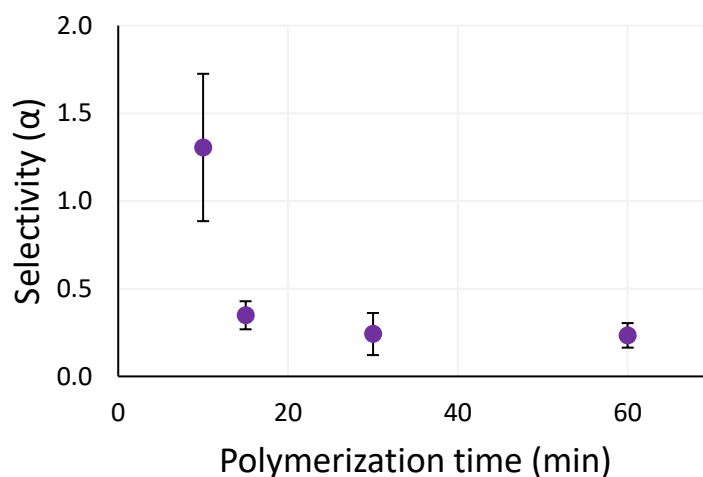


Figure 4-7 - Selectivity calculated on the levofloxacin/ciprofloxacin binding constant ratio of the acn nanoMIPs in function of the polymerization time. Error bars indicate 1 standard error unit.

4.3.5 Discussion

Recently it has been shown that in the SPPS the composition of the polymerization mixture – very poor in cross-linker component (2% of total moles in this work) – is such that the concept about the formation of a rigid and well-defined binding site within a highly cross-linked network of polymeric chains must be discarded. Alternatively, it has been proposed a model where the molecular imprinting of nanoparticles is the result of the dynamic interaction between the template molecules grafted onto the surface of the solid phase and the lightly cross-linked chains being formed at the interface between the solution and the glass surface [1].

Within the framework of this model, as the polymeric chains grow progressively over time and rearrange themselves around the immobilized template, the binding properties of nanoMIPs depend not only on the classic parameters typical of molecular imprinting, such as, for example, the ability of functional monomers to interact with the template, but also on the length of the polymerization process, that is the actual dimensions of the nanopolymers.

The experimental results reported in this work confirm that the polymerization time in the solid phase polymerization method has different effects on the binding behavior of the resulting nanoMIPs. For the nanoMIPs synthesized in water we can identify three different phases: (A) short polymerization times, with nanoparticles characterized by high binding affinity but low selectivity ($K_{eq} > 10^7 \text{ M}^{-1}$, $\alpha \approx 1$), (B) medium polymerization times, with nanoparticles characterized by high binding affinity and selectivity ($K_{eq} \geq 10^6 \text{ M}^{-1}$, $\alpha < 1$), and (C) long polymerization times, with nanoparticles characterized by low binding affinity, faster dissociation kinetics and low selectivity ($K_{eq} \leq 10^6 \text{ M}^{-1}$, $k_{dis} \gg 0.2 \text{ min}^{-1}$, $\alpha \approx 1$).

To try to evaluate this complex behaviour, it is necessary to consider that during the polymerization process the nanoparticles continue to grow, both when they are bonded to the solid phase and when they are free in solution. As it is plausible that in the early stage of the polymerization the conformation of the growing polymeric chains is very flexible and able to rapidly rearrange and maximize the interaction with the template on solid phase. In these conditions there are no binding sites with a stiff and defined structure yet, even if, once dissociated, nanoparticles are able to maintain – at least in part – the binding conformation but with limited selectivity towards molecular other than the template. As a consequence, nanoMIPs prepared in very short polymerization time show a type-A binding behaviour, with high binding affinity and fast association kinetics but poor or absent selectivity.

When the polymerization process continues for longer times, nanoparticles become larger and more structured, with chains conformation restrained and intertwined, leading to binding sites well defined but stiffer and – after dissociation from the solid phase – less accessible to ligands. In this condition nanoMIPs show a type-B binding behaviour: the association rate constant and the binding affinity decrease but selectivity increases.

Further prolonging the polymerization time causes further growth of the nanoparticles. Under these conditions the polymer structure becomes more and more rigid, sterically hindering the binding sites to the point that they cannot effectively bind the ligands during the rebinding process. In this condition nanoMIPs show a type-C binding behaviour: the binding properties come to coincide with those of not-imprinted nanoparticles, depending no more on the presence of accessible binding sites, but only from the presence of randomly dispersed functional groups on the surface of the nanoparticles.

If we can demonstrate these three-classes classification for the MIPs imprinted in water environment, for the nanoMIPs imprinted in acetonitrile we observe different behaviours. At first, we have a similar recognition capability for the template and the levofloxacin from the imprinted nanoparticles, that means a medium affinity but a low selectivity. With an increase of the polymerization time, the affinity for the ciprofloxacin grows and the affinity for the levofloxacin goes down with an increase of the selectivity. From 30 to 60 minutes the values keep constant. For a lack of experiments, we don't know the behaviour after 1 hour of polymerization.

In this case we observe a more classical behaviour, when the capability to recognize the template molecule increase over the time to become constant after a specific time. The binding site evolves around the template molecule to assume a rigid conformation that doesn't change over a specific time. It is explainable with the used monomeric formulation: there is more crosslinker than in the water synthesis formulation; That means a greater rigidity of the binding sites, that can't change the conformation during the polymerization process.

4.4 CONCLUSIONS

The results reported in this work show that polymerization time plays a pivotal role in determining the binding properties of nanoMIPs in both synthesis environments. It is reasonable to assume that, since the growth rate of the nanoparticles certainly depends on many variables such as the chemical properties of the monomers, the solvent and the polymerization temperature and, last but not least, the type of radical initialization, the results reported here are to be considered representative of this system in particular. However, there is no reason to believe that the overall behavior implied by the experimental results reported here cannot be extended to different polymerization mixtures and experimental conditions, and is therefore of general validity for nanoMIPs prepared by solid phase synthesis. Finally, we conclude by stressing that the control of the polymerization time allows to calibrate not only the binding capacity of the nanoMIPs towards the template, both in terms of affinity and association kinetics, but also the selectivity towards related molecules. This result seems to us particularly interesting for future applications that will require nanoMIPs with a high capacity to discriminate between ligands with similar molecular structures.

4.5 BIBLIOGRAPHY

- [1] T. Cowen, E. Stefanucci, E. Piletska, G. Marrazza, F. Canfarotta, S.A. Piletsky. Synthetic mechanism of molecular imprinting at the solid phase. *Macromolecules*, **2020**, *53*, 1435–1442, doi: 10.1021/acs.macromol.9b01913.
- [2] A. Poma, A. Guerreiro, M.J. Whitcombe, E. Piletska, A.P.F. Turner, S.A. Piletsky. Solid-phase synthesis of molecularly imprinted polymer nanoparticles with a reusable template – “plastic antibodies”. *Adv Funct Mater*, **2013**, *2*, 2821-2827, doi:10.1002/adfm.201202397.
- [3] K. Muzyka, K. Karim, A. Guerreiro, A. Poma, S. Piletsky. Optimisation of the synthesis of vancomycin-selective molecularly imprinted polymer nanoparticles using automatic photoreactor. *Nanoscal Res Lett*, **2014**, *9*, 154-154, doi: 10.1186/1556-276X-9-154.
- [4] X.H. Wang, L. Tang, F.F. Yang, L.L. Ying, Y.P. Huang, Z.S. Liu. Green synthesis of water-compatible and thermo-responsive molecularly imprinted nanoparticles. *European Polymer Journal*, **2017**, *92*, 174–184, doi: 10.1016/j.eurpolymj.2017.05.012.
- [5] S. Noël, V. Gasser, B. Pesset, F. Hoegy, D. Rognan, I.J. Schalka, G.L.A. Mislin. Synthesis and biological properties of conjugates between fluoroquinolones and a N³”-functionalized pyochelin. *Org. Biomol. Chem.* **2011**, *9*, 8288–8300, doi: 10.1039/C1OB06250F.
- [6] F. Canfarotta, A. Poma, A. Guerreiro, S.A. Piletsky. Solid-phase synthesis of molecularly imprinted nanoparticles. *Nat. Protocols*, **2016**, *11*, 443-455, doi:10.1038/nprot.2016.030.

5 RABBIT IGG-IMPRINTED NANOMIPS: EFFECT OF THE CROSS-LINKER ON AFFINITY AND SELECTIVITY

5.1 INTRODUCTION

As seen in previous chapters, the synthesis of nanoMIPs by SPPS performed in water uses a monomeric mixture which includes a large excess – up to 98% by moles – of functional monomers. For big molecules, the selection of the functional monomers seems to be of lesser importance than in the case of templates consisting of small molecules, because it has been shown that functional monomers that differ in their chemical properties are in any case able to interact with different functions present on the big templates, invariably leading to nanoMIPs with good molecular recognition properties [1]. About the cross-linker, it is added in a much more limited amount, and invariably is N,N'-methylene-bis-acrylamide (BIS) [2]. Its prevalent use may be justified by its good solubility in water. Nevertheless, it is possible to consider using other cross-linkers, of which, however, the effect on the binding properties of nanoMIPs has never been reported in literature to date, with the remarkable exception of the use of N,N'-ethylene dimethacrylamide for the solid phase synthesis of adenosine monophosphate-binding nanoMIPs [3]. Theoretically, we can suppose that a so small amount of a substance, that doesn't directly bind the target molecule, cannot have a big influence on the nanoMIPs binding properties. Anyway, the following results tell another story.

5.1.1 Why the IgG?

Immunoglobulins G (IgG) are the most abundant proteins with immunological activity, accounting for 75-80% of all immunoglobulins. They strongly bind the corresponding antigens – usually foreign biomacromolecules to the organism – with high specificity, playing a key role in the immune system of the mammals [4]. For this reason, IgG are extremely relevant not only in diagnostics [5,6], therapeutics [7,8] and theragnostics [9], but also in applications where very high selectivity towards a target molecule is mandatory, as (bio)sensoristics [10,11] and affinity chromatography [12,13]. IgG can be conveniently isolated from plasma by the classical Cohn's method based on the fractional precipitation of serum proteins by ethanol [14]. Unfortunately, this method does not assure complete separation of IgG from other serum proteins, and more efficient downstream purification strategies must be used to obtain pure IgG fractions. Several methods based on affinity ligands of natural or artificial origin have been proposed but, at the present, affinity chromatography based on Protein A - a 42 kDa protein with high affinity for the Fc region of IgG - is the preferred method for preparative and

industrial purposes [15-17]. However, this method suffers from high costs and limited stability of the Protein A, and harsh elution conditions, which can sometimes lead to irreversibly IgG damage. Thus, man-made IgG-binding materials based on the molecular imprinting technology, which could overcome these drawbacks, are of significant interest. In the last 10 years, several papers describing different approaches to IgG imprinting have been published: cryogels [18,19], films [20-22], hydrogels [23], interpenetrating polymers [24], magnetic particles [25,26], membranes [27,28], microbeads [29,30] and nanoparticles (nanoMIPs) prepared by solid phase synthesis (SPPS) [31].

This latter approach has proved particularly useful for obtaining high affinity protein-imprinted nanoparticles, characterized by good selectivity for the template and complete compatibility with aqueous environments [32-39]. Moreover, as the template is covalently grafted onto the solid phase, the isolation and purification of nanoMIPs is an easy task, and no residual protein remains trapped in the nanoparticles, avoiding product contamination.

5.1.2 Aim of the work and objectives

In this work, in order to investigate the effect of different cross-linkers in rabbit IgG-imprinted nanoMIPs prepared by SPPS, alongside BIS, some other similar cross-linkers were considered, whose structural formulas are shown in figure 5-1: N,N'-ethylene dimethacrylamide (EDAM), N,O-bis-methacryloylethanolamine (NOBE), ethylene glycol dimethacrylate (EDMA) and glycerol dimethacrylate (GDMA). These crosslinkers replaced the BIS in monomeric mixtures without changing the molar proportions of the functional monomers. The binding properties of the nanoMIPs were measured by equilibrium partition experiments with the template - rabbit IgG (RIgG) - and the selectivity was valued with respect to other three proteins of interest: bovine IgG (BIgG), bovine serum albumin (BSA) and hen egg lysozyme (LZM). The non-imprinted binding was evaluated preparing the same five nanoMIPs but imprinted for the Diclofenac, a small molecule, and measuring their binding for RIgG. Also, shape and morphology of the nanoparticles were studied through the AFM and NTA techniques, to investigate the influence of the crosslinkers on these parameters.

5.2 EXPERIMENTAL

5.2.1 Materials

Glass beads were Spherglass-2429 70-100 μm average particle size (Potters, UK). Ciprofloxacin was purchased from Supelco (Milan, Italy).

N,O-Bis-methacryloylethanolamine (NOBE) was prepared in according with literature [40].

Acrylic acid (AA), 3-(aminopropyl)trimethoxysilane (APTMS), ammonium persulphate (APS), 1-ethyl-3-(3-dimethylaminopropyl)carbodiimide (EDC), ethylene dimethacrylate (EDMA), hexamethyldisilazane (HMDS), N-hydroxysuccinimide (NHS), N-isopropylacrylamide (NIPAm), N'-methylen-bis-acrylamide (BIS), morpholinethansulphonic acid (sodium salt, MES), N-tert-butylacrylamide (TBAm), N,N,N',N'-tetramethylethylenediamine (TEMED), IgG (BIgG), bovine serum albumin (BSA), N,N'-diisopropylcarbodiimide (DIC), 4-(N,N-dimethylamino)pyridine (DMAP), ethanolamine, N,N'-ethylenedimethacrylamide (EDAM), glycerol dimethacrylate (GDMA, mixture of 1,2 and 1,3 isomers) were purchased from Sigma-Merck (Milan, Italy). Hen egg lysozyme (LZM) was purchased from Boehringer Ingelheim (Milan, Italy).

Solvents and all other chemicals were purchased from Sigma-Merck (Milan, Italy). All the solvents were of HPLC grade, whereas all chemicals were of analytical grade.

The water used was ultra-purified in Purelab Prima System from Elga (Marlow, UK). Polymerization inhibitors in the monomers were removed by filtration through activated basic alumina.

Protein stock solutions were prepared by dissolving 25 mg of protein in 25 mL of phosphate buffer (20 mM, pH 7.4) and stored in the dark at $-20\text{ }^{\circ}\text{C}$. Coomassie Blu G250 protein assay reagent was from VWR International (Milan, Italy).

5.2.2 Glass beads amination

In a 100-mL round-bottomed flask, 25 g of glass beads in 50 mL of 1 M aqueous NaOH and boiled for 1 h. Then, they were diluted with 50 mL of ultrapure water and filtered on a 0.22 μm nylon membrane. The glass beads were washed with 100 mL of 1 M aqueous HCl and with ultrapure water till neutrality. Then they were rinsed twice with acetone and dried at $60\text{ }^{\circ}\text{C}$ overnight.

The dried glass beads were transferred in a 1-L round-bottomed flask and dispersed in 50 mL of toluene, removing water by azeotropic distillation. Then, the flask was cooled to room temperature, 10 mL of APTMS were added, and the mixture let to react overnight. The glass beads were filtered on a 0.22 μm nylon membrane and washed with 3x50 mL of toluene.

To end-cap the residual silanols, the glass beads were transferred in a 250-mL round-bottomed flask and dispersed in 50 mL of toluene, removing water by

azeotropic distillation. Then, the flask was cooled to room temperature, 1 mL of HMDS was added to the dispersion and the mixture let to react overnight. The end-capped glass beads, named “short-chain beads” (SC-beads) were filtered on a 0.22 μm nylon membrane, rinsed twice with acetone and dried at 60 $^{\circ}\text{C}$ overnight. After silanization, the amino groups available on the silanized glass beads surface were determined by Kaiser’s method as 1,1 $\mu\text{mol/g}$.

5.2.3 Template immobilization

In a 100-mL round-bottom flask provided of reflux condenser, 10 g of aminated glass beads, 50 mg (0.50 mmol) of succinic anhydride and about 1 mg of DMAP as catalyst were suspended into 40 mL of anhydrous pyridine. The mixture was heated at 90 $^{\circ}\text{C}$ for six hours, cooled, filtered on a 0.22 μm nylon membrane, and washed with dimethylformamide and HCl 1 M.

The hemisuccinated beads were transferred in a 100-mL flat-bottom flask containing 40 mL of dimethylformamide 6 mg of NHS (0.050 mmol) and 8 μL of DIC (0.052 mmol). The suspension was incubated at 4 $^{\circ}\text{C}$ for 60 min onto a horizontal roller, filtered on a 0.22 μm nylon membrane, washed with cold dimethylformamide and dried under vacuum suction.

The activated glass beads were transferred in a 100-mL flat-bottom flask and 40 mL of 1 mg/mL of rabbit IgG dissolved in bicarbonate buffer (150 mM, pH 8.5) were added. The suspension was incubated at room temperature overnight onto a horizontal roller, filtered on a 0.22 μm nylon membrane, washed with water, dried under vacuum suction and stored in the dark at 4 $^{\circ}\text{C}$.

5.2.4 Synthesis of nanoMIPs

The polymerization mixtures were prepared in according with the literature and previous works [1]. A pre-polymerization mixture (molar ratio crosslinker : AA : NIPAm : TBAm = 2 : 20 : 30 : 48) was made in 25 mL of ultrapure water by mixing under sonication 0.0065 mmol of cross-linker (BIS: 1 mg, EDAM: 1.1 mg, NOBE: 1.3 mg, EDMA: 1.3 mg, GDMA: 1.5 mg), 4.7 mg of AA (0.065 mmol), 11 mg of NIPAm (0.097 mmol) and 19.8 mg of TBAm (0.156 mmol, dissolved in 0.5 mL of ethanol). Then, 5 mL of mixture was added to 50-mL polypropylene SPE cartridges containing 2.5 g of functionalized glass beads. The cartridges were purged with nitrogen for 5 min. 3 μL of TEMED and 100 μL of 30 mg mL^{-1} aqueous solution of APS were added and the polymerization was carried out at room temperature for 60 min in a roller-equipped incubator. The supernatant was drained by vacuum aspiration, the dry cartridges were cooled to 4 $^{\circ}\text{C}$ and polymerization by-products and low-affinity nanoMIPs were washed with 10 \times 2 mL of ice-cold water. High affinity nanoMIPs were collected by eluting the cartridges at room temperature with 5 \times 3 mL of 0.1 M^{-1} aqueous HCl. The eluates were immediately neutralized

with aqueous ammonium hydroxide 1 M^{-1} and purified by gel-filtration in ultrapure water onto a $26 \times 250 \text{ mm}$ Sephadex G25 column. The nanoMIPs were isolated by centrifugation at $14000 \times g$, dried by lyophilisation and stored at $4 \text{ }^\circ\text{C}$.

Not-imprinted polymers (nanoNIPs) were prepared in the same experimental conditions in terms of composition of the polymerization mixture and polymerization time but using glass-beads functionalized with diclofenac as solid phase [41].

5.2.5 Determination of nanoMIPs size and charge

Hydrodynamic particle size and zeta potential were measured with a ZetaView® Nanoparticle Tracking Analyzer PMX-120, (Analytik, Cambridge, UK) using a laser source at 488 nm . Solid samples of each nanoMIPs were dissolved to the working dilution with ultrapure water under sonication. pH was adjusted with HCl 0.1 M , and about 2 mL of sample immediately injected in the analyzer. Results are the average of three distinct measurements made at $25.5 \pm 0.1 \text{ }^\circ\text{C}$.

5.2.6 Atomic force microscopy of nanoMIPs

Borosilicate glass slides, $10 \times 10 \text{ mm}$, were washed with 'piranha' solution (98% sulphuric acid + 30% hydrogen peroxide, 3+1 v/v. Caution! It reacts violently with organic materials) for 10 min, rinsed with ultrapure water, dried under nitrogen and immersed overnight in a 1% v/v solution of APTMS in dry toluene. The aminated slides were washed with ethanol and ultrapure water and covered with an adequate volume of MES buffer (50 mM , pH 4.7) containing 1 mg mL^{-1} of NHS-activated nanoMIPs (see below), incubated at room temperature overnight, rinsed with ultrapure water and dried under nitrogen.

The Atomic Force Microscopy imaging was performed with a Park System XE-100 microscopes (Park Systems Europe GmbH, Mannheim, Germany) in non-contact mode (scan rate 0.4 Hz) using ACTA-10M cantilevers (Applied Nano Structures, Mountain View, USA).

5.2.7 Coupling of nanoMIPs to glass beads

In 4-mL glass vials 1 mg of nanoMIPs were dissolved under sonication in 1 mL of MES buffer (50 mM , pH 4.7), 8 mg of NHS (0.069 mmol) and 21.5 mg of EDC (0.138 mmol) were added and the solutions incubated at room temperature for 60 min. Then, they were transferred in 10-mL flasks containing 1 g of aminated glass beads. The suspensions were incubated at room temperature overnight, filtered on $0.22 \text{ }\mu\text{m}$ nylon membranes, washed with ultrapure water, rinsed twice

with acetone, dried under vacuum at room temperature and stored in the dark at 4 °C.

5.2.8 Protein determination

The protein determination was carried out by Bradford assay method. Briefly, 150 µL of protein sample was added to 150 µL of protein assay reagent in polystyrene microplates (12x8 wells, flat bottom, VWR International, Milan, Italy). After shaking for 10 s the absorbance was read at 450 and 595 nm. Concentrations were calculated from a calibration graph covering the 0.5-50 µg mL⁻¹ range of protein diluted in same phosphate buffer plotting the ratio A₅₉₅/A₄₅₀ vs. the concentration [42].

5.2.9 Determination of binding properties

To measure binding isotherms, about 40 mg of glass beads supporting nanoMIPs were exactly weighed in 4 mL flat bottom amber glass vials. Then, 1.0 mL of phosphate buffer (20 mM, pH 7.4) containing increasing amounts of protein ranging from 0.5 to 50 µg was added. The vials were incubated for 2 hours at room temperature under continuous agitation on a horizontal rocking table. Then, the solutions were filtered on 0.22 µm nylon membranes and the free amounts of target protein were measured by Bradford assay. Each experimental point was assessed as the average of two repeated measures.

Binding parameters were calculated by using SigmaPlot 12 (Systat Software Inc., Richmond, CA, USA). Non-linear least square fitting was applied to the averaged experimental data. Binding isotherm parameters were calculated by using a Langmuir binding isotherm model.

The binding selectivity, α , was calculated as:

$$\alpha = \frac{K_{eq}Protein}{K_{eq}Rabbit\ IgG}$$

where K_{eq} (Rabbit IgG) and K_{eq} (protein) are the equilibrium binding constants calculated for Rabbit IgG and any other protein, respectively.

5.3 RESULTS AND DISCUSSIONS

In order to investigate the effect of different cross-linkers in IgG-imprinted nanoMIPs, in the pre-polymerization mixtures BIS was replaced with other similar cross-linkers: N,N'-ethylene dimethacrylamide (EDAM), N,O-bis-methacryloylethanolamine (NOBE), ethylene glycol dimethacrylate (EDMA) and glycerol dimethacrylate (GDMA), without changing the molar proportions with functional monomers and using the same persulfate/TEMED-induced radical polymerization protocol in water at room temperature.

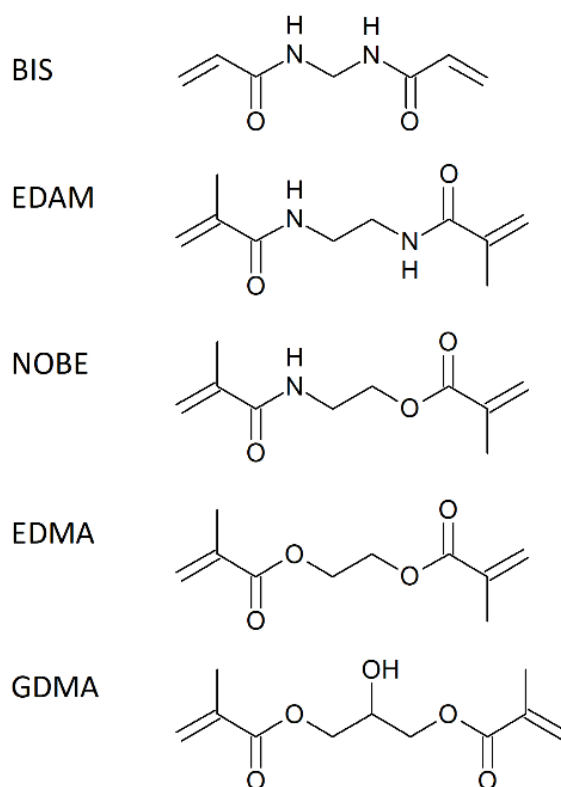


Figure 5-1 - The five crosslinker used

After gel filtration, centrifugation and drying, nanoMIPs were collected as white solids, with yields calculated with respect to the amount of monomers in the polymerization mixtures of 15-18% (1-1.2 mg). When dissolved in water, nanoMIPs gave transparent and colourless solutions, without any perceivable turbidity. Nanoparticles composition can be influenced by the different reactivity of the monomers, as well as the effective degree of crosslinking, but, because of the limited quantity of nanoparticles obtained, no attempts were made to establish the effective degree of crosslinking. Therefore, as a first approximation, we assume that it does not vary significantly between the different polymers.

5.3.1 Size and charge of nanoMIPs

In the table 5-1 are reported, for each nanoMIPs, the measured properties of ζ potential, polydispersity index (PDI), and hydrodynamic diameter measured through a NTA instrument.

Table 5-1 - Hydrodynamic diameter (dp) \pm s.d., relative increase (swelling capacity) of the nanoparticle volume between pH 7 and pH 3 (dV), polydispersity index (PDI), zeta potential (ζ) and absolute difference of zeta potential between pH 3 and pH 7 ($\Delta\zeta$) measured for nanoMIPs

Cross-linker	dp (nm)			PDI		ζ , mV		
	pH 3	pH 7	ΔV	pH 3	pH 7	pH 3	pH 7	$\Delta\zeta$
BIS	171 \pm 83	129 \pm 66	2.34	0.24	0.26	+7.7	-23.9	31.6
EDAM	189 \pm 94	169 \pm 84	1.40	0.25	0.25	+10.4	-8.3	18.7
NOBE	186 \pm 87	148 \pm 72	1.98	0.22	0.24	+15.1	-18.0	33.1
EDMA	158 \pm 79	140 \pm 73	1.44	0.25	0.27	+1.0	-22.2	23.2
GDMA	147 \pm 77	129 \pm 71	1.48	0.27	0.30	+10.6	-7.4	18.0

Acrylic acid was used as charged functional monomer, thus nanoMIPs can be seen as charged polyelectrolytes at neutral pH. This is confirmed by ζ potential measurements, where at pH 7 all the nanoMIPs show a net negative potential, with ζ values between -7.4 mV (GDMA) and -23.9 mV (BIS), while at pH 3, in more acidic conditions where carboxyls are fully protonated, ζ turns positive, with values between +1.0 mV (EDMA) and +15.1 (NOBE). The little values of ζ potential in both the conditions mean the possibility for the nanoMIPs to aggregate themselves. In figure 5-2 they are graphical reported these values.

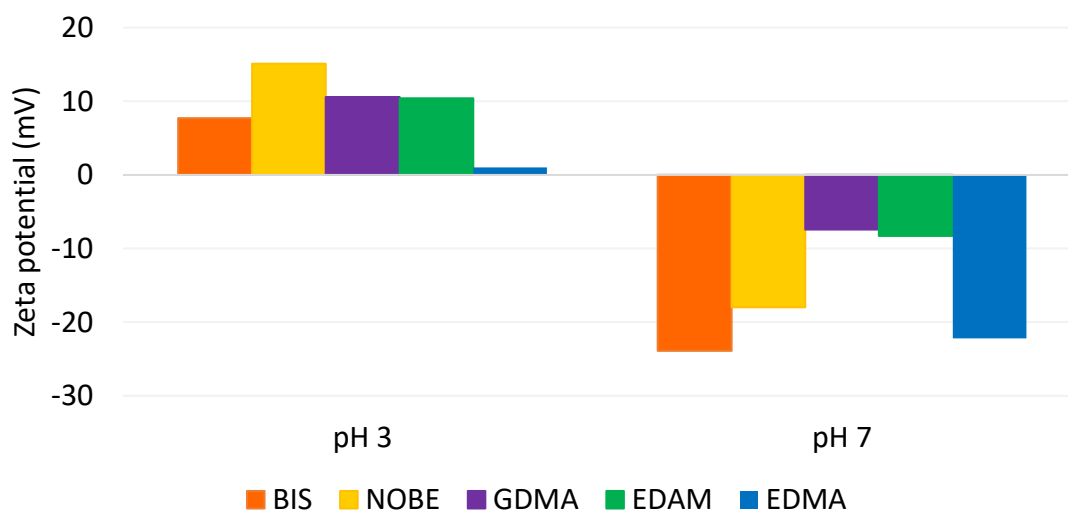


Figure 5-2 - Zeta potential for the five nanoMIPs in the two pH conditions

The hydrodynamic diameter, d_p , measured by laser nanoparticle tracking at pH 7, shows nanoparticles with average diameters just over a hundred nm, ranging from 129 nm (BIS) to 169 nm (EDAM), and with polydispersity index between 0.24 (NOBE) and 0.30 (GDMA), corresponding to moderately polydispersed nanoparticles. In the figure 5-3 are graphically reported the diameters of the nanoparticles. In more acidic environment, at pH 3, the formation of aggregates larger than 1 μm (instrumental limit of the particle tracker set-up), was indirectly observed, because the nanoparticles count fell by two orders of magnitude from 10^5 to 10^3 . About the fraction of nanoparticles remained in solution, the polydispersity index remains essentially constant, but diameters increase markedly, ranging from 147 nm (GDMA) to 189 nm (EDAM). These results show that in the solid phase synthesis the cross-linker structure marginally affect the dimensions of the resulting nanoparticles, which are probably mainly controlled by the formation of dangling long chains of monomers, some or most not cross-linked. Anyway cross-linker in some manner is yet capable of influencing nanoMIP flexibility. In fact, while nanoparticles containing BIS or NOBE are able to double their volume from pH 7 to pH 3, nanoparticles containing EBIS, EDMA or GDMA swell significantly less. It must be noted that nanoparticles swelling ability does not seem to be related to the binding properties (see the section 5.3.3 for experimental binding results), as BIS- and GDMA-based nanopolymers show comparable binding constants but very different swelling ability from pH 7 to pH 3. It is also noteworthy that the absolute difference in the ζ values measured between pH 7 and pH 3 is proportional to the swelling ability of the nanoparticles. This is not unexpected because as the volume changes, the surface charge density changes proportionally (whatever its sign), equally affecting the resulting $\Delta\zeta$ potential.

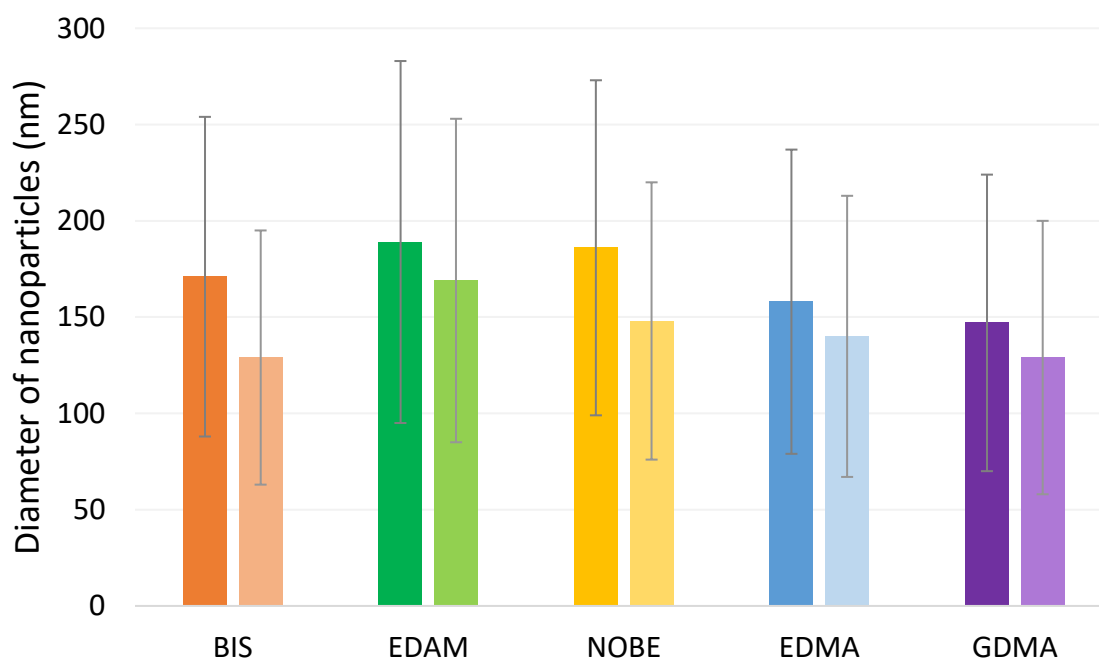


Figure 5-3 - Variation of the hydrodynamic diameter of the nanoparticles for the five nanoMIPs influenced by pH condition. pH 3 = dark color, pH 7 = light color

5.3.2 AFM imaging of nanoMIPs

The results obtained by laser nanoparticle tracking are confirmed by atomic force microscopy performed onto nanoMIPs covalently grafted onto aminosilanized glass slides. NanoMIPs were covalently grafted onto the glass slides at pH 4.7, in conditions within the pH jump covered by the tracking measurements (from pH 7 to pH 3), thus the formation of these structures is likely to be due to grafting of clustered nanoparticles stabilized by electrostatic interactions. In the follow table 5.2 are reported the image for all five polymers obtained at higher resolution (x25) on an area of 2 x 2 μm .

The preliminary images performed on relatively large area of 10 x 10 μm show that the glass surface is randomly covered with what seems to be sparse clusters of nanoparticles. The imaging of the clusters in high resolution shows an overall shape rather irregular, with an approximate size of some μm^2 and with thickness of hundreds of nm, apparently composed of several tightly packed globular objects with a slightly wrinkled surface and with individual diameters comparable to those measured by nanoparticles laser tracking, therefore compatible with an aggregate of nanoparticles. There isn't visible difference between the different types of nanoMIPs. This means that the crosslinker has not an influence on the morphology of the nanoparticles.

A further evidence of nanoparticles clustering induced by electrostatic interactions comes from imaging of deposited nanoMIPs at higher ionic strength (0.1 M⁻¹ NaCl). In this case, clusters are significantly larger for all the nanoparticles examined, often exceeding dimensions of 2 x 2 μm , even if their height with respect to the underlying glass surface does not seem to grow proportionally.

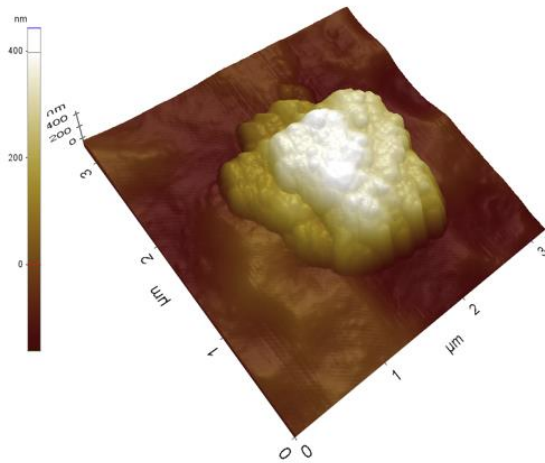


Figure 5-4 - EBIS

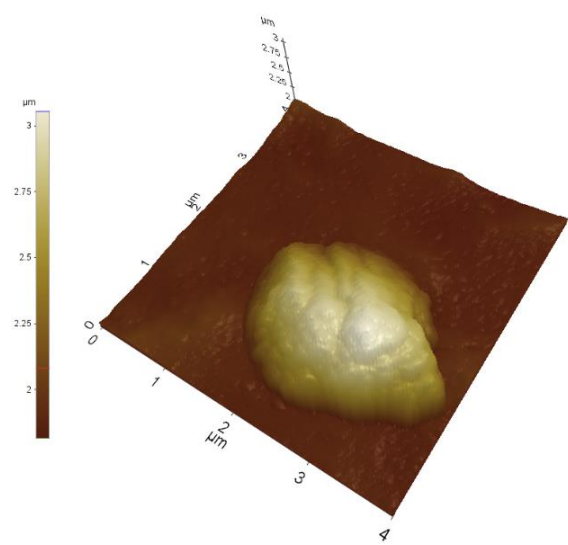


Figure 5-5 - NOBE

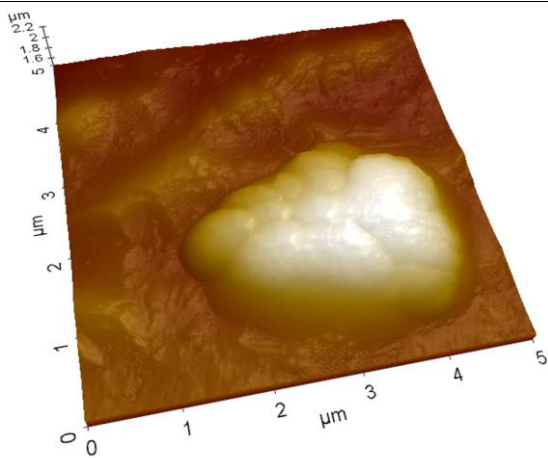


Figure 5-6 - BIS

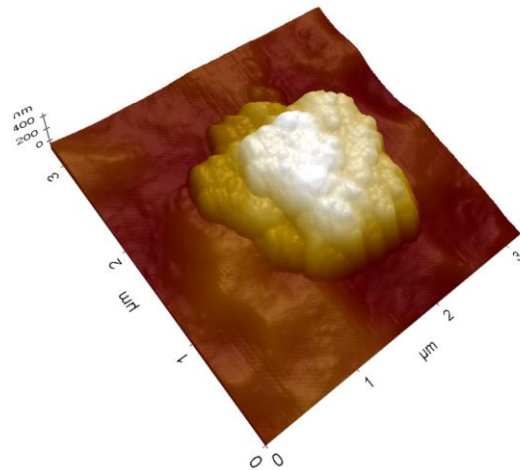


Figure 5-7 - EDAM

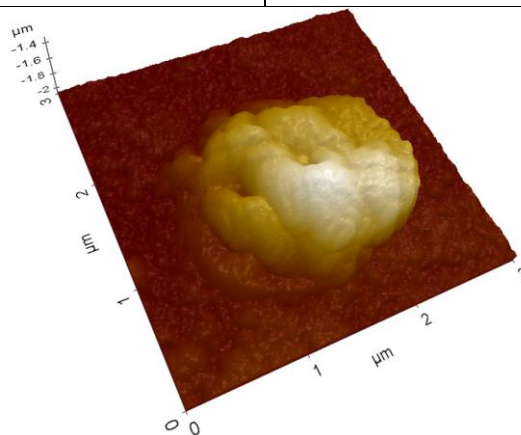


Figure 5-8 - GDMA

Table 5-2 - AFM images for the different five polymers nanoMIPs. It is possible observe only aggregates of nanoparticles and no single nanoparticles

5.3.3 Binding properties of nanoMIPs

In the traditional molecular imprinting techniques (bulk, suspension/emulsion, etc.) BIS is very little used and the cross-linker constitutes up to 80% molar of the polymerization mixture, thus exerting a deep effect not only on the morphology of the polymer and its bulk properties, but also on the binding properties [43-45]. On the contrary, in SPPS technique BIS is the preferred cross-linker, and in the pre-polymerization mixture it is added in a much more limited amount, practically never more than 3% by moles. Consequently, it is to be expected that the effect on molecular recognition properties by the cross-linker is limited, and that the presence of structurally different cross-linkers is not able to affect these properties.

In the table 5-3 are reported the equilibrium binding constants measured in phosphate buffer (20 mM, pH 7.4) for RIgG, BIgG, BSA and LZM on RIgG-imprinted (nMIP) and not imprinted (nNIP, aka nMIP imprinted for the diclofenac molecules) nanoparticles supported onto glass beads.

Table 5-3 - K_{eq} values ($M^{-1} \times 10^6$) ± 1 s.e

Crosslinker		RIgG	BIgG	BSA	LZM
BIS	nMIP	16.0 \pm 1.3	3.5 \pm 0.4	2.2 \pm 0.3	1.7 \pm 0.3
	nNIP	1.3 \pm 0.3	3.4 \pm 0.7	1.0 \pm 0.2	0.6 \pm 0.2
EDAM	nMIP	8.8 \pm 1.9	3.3 \pm 0.8	2.1 \pm 0.5	2.3 \pm 0.6
	nNIP	1.6 \pm 0.3	2.8 \pm 0.9	0.3 \pm 0.2	1.3 \pm 0.2
NOBE	nMIP	15.9 \pm 2.5	6.2 \pm 1.2	0.6 \pm 0.3	0.2 \pm 0.2
	nNIP	2.2 \pm 0.5	1.7 \pm 0.1	0.3 \pm 0.1	0.2 \pm 0.1
EDMA	nMIP	3.4 \pm 0.7	2.4 \pm 0.4	1.4 \pm 0.4	0.3 \pm 0.1
	nNIP	1.2 \pm 0.4	1.6 \pm 0.4	0.9 \pm 0.2	0.1 \pm 0.0
GDMA	nMIP	12.8 \pm 1.5	4.3 \pm 1.0	1.8 \pm 0.3	1.4 \pm 0.3
	nNIP	1.1 \pm 0.3	1.8 \pm 0.5	0.6 \pm 0.2	0.6 \pm 0.0

Surprisingly, the determination of the equilibrium binding constant, K_{eq} , by equilibrium partition experiments shows a distinctly different situation. In fact, all the cross-linker used for the imprinting of RIgG gives nanoMIPs with K_{eq} around $10^7 M^{-1}$, with the remarkable exception of EDMA, which gives a significantly lower value of $3.4 \times 10^6 M^{-1}$. In comparison, the corresponding nanoNIPs, prepared by SPPS with diclofenac as template, show K_{eq} with values significantly lower than the values for the corresponding nanoMIPs and indistinguishable from each other (t-test: $\alpha=0.05$, $n=10$, $t<2.101$).

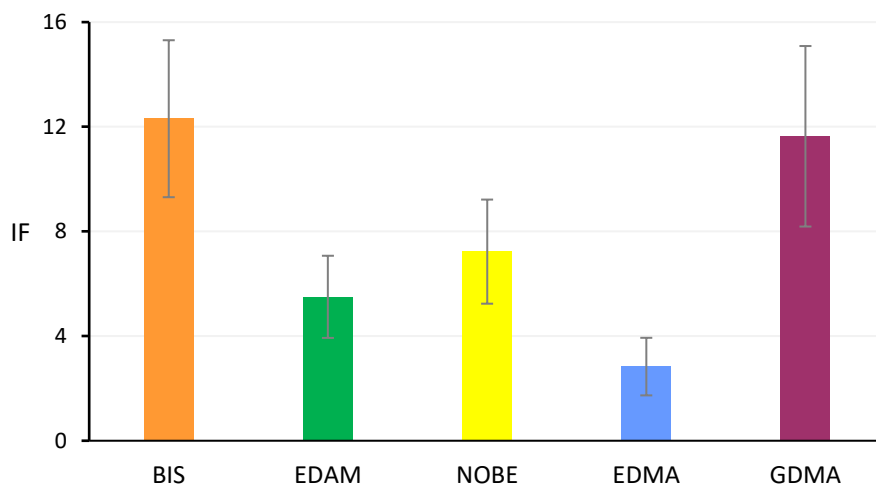


Figure 5-9 - Imprinting factor for the different five polymers nanoMIPs calculated on the binding capability of the correspondent nanoMIP

The differing values of K_{eq} obtained for each nanoMIP have an obvious influence on the imprinting factor (IF) that is an estimate of how much the binding affinity increases for an imprinted polymer respect to a not imprinted one of identical composition. In Figure 5-9 all five nanoMIPs show IF values higher than unity, confirming the success of the SPPS technique in the imprinting of RIgG. However, while nanoMIPs containing BIS and GDMA show IF values higher than 10 (BIS: 12.3 ± 3.0 , GDMA 11.6 ± 3.5), corresponding to a very strong imprinting effect, the others show markedly lower IF values (EDAM: 5.5 ± 1.6 , NOBE: 7.2 ± 2.0), demonstrating that the choice of right cross-linker is important to achieve an efficient SPPS process, regardless of whether the cross-linker itself is present in the pre-polymerization mixture in very limited quantities, compared to the other monomers. It should be noted that the GDMA-based nanoMIPs are to be considered structurally more complex than the other nanoMIPs, as they are composed of an almost equimolar mixture of two different cross-linkers, respectively glycerol 1,2- and 1,3-dimethacrylate. However, the resulting nanoMIP does not appear to behave significantly differently from other nanoMIPs, except, of course, for those based on EDMA. It is also noteworthy that the polymer with the lowest IF value (2.8 ± 1.1) contains EDMA, which represents the predominant cross-linker used to prepare imprinted polymers with the traditional approaches. This fact is a strong evidence of how the SPPS technique differs from the other molecular imprinting approaches, and how it is necessary to paid attention to transfer pre-polymerization mixtures formulations from one approach to another without a careful preliminary evaluation.

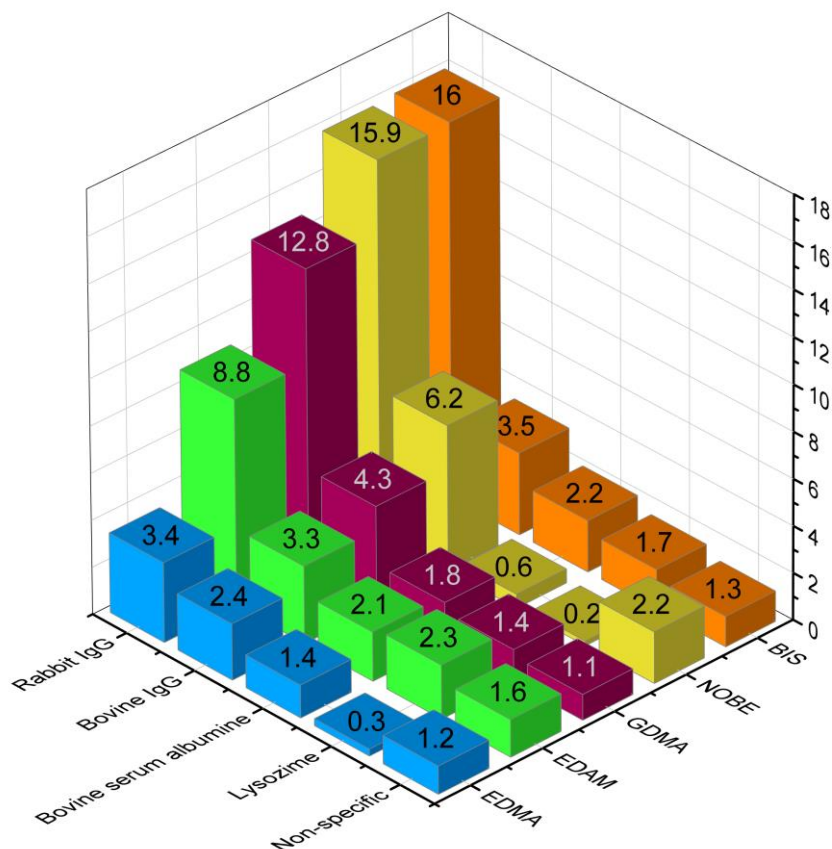


Figure 5-10 - K_{eq} ($10^6 M^{-1}$) values of nanoMIPs binding for the Rabbit IgG, Bovine IgG, BSA, Lysozyme and the non-specific binding of the rabbit IgG on the correspondent NIP

In addition to the magnitude of the binding constant and imprinting factor, a third essential parameter for evaluating the molecular recognition properties of nanoMIPs is binding selectivity, α . In this work we evaluated the selectivity of Rabbit IgG-imprinted nanoMIPs towards a structurally very similar protein such as bovine IgG, a protein structurally different but of similar isoelectric point, bovine serum albumin (BSA), and a protein of different structure and isoelectric point such as hen egg lysozyme (LZM).

The values in Figure 5-10 show that all the nanopolymers characterized by high affinity ($K_{eq} \sim 10^7 M^{-1}$) are selective towards the template RIgG, with a limited but substantial recognition ($0.2 \leq \alpha \leq 0.4$) towards BIgG, confirming the results reported in literature for human IgG-imprinted nanoMIPs [31]. This limited recognition can be explained on the basis of the shared presence in the IgG structure of the Fc fragment, which differs little between proteins of different species [4]. As a template Rabbit IgG is randomly grafted on the surface of the glass beads, and nanoMIPs produced by SPPS will have molecular recognition properties towards different parts of the template structure. Some will have binding sites recognizing the Fc fragment, common to IgG from different species, while others will recognize other portions of the protein, which are typical for IgG of a particular species. Therefore, during the rebinding of BIgG, some nanoMIPs will preferentially bind the Fc fragment, regardless of its origin (rabbit or bovine),

while others, more selective, will not be able to bind the BIgG. Thus, the resulting binding will be an average between the full (Fc-binding nanoMIPs) and the weak (non-Fc-binding nanoMIPs) recognition of Bovine IgG.

On the contrary, because of the low affinity resulting in a limited imprinting factor, with EDMA-based nanoMIPs RIgG and BIgG are recognized almost in the same way, confirming a substantial absence of selectivity. It must be noted that the low values of K_{eq} measured for EDMA-based nanoMIPs ($2.4 \pm 0.4 \times 10^6 \text{ M}^{-1}$) and nanoNIPs ($1.6 \pm 0.4 \times 10^6 \text{ M}^{-1}$) are statistically indistinguishable from each other (t-test: $\alpha=0.05$, $n=10$, $t=1.414$). Therefore, in this case the binding to BIgG cannot be attributed for certain to the presence of imprinted binding sites.

Concerning BSA and LZM, as these proteins are very different from IgG, for all the nanopolymers the molecular recognition results very limited, lower than that observed for BIgG. However, it should be noted that the binding behaviour presents significant differences, since for BIS-, EDMA- and GDMA-based nanopolymers the recognition follows the order of similarity, i.e. BIgG > BSA > LZM, while in the case for EDAM- and NOBE-based nanopolymers it is different, as the first recognizes the three proteins in the same way, while for the second, BSA and LZM show almost no recognition, confirming that small changes in the nature of the cross-linker – i.e. the replacement of an amide group with an ester group (NOBE vs. EDAM) – exert a significant effect on the binding properties of the nanoMIPs.

A two-way ANOVA was conducted on the K_{eq} values, for the type of nanoMIPs and the different proteins. For the difference between the five nanoMIPs, we obtained a Fp value lower than the F value ($1.570 < F_{(4, 16)} 3.007$), that means that the behaviour of the five nanoMIPs is comparable. For the proteins, it confirmed the difference of the bovine IgG recognition on the non-specific binding ($5.03 < F_{(3, 12)} 3.49$), and the absence of difference between BSA and LZM to the nonspecific binding ($0.64 < F_{(2, 8)} 4.46$).

5.4 CONCLUSIONS

The results reported in this work confirm the relevance of the cross-linker structure in the SPPS technique. Although present in minimal quantities compared to the other monomers in the pre-polymerization mixture, they are able to influence the binding affinity and selectivity of protein-imprinted nanoparticles through subtle differences in their structure, *i.e.* the replacement of an amide group with an ester group (NOBE vs. EDAM), the presence of a hydroxyl group (GDMA vs. EDMA) or the number of atoms in the molecular bridge (BIS vs. EDAM). The experimental results currently available are not sufficient to advance quantitative hypotheses on the relationship between binding properties of nanoMIPs and structural properties of cross-linkers, but it is plausible that a further expansion of the number of cross-linkers tested could provide robust indications on the type of molecular structures optimal to obtain nanoMIPs with high affinity and selectivity for the target molecule.

Also, we obtained several nanoMIPs with the capability to selectively bind the template molecule for rabbit IgG and able to distinguish protein with different structure than IgG. The capability to discriminate IgG from other animal species is low, and is possible an application of this nanoMIPs in a “protein A substitution system”.

5.5 BIBLIOGRAPHY

- [1] T.S. Bedwell, N. Anjum, Y. Ma, J. Czulak, A. Poma, E. Piletska, M.J. Whitcombe, S.A. Piletsky. New protocol for optimisation of polymer composition for imprinting of peptides and proteins. *RSC Adv*, **2019**, *9*, 27849-27855, doi: 10.1039/c9ra05009d.
- [2] F. Canfarotta, A. Poma, A. Guerreiro, S. Piletsky. Solid-phase synthesis of molecularly imprinted nanoparticles. *Nature Protocols*, **2016**, *11*, 443-455, doi: 10.1038/nprot.2016.030.
- [3] C.A. Mourão, F. Bokeloh, J. Xu, E. Prost, L. Duma, F. Merlier, S.M. Bueno, K. Haupt, B.T. Bui. Dual-oriented solid-phase molecular imprinting: toward selective artificial receptors for recognition of nucleotides in water. *Macromolecules*, **2017**, *50*, 7484-7490, doi: 10.1021/acs.macromol.7b01782.
- [4] G. Vidarsson, G. Dekkers, T. Rispens. IgG subclasses and allotypes: from structure to effector functions. *Front Immunol*, **2014**, *20*, 520, doi: 10.3389/fimmu.2014.00520.
- [5] S.K. Vashist, P.B. Luppá, L.Y. Yeo, A. Ozcan, J.H.T. Luong. Emerging technologies for next-generation point-of-care testing. *Trends Biotechnol*, **2015**, *33*, 692-705, doi: 10.1016/j.tibtech.2015.09.001.
- [6] C. Dincer, R. Bruch, A. Kling, P.S. Dittrich, G.A. Urban. multiplexed point-of-care testing - xPOCT. *Trends Biotechnol*, **2017**, *35*, 728-742, doi: 10.1016/j.tibtech.2017.03.013.
- [7] P. Sharma, J.P. Allison. Immune checkpoint targeting in cancer therapy: toward combination strategies with curative potential. *Cell*, **2015**, *161*, 205-14, doi: 10.1016/j.cell.2015.03.030.
- [8] A. Beck, L. Goetsch, C. Dumontet, N. Corvaia. Strategies and challenges for the next generation of antibody-drug conjugates. *Nat Rev Drug Discov*, **2017**, *16*, 315-337, doi: 10.1038/nrd.2016.268.
- [9] T. Lammers, S. Aime, W.E. Hennink, G. Storm, F. Kiessling. Theranostic nanomedicine. *Acc Chem Res*, **2011**, *44*, 1029-38, doi: 10.1021/ar200019c.
- [10] F.S. Felix, L. Angnes. Electrochemical immunosensors - a powerful tool for analytical applications. *Biosens Bioelectron*, **2018**, *15*, 470-478, doi: 10.1016/j.bios.2017.11.029.

- [11] A. Jones, L. Dhanapala, R.N.T. Kankanamage, C.V. Kumar, J.F. Rusling. Multiplexed immunosensors and immunoarrays. *Anal Chem*, **2020**, *92*, 345-362, doi: 10.1021/acs.analchem.9b05080.
- [12] N. Delaunay-Bertoncini, V. Pichon, M.C. Hennion. Experimental comparison of three monoclonal antibodies for the class-selective immunoextraction of triazines. Correlation with molecular modeling and principal component analysis studies. *J Chromatogr A*, **2003**, *999*, 3-15, doi: 10.1016/S0021-9673(03)00425-4.
- [13] E.L. Rodriguez, S. Poddar, S. Iftekhar, K. Suh, A.G. Woolfork, S. Ovbude, A. Pekarek, M. Walters, S. Lott, D.S. Hage. Affinity chromatography: A review of trends and developments over the past 50 years. *J Chromatogr B Analyt Technol Biomed Life Sci*, **2020**, *1157*, 122332, doi: 10.1016/j.jchromb.2020.122332.
- [14] E.J. Cohn, L.E. Strong, W.L. Hughes, D.J. Mulford, J.N. Ashworth, M. Melin, H.L. Taylor. Preparation and properties of serum and plasma proteins. iv. a system for the separation into fractions of the protein and lipoprotein components of biological tissues and fluids. *Journal of the American Chemical Society*, **1946**, *68*, 459-475, doi: 10.1021/ja01207a034.
- [15] K. Huse, H.J. Böhme, G.H. Scholz. Purification of antibodies by affinity chromatography. *J Biochem Biophys Methods*, **2002**, *51*, 217-31, doi: 10.1016/S0165-022X(02)00017-9.
- [16] A.C.A. Roque, C.S.O. Silva, M.Â. Taipa. Affinity-based methodologies and ligands for antibody purification: Advances and perspectives. *Journal of Chromatography A*, **2007**, *1160*, 44-55, doi: 10.1016/j.chroma.2007.05.109.
- [17] P. Gagnon. Technology trends in antibody purification. *J Chromatogr A*, **2012**, *1221*, 57-70, doi: 10.1016/j.chroma.2011.10.034.
- [18] S. Ashlyüce, L. Uzun, R. Say, A. Denizli. Immunoglobulin G recognition with Fab fragments imprinted monolithic cryogels: Evaluation of the effects of metal-ion assisted-coordination of template molecule. *Reactive & Functional Polymers*, **2013**, *73*, 813-820, doi: 10.1016/j.reactfunctpolym.2013.03.009.
- [19] I. Perçin, N. Idil, A. Denizli. Molecularly imprinted poly(N-isopropylacrylamide) thermosensitive based cryogel for immunoglobulin G purification. *Process Biochemistry*, **2019**, *80*, 181-189, doi: 10.1016/j.procbio.2019.02.001.17.
- [20] A. Tretjakov, V. Syritski, J. Reut, R. Boroznjak, O. Volobujeva, A. Öpik. Surface molecularly imprinted polydopamine films for recognition of

- immunoglobulin G. *Microchimica Acta*, **2013**, *15*, 180, 1433 – 1442, doi: 10.1007/s00604-013-1039-y.
- [21] R. Bai, Y. Sun, Me. Zhao, Z. Han, J. Zhang, Y. Sun, W. Dong, S. Li. Preparation of IgG imprinted polymers by metal-free visible-light-induced ATRP and its application in biosensor. *Talanta*, **2021**, *226*, 122160, doi: 10.1016/j.talanta.2021.122160.
- [22] F. Torrini, F. Battaglia, P. Palladino, S. Scarano, M. Minunni. Imprinted biopolymers as green abiotic route in immunoglobulin affinity plasmonic sensing. *Biosensors and Bioelectronics*, **2022**, *217*, 114706, doi: 10.1016/j.bios.2022.114706.
- [23] M. Cui, Y. Gong, M. Du, K. Wang, T. Li, X. Zhu, S. Wang, X. Luo. An antifouling electrochemical biosensor based on a protein imprinted hydrogel for human immunoglobulin G recognition in complex biological media, *Sensors and Actuators B: Chemical*, **2021**, *337*, 129820, doi: 10.1016/j.snb.2021.129820.
- [24] A. Nematollahzadeh, P. Lindemann, W. Sun, J. Stute, D. Lütkemeyer, B. Sellergren. Robust and selective nano cavities for protein separation: an interpenetrating polymer network modified hierarchically protein imprinted hydrogel. *Journal of chromatography A*, **2014**, *1345*, 154-63, doi: 10.1016/j.chroma.2014.04.030.
- [25] J. Zhou, N. Gan, T. Li, F. Hu, X. Li, L. Wang, L. Zheng. A cost-effective sandwich electrochemiluminescence immunosensor for ultrasensitive detection of HIV-1 antibody using magnetic molecularly imprinted polymers as capture probes. *Biosensors and Bioelectronics*, **2014**, *54*, 199-206, doi: 10.1016/j.bios.2013.10.044.
- [26] A. Axin Liang, B. Huipeng Hou, C. Shanshan Tang, D. Liquan Sun, E. Aiqin Luo. An advanced molecularly imprinted electrochemical sensor for the highly sensitive and selective detection and determination of Human IgG. *Bioelectrochemistry*, **2021**, *137*, 107671, doi: 10.1016/j.bioelechem.2020.107671.
- [27] D. Yin, M. Ulbrich., Antibody-imprinted membrane adsorber via two-step surface grafting. *Biomacromolecules*, **2013**, *14*, 4489-4496, doi: 10.1021/bm401444y.
- [28] S. Schwark, W. Sun, J. Stute, D. Lütkemeyer, M. Ulbricht, B. Sellergren. Monoclonal antibody capture from cell culture supernatants using epitope imprinted macroporous membranes. *RSC Advances*, **2016**, *6*, 53162-53169, doi: 10.1039/C6RA06632A.

- [29] Y. Saylan, R. Uze, L. Uzun, A. Denizli. Surface imprinting approach for preparing specific adsorbent for IgG separation. *Journal of biomaterials science, Polymer edition*, **2014**, *25*, 1-14, doi: 10.1080/09205063.2014.911569.
- [30] W. Shi, K.B. Li, S.Q. Zhang, H.L. Lu, R.H. Shi, Y.G. Zhan, Z.L. Tong, D.M. Han. Improvement of adsorption selectivity of ion-exchange chromatography through the double-recognition mode. *Journal of Chemical & Engineering Data*, **2019**, *64*, 5385-5397, doi: 10.1021/acs.jced.9b00594.
- [31] E. Moczko, A. Guerreiro, C. Cáceres, E. Piletska, B. Sellergren, S.A. Piletsky. Epitope approach in molecular imprinting of antibodies. *Journal of Chromatography B*, **2019**, *1124*, 1-6, doi: 10.1016/j.jchromb.2019.05.024.
- [32] S. Ambrosini, S. Beyazit, K. Haupt, B. Tse Sum Bui. Solid-phase synthesis of molecularly imprinted nanoparticles for protein recognition. *Chem Commun*, **2013**, *49*, 6746-6748, doi: 10.1039/C3CC41701H.
- [33] A. Poma, A. Guerreiro, S. Caygill, E. Moczko, S. Piletsky. Automatic reactor for solid-phase synthesis of molecularly imprinted polymeric nanoparticles (MIP NPs) in water. *RSC Adv*, **2014**, *4*, 4203-4206, doi: 10.1039/C3RA46838K.
- [34] J. Xu, S. Ambrosini, E. Tamahkar, C. Rossi, K. Haupt, B. Tse Sum Bui. Toward a universal method for preparing molecularly imprinted polymer nanoparticles with antibody-like affinity for proteins. *Biomacromolecules*, **2016**, *17*, 345-53, doi: 10.1021/acs.biomac.5b01454.
- [35] J. Ashley, Y. Shukor, R. D'Aurelio, L. Trinh, T.L. Rodgers, J. Temblay, M. Pleasants, I.E. Tothill. Synthesis of molecularly imprinted polymer nanoparticles for α -casein detection using surface plasmon resonance as a milk allergen sensor. *ACS Sensors*, **2018**, *3*, 418-424, doi: 10.1021/acssensors.7b00850.
- [36] X. Feng, J. Ashley, T. Zhou, A. Halder, Y. Sun. Molecularly imprinted nanoparticles for inhibiting ribonuclease in reverse transcriptase polymerase chain reaction. *Analyst*, **2018**, *143*, 2750-2754, doi: 10.1039/C8AN00711J.
- [37] K. Smolinska-Kempisty, A. Guerreiro, J. Czulak, S. Piletsky. Negative selection of MIPs to create high specificity ligands for glycosylated haemoglobin. *Sensors and Actuators B: Chemical*, **2019**, *301*, 126967, doi: 10.1016/j.snb.2019.126967.
- [38] C. Cáceres, E. Moczko, I. Basozabal, A. Guerreiro, S. Piletsky. Molecularly imprinted nanoparticles (nanoMIPs) selective for proteins: optimization of

- a protocol for solid-phase synthesis using automatic chemical reactor. *Polymers*, **2021**, *13*, 314, doi: 10.3390/polym13030314.
- [39] S.S. Piletsky, E. Piletska, M. Poblocka, A. Macip, D.J.L. Jones, M. Braga, T.H. Cao, R. Singh, A.C. Spivey, E.O. Aboagye, S. Piletsky. Snapshot imprinting: rapid identification of cancer cell surface proteins and epitopes using molecularly imprinted polymers. *Nano Today*, **2021**, *41*, 101304, doi: 10.1016/j.nantod.2021.101304.
- [40] D.S. Meador, D.A. Spivak. Absolute configuration determination using enantiomeric pairs of molecularly imprinted polymers. *Organic letters*, **2014**, *16*, 1402-1405, doi: 10.1021/ol500173y.
- [41] A. Poma, A. Guerreiro, M.J. Whitcombe, E. Piletska, A.P.F. Turner, S. Piletsky. Solid-phase synthesis of molecularly imprinted polymer nanoparticles with a reusable template – “plastic antibodies”. *Adv Funct Mater*, **2013**, *2*, 2821-2827, doi: 10.1002/adfm.201202397.
- [42] T. Zor, Z. Selinger. Linearization of the Bradford protein assay increases its sensitivity: theoretical and experimental studies. *Anal Biochem*, **1996**, *236*, 302-308, doi: 10.1006/abio.1996.0171.
- [43] E.M.A. Dourado, C. Herdes, P.R.V. Tassel, L. Sarkisov. Molecular recognition effects in atomistic models of imprinted polymers. *Int J Mol Sci*, **2011**, *12*, 4781-4804, doi: 10.3390/ijms12084781.
- [44] S. Shoravi, G.D. Olsson, B.C. Karlsson, I.A. Nicholls. On the influence of crosslinker on template complexation in molecularly imprinted polymers: a computational study of prepolymerization mixture events with correlations to template-polymer recognition behavior and NMR spectroscopic studies. *Int J Mol Sci*, **2014**, *15*, 10622-10634, doi: 10.3390/ijms150610622.
- [45] K. Golker, B.C.G. Karlsson, G.D. Olsson, A.M. Rosengren, I. Nicholls. Influence of composition and morphology on template recognition in molecularly imprinted polymers. *Macromolecules*, **2013**, *46*, 1408-1414, doi: 10.1021/ma3024238.

6 THE USE OF THE MIMIC TEMPLATE IN THE SOLID-PHASE SYNTHESIS: THE EXAMPLE OF AN OCHRATOXIN A-IMPRINTED NANOMIP

6.1 INTRODUCTION

In classical imprinting methods such as the bulk synthesis, the presence in the final product of unwashed template molecules is an enormous problem. With the normal analytical use of the imprinted particles, the lattice structure can degrade, and an amount of the trapped template molecules is released at every use of the MIP particles. Historically, this has represented the principal limit to the MIP application in the solid-phase extraction. This phenomenon takes the name of “bleeding” [1, 2]. To overcome this problem, the technique of the “mimic template”, also known as “dummy template” [3-5], was introduced in bulk synthesis method. This technique consists into imprinting not the real template/target molecule itself, but one of its structural homologues. So, in the final MIP particles it is not the target substance that is trapped but a different one, so that the former does not pollute the analysis.

In the solid-phase polymerization the template molecules are not trapped in the final product, because all of them are moved away together with the silica microspheres after the synthesis, and for this reason the use of the mimic template may appear useless. But this technique allows achieving another advantage beside avoiding the bleeding phenomenon: limiting the use of expensive or dangerous templates. Indeed, in the case of dangerous target molecules, such as ochratoxin A, limiting their employment represents a security issue.

Ochratoxin A (OTA) is a mycotoxin with a potential carcinogenic effect, and it is an important and dangerous food-contaminant [6] with an enormous analytical interest. The individuation and the quantification of OTA in food samples is required by the law in several countries [7]. In literature a lot of studies about OTA-imprinted MIPs are present [8-10], with some of them leveraging the mimic template technique.

6.1.1 Aim of the work and objectives

The principal goal of this work was exploring the possibility to use the mimic template strategy also in the solid-phase synthesis and measuring the efficiency of this approach. Secondly, the focus was put on producing a nanoMIP against OTA. For this purpose, we selected a phenylalanine derivate as a mimic template, namely N-(4-chloro-1-hydroxy-2-naphthoylamido)-(L)-phenylalanine, shortened in CHNA-Phe. This type of structural homologue has a less toxic effect than OTA.

The principal responsible of the protein synthesis inhibition behavior of the mycotoxin is in the isocoumarin moiety [11]. This structure is different in CHNA-Phe with respect to OTA. This mimic template was previously successfully used for OTA-binding-MIPs in several works [8, 9]. All these works used the bulk synthesis to obtain the MIP.

The monomeric formulation was selected by a previous work of López-Puertollano et al. [9]. To evaluate the binding capability of the CHNA-Phe-imprinted nanoMIP, we measured the binding constant for the mimic template itself, and for the original OTA. Also, we measured the non-specific binding for each of the target substances with a nanoMIP imprinted for diclofenac with the same formulation.

6.2 EXPERIMENTAL

6.2.1 Materials

Glass beads were Spherglass-2429, with 70-100 μm average particle size (Potters, UK).

Acrylic acid (AA), 2-aminoethylmethacrylate hydrochloride (AEMA), 3-(aminopropyl)trimethoxysilane (APTMS), ammonium persulphate (APS), N,N'-diisopropylcarbodiimide (DIC), ethylenglycole methacrylate phosphate (EGMP), hexamethyldisilazane (HMDS), N-hydroxysuccinimide (NHS), N-isopropylacrylamide (NIPAm), N,N'-methylenN,N'-N,N'-methylen-bis-acrylamide (BIS), morpholinethansulphonic acid (sodium salt, MES), N-tertbutylacrylamide (TBAm) and N,N,N',N'-tetramethylethyldiamine (TEMED), N-(4-chloro-1-hydroxy-2-naphthoic acid) (CHNA), L-phenylalanine (Phe), N,N-dicyclohexylcarbodiimide were purchased by Sigma-Merck (Milan, Italy). Solvents and all other chemicals were purchased from Sigma-Merck (Milan, Italy). All the solvents were of HPLC grade, whereas all chemicals were of analytical grade.

The used water was ultra-purified in Purelab Prima System from Elga (Marlow, UK). Polymerization inhibitors in the monomers were removed by filtration through activated basic alumina.

CHNA-Phe and OTA stock solutions were prepared by dissolving 10 mg of the substance in 25 mL of methanol then stored in the dark at $-20\text{ }^{\circ}\text{C}$.

6.2.2 Glass beads amination

In a 100-mL round-bottomed flask, 25 g of glass beads was dispersed in 50 mL of 1 M aqueous NaOH and boiled for 1 h. Then, they were diluted with 50 mL of ultrapure water and filtered on a $0.22\text{ }\mu\text{m}$ nylon membrane. The glass beads were washed with 100 mL of 1 M aqueous HCl and with ultrapure water till neutrality. Then they were rinsed twice with acetone and dried at $60\text{ }^{\circ}\text{C}$ overnight.

The dried glass beads were transferred in a 1-L round-bottomed flask and dispersed in 50 mL of toluene, removing water by azeotropic distillation. Then, the flask was cooled to room temperature, 10 mL of APTMS was added, and the mixture let to react overnight. The glass beads were filtered on a $0.22\text{ }\mu\text{m}$ nylon membrane and washed with $3 \times 50\text{ mL}$ of toluene.

To end-cap the residual silanols, the glass beads were transferred in a 250-mL round-bottomed flask and dispersed in 50 mL of toluene, removing water by azeotropic distillation. Then, the flask was cooled to room temperature, 1 mL of HMDS was added to the dispersion and the mixture was let to react overnight. The end-capped glass beads, named "short-chain beads" (SC-beads) were filtered on a $0.22\text{ }\mu\text{m}$ nylon membrane, rinsed twice with acetone and dried at $60\text{ }^{\circ}\text{C}$ overnight.

After silanization, the amino groups available on the silanized glass beads surface were determined by Kaiser's method as 1,1 $\mu\text{mol/g}$ [12].

6.2.3 Synthesis of the OTA analog

The synthesis of the OTA analog N-(4-chloro-1-hydroxy-2-naphthoylamido)-(L)-phenylalanine (CHNA-Phe) reported in Figure 6-1, was developed utilizing the reaction between a primary amine and the N-hydroxysuccinimidyl derivative of a carboxylic acid according to the procedure previously reported in literature with minor modifications [8].

In a 250-mL round-bottom flask containing 500 mg (2.25 mmol) of CHNA dissolved into 50 mL of ice-cold anhydrous tetrahydrofuran, 271 mg (2.36 mmol) of NHS and 487 mg (2.36 mmol) of freshly crystallized N,N-dicyclohexylcarbodiimide were added in sequence. The mixture was stirred for 2 h at 4 °C, the obtained N,N-dicyclohexylurea was separated by filtration with a G4 Büchner funnel, and then rapidly added drop by drop under vigorous stirring in a solution of 1.12 g (6.75 mmol) of Phe dissolved in 50 mL of 0.1 M NaHCO_3 . The reaction mixture was stirred at room temperature overnight, then evaporated in a rotavapor. The residue was acidified to pH 2 with 0.1 M aqueous HCl, dispersed under sonication into 50 mL of ethylacetate and washed three times with 50 mL of acidified water. The organic layer was dried over anhydrous Na_2SO_4 and evaporated under a stream of air. The obtained raw product was recrystallized twice in absolute ethanol, giving the product as a white powder (648 mg, 78% yield), deemed pure by HPLC-MS with a mobile phase constituted by MeCN–AcOH, 99/1 v/v (eluent A) and H_2O –AcOH, 99/1 v/v (eluent B) in A + B gradient, from 1/9 (1 min) to 9/1 (6 min), then in isocratic conditions up to 7 min.

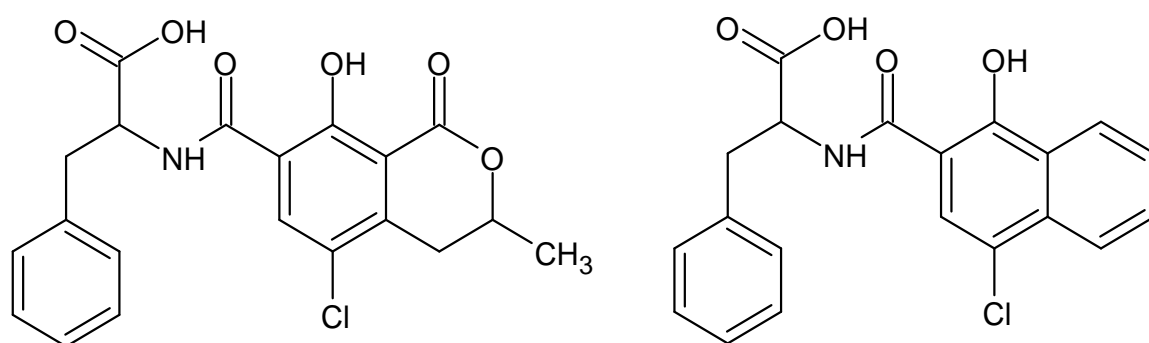


Figure 6-5-11 - The OTA (left) and CHNA-Phe (right) molecular structures

6.2.4 Template immobilization

In a 25-mL glass vial, 111 mg (0.300 mmol) of template was dissolved in 10 mL of DMF, 38 mg of NHS (0.330 mmol) and 52 μL of DIC (0.332 mmol) were added

and the solution incubated at 4 °C for 60 min. Then, it was transferred into a 50-mL vial containing 5 g of aminated glass beads. The mixture was incubated at room temperature overnight onto a horizontal roller, filtered on a 0.22 µm nylon membrane, washed with DMF and ultrapure water, rinsed twice with acetone, dried under vacuum at room temperature and stored in the dark at 4 °C.

6.2.5 Synthesis of the nanoMIPs

The polymerization mixtures were prepared according to the literature [9, 13] and to previous experiments performed within our research group. A pre-polymerization mixture was made in 100 mL of ultrapure water by mixing, under sonication, 1.1 µL of AA (0.016 mmol), 1 mg of AEMA (0.006 mmol), 33.6 mg of EGMP (0.16 mmol), 19 mg of NIPAm (0.17 mmol), 16.5 mg of TBAm (0.13 mmol, predissolved in 0.5 mL of ethanol) and 1 mg of BIS (0.0065 mmol). Then, 8 mL of mixture was added to 50-mL polypropylene SPE cartridges containing 5 g of template-functionalized glass beads. The cartridges were purged with N₂ for 5 min. 30 µL of TEMED and 500 µL of 30 mg mL⁻¹ aqueous solution of APS were added and the polymerization was carried out at room temperature for 1 h in a roller-equipped incubator. The supernatant was drained by vacuum aspiration, the dry cartridges were cooled to 4 °C and polymerization by-products and low-affinity nanoMIPs were washed away with 10×2 mL of ice-cold water. High-affinity nanoMIPs were collected by eluting the cartridges at room temperature with 5×3 mL hot water and 5×1 mL of 90% methanol/10% acetic acid v/v. The eluates were purified by gel-filtration in ultrapure water onto a 26 x 250 mm Sephadex G25 column. The nanoMIPs were isolated by centrifugation at 14000 x g, dried by lyophilisation and stored at 4 °C.

Non-imprinted polymers (nanoNIPs) were prepared in the same experimental conditions in terms of composition of the polymerization mixture and polymerization time but using glass-beads functionalized with diclofenac as solid phase.

6.2.6 Coupling of nanoMIPs to glass beads

In 4-mL glass vials, 1 mg of nanoMIPs was dissolved under sonication in 1 mL of MES buffer (50 mM, pH 4.7), 8 mg of NHS (0.069 mmol) and 21.5 mg of EDC (0.138 mmol) were added and the solutions incubated at room temperature for 60 min. Then, they were transferred in 10-mL flasks containing 1 g of aminated glass beads. The suspensions were incubated at room temperature overnight, filtered on 0.22 µm nylon membranes, washed with ultrapure water, rinsed twice with acetone, dried under vacuum at room temperature and stored in the dark at 4 °C.

6.2.7 HPLC method

Reverse-phase HPLC analysis was used for OTA and CHNA-Phe determination. The HPLC apparatus (Merck-Hitachi, Milan, Italy) was a LaChrom Elite system composed of a programmable binary pump L-2130, an auto-sampler L-2200, a fluorescence detector L-2480, provided with EZChrom Elite software for the instrumental programming, data acquisition and data processing. The used column was a 100 mm × 4.6 mm Chromolith RP-18 (Merck, Milan, Italy). The mobile phase was water/acetonitrile 50/50, acetic acid 1% (v/v). Elution was performed in isocratic conditions at a flow rate of 0.5 mL/min. The sample volume that was injected was 5 µL and the fluorescence wavelengths were: CHNA-Phe: $\lambda_{\text{ex}} = 350 \text{ nm}/\lambda_{\text{em}} = 416 \text{ nm}$; OTA: $\lambda_{\text{ex}} = 333 \text{ nm}/\lambda_{\text{em}} = 460 \text{ nm}$. Standard solutions between 5 and 80 ng/mL were prepared in the eluent immediately before use. The solutions were analyzed in triplicate and mean peak areas were plotted against standard concentration. The calibration plot was drawn by using a weighted linear regression (weight = 1/conc).

6.2.8 Determination of binding properties

To measure binding isotherms, about 40 mg of glass beads supporting nanoMIPs were exactly weighed in 4-mL flat bottom amber glass vials. Then, 1.0 mL of 20 mM buffer with different pH (from 4 to 8) containing increasing amounts of target molecule ranging from 0.5 to 10 µg was added. The vials were incubated for 2 h at room temperature under continuous agitation on a horizontal rocking table. Then, the solutions were filtered on 0.22 µm nylon membranes and the free amounts of target molecule were measured by HPLC-fluorescence analysis. Each experimental point was assessed as the average of two repeated measures.

Binding parameters were calculated by using SigmaPlot 12 (Systat Software Inc., Richmond, CA, USA). Non-linear least square fitting was applied to the averaged experimental data. Binding isotherm parameters were calculated by using a Langmuir binding isotherm model.

The binding selectivity, α , was calculated as:

$$\alpha = \frac{K_{\text{eq}} \text{OTA}}{K_{\text{eq}} \text{CHNA} - \text{phe}}$$

where $K_{\text{eq}} \text{OTA}$ and $K_{\text{eq}} \text{CHNA-Phe}$ are the equilibrium binding constants calculated for OTA and CHNA-Phe, respectively.

6.3 RESULTS AND DISCUSSIONS

6.3.1 Binding properties of the nanoMIP

To evaluate the possibility of using the strategy of the mimic template in the SPSS type of synthesis, we have measured the bindings of a CHNA-Phe-imprinted nanoMIP for the mimic template itself and for the original OTA. We have also tested different pH conditions for the rebinding experiments environment. The testing of different pH was performed to find the best rebinding conditions, because both the CHNA-Phe and OTA molecules present several polar atoms like oxygen and nitrogen that can modify binding in function of their protonation state. In Table 6-1 and in the Figure 6-2 the K_{eq} values are reported.

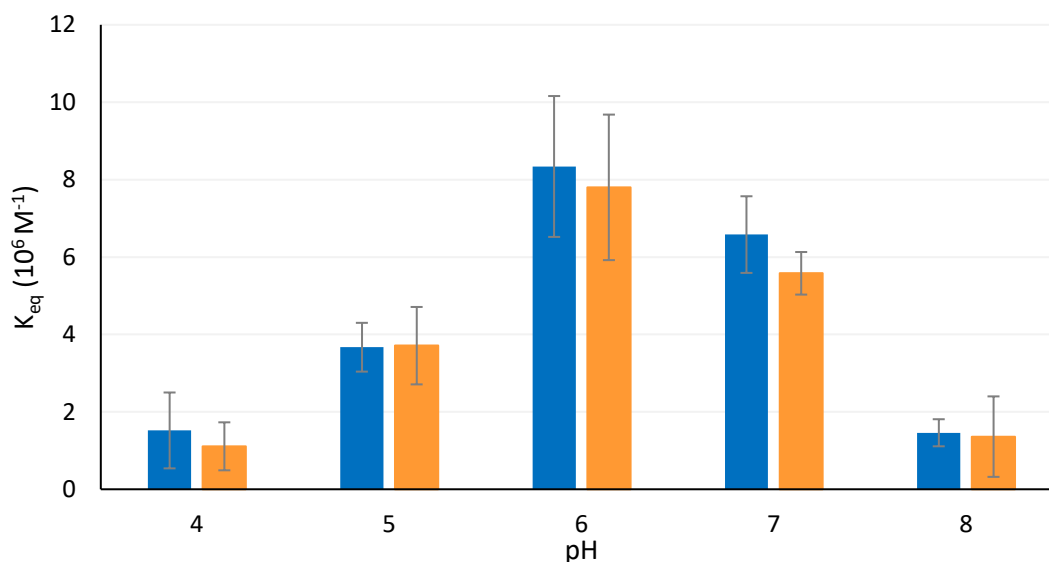


Figure 6-2 - K_{eq} ($10^6 M^{-1}$) values of bindings between nanoMIP and CHNA-Phe (blue) or OTA (orange) at different pH. Error bars indicate 1 standard error unit.

Table 6-1 - K_{eq} ($10^6 M^{-1}$) values of binding of the nanoMIP and nanoMIP with the CHNA and the OTA at different pH.

pH	MIP		NIP	
	CHNA-Phe	OTA	CHNA-Phe	OTA
4	1.52 ± 0.98	1.11 ± 0.62	0.54 ± 0.30	0.60 ± 0.53
5	3.67 ± 0.63	3.71 ± 1.00	1.61 ± 0.43	1.92 ± 0.71
6	8.34 ± 1.82	7.80 ± 1.88	1.91 ± 0.33	1.88 ± 0.87
7	6.58 ± 0.99	5.58 ± 0.55	1.33 ± 0.22	1.87 ± 0.41
8	1.46 ± 0.35	1.36 ± 1.04	0.88 ± 0.66	1.32 ± 0.34

For the buffer pH dependence of the CHNA-Phe binding, the K_{eq} presents a perfect gaussian behavior ($r^2 = 0.973$, $a = 8.7 \pm 0.7$, $b = 6.3 \pm 0.1$, $c = 0.9 \pm 0.1$), with a maximum binding at pH 6.3. This pH is near to the pH of the synthesis environment (neutral water with a slight presence of acrylic acid), and thus it is reasonable to think that the target molecule is in the same ionization condition of the template molecules employed to form the binding sites. Like in the case of CHNA-Phe, for OTA the best binding condition is found to occur at pH 6. A statistical comparison (t-test: = 0.05, $n = 20$, $t < 2.101$) between the equilibrium binding constants for CHNA-Phe and OTA measured onto the nanoMIP show that the values for the corresponding nanoMIPs and indistinguishable from each other.

In Table 6-1 the binding values for CHNA-Phe and OTA for the non-imprinted polymer are also reported. The values are lower than the specific, and a similar trend is observed. At pH 5 and 6, the non specific binding is higher, probably for the optimal ionization states of the target molecules and the nanoparticles surface functionality. At the extremes, the values of the specific binding for OTA and CHNA-Phe are the same as those of the non-specific binding. Instead, at central pH values, specific binding is much higher than the non-specific one, with imprinting factors over 4. In the figure 6-3 are reported the imprinting factor values.

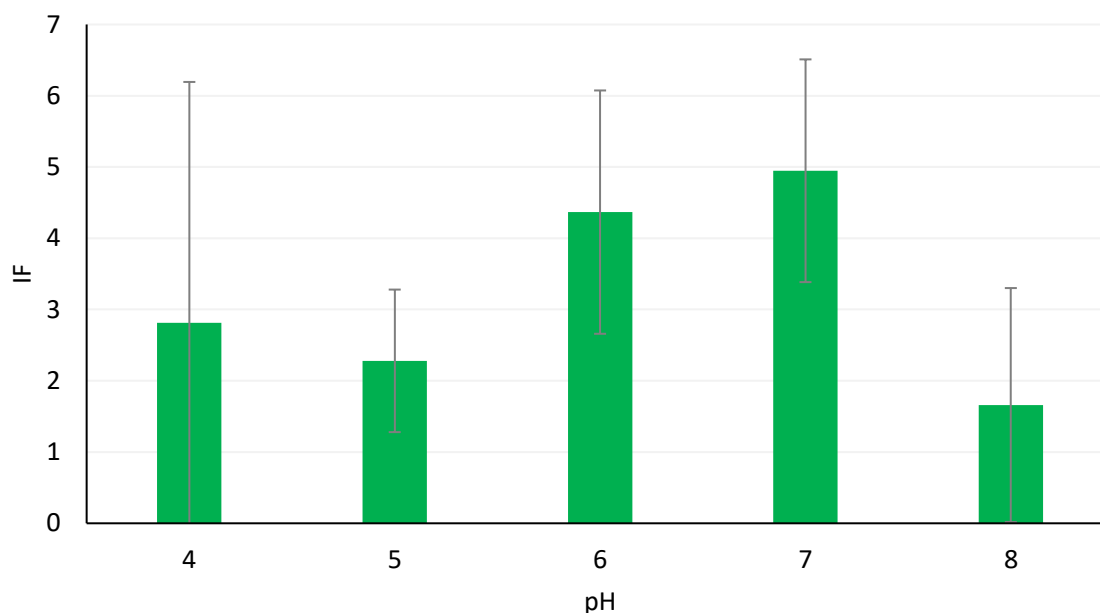


Figure 6 3 – Imprinting factor values (IF) for the nanoMIP at different pH. Error bars indicate 1 standard error unit.

Figure 6-4 reports the selectivity values, calculated as a ratio between the K_{eq} of the OTA binding over the K_{eq} of the CHNA-Phe binding at every pH condition. No general behaviour is observed, and the binding is better for the CHNA-Phe or for the OTA template without any understandable trend. If focus is put onto the central pH 6 – the condition with the higher binding constants – there is an absolute equality in the recognition of the targets. Compared to work presented in the previous chapters, for this nanoMIP the goal was obtain the smaller selectivities, because with the mimic template strategy it is backfired obtain a large selectivity.

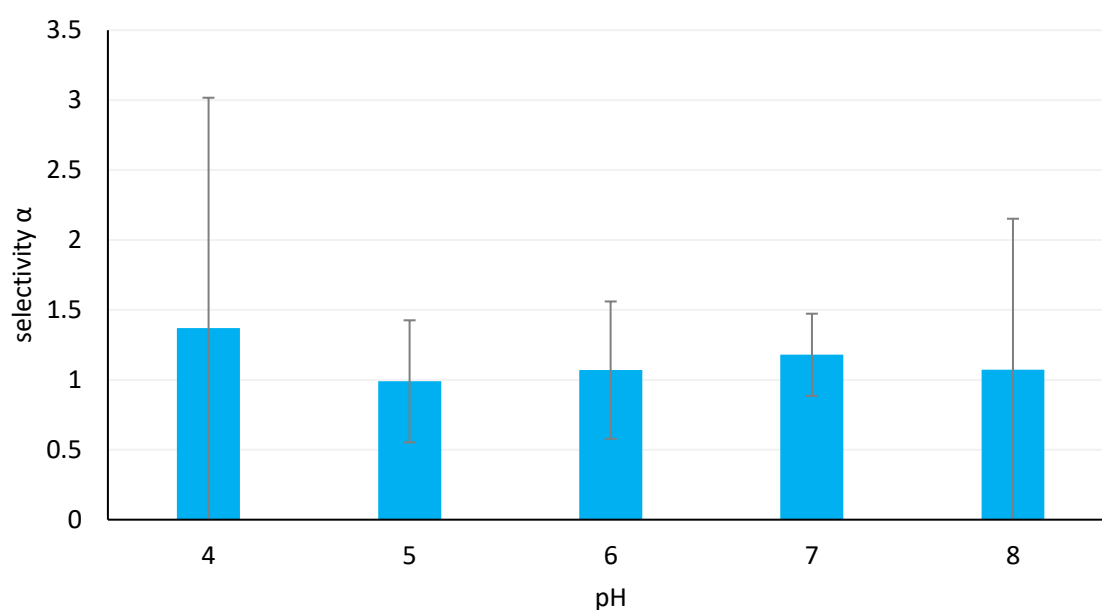


Figure 6-4 – Selectivity values (α) for the nanoMIP at different pH. Error bars indicate 1 standard error unit.

6.4 CONCLUSIONS

According to the experimental results, we have demonstrated that the strategy of the mimic template is a successful way to obtain solid-phase nanoMIPs for dangerous and expensive substances, such as ochratoxin A. We have obtained a nanoMIP imprinted for a mimic molecule that, in the best buffer conditions, binds the effective imprinted mimic molecule as efficiently as the original dangerous target. The binding constants have very high values in both cases (10^7 M^{-1}).

We have also observed that the rebinding buffer pH conditions are very important, similarly to what was discussed in Chapter 2. Adopting pH conditions close to the synthesis conditions is best, while increasing/decreasing pH of 2 units determines the near disappearance of selective binding, leaving only non-specific binding. Thus, the pH of the synthesis environment is deemed fundamental for the following rebinding experiment. In the future, it will be necessary to study the possibility of regulating the pH of the synthesis environment (especially in aqueous media) to better control the binding capability of the nanoMIP as a function of the ionic state of the template molecule.

6.5 BIBLIOGRAPHY

- [1] L. Chen, S. Xu, J. Li. Recent advances in molecular imprinting technology: current status, challenges and highlighted applications. *Chemical Society Reviews*, **2011**, *40*, 2922–2942, doi:10.1039/c0cs00084a.
- [2] Å. Zander, P. Findlay, T. Renner, B. Sellergren, A. Swietlow. Analysis of nicotine and its oxidation products in nicotine chewing gum by a molecularly imprinted solid-phase extraction. *Anal Chem*, **1998**, *70*, 3304–3314, doi:10.1021/ac971272w.
- [3] L.I. Andersson, A. Paprica, T. Arvidsson. A highly selective solid phase extraction sorbent for pre-concentration of sameridine made by molecular imprinting. *Chromatographia*, **1997**, *46*, 57–62, doi: 10.1007/BF02490930.
- [4] J.L. Urraca, M.D. Marazuela, E.R. Merino, G. Orellana, M.C. Moreno-Bondi. Molecularly imprinted polymers with a streamlined mimic for zearalenone analysis. *Journal of Chromatography A*, **2006**, *1116*, 127–134, doi: 10.1016/j.chroma.2006.03.032.
- [5] J. Matsui, K. Fujiwara, T. Takeuchi. Atrazine-selective polymers prepared by molecular imprinting of Trialkylmelamines as dummy template species of atrazine. *Analytical Chemistry*, **2000**, *72*, 1810–1813, doi: 10.1021/ac9911950.
- [6] 15th Report on Carcinogens, **2021**, *National Toxicology Program*, U.S. Department of Health and Human Services.
- [7] Commission regulation (EU) 2022/1370 of 5 August 2022 amending Regulation (EC) No 1881/2006 as regards maximum levels of ochratoxin A in certain foodstuffs.
- [8] C. Baggiani, F. Biagioli, L. Anfossi, C. Giovannoli, C. Passini, G. Giraudi. Effect of the mimic structure on the molecular recognition properties of molecularly imprinted polymers for Ochratoxin A prepared by a fragmental approach. *React Funct Polym*, **2013**, *73*, 833–837, doi: 10.1016/j.reactfunctpolym.2013.03.018.
- [9] D. López-Puertollano, T. Cowen, Á. García-Cruz, E. Piletska, A. Abad-Somovilla, A. Abad-Fuentes, S. Piletsky. Study of epitope imprinting for small templates: Preparation of nanoMIPs for Ochratoxin A. *ChemNanoMat*, **2019**, *5*, 651–657, doi: 10.1002/cnma.201900050.
- [10] C. Baggiani, L. Anfossi, C. Giovannoli. Artificial systems for molecular recognition of mycotoxins. In: M. Rai, A. Varma (eds). *Mycotoxins in food, feed and bioweapons*. Springer, Berlin, Heidelberg, **2010**, doi:

10.1007/978-3-642-00725-5_1.

- [11] T. Kőszegi, M. Poór. Ochratoxin A: molecular interactions, mechanisms of toxicity and prevention at the molecular level. *Toxins*, **2016**, *8*, 111, doi: 10.3390/toxins8040111.
- [12] E. Poli, V. Chaleix, C. Damia, Z. Hjezi, E. Champion, V. Sol. Efficient quantification of primary amine functions grafted onto apatite ceramics by using two UV-Vis spectrophotometric methods. *Anal Methods*, **2014**, *6*, 9622–9627, doi: 10.1039/c4ay02012j.
- [13] F. Canfarotta, A. Poma, A. Guerreiro, S.A. Piletsky. Solid-phase synthesis of molecularly imprinted nanoparticles. *Nat Protoc*, **2016**, *11*, 443-455, doi: 10.1038/nprot.2016.030.

7 THE EFFECT OF THE PRESENCE OF AN ENANTIOMERIC TEMPLATE: THE EXAMPLE OF LEVOTHYROXINE NANOMIPs

7.1 INTRODUCTION

Discriminating different chiral isomers is one of the most important goals of chemical sciences. In nature a lot of molecules present chirality, and in living systems it is common that only one of the possible enantiomers of a molecule presents biological activity. Examples of this are amino acids, for which only the L enantiomers are used by organisms to build proteins. Moreover, natural antibodies have a great capability of discriminating different enantiomers [1, 2].

In the MIP technology the possibility to make systems with chiral recognition properties has been a goal for a long time. The first MIP imprinted to a chiral molecule was produced by Wulff et al. in 1978, namely a MIP imprinted for the 4-nitrophenyl- α -D-mannopyranoside, with a recognition of the D enantiomer twice as efficient as that of the L enantiomer [3]. With the classical bulk synthesis method, the imprinting of chiral substances has found large applications, both with normal and chiral monomers [4]. The principal application of enantioselective MIPs is in separation techniques such as SPE, HPLC and sensors [5]. In general, all the MIPs imprinted for a chiral enantiomer present a good enantiomeric selectivity. It is important to remember that a lot of template molecules – especially in the case of big molecules - present several chiral centers, but “chiral templates” are usually employed to isolate the only enantiomer which is most commonly found. For example, cholesterol presents eight chiral centers, but one enantiomer is predominant [6].

7.1.1 Aim of the work and objectives

To evaluate the possibility of obtaining a nanoMIP with the solid-phase polymerization synthesis characterized by chiral recognition capabilities, we selected levothyroxine (LT4) as a template. This molecule is a derivate of aminoacid tyrosine produced by the thyroid gland, and together with the L-triiodothyronine (LT3) it forms the class of the thyroid hormones. In the human organism, the L isomers present the principal active effect, while the D isomers are not used in the pharmacological treatment of hypothyroidism [7, 8]. Besides, the D isomers also display secondary effects on the organism [9]. An enantioselective MIP for this substance is already present in literature but was not obtained with the SPPS technique [10]. To study the influence of the template chiral center in the imprinting process, we immobilized the template molecule onto the glass beads

through two different positions (Figure 7-1): the ammino group on the chiral center (template A) and the phenolic group (template B).

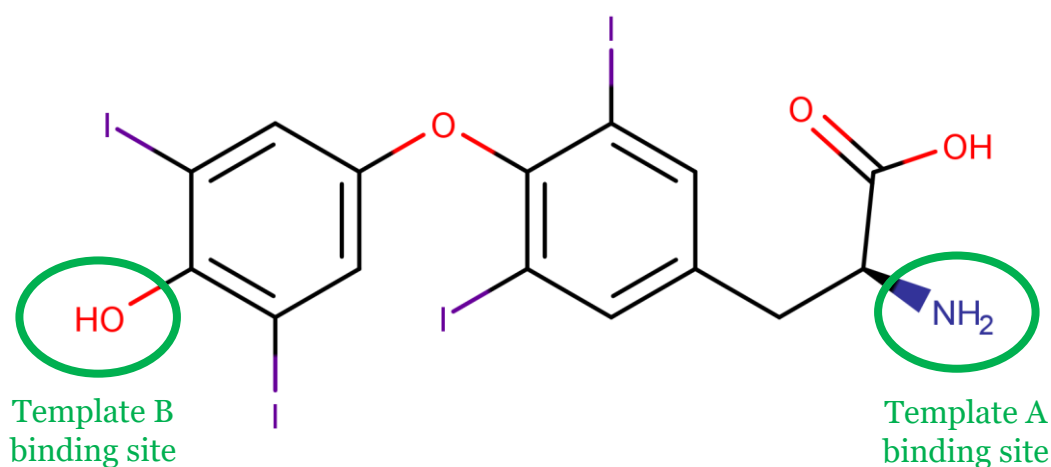


Figure 7-1 - The levothyroxine molecular structure and the template's immobilization sites.

For the two different template nanoMIPs – in addition to the affinity for the template molecule - two types of selectivities were measured. Firstly, the classical chemical selectivity on the structural homologues was measured. For this purpose, we measured the binding for the less iodine-substituted structural homologues of L T₄, namely L T₃ and 3',5'-diiodo- L -thyronine (L T₂). Also, we measured the chiral selectivity using the alternative enantiomers of L T₄ and L T₃, i.e., D T₄ and D T₃. The non-specific binding was measured with the use of a nanoMIP imprinted in the same conditions as for diclofenac and measuring the affinity for all thyroid hormones.

7.2 EXPERIMENTAL

7.2.1 Materials

Glass beads were Spheriglass-2429, with 70-100 μm average particle size (Potters, UK).

Acrylic acid (AA), 3-(aminopropyl)trimethoxysilane (APTMS), ammonium persulphate (APS), azobisisobutyronitrile (AIBN), 1-ethyl-3-(3-dimethylaminopropyl)carbodiimide (EDC), hexamethyldisilazane (HMDS), N-hydroxysuccinimide (NHS), N-isopropylacrylamide (NIPAm), N,N'-methyleneN,N'-N,N'-methylene-bis-acrylamide (BIS), morpholinethansulphonic acid (sodium salt, MES), sodium borohydride, N-tert-butylacrylamide (TBAm), N,N,N',N'-tetramethylethylenediamine (TEMED), N,N-dimethylaminopyridine (DMAP), N,N'-dicyclohexylcarbodiimide (DCC), borabicyclo[3.3.1]nonane (9-BBN), levothyroxine (LT4), dextrothyroxine (DT4), L-triiodothyronine (LT3), D-triiodothyronine (DT3), 3',5'-diiodo-L-thyronine (LT2), succinic anhydride, N,N'-diisopropylcarbodiimide (DIC), 4-dimethylaminopyridine (DMAP) were purchased by Sigma-Merck (Milan, Italy).

Solvents and all other chemicals were purchased from Sigma-Merck (Milan, Italy). All the solvents were of HPLC grade, whereas all chemicals were of analytical grade.

The used water was ultra-purified in Purelab Prima System from Elga (Marlow, UK). Polymerization inhibitors in the monomers were removed by filtration through activated basic alumina.

Hormone stock solutions were prepared by dissolving 10 mg of the substance in 25 mL of DMF/1 M NaOH 80/20 (v/v) then stored in the dark at $-20\text{ }^{\circ}\text{C}$.

7.2.2 Glass beads amination

In a 100-mL round-bottomed flask, 25 g of glass beads was dispersed in 50 mL of 1 M aqueous NaOH and boiled for 1 h. Then, they were diluted with 50 mL of ultrapure water and filtered on a 0.22 μm nylon membrane. The glass beads were washed with 100 mL of 1 M aqueous HCl and with ultrapure water until neutrality was achieved. Then they were rinsed twice with acetone and dried at $60\text{ }^{\circ}\text{C}$ overnight.

The dried glass beads were transferred in a 1-L round-bottomed flask and dispersed in 50 mL of toluene, removing water by azeotropic distillation. Then, the flask was cooled to room temperature, 10 mL of APTMS was added, and the mixture was let to react overnight. The glass beads were filtered on a 0.22 μm nylon membrane and washed with 3x50 mL of toluene.

To end-cap the residual silanols, the glass beads were transferred into a 250-mL round-bottomed flask and dispersed in 50 mL of toluene, removing water by

azeotropic distillation. Then, the flask was cooled to room temperature, 1 mL of HMDS was added to the dispersion and the mixture was let to react overnight. The end-capped glass beads, named “short-chain beads” (SC-beads) were filtered on a 0.22 μm nylon membrane, rinsed twice with acetone and dried at 60 °C overnight. After silanization, the amino groups available on the silanized glass beads surface were determined by Kaiser’s method as 1,1 $\mu\text{mol/g}$.

7.2.3 Glass beads hemisuccination

10 g of aminated glass beads was added to 20 g of succinic anhydride in 20 mL of pyridine at 90 °C for 12 h. A few grains of DMAP were added to catalyze the reaction. After the reaction the solid were separated with a filtration on glass filter and washed with pyridine and water.

7.2.4 Template A immobilization

To bind the template molecule $\text{L}T_4$ to the glass beads through the chiral center (template A), $\text{L}T_4$ was introduced into the reaction environment without any modification. 5 g of hemisuccinated glass beads was placed in a 25-mL glass vial, with 7.6 mg of NHS, 10 μL of DCC and 10 mL of anhydrous DMF, and the mixture was moderately stirred for 60 min. Meanwhile, 235 mg of $\text{L}T_4$ was dissolved in 13 mL of DMF, while adding 2 drops of trimethylamine. The $\text{L}T_4$ solution was then added to the stirred glass beads suspension. The mixture was incubated at room temperature overnight onto a horizontal roller, filtered on a 0.22 μm nylon membrane, washed with DMF and ultrapure water, rinsed twice with acetone, dried under vacuum at room temperature and stored in the dark at 4 °C.

7.2.5 Synthesis of T4-CME (template B)

The synthesis of 4'-carboxymethoxy-3,5,3',5'-tetraiodothyronine (T4-CME), i.e., template B, was conducted according to literature [11], and consists of four reaction steps. In the Figure 7-2 the synthesis procedure is reported.

In the first step, the nucleophile groups were protected. 100 g (1.29 mmol) of $\text{L}T_4$ was dissolved in 10.0 mL of 1 M aqueous NaOH at 4 °C. The solution was diluted with water and 1 M aqueous NaOH to 70 mL (pH 11) and it was stirred for 20 min. The pH was brought to 10.5 with 0.1 M aqueous HCl, and then 0.70 mL of acetic anhydride (Ac_2O) was added. The pH was kept constant at 10.5 with 5 mL of 2 M aqueous NaOH and stirred for 2 h. 0.10 g of activated charcoal was added, and all was stirred for another 30 min at 10 °C. The suspension was filtered on a Gooch filter and the activated charcoal washed away with 3 mL of 1 M aqueous HCl. The solution was left overnight at 4 °C. The resulting white suspension (N,O-diacetyl-

L-3,5,3',5'-tetraiodothyroxine) was filtered on a 0.22 μm membrane filter. This product is instable and needs to be used as soon as possible.

In the second step, the phenolic moiety was deprotected. The previous product was dissolved in 50 mL of methanol (CH_3OH) and 17 mL of aqueous NH_3 25% v/v and left overnight at 4 $^\circ\text{C}$. 0.10 g of activated charcoal was added and the mixture was stirred for 30 min, and then filtered on a Gooch filter. The resulting solution was evaporated to reduce the volume to 66% of the initial one in a rotavapor instrument under 30 $^\circ\text{C}$. The initial volume was restored by adding water and the pH was brought to 5. After an overnight wait at 4 $^\circ\text{C}$, a gel precipitate (N-acetyl-L-3,5,3',5'-tetraiodothyroxine) was separated on a 0.22 μm membrane filter. This product is stable over time if it is held away from light and humidity.

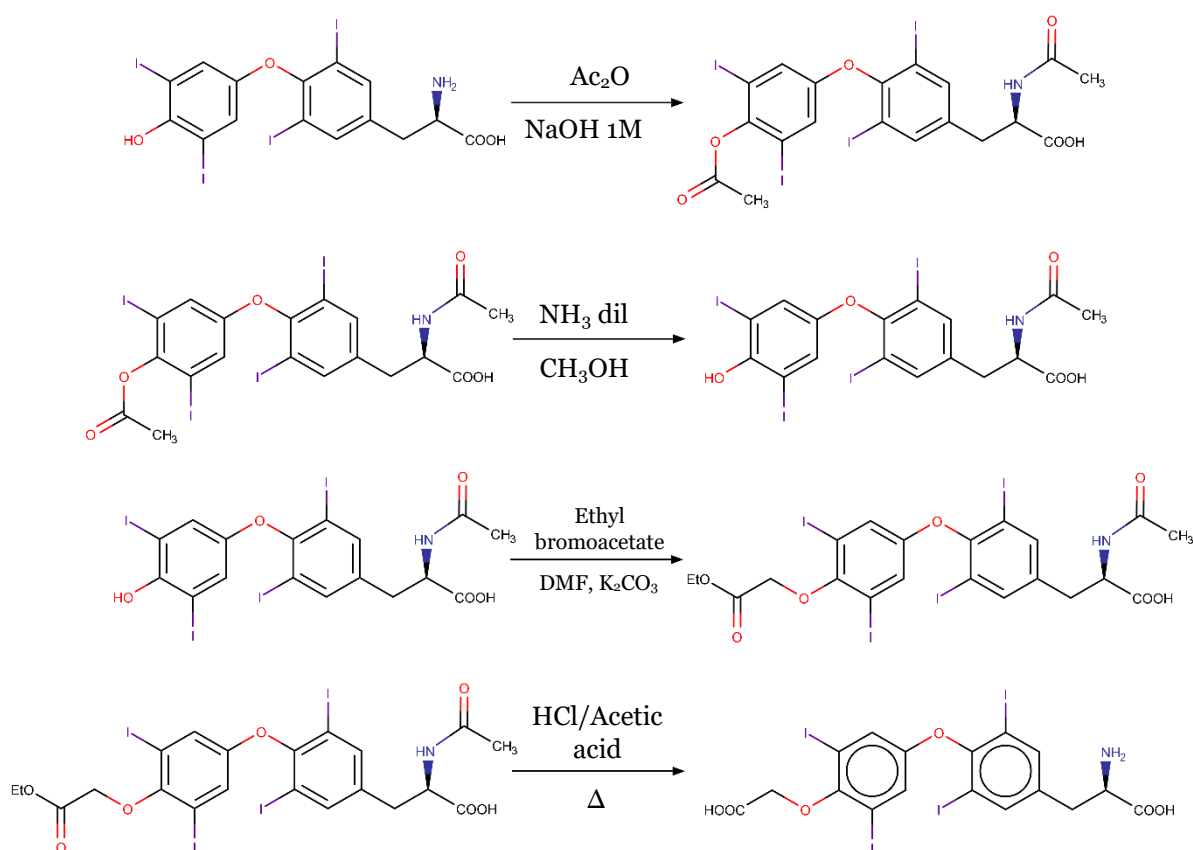


Figure 7-2 - Synthesis scheme of T4-CME (template B)

In the third step, the phenolic group was carboxymethylated. The previous product was dissolved in 12 mL of anhydrous DMF with 50 mg of dried K_2CO_3 . Under stirring, 0.11 mL of ethyl bromoacetate was added. The solution was stirred for 3 h at room temperature in the dark. After this time, 20 mL of cold water (4 $^\circ\text{C}$) was added. The solution was evaporated to reduce the volume to 66% of the initial one in a rotavapor instrument under 30 $^\circ\text{C}$ in the dark. The volume was restored by adding water and the pH was brought to 5. After an overnight wait at 4 $^\circ\text{C}$, a gel

precipitate (4'-carboxymethoxy-N-acetyl-L-3,5,3',5'-tetraiodothyroxine) was separated on a 0.22 μm membrane filter and dried in a dessicator. This product is stable over time if it is held away from light and humidity.

In the last step, the protecting groups on O and N were hydrolyzed. The previous product was dissolved in 16 mL of an acetic acid/37% HCl 50/50 v/v solution and refluxed in the dark for 4 h. After this time, the solution was reduced to half its volume using a rotavapor in the dark. The T4-CME product precipitated as a grey solid. This was separated on a 0.22 μm membrane filter and dried in a dessicator. This product is stable over time if stored in the dark at 4 $^{\circ}\text{C}$.

7.2.6 Template B immobilization

To bind the template molecule L^{T4} to the glass beads with the phenolic moiety (template B), L^{T4} was introduced into the reaction environment in the form of T4-CME and with a protecting group on the chiral moiety.

To protect the chiral moiety [12,13], 50 mg of T4-CME (0.061 mmol) was introduced into a 100-mL flask with 7.5 mg of 9-BBN (0.062 mmol). The solids were dissolved in 50 mL of methanol and refluxed for 3 h. After this time the methanol was evaporated through a rotavapor.

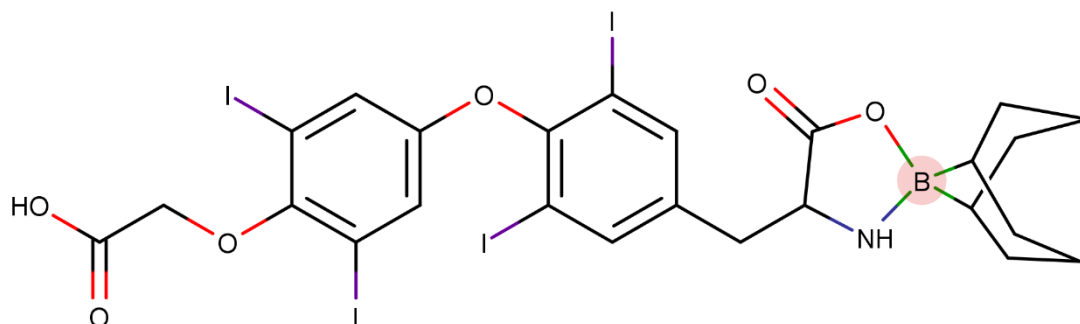


Figure 7-3 – Molecular structure of the T4-CME - 9-BBN adduct

In 25-mL glass vials, 50 mg of protected T4-CME (0.061 mmol) was dissolved in 8 mL of DMF, 7.6 mg of NHS (0.066 mmol) and 10 μL of DCC (0.064 mmol) were added and the solutions incubated for 60 min. Then, they were transferred in 25-mL flasks containing 5 g of aminated glass beads. The suspensions were incubated at room temperature overnight, filtered on a 0.22 μm nylon membrane, washed with DMF, rinsed twice with acetone, dried under vacuum at room temperature and stored in the dark at 4 $^{\circ}\text{C}$.

The protecting group was removed incubating the template-glass beads conjugate overnight with 10 mL of methanol/chloroform 90/10 v/v. The solid was washed with 20 mL of methanol and 25 mL of ultrapure water.

7.2.7 Synthesis of nanoMIPs

The polymerization mixtures were prepared according to the literature [14] and previous experiments performed within our research group. A pre-polymerization mixture (Formulation G, molar ratio BIS : AA : NIPAm : TBAm = 2 : 20 : 30 : 48) was prepared in 25 mL of ultrapure water by mixing under sonication 1 mg of cross-linker (BIS: 0.0065 mmol), 4.7 mg of AA (0.065 mmol), 11 mg of NIPAm (0.097 mmol) and 19.8 mg of TBAm (0.156 mmol, dissolved in 0.5 mL of ethanol). Then, 8 mL of mixture was added to 50-mL polypropylene SPE cartridges containing 5 g of template-functionalized glass beads. The cartridges were purged with N₂ for 5 min. 30 µL of TEMED and 500 µL of 30 mg mL⁻¹ aqueous solution of APS were added and the polymerization was carried out at room temperature for 1 h in a roller-equipped incubator. The supernatant was drained by vacuum aspiration, the dry cartridges were cooled to 4 °C and polymerization by-products and low-affinity nanoMIPs were washed away with 10×2 mL of ice-cold water. High-affinity nanoMIPs were collected by eluting the cartridges at room temperature with 5×3 mL hot water and 5×1 mL of 90% methanol/10% acetic acid v/v. The eluates were purified by gel-filtration in ultrapure water onto a 26 x 250 mm Sephadex G25 column. The nanoMIPs were isolated by centrifugation at 14000 x g, dried by lyophilization and stored at 4 °C.

Non-imprinted polymers (nanoNIPs) were prepared in the same experimental conditions in terms of composition of the polymerization mixture and polymerization time but using glass beads functionalized with diclofenac as a solid phase.

7.2.8 Coupling of nanoMIPs to glass beads

In 4-mL glass vials, 1 mg of nanoMIPs was dissolved under sonication in 1 mL of MES buffer (50 mM, pH 4.7), 8 mg of NHS (0.069 mmol) and 21.5 mg of EDC (0.138 mmol) were added and the solutions incubated at room temperature for 60 min. Then, they were transferred in 10-mL flasks containing 1 g of aminated glass beads. The suspensions were incubated at room temperature overnight, filtered on 0.22 µm nylon membranes, washed with ultrapure water, rinsed twice with acetone, dried under vacuum at room temperature and stored in the dark at 4 °C.

7.2.9 HPLC-MS method

Reverse-phase HPLC-MS analysis was used for target determination. The HPLC apparatus (ThermoScientific) was an Accela LC system composed of a programmable quaternary pump, an auto-sampler and a mass spectrometer with an LCQ Fleet single ion trap and an ESI ion source, provided with Xcalibur and LCQFleet softwares for the instrumental programming, data acquisition and data processing. The used column was a 150 mm × 4.6 mm Kinetex XB-C18A 5 µm

(Phenomenex). The mobile phase was methanol/water 70/30, formic acid 1% (v/v). Elution was performed in isocratic conditions at a flow rate of 0.5 mL/min. The injected sample volume was 50 μ L. The ESI parameters were: sheath gas flow rate 35 au, aux gas flow rate 5 au, sweep gas flow rate 0 au, spray voltage 4.50 kV, capillary temperature 260 $^{\circ}$ C, capillary voltage 44 V, tube lens 120 V. The analyses were conducted in SRM method with the selection of the molecular ions and their following fragmentation in a MS² experiments. Standard solutions between 10 and 100 ng/mL were prepared in the eluent immediately before use. The solutions were analyzed in duplicate and mean peak areas were plotted against standard concentration. The calibration plot was drawn by using a weighted linear regression (weight = 1/conc).

7.2.10 Determination of binding properties

To measure binding isotherms, about 40 mg of glass beads supporting nanoMIPs were exactly weighed in 4-mL flat bottom amber glass vials. Then, 1.0 mL of 20 mM phosphate buffer at pH 7.4 containing increasing amounts of target molecule ranging from 0.5 to 10 μ g was added. The vials were incubated for 2 h at room temperature under continuous agitation on a horizontal rocking table. Then, the solutions were filtered on 0.22 μ m nylon membranes and the free amounts of target molecules were measured by HPLC-MS analysis. Each experimental point was assessed as the average of two repeated measures.

Binding parameters were calculated by using SigmaPlot 12 (Systat Software Inc., Richmond, CA, USA). Non-linear least square fitting was applied to the averaged experimental data. Binding isotherm parameters were calculated by using a Langmuir binding isotherm model.

The binding selectivity, α , was calculated as:

$$\alpha = \frac{K_{eq} \text{target molecule}}{K_{eq} \text{LT4}}$$

where K_{eq} target molecule and K_{eq} LT4 are the equilibrium binding constants calculated for the other molecule and LT4, respectively.

7.3 RESULTS AND DISCUSSION

7.3.1 Binding properties of the nanoMIP

To evaluate the binding properties of the nanoMIPs, they were measured for the two different-oriented template nanoMIPs through rebinding experiments with different thyroid hormones. Firstly, the affinity for L T₄, the template molecule, was measured, to evaluate how well the two MIPs could bind it. The same was applied to the binding affinity to thyroid hormones with fewer iodine atoms (summarized in Figure 7-4): L T₃ (one I atom less than L T₄) and L T₂ (two I atoms less than L T₄), to evaluate the selectivity of the nanoMIPs for the template structural homologues. The affinity for the enantiomers of the L T₄ and L T₃ hormones was measured as well, to evaluate the chiral selectivity of the nanoMIPs. In Table 7-1 and in Figure 7-5 the resulting K_{eq} values for these target substances, and their relative non-specific bindings, are summarized.

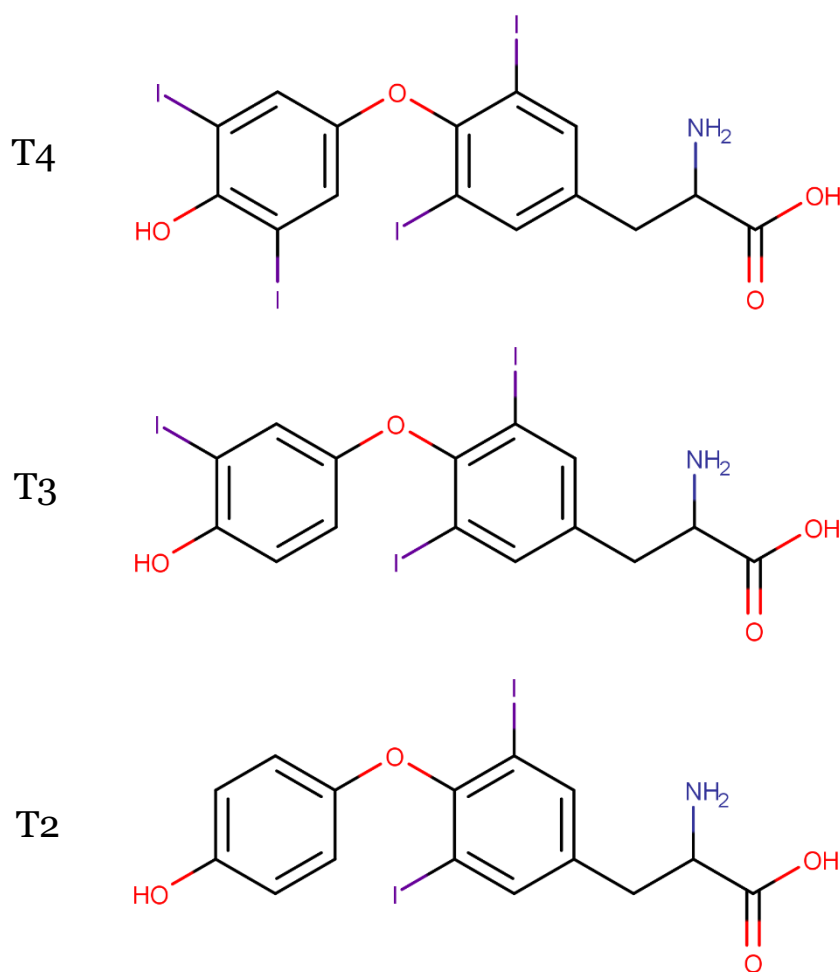


Figure 7-4 - Molecular structures of the thyroid hormones used to evaluate the selectivity of the nanoMIPs. T₄, T₃ and T₂ are general abbreviations for both the L and D enantiomers.

Table 7-1 - K_{eq} ($10^6 M^{-1}$) values of the thyroid hormones binding with the two nanoMIPs (template A and template B) and the diclofenac-imprinted nanoMIP (non-specific). The values are reported with ± 1 standard deviation.

	Template A MIP	Template B MIP	Non-specific
L _T 4	25.4 ± 13.4	107.9 ± 45.5	4.4 ± 2.2
D _T 4	22.3 ± 7.7	26.0 ± 6.8	5.9 ± 4.4
L _T 3	14.3 ± 6.9	29.4 ± 15.9	4.8 ± 5.0
D _T 3	15.9 ± 0.7	11.8 ± 5.8	3.6 ± 1.7
L _T 2	5.1 ± 1.3	2.7 ± 1.23	3.1 ± 1.6

For the template molecule, each nanoMIP displays a good affinity, but the template B nanoMIP – i.e., the one imprinted for the L_T4 bound to the opposite of the chiral center – presents a better value, in the range of $10^8 M^{-1}$. The template B nanoMIP presents a K_{eq} 4 times higher than that of the template A nanoMIP. In agreement with the decrease of the number of iodine atoms, for the selectivity of the other thyroid hormones a decrease of the recognition capability for both the nanoMIPs is observed, although the rest of the molecular structure remains identical. This is explainable with the entropic gain of the binding between the target molecule and the nanoMIP binding site compared to the initial entropic state, in which the molecule is solvated. With a decrease of the number of iodine substituents, this gain disappears. For T₂, the specific portion of the binding is empty, and the K_{eq} values for both the nanoMIPs are the same of the non-specific binding.

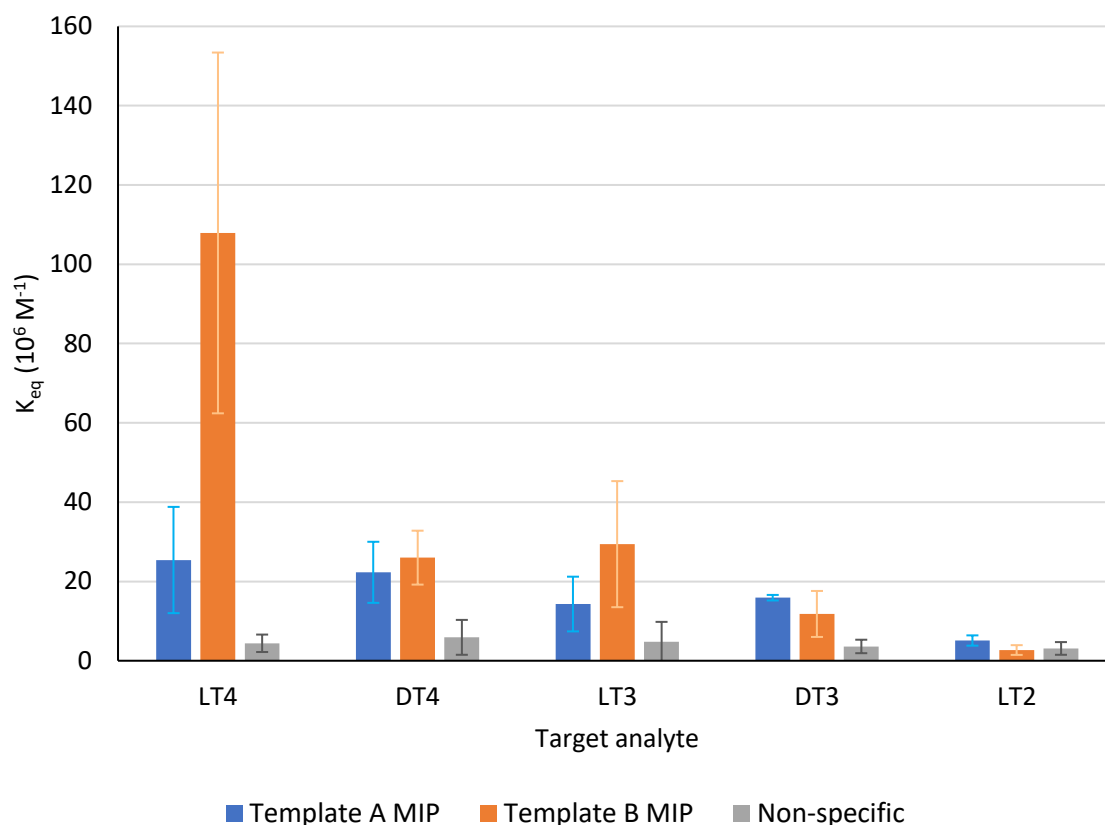


Figure 7-5 - K_{eq} ($10^6 M^{-1}$) values of the thyroid hormones binding the two nanoMIPs (template A and template B) and the diclofenac-imprinted nanoMIP (non-specific). Error bars indicate 1 deviation standard unit.

Observing the data, another behaviour can be observed. If the template A nanoMIP binds the D and L isomers equally for both T4 and T3 molecules, the same does not apply to the template B nanoMIP. Indeed, this binds the L isomers much better than the D ones. This behavior is explainable with the binding position of the template on the glass beads. For template A, the binding on the chiral site creates a steric hindrance, which leads the binding site to being “badly imprinted” on this side of the molecule. Also, in this template one of the most polar groups of the molecule – the amino group – is lost, which implies a lower imprinting potential, translating into a smaller affinity for the template. For template B, the binding with the glass beads occurs on the phenolic group, and the chiral moiety is well exposed. In fact, this nanoMIP has a good chiral recognition capability: L isomers are bound 4.15 times better in the case of T4 and 2.5 times better in the case of T3 than the D isomers. Also, the exposition of the amino group means a major recognition capability, which translates into a higher binding affinity (imprinting factor of 24.5 for L T4).

7.4 CONCLUSIONS

According to the data, with the solid-phase polymerization synthesis it is possible to obtain nanoMIPs imprinted to chiral molecules with high enantioselectivity of the binding site. At the same time, it is fundamental for this type of molecule to choose the best functional group to bind with the glass beads, to maximize enantioselectivity. In cases such as that of the template A nanoMIP, a binding of the template on the chiral center itself can cancel out all the chiral selectivity on the resulting nanoMIP. In contrast, a good choice to maximize the enantiomeric selectivity may introduce an additional binding pivot over the geometricity of the molecule and the chemistry of the functional groups, obtaining higher affinity. Although, this last point needs additional experiments and studies to be confirmed.

At the same time, a nanoMIP (i.e., the template B nanoMIP) with very good properties was developed for L T₄, with the capability to discriminate very well both the L enantiomer from the D one and LT₄ from the other thyroid hormones that are present in the organism, such as L T₃. In the future, it will be possible to apply this nanoMIP to an analytical system.

7.5 BIBLIOGRAPHY

- [1] T.K. Nevanen, L. Söderholm, K. Kukkonen, T. Suortti, T. Teerinen, M. Linder, H. Söderlund, T.T. Teeri. Efficient enantioselective separation of drug enantiomers by immobilised antibody fragments. *Journal of Chromatography A*, **2001**, 925, 189-97, doi:10.1016/S0021-9673(01)01021-4
- [2] S.B. Lee, D.T. Mitchell, L. Trofin, T.K. Nevanen, H. Söderlund, C.R. Martin. Antibody-based bio-nanotube membranes for enantiomeric drug separations. *Science*, **2002**, 296, 2198–2200, doi: 10.1126/science.1071396.
- [3] G. Wulff, W. Vesper. Preparation of chromatographic sorbents with chiral cavities for racemic resolution. *Journal of Chromatography A*, **1978**, 167, 171-186, doi: 10.1016/S0021-9673(00)91156-7.
- [4] M. Rutkowska, J. Płotka-Wasyłka, C. Morrison, P.P. Wiczorek, J. Namieśnik, M. Marć. Application of molecularly imprinted polymers in analytical chiral separations and analysis. *TrAC Trends in Analytical Chemistry*, **2018**, 102, 91-102, doi: 10.1016/j.trac.2018.01.011.
- [5] N.M. Maier, W. Lindner. Chiral recognition applications of molecularly imprinted polymers: a critical review. *Anal Bioanal Chem*, **2007**, 389, 377–397, doi: 10.1007/s00216-007-1427-4.
- [6] M.J. Whitcombe, M.E. Rodriguez, P. Villar, E. N. Vulfson. A new method for the introduction of recognition site functionality into polymers prepared by molecular imprinting: synthesis and characterization of polymeric receptors for cholesterol. *Journal of the American Chemical Society*, **1995**, 117, 7105-7111, doi: 10.1021/ja00132a010.
- [7] C.A. Gorman, N.S. Jiang, R.D. Ellefson, L.R. Elveback. Comparative effectiveness of dextrothyroxine and levothyroxine in correcting hypothyroidism and lowering blood lipid levels in hypothyroid patients. *The Journal of Clinical Endocrinology & Metabolism*, **1979**, 49, 1–7, doi: 10.1210/jcem-49-1-1.
- [8] Y. Lee, E. Bang, W. Lee, Y.C. Na. Simultaneous enantioselective separation method for thyroid hormones using liquid chromatography–tandem mass spectrometry and its applications. *Journal of Pharmaceutical and Biomedical Analysis*, **2021**, 196, 113904, doi: 10.1016/j.jpba.2021.113904.
- [9] C. Bommer, E. Werle, I. Walter-Sack, C. Keller, F. Gehlen, C. Wanner, M. Nauck, W. März, H. Wieland, J. Bommer. D-thyroxine reduces lipoprotein serum concentration in dialysis patients. *Journal of the American Society of Nephrology*, **1998**, 9, 90-96, doi: 10.1681/ASN.V9190.

- [10] B.B. Prasad, M.P. Tiwari, R. Madhuri, P.S. Sharma. Enantioselective quantitative separation of d- and l-thyroxine by molecularly imprinted micro-solid phase extraction silver fibre coupled with complementary molecularly imprinted polymer-sensor. *Journal of Chromatography A*, **2010**, *1217*, 4255-4266, doi: 10.1016/j.chroma.2010.04.055.
- [11] H. Rokos, E. Scheiffele, H. Steinmaus, R. Thoma. Arzneimittel oder diagnostikum zur behandlung oder feststellung von schilddruesenfunktionsstoerungen und verfahren zu dessen herstellung. Patent DE2737802A1, **1977**, Federal republic of Germany, Deutsches Patentamt.
<https://depatisnet.dpma.de/DepatisNet/depatisnet?action=bibdat&docid=DE000002737802A1>
- [12] T. Ankner, T. Norberg, J. Kihlberg. Mild oxidative cleavage of 9-BBN-protected amino acid derivatives. *Eur J Org Chem*, **2015**, 3767-3770, doi: 10.1002/ejoc.201500361.
- [13] W.H. Dent, W. Randal Erickson, S. C. Fields, M.H. Parker, E.G. Tromiczak. 9-BBN: an amino acid protecting group for functionalization of amino acid side chains in organic solvents. *Organic Letters*, **2002**, *4*, 1249-1251, doi: 10.1021/ol017241b.
- [14] F. Canfarotta, A. Poma, A. Guerreiro, S.A. Piletsky. Solid-phase synthesis of molecularly imprinted nanoparticles. *Nat Protoc*, **2016**, *11*, 443-455, doi: 10.1038/nprot.2016.030.

8 NANOMIP-BASED SOLID PHASE EXTRACTION OF FLUOROQUINOLONES FROM HUMAN URINE

8.1 INTRODUCTION

Molecularly imprinted polymers (MIPs) find in the so called “molecularly imprinted solid phase extraction” (MISPE) technique one of their most popular applications, consisting of selectively extracting target analytes in the presence of interfering substances and complex matrices. Whether in the form of cartridges [1], monoliths [2], magnetic particles [3], or nanofibers [4], the application of MIPs to extraction problems is certainly competitive due to their resistance to chemical and biological degradation, the versatility of their applications and the operative costs (if compared to similar methods based on natural receptors such as immunoaffinity extraction) [5,6].

Despite these advantageous characteristics, the MISPE technique shows several drawbacks which limit its wider applicability. First, the preparation of the imprinted material requires the introduction into the polymerization mixture of a fair amount of the target molecule that must act as a template [7]. Thus, the preparation of an adequate quantity of the polymer requires a large quantity of the template, which cannot always be recovered and recycled. In the case of analytes that are difficult to find, expensive or unstable, or those that represent a hazard to health or safety, this is a practical obstacle that cannot be easily overcome. Furthermore, the complete removal of the template from the imprinted polymer is frequently rather difficult [8,9] and the unextracted residues can slowly leach out in the so-called “bleeding effect”, contaminating the samples in the solid phase extraction process and irreparably compromising the results of the analysis.

To overcome these drawbacks, the “mimic template” technique has been introduced, where a putative molecule that is structurally similar to the target molecule is able to raise imprinted binding sites but does not interfere with the subsequent analytical technique. This approach avoids the bleeding effect, but still requires the availability of large quantities of the mimic template, which frequently must be prepared by ad hoc synthesis [10].

An innovative approach for solving all these issues is presented by the solid phase synthesis of nanoMIPs [11,12]. However, to date only limited attention has been paid to the use of nanoMIPs in solid phase extraction [13]. Therefore, since nanoMIPs show close similarities, in terms of binding behavior, to natural antibodies, it seems relevant to check whether it is possible to use them as substitutes of natural antibodies in immunoextraction methods.

8.1.1 Aim of the work and objectives

As a proof-of-concept study, we decided to prepare a MISPE system with the “standard” nanoMIP imprinted for the ciprofloxacin, with the previous optimized synthesis method (formulation mixture G for synthesis in water, 1 hour polymerization). The ciprofloxacin has a relevant interest as an analytical target in MISPE [14-16]. As extraction matrix, the human urine was selected. There is a real interest in the individuation and quantification of the ciprofloxacin and other fluoroquinolones in urine, to prevent the release into the environment of large amounts of antibiotics. This also means to prevent the strengthening of antibiotic resistance [17].

To develop the MISPE system, we started from a simplified model where the human urine was substituted with a “synthetic urine”: a buffer with several salts and proteins that mimics the natural compound. This approach eliminates the matrix effect caused by human’s individual variability. The extraction parameters were optimized with this artificial matrix. Therefore, with real human urine, the system was tested in real conditions of use.

8.2 EXPERIMENTAL

8.2.1 Materials

Glass beads were Spherglass-2429 70-100 μm average particle size (Potters, UK). Ciprofloxacin was purchased from Supelco (Milan, Italy).

Acrylic acid (AA), 3-(aminopropyl)trimethoxysilane (APTMS), ammonium persulphate (APS), azo-bis-isobutyronitrile (AIBN), chlorotetracycline (CYX), 1-ethyl-3-(3-dimethylaminopropyl)carbodiimide (EDC), hexamethyldisilazane (HMDS), N-hydroxysuccinimide (NHS), N-isopropylacrylamide (NIPAm), N,N'-methylene-bis-acrylamide (BIS), morpholinethansulphonic acid sodium salt (MES), sodium borohydride, N-tert-butylacrylamide (TBAm), N,N,N',N'-tetramethylethylenediamine (TEMED), ciprofloxacin (CPX), levofloxacin (LVX), danofloxacin (DAN), enrofloxacin (ENR), moxifloxacin (MOX), norfloxacin (NOR), lomefloxacin (LOM), sarafloxacin (SAR), N,N'-diisopropylcarbodiimide (DIC), N,N-dimethylaminopyridine (DMAP), succinic anhydride and trimethylolpropane trimethacrylate (TRIM) were purchased from Sigma-Merck (Milan, Italy).

Solvents and all other chemicals were purchased from Sigma-Merck (Milan, Italy). All the solvents were of HPLC grade, whereas all chemicals were of analytical grade.

The water used was ultra-purified in Purelab Prima System from Elga (Marlow, UK). Polymerization inhibitors in the monomers were removed by filtration through activated basic alumina.

Antibiotic stock solutions were prepared by dissolving 10 mg of the substance in 25 mL of methanol/acetic acid 95/5 (v/v) then stored in the dark at $-20\text{ }^{\circ}\text{C}$. Synthetic urine was prepared as previously reported [18], stored at $4\text{ }^{\circ}\text{C}$ and discarded no later than a week after its preparation.

8.2.2 Glass beads amination

In a 100-mL round-bottomed flask, 25 g of glass beads in 50 mL of 1 M aqueous NaOH and boiled for 1 h. Then, they were diluted with 50 mL of ultrapure water and filtered on a $0.22\text{ }\mu\text{m}$ nylon membrane. The glass beads were washed with 100 mL of 1 M aqueous HCl and with ultrapure water till neutrality. Then they were rinsed twice with acetone and dried at $60\text{ }^{\circ}\text{C}$ overnight.

The dried glass beads were transferred in a 1-L round-bottomed flask and dispersed in 50 mL of toluene, removing water by azeotropic distillation. Then, the flask was cooled to room temperature, 10 mL of APTMS were added, and the mixture let to react overnight. The glass beads were filtered on a $0.22\text{ }\mu\text{m}$ nylon membrane and washed with $3 \times 50\text{ mL}$ of toluene.

To end-cap the residual silanols, the glass beads were transferred in a 250-mL round-bottomed flask and dispersed in 50 mL of toluene, removing water by

azeotropic distillation. Then, the flask was cooled to room temperature, 1 mL of HMDS was added to the dispersion and the mixture let to react overnight. The end-capped glass beads, named “short-chain beads” (SC-beads) were filtered on a 0.22 μm nylon membrane, rinsed twice with acetone and dried at 60 °C overnight. After silanization, the amino groups available on the silanized glass beads surface were determined by Kaiser’s method as 1,1 $\mu\text{mol/g}$.

8.2.3 Synthesis of ciprofloxacin hemisuccinamide

The template molecule, ciprofloxacin hemisuccinamide (CPX-HS), was synthesized according to a modification of the procedure given by Noël et al. [19]. Succinic anhydride (100 mg, 1 mmol) was added to a suspension of CPX (331 mg, 1 mmol) in DMSO (2.0 mL) containing a catalytical amount of DMAP. The reaction mixture was stirred under nitrogen overnight at 95 °C and cooled down to room temperature. The resulting precipitate was filtered, washed successively with water and diethylether, and dried under reduced pressure. The expected hemisuccinamide was isolated as a fluffy white powder (98 mg, yield 75%), deemed pure by MS-HPLC (ESI: m/z 431.1 [MH⁺]).

8.2.4 Template immobilization

In 25-mL glass vials 10 mg of hemisuccinade ciprofloxacin (0.231 mmol) were dissolved in 10 mL of DMF, 26.7 mg of NHS (0.232 mmol) and 29.3 mg of DIC (0.232 mmol) were added and the solutions incubated for 60 min. Then, they were transferred in 25-mL flasks containing 5 g of aminated glass beads. The suspensions were incubated at room temperature overnight, filtered on a 0.22 μm nylon membrane, washed with DMF, rinsed twice with acetone, dried under vacuum at room temperature and stored in the dark at 4 °C.

8.2.5 Synthesis of nanoMIPs

The polymerization mixtures were prepared in according with the literature [20] and previous experiments by us. A pre-polymerization mixture (molar ratio BIS : AA : NIPAm : TBAm = 2 : 20 : 30 : 48) was made in 25 mL of ultrapure water by mixing under sonication 0.0065 mmol of cross-linker (BIS: 1 mg), 4.7 mg of AA (0.065 mmol), 11 mg of NIPAm (0.097 mmol) and 19.8 mg of TBAm (0.156 mmol, dissolved in 0.5 mL of ethanol). Then, 5 mL of mixture was added to 50-mL polypropylene SPE cartridges containing 2.5 g of template functionalized glass beads. The cartridges were purged with nitrogen for 5 min. 3 μL of TEMED and 100 μL of 30 mg mL^{-1} aqueous solution of APS were added and the polymerization was carried out at room temperature 1 hour in a roller-equipped incubator. The supernatant was drained by vacuum aspiration, the dry cartridges were cooled to 4

°C and polymerization by-products and low-affinity nanoMIPs were washed with 10×2 mL of ice-cold water. High affinity nanoMIPs were collected by eluting the cartridges at room temperature with 5×3 mL hot water and 5×1 mL of 90% methanol/10% acetic acid v/v. The eluates were purified by gel-filtration in ultrapure water onto a 26 x 250 mm Sephadex G25 column. The nanoMIPs were isolated by centrifugation at 14000 x g, dried by lyophilisation and stored at 4 °C.

8.2.6 Coupling of nanoMIPs to glass beads

In 4-mL glass vials 1 mg of nanoMIPs were dissolved under sonication in 1 mL of MES buffer (50 mM, pH 4.7), 8 mg of NHS (0.069 mmol) and 21.5 mg of EDC (0.138 mmol) were added and the solutions incubated at room temperature for 60 min. Then, they were transferred in 10-mL flasks containing 1 g of amminated glass beads. The suspensions were incubated at room temperature overnight, filtered on 0.22 µm nylon membranes, washed with ultrapure water, rinsed twice with acetone, dried under vacuum at room temperature and stored in the dark at 4 °C.

8.2.7 HPLC method

Reverse phase HPLC analysis was used for fluoroquinolones determination. The HPLC apparatus (Merck-Hitachi, Milan, Italy) was a LaChrom Elite system composed of a programmable binary pump L-2130, an auto-sampler L-2200, a fluorescence detector L-2480, provided with EZChrom Elite software for the instrumental programming, data acquisition and data processing. The column used was a 100 mm × 4.6 mm Chromolith RP-18 (Merck, Milan, Italy). The mobile phase was water/acetonitrile 85+15, acetic acid 1% (v/v) for the fluoroquinolones and a 50 mM acetate buffer and pH 8.1/methanol 40 + 60 (v/v) for chlortetracycline. Elution was performed in isocratic conditions at a flow rate of 0.7 mL/min. The sample volume that was injected was 5 µL and the fluorescence wavelengths were: CPX, DAN, ENR, LOM, NAR, SAR: $\lambda_{ex} = 280/\lambda_{em} = 440$ nm; LVX: $\lambda_{ex} = 278/\lambda_{em} = 540$ nm; MOX: $\lambda_{ex} = 294/\lambda_{em} = 503$ nm; and CTX: $\lambda_{ex} = 380/\lambda_{em} = 532$ nm. Fluoroquinolone solutions between 5 and 500 ng/mL were prepared in the eluent immediately before use. The solutions were analyzed in duplicated and mean peak areas were plotted against fluoroquinolone concentration. The calibration plot was drawn by using a weighted linear regression (weight = 1/conc).

8.2.8 Preparation of MISPE Cartridges

Adequate amounts of glass beads grafted with nanoMIPs (1 g) were suspended in water and packed into 5 mL capacity, empty polypropylene SPE cartridges that

were provided with frits to secure the packing and outlet stopcocks. The columns were connected to a vacuum manifold and washed extensively with water, then dried under a vacuum. Immediately before any use, the cartridges were activated with 500 μL of MES buffer 50 mM at pH 4.5. When necessary, the columns were cleaned and regenerated by washing with 500 μL of water/acetic acid 9 + 1 v/v and $3 \times 500 \mu\text{L}$ of water.

8.2.9 Optimization of the MISPE Method

In order to optimize the procedure of fluoroquinolone extraction, different protocols were applied during the loading and washing steps. In the subsequent experiments, each extraction was repeated three times and the amount of analyte recovery was evaluated as the average of the single values that were measured.

To investigate the effects of the different loading solutions, ciprofloxacin (200 ng mL^{-1}) in synthetic urine was diluted 1 + 9 v/v with 50 mM MES (pH 4.5–5.5) or phosphate buffers (pH 6.5–8.5), and then 250 μL of diluted solution was loaded into the cartridge. After the sample loading, the cartridge was washed with 250 μL of methanol/acetic acid 9 + 1 v/v.

To investigate the effects of the different washing solutions, ciprofloxacin (200 ng mL^{-1}) in synthetic urine was diluted 1 + 9 v/v with 50 mM MES buffer, pH 4.5, then 250 μL of diluted solution was loaded into the cartridge. After the sample loading, air was passed through the cartridge for 10 min in order to remove all of the residual traces of the solution. Then, the cartridge was washed with 250 μL of 50 mM MES buffer, pH 4.5, ultrapure water, methanol, acetonitrile, acetone, tetrahydrofuran or ethyl acetate. Air was passed through the cartridge for 10 min to remove all the residual traces of the washing solution and the retained ciprofloxacin was eluted with 250 μL of methanol/acetic acid 9 + 1 v/v.

To investigate the effects of the different loading volumes, ciprofloxacin (200 ng mL^{-1}) in synthetic urine was diluted 1 + 9 v/v with 50 mM MES buffer, pH 4.5 and 0.10, 0.25, 0.50, 1.00, 2.00 or 5.00 mL of diluted solution was loaded into the cartridge. Then, air was passed through the cartridge for 10 min to remove all of the residual traces of the loading solution and the retained ciprofloxacin was eluted with 250 μL of methanol/acetic acid 9 + 1 v/v.

8.2.10 MISPE Selectivity

To investigate the selectivity of the optimized extraction protocol in the loading solution, ciprofloxacin was substituted with 7 other fluoroquinolones (danofloxacin, enrofloxacin, levofloxacin, lomefloxacin, moxifloxacin, norfloxacin and sarafloxacin), and chlortetracycline, which was chosen as an unrelated substance. For each of these ligands, a standard solution of 200 ng mL^{-1} in synthetic urine was diluted 1 + 9 v/v with 50 mM MES buffer, pH 4.5 and then 250

μL of this diluted solution was loaded into the cartridge. Then, air was passed through the cartridge for 10 min to remove all the residual traces of the solution. The retained ligands were eluted with 250 μL of methanol/acetic acid 9 + 1 v/v.

8.2.11 MISPE of Real Samples

Blank urine samples collected from four individuals (two men and two women) were mixed and then filtered through a 0.22 μm polypropylene membrane. The resulting 10 mL samples were spiked with known amounts of ciprofloxacin (ranging from 2 to 20 μg), or a mixture of ciprofloxacin, danofloxacin and norfloxacin (20 μg each), and then immediately extracted with the optimized protocol reported in Section 8.2.9. To evaluate the reproducibility of the MISPE protocol, each extraction was repeated five times and the rate of analyte recovery was evaluated as the average of the single values that were measured.

8.3 RESULTS AND DISCUSSIONS

8.3.1 Optimization of the MISPE Protocol

To optimize the procedure for fluoroquinolone extraction, the attention was initially focused on the composition of the loading and washing solutions. Synthetic urine containing 200 ng mL^{-1} of ciprofloxacin was diluted 1 + 9 with buffers with different pH levels. As reported in Figure 8-1, there is a clear effect of the buffer's pH on the retention of ciprofloxacin, as the acidic buffer shows a limited loss of analytes while the neutral and basic pH buffers do not quantitatively retain them. This result confirms the results saw in the chapter 2, where ciprofloxacin-binding nanoMIPs show a decreasing of the binding constants when pH increases.

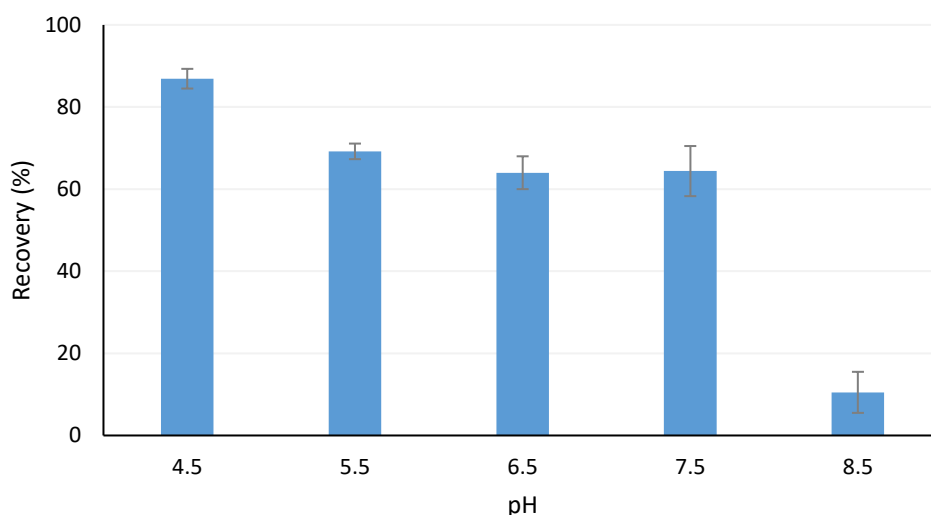


Figure 8-1 - Effect of pH on loading of 1 mL of synthetic urine containing 200 ng mL^{-1} of ciprofloxacin, diluted 9 + 1 v/v with 50 mM buffers.

Once optimal loading conditions were defined (pH 4.5), the effect of the washing solutions was evaluated. They were considered 1 mL of water, an MES buffer at pH 4.5 and organic solvents of decreasing polarity (methanol, acetonitrile, acetone, tetrahydrofuran and ethyl acetate). As reported in Figure 8-2, none of these solutions, except for the less-polar ethyl acetate, is capable of quantitatively retaining ciprofloxacin. It should be noted that the loading buffer is also unable to fully retain the analyte, even if the loss is significantly less (~25%) than that of all the other solutions. As a consequence of this result and taking into account that, by eluting the cartridges loaded with real urine samples with ethyl acetate, the corresponding chromatogram does not show any peak whatsoever, it was therefore decided to omit the washing step, limiting the process to drying the cartridges carefully after loading the sample.

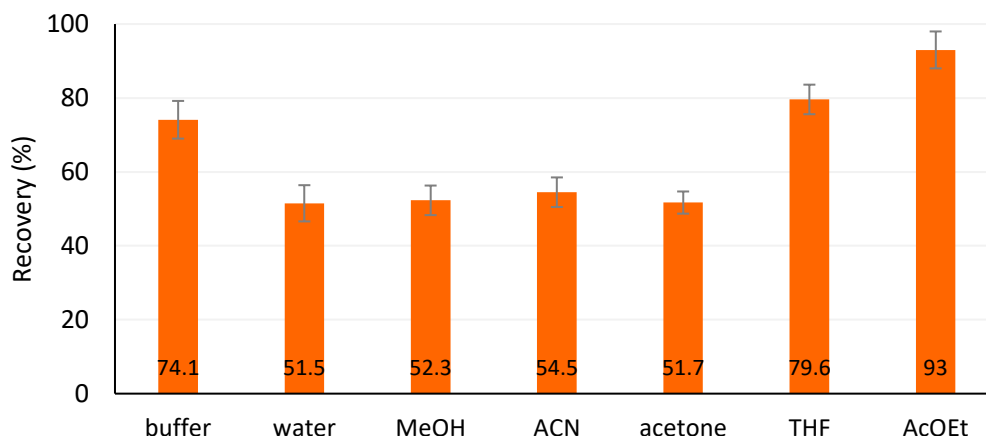


Figure 8-2 - Effect of 1 mL of washing solutions on retention of ciprofloxacin after loading of 1 mL of synthetic urine containing 200 ng mL^{-1} of ciprofloxacin, diluted 9 + 1 v/v with 50 mM MES buffer, pH 4.5.

The effect of increasing loading volumes was evaluated considering samples of synthetic urine spiked with ciprofloxacin at a fixed concentration of 200 ng mL^{-1} and diluted 1 + 9 v/v with 50 mM of MES buffer. The results, reported in Figure 8-3, show that when the loading volumes are larger than 0.25 mL, the recovery of the analyte drops sharply, becoming very small when 5 mL of the sample is loaded. This is unexpected, as the nanoMIP G (see chapter 3) that was used to prepare the MISPE cartridges shows a binding site concentration of $9.5 \pm 1.4 \text{ nmol g}^{-1}$. This is a static binding capacity of $\sim 3 \text{ }\mu\text{g/cartridge}$ of ciprofloxacin, corresponding to 3 times greater than the amount present in 5 mL of the sample. The cause of this poor loading capacity is probably related for the non-equilibrium condition of the system, because the binding time of 10 minutes is not enough to achieve the thermodynamic equilibrium. In any case, a loading volume of 0.25 mL ensures a good retention of the analyte in the MISPE protocol reported here.

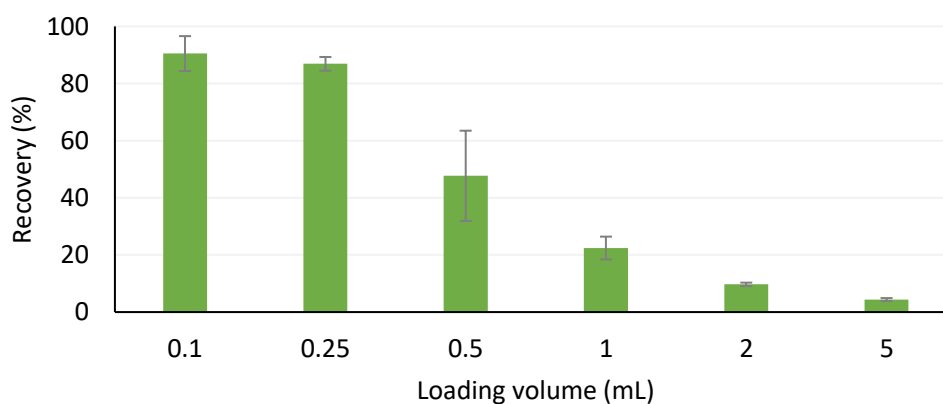


Figure 8-3 - Effect of sample loading volumes on retention of ciprofloxacin, 200 ng mL^{-1} in synthetic urine, diluted 9 + 1 v/v with 50 mM MES buffer, pH 4.5.

8.3.2 MISPE Selectivity

The selectivity of the optimized MISPE protocol was investigated by extracting several analogues that are related to different generations of antibiotics [21], the molecular structures of which are reported in figure 8-4. They are different from ciprofloxacin by substituents, but they share the common fluoroquinolone nucleus (highlighted in red in the structures).

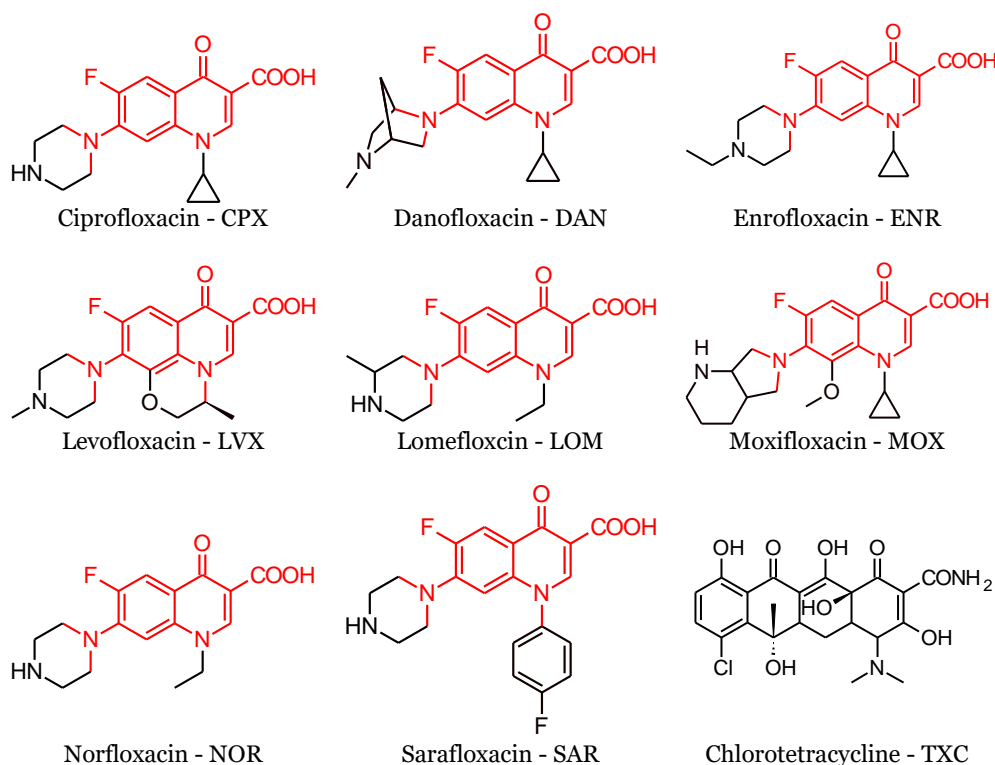


Figure 8-4 - Template, fluoroquinolones with similar molecular structure and chlortetracycline.

The results, reported in Figure 8-5, show that the imprinted cartridge is able to retain all of the examined fluoroquinolones with recovery rates greater than 80%, while chlortetracycline (an antibiotic substance with a molecular structure completely different from that of fluoroquinolones) is poorly retained. The group selectivity shown by the nanoMIPs can be explained by considering that the positions on the rigid molecular structure of the fluoroquinolone, which presumably are most responsible for the interaction with the binding site, correspond to the positions C3 (carboxyl) and C4 (quinone); these are far from the positions N1 and C7 that determine structural differences. It follows that the significant molecular recognition of all fluoroquinolones is essentially determined by the presence of some ubiquitous structures on this class of molecules. These ubiquitous structures are the condensed ring systems that give shape and size to the binding site and the presence of the carboxyl-quinone system in positions C3-C4, which guarantees the same non-covalent interaction mechanism for all

molecules. Moreover, it is clear that the basic shape of the ligands is equally important. Chlortetracycline, which possesses a pair of substituents in the C1-C2 positions (like the carboxyl-quinone system) but exhibits a radically different condensed ring system, is poorly recognized by nanoMIPs.

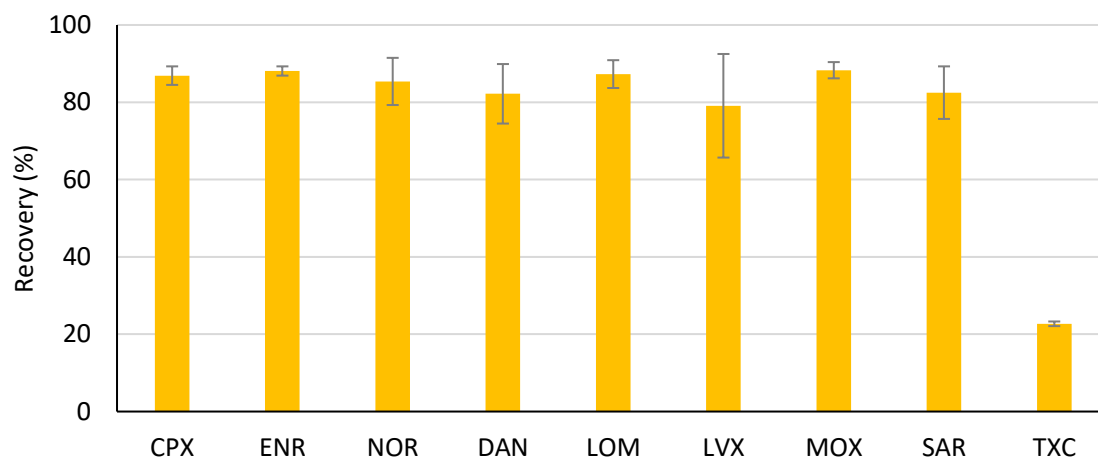


Figure 8-5 - Selectivity after loading of 1 mL of synthetic urine containing 200 ng mL⁻¹ of analyte, diluted 9 + 1 v/v with 50 mM MES buffer, pH 4.5

8.3.3 MISPE of Real Samples

To evaluate the ability of the MISPE cartridges to extract from real samples of human urine, blanks were spiked with known amounts of ciprofloxacin or a mixture of three different fluoroquinolones (ciprofloxacin, danofloxacin, and norfloxacin).

The recovery of ciprofloxacin was determined by comparing the HPLC detector responses of five different urine samples. The recovery rates, reported in Table 8-1, were determined at five concentration levels of ciprofloxacin (between 0.2 to 2 µg mL⁻¹), resulting in levels between about 82% and 85% with a relative standard deviation <5%. Moreover, pairwise t-tests performed to compare the recovery rates obtained at different ciprofloxacin concentrations showed no statistical differences between the groups, with t-values (n = 5, α = 0.05) between 0.290 and 0.938 (see Table 8-2). These results show that the extraction protocol performed well, with good recovery rates and a substantial insensitivity to varying concentration levels.

Table 8-1 - Recovery of ciprofloxacin in human urine after dilution 9 + 1 v/v with 50 mM MES buffer, pH 4.5 and MISPE. Values are the mean \pm 1 σ of 5 samples.

Ciprofloxacin, $\mu\text{g mL}^{-1}$	Recovery, %
0.2	84.8 \pm 4.4
0.5	82.7 \pm 4.5
1.0	85.4 \pm 4.5
1.5	82.9 \pm 3.6
2.0	85.0 \pm 3.1

Table 8-2 - Recovery of ciprofloxacin in human urine after dilution 9 + 1 v/v with 50 mM MES buffer, pH 4.5 and MISPE. *t*-values for pairwise comparison of samples at different concentration.

$\mu\text{g mL}^{-1}$	0.2	0.5	1.0	1.5	2.0
0.2	-	0.432	0.821	0.477	0.910
0.5	0.432	-	0.316	0.938	0.290
1.0	0.821	0.316	-	0.352	0.880
1.5	0.477	0.938	0.352	-	0.334
2.0	0.910	0.290	0.880	0.334	-

Satisfactory sample clean-up was achieved: this can be seen in the example reported in Figure 8-6, where the chromatograms of before and after the MISPE of the urine spiked with the fluoroquinolone mixture at a concentration level of 2 $\mu\text{g mL}^{-1}$ are reported. When comparing the chromatograms, fluoroquinolones can be detected with some difficulty when a sample of urine is separated directly by reverse phase-HPLC without preliminary MISPE, while the same sample that was analyzed after MISPE shows a cleaner chromatographic trace, where the peaks corresponding to fluoroquinolones can be more easily detected and, therefore, quantified.

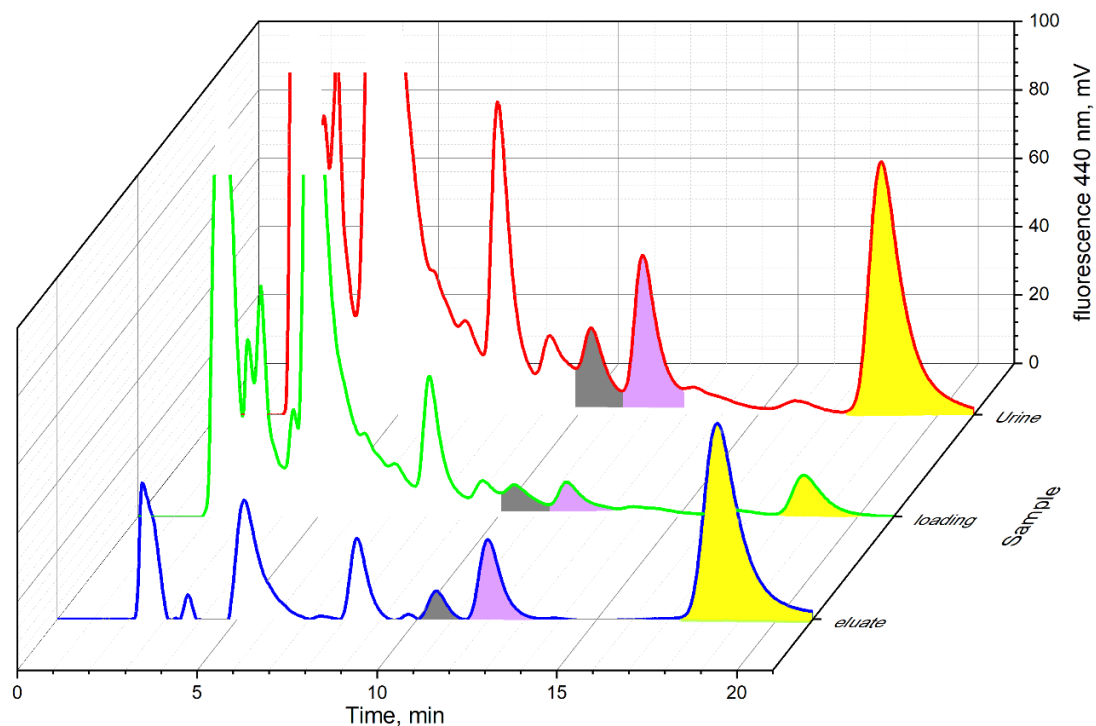


Figure 8-6 - HPLC chromatograms of human urine spiked with ciprofloxacin (violet area), danofloxacin (yellow area), and norfloxacin (grey area) at final concentration of $2 \mu\text{g mL}^{-1}$ and diluted 9 + 1 v/v with 50 mM MES buffer, pH 4.5.

RED LINE: sample injected without MISPE; **GREEN LINE:** not retained loading.
BLUE LINE: eluate from MISPE cartridge.

8.4 CONCLUSIONS

In this work, it was demonstrated that is possible to use nanoMIPs prepared by solid-phase synthesis to develop a MISPE technique suitable with real matrices. Unlike materials prepared with more traditional molecular imprinting techniques, solid-phase synthesis allows the preparation of nanopolymers only in very small quantities, at the level of mg per synthesis cycle. Furthermore, due to their typical dimensions, nanoMIPs are not directly usable as packing materials for SPE cartridges. Therefore, nanoMIPs were supported on glass microspheres, based on an experimental approach previously used to successfully measure the binding isotherms of this type of nanomaterials. We also considered it feasible to use very limited amounts of the nanoMIPs by designing their use in this study to align with the use of natural antibodies in the preparation of cartridges for immunoaffinity studies. In fact, even in this case, the typical quantity of antibodies that are covalently bond to the supports is very small. Nonetheless, this small amount does not affect the extraction efficiency of the method [22]. However, it should be noted that the attempt to preconcentrate the samples to further increase the method's sensitivity was not effective, as the ability of MISPE cartridges to retain the analytes with loading volumes greater than 0.25 mL involves a significant drop in the recovery rate.

In conclusion, the experimental results reported here show a MISPE/HPLC method allowing the direct extraction of fluoroquinolones from buffered urine samples at the $\mu\text{g mL}^{-1}$ level, with good recovery rates and precision, without interference from the matrix. We believe that these results are, although limited to a small number of analytes in a single real matrix, a good proof-of-concept for the use of nanoMIPs in MISPE methods.

8.5 BIBLIOGRAPHY

- [1] V. Pichon, N. Delaunay, A. Combès. Sample preparation using molecularly imprinted polymers. *Anal Chem*, **2019**, *92*, 16–33, doi: 10.1021/acs.analchem.9b04816.
- [2] E. Turiel, A. Martín-Esteban. Molecularly imprinted polymers-based microextraction techniques. *TrAC Trends Anal Chem*, **2019**, *118*, 574–586, doi: 10.1016/j.trac.2019.06.016.
- [3] S. Ansari. Application of magnetic molecularly imprinted polymer as a versatile and highly selective tool in food and environmental analysis: recent developments and trends. *TrAC Trends Anal Chem*, **2017**, *90*, 89–106, doi: 10.1016/j.trac.2017.03.001.
- [4] S.A. Zaidi. Recent developments in molecularly imprinted polymer nanofibers and their applications. *Anal Methods*, **2015**, *7*, 7406–7415, doi: 10.1039/C5AY01609F.
- [5] T. Zhou, L. Ding, G. Che, W. Jiang, L. Sang. Recent advances and trends of molecularly imprinted polymers for specific recognition in aqueous matrix: preparation and application in sample pretreatment. *TrAC Trends Anal Chem*, **2019**, *114*, 11–28, doi: 10.1016/j.trac.2019.02.028.
- [6] M. Arabi, A. Ostovan, A.R. Bagheri, X. Guo, L. Wang, J. Li, X. Wang, B. Li, L. Chen. Strategies of molecular imprinting-based solid-phase extraction prior to chromatographic analysis. *TrAC Trends Anal Chem*, **2020**, *128*, 115923, doi: 10.1016/j.trac.2020.115923.
- [7] P.A. Cormack, A.Z. Elorza. Molecularly imprinted polymers: synthesis and characterisation. *J Chromatogr B*, **2004**, *804*, 173–182, doi: 10.1016/j.jchromb.2004.02.013.
- [8] A. Ellwanger, L. Karlsson, P.K. Owens, C. Berggren, C. Crecenzi, K. Ensing, S. Bayouhd, P. Cormack, D. Sherrington, B. Sellergren. Evaluation of methods aimed at complete removal of template from molecularly imprinted polymers. *Analyst*, **2001**, *126*, 784–792, doi: 10.1039/b009693h.
- [9] R.A. Lorenzo, A.M. Carro, C. Alvarez-Lorenzo, A. Concheiro. To remove or not to remove? The challenge of extracting the template to make the cavities available in molecularly imprinted polymers (MIPs). *Int J Mol Sci*, **2011**, *12*, 4327–4347, doi: 10.3390/ijms12074327.
- [10] C. Baggiani, L. Anfossi, C. Giovannoli. Solid phase extraction of food contaminants using molecular imprinted polymers. *Anal Chim Acta*, **2007**, *591*, 29–39, doi: 10.1016/j.aca.2007.01.056.

- [11] A. Poma, A. Guerreiro, M.J. Whitcombe, E. Piletska, A. Turner, S.A. Piletsky. Solid-phase synthesis of molecularly im-printed polymer nanoparticles with a reusable template- “plastic antibodies”. *Adv Funct Mater*, **2013**, *23*, 2821–2827, doi: 10.1002/adfm.201202397.
- [12] S. Ambrosini, S. Beyazit, K. Haupt, B.T.S. Bui. Solid-phase synthesis of molecularly imprinted nanoparticles for protein recognition. *Chem Commun*, **2013**, *49*, 6746–6748, doi: 10.1039/c3cc41701h.
- [13] Z. Altintas, A. Guerreiro, S.A. Piletsky, I.E. Tothill. NanoMIP based optical sensor for pharmaceuticals monitoring. *Sensors Actuators B: Chem*, **2015**, *213*, 305–313, doi: 10.1016/j.snb.2015.02.043.
- [14] E. Benito-Peña, S. Martins, G. Orellana, M.C. Moreno-Bondi. Water-compatible molecularly imprinted polymer for the selective recognition of fluoroquinolone antibiotics in biological samples. *Anal Bioanal Chem*, **2008**, *393*, 235–245, doi: 10.1007/s00216-008-2405-1.
- [15] H.L. de Oliveira, S.D.S. Anacleto, A.T.M. da Silva, A. Pereira, W. Borges, E. Figueiredo, K.B. Borges. Molecularly imprinted pipette-tip solid phase extraction for selective determination of fluoroquinolones in human urine using HPLC-DAD. *J Chromatogr B*, **2016**, *1033-1034*, 27–39, doi: 10.1016/j.jchromb.2016.08.008.
- [16] F. Barahona, B. Albero, J.L. Tadeo, A. Martín-Esteban. Molecularly imprinted polymer-hollow fiber microextraction of hydrophilic fluoroquinolone antibiotics in environmental waters and urine samples. *J Chromatogr A*, **2018**, *1587*, 42–49, doi: 10.1016/j.chroma.2018.12.015.
- [17] S. Singha, K.H. Ahn. detection of ciprofloxacin in urine through sensitized lanthanide luminescence. *Sensors (Basel)*, **2016**, *16*, 2065, doi: 10.3390/s16122065.
- [18] F. Di Nardo, S. Occhipinti, P. Gontero, S. Cavallera, M. Chiarello, C. Baggiani, L. Anfossi. Detection of urinary prostate specific antigen by a lateral flow biosensor predicting repeat prostate biopsy outcome. *Sens Actuators B Chem*, **2020**, *325*, 128812, doi: 10.1016/j.snb.2020.128812.
- [19] S. Noël, V. Gasser, B. Pesset, F. Hoegy, D. Rognan, I.J. Schalk, G.L.A. Mislin. Synthesis and biological properties of con-jugates between fluoroquinolones and a N3''-functionalized pyochelin. *Org Biomol Chem*, **2011**, *9*, 8288–8300, doi: 10.1039/c1ob06250f.
- [20] F. Canfarotta, A. Poma, A. Guerreiro, S. Piletsky. Solid-phase synthesis of molecularly imprinted nanoparticles. *Nature Protocols*, **2016**, *11*, 443–455, doi: 10.1038/nprot.2016.030.

- [21] P. Ball. Quinolone generations: natural history or natural selection? *J Antimicrob Chemother*, **2000**, 46, 17–24, doi: 10.1093/oxfordjournals.jac.a020889.
- [22] V. Pichon, N. Delaunay-Bertoncini, M.C. Hennion, Chapter 33—Immunosorbents in sample preparation. In: *Comprehensive analytical chemistry—sampling and sample preparation for field and laboratory*; Pawliszyn, J., Ed.; Elsevier: Amsterdam, The Netherlands, **2002**; Volume XXXVII, pp.1088–1090.

9 GENERAL CONCLUSIONS

In these three years of PhD, several aspects of the innovative MIP synthesis approach called solid-phase polymerization synthesis were thoroughly explored. A large part of the research was dedicated to increase the knowledge about this technique. In particular, the exploration of the parameters involved in the polymerization mechanism and their influence on the final binding properties is one of the most important focuses of this PhD work. The application of the technique to analytical systems, though, will need to be addressed in-depth in the near future.

As a main aim of the work, some great differences between the SPPS mechanism and the traditional synthesis in the effect of the cross-linker and the polymerization time were successfully highlighted. In Chapter 5 it was observed that a change in the cross-linker structure can have an enormous impact on the binding properties of the nanoMIPs, but a less pronounced one on the morphology of the nanoparticles. This unexpected behaviour represents yet today a mystery, which will certainly act as a source of further studies. In particular, further attention needs to be directed to the understanding of why such a little amount of a molecular compound unrelated to the binding with the template during the polymerization step and the rebinding phase can modify the binding itself in such a significative way? A secondary question to be addressed is whether this effect is template-correlated. This behaviour was observed on a nanoMIP imprinted for the RIgG – a big molecule – but no similar trials were performed on smaller templates such as the over-studied ciprofloxacin. As observed in literature, for large molecular templates the influence of the monomeric mixture is secondary [1], but in Chapter 3 it was found that this is not true for small templates. Additional future studies on this effect are fundamental, and in this sense in-silico calculations can be explored as a means to identify the cross-linker properties involved by this effect (e.g., polarity, hydrophobicity, rigidity, etc.). Nonetheless, the N,N'-methylenN,N'-N,N'-methylen-bis-acrylamide (BIS) cross-linker showed a very high flexibility in its application. Besides providing the best binding properties to the IgG nanoMIPs, this cross-linker was indeed used to make nanoMIPs imprinted for ciprofloxacin (Chapters 2, 3, 4 and 8), LT4 (Chapter 7) and CHNA-Phe (Chapter 6). In a sense, it can be claimed that BIS, which has rarely used in the classical synthesis approach, has become a pivotal component of the SPPS technique. In Table 9-1 all the best binding values obtained in the previous chapters for BIS nanoMIPs are reported.

All these nanoMIPs have K_{eq} values in the order of $10^6 - 10^8 \text{ M}^{-1}$, which are usually very high for MIPs, comparable to those involved in the field of the natural antibodies [2]. With these data, it is not possible to affirm that BIS is the absolute best cross-linker for SPPS, but undoubtedly its use is applicable to several types of templates with good results.

Table 9-1 - Binding properties of the BIS nanoMIPs

Template	Chapter	Experimental Condition	K_{eq} , $10^6 M^{-1}$	B_{max} , nmol/g
CPX	2	wLC-MIP, rebinding pH 4	15.40 ± 1.26	1.65 ± 0.01
CPX	3	monomeric form. C	4.01 ± 0.62	8.8 ± 0.7
CPX	4	15' synthesis time	15.39 ± 2.14	1.05 ± 0.10
RIgG	5		16.0 ± 1.3	1.37 ± 0.03
CHNA-Phe	6	rebinding pH 6	12.43 ± 2.61	1.00 ± 0.10
LT4	7	template B	107.9 ± 45.5	1.75 ± 0.17

The polymerization time is, perhaps, the principal factor to consider during the polymerization process. As observed in Chapter 4, the choice of the correct polymerization time is able to alter the balance between the affinity and the selectivity of the nanoMIP. Unlike the traditional MIP, for which the influence of the polymerization time is in the order of hours [3], a difference of few minutes can induce a huge modification of these properties. Moreover, the polymerization time has a big effect on the morphology of the nanoparticles. The polymerization appears to proceed until the exhaustion of the monomers in the solution. With the monomer quantities employed in the discussed works, this happens about two hours after the start of polymerization, after which the nanoparticles no longer grow, and their rigidity increases. All the nanoMIPs produced in this PhD work (except those in Chapter 3), displayed polymerization times of one hour, which is reasonable for the preparation of good quality nanoMIPs. It can be supposed that this is a general behavior and is not related to the ciprofloxacin template only.

In general, the water synthesis proved to be the main strength of the SPPS technique. Without having extensively studied the synthesis in organic solvents, the results of both Chapters 2 and 3 showed that the water-synthesized nanoMIPs have better binding properties than their counterparts obtained in other solvents. Water synthesis allows for the elimination of the organic solvents in the polymerization process, granting a greener and cheaper production and a simplification of the nanoMIPs collecting step. At the same time, the templates used in this work display logD values that fall in the middle of the employed logD scale (log D at pH 7.4 between -0.76 and 3.44). Template molecules at the extreme of this scale, extremely hydrophobic or hydrophilic, may not be suitable for water synthesis and additional studies in this direction are needed. Also, like the previous literature has shown (see Introduction), in Chapter 5 the easy applicability of water synthesis to proteins and other biomacromolecules, previously inaccessible as templates to the SPPS technique, was demonstrated.

In Chapters 6 and 7 the flexibility of the SPPS technique was explored for particular cases: that of the mimic template and that of the chiral template. In both instances, the SPPS technique responded perfectly, providing nanoMIPs with the

ability to bind a structural analogue of a dangerous target molecule in one case and with enantiomeric selectivity in the other one. These results open the door to a large number of applications for which these properties are much needed.

One of the most evident limits of the nanoMIPs obtained with SPPS is the low number of binding sites, expressed by their B_{\max} values. Nevertheless, these few binding sites on the surface of the nanoparticles exhibit very elevated binding capability. This is explainable with the position of the template molecules on the surface of the glass beads. During the polymerization step only a limited surface area of the forming nanoparticle is exposed to the template molecules, and the majority of the nanoparticle surface does not expose any binding sites, which leads to low B_{\max} values. This aspect was of critical importance in the work presented in Chapter 8, since the obtained ciprofloxacin MISPE system presented a very low binding capability (nmol/g). This is an important difference compared to classical MIPs, in which the number of binding site is generally elevated ($\mu\text{mol/g}$) [2]. To overcome this limit, efforts will be made to study a way of controlling the number of template molecules on the glass microspheres.

In conclusion, the SPPS technique was proved to be a strongly innovative approach to make nanoMIPs. Some of its mechanisms need further studies to be fully understood, but the very high quality of the obtained nanoMIPs paves the way to a possible application of nanoMIPs in the field of immunochemistry. The road to this goal is far from simple: many parameters will have to be taken account of, and in some instances, many more, as of now yet unknown, will need to be unearthed.

9.1.1 Bibliography

- [1] T.S. Bedwell, N. Anjum, Y. Ma, J. Czulak, A. Poma, E. Piletska, M.J. Whitcombe, S.A. Piletsky. New protocol for optimisation of polymer composition for imprinting of peptides and proteins. *RSC Adv*, **2019**, 9, 27849-27855, doi: 10.1039/c9ra05009d.
- [2] C. Baggiani, L. Anfossi, C. Giovannoli. MIP-based immunoassays: State of the art, limitations and perspectives. *Molecular Imprinting*, **2013**, 1, 41–54, doi: 10.2478/molim-2013-0002.
- [3] E. Piletska, A.R. Guerreiro, M.J. Whitcombe, S.A. Piletsky. Influence of the polymerization conditions on the performance of molecularly imprinted polymers. *Macromolecules*, **2009**, 42, 4921-4928, doi: 10.1021/ma900432z.

10 APPENDICES

10.1 ADDITIONAL WORK OUTSIDE THE SCOPE OF THE THESIS

In addition to the scientific activities described in the previous chapter of this thesis, I have collaborated on other research projects. These projects took place within my research group, and they are focused always on development or application of molecular recognition systems, both MIPs and immunochemistry methods like lateral flow devices and ELISAs. Most of these works resulted in publications. Below are reported the papers' abstracts.

Effect of surfactants on the binding properties of a molecularly imprinted polymer [1]

In molecularly imprinted polymers, non-specific interactions are generally based on weak forces between the polymer surface and the sample matrix. Thus, additives able to interfere with such interactions should be able to significantly reduce any non-specific binding effect. Surfactants represent an interesting class of substances as they are cheap and easily available. Here, we present a study of the effect of three surfactants (the anionic sodium dodecylsulphate, SDS, the cationic cetyltrimethylammonium bromide (CTAB) and the non-ionic polyoxyethylene-(20)-sorbitan monolaurate Tween 20) on the binding affinity of a 2,4,5-trichlorophenoxyacetic acid (2,4,5-T)-imprinted polymer for the template and its analogue 2,4-dichlorophenoxyacetic acid (2,4-D). The experimental results indicate that increasing amounts of surfactant decrease the binding affinity for the ligands strongly for the ionic ones, and weaker for the non-ionic one. This effect is general, as it occurs for both 2,4,5-T and 2,4-D and for both the imprinted and the not-imprinted polymers. It also proves that the magnitude of this effect mainly depends on the presence or absence of an ionic charge, and that the hydrophobic "tail" of surfactants plays only a minor role.

Selective enrichment of aianthone from leaves of aianthus altissima by tandem reverse phase/molecularly imprinted solid phase extraction [14]

The biological activity of extracts from *Ailanthus altissima* is mainly due to the presence of aianthone, a compound belonging to the quassinoid class. Recently, attention has been paid to its strong cytostatic activity. However, the extraction of aianthone is based on very long and demanding procedures, which keep the price

of the commercial product very high. Thus, the development of selective adsorbents for the purification of aianthone from *A. altissima* leaves extracts could help in reduce the costs of production. In this work, we describe the rational design of a molecularly imprinted polymer selective for aianthone based on the screening of a 96- members not-imprinted polymeric library to rapidly identify pre-polymerization mixtures able to generate MIPs with enhanced binding properties. A 4-vinylpyridine-co-trimethylolpropane trimethacrylate polymer showed high binding towards aianthone. It was used to prepare an imprinted polymer with acetonitrile showed interesting binding affinity ($K_{eq} = 18.3 \times 10^3 \text{ M}^{-1}$), high imprinting factor ($IF = 3.8$) and fast binding kinetics ($k_{ass} = 0.390 \text{ min}^{-1}$, $k_{dis} = 0.021 \text{ M}^{-1} \text{ min}^{-1}$). The imprinted polymer was used to develop a successful purification protocol of extracts from *Ailanthus altissima* leaves. The purification was based on the combination of a preliminary clean-up of Soxhlet extracts onto a reverse phase-C18 cartridge and the subsequent isolation of aianthone by a molecularly imprinted solid phase extraction. This approach allowed efficiently purifying the aianthone contained in aqueous or methanolic Soxhlet extracts with high yields compared to the quantities reported in literature (water: $0.756 \pm 0.027 \text{ mg g}^{-1}$; methanol: $0.770 \pm 0.030 \text{ mg g}^{-1}$). Moreover, it allows processing sample volumes up to 15 mL without significant losses of the target compound.

Enzyme immunoassay for measuring aflatoxin B1 in legal cannabis [15]

The diffusion of the legalization of cannabis for recreational, medicinal and nutraceutical uses requires the development of adequate analytical methods to assure the safety and security of such products. In particular, aflatoxins are considered to pose a major risk for the health of cannabis consumers. Among analytical methods that allows for adequate monitoring of food safety, immunoassays play a major role thanks to their cost-effectiveness, high-throughput capacity, simplicity and limited requirement for equipment and skilled operators. Therefore, a rapid and sensitive enzyme immunoassay has been adapted to measure the most hazardous aflatoxin B1 in cannabis products. The assay was acceptably accurate (recovery rate: 78–136%), reproducible (intra- and inter-assay means coefficients of variation 11.8% and 13.8%, respectively), and sensitive (limit of detection and range of quantification: 0.35 ng mL^{-1} and $0.4\text{--}2 \text{ ng mL}^{-1}$, respectively corresponding to 7 ng g^{-1} and $8\text{--}40 \text{ ng g}^{-1}$ in the plant) and provided results which agreed with a HPLC-MS/MS method for the direct analysis of aflatoxin B1 in cannabis inflorescence and leaves. In addition, the carcinogenic aflatoxin B1 was detected in 50% of the cannabis products analyzed (14 samples collected from small retails) at levels exceeding those admitted by the European Union in commodities intended for direct human consumption, thus envisaging the need for effective surveillance of aflatoxin contamination in legal cannabis.

A multi-target lateral flow immunoassay enabling the specific and sensitive detection of total antibodies to SARS COV-2 [10]

A rapid test for detecting total immunoglobulins directed towards the nucleocapsid protein (N) of severe acute syndrome coronavirus 2 (SARS CoV-2) was developed, based on a multi-target lateral flow immunoassay comprising two test lines. Both test lines bond to several classes of immunoglobulins (G, M, and A). Specific anti-SARS immunoglobulins were revealed by a colorimetric probe formed by N and gold nanoparticles. Targeting the total antibodies response to infection enabled achieving 100% diagnostic specificity (95.75–100, C.I. 95%, n = 85 healthy and with other infections individuals) and 94.6% sensitivity (84.9–98.9, C.I. 95%, n = 62 SARS CoV-2 infected subjects) as early as 7 days post confirmation of positivity. Agreeing results with a reference serological ELISA were achieved, except for the earlier detection capability of the rapid test. Follow up of the three seroconverting patients endorsed the hypothesis of the random rise of the different immunoglobulins and strengthened the ‘total antibodies’ approach for the trustworthy detection of serological response to SARS CoV-2 infection.

Switching from multiplex to multimodal colorimetric lateral flow immunosensor [13]

Multiplex lateral flow immunoassay (LFIA) is largely used for point-of-care testing to detect different pathogens or biomarkers in a single device. The increasing demand for multitargeting diagnostics requires multi-informative single tests. In this study, we demonstrated three strategies to upgrade standard multiplex LFIA to multimodal capacity. As a proof-of-concept, we applied the strategies to the differential diagnosis of Human Immunodeficiency Virus (HIV) infection, a widespread pathogen, for which conventional multiplex LFIA testing is well-established. In the new two-parameter LFIA (x2LFIA), we exploited color encoding, in which the binding of multiple targets occurs in one reactive band and the color of the probe reveals which one is present in the sample. By combining the sequential alignment of several reactive zones along the membrane of the LFIA strip and gold nanoparticles and gold nanostars for the differential visualization, in this demonstration, the x2LFIA can furnish information on HIV serotype and stage of infection in a single device. Three immunosensors were designed. The use of bioreagents as the capturing ligand anchored onto the membrane or as the detection ligand labelled with gold nanomaterials affected the performance of the x2LFIA. Higher detectability was achieved by the format involving the HIV-specific antigens as capturing agent and labelled secondary bioligands (anti-human immunoglobulins M and protein G) as the probe.

Detection of urinary prostate specific antigen by a lateral flow biosensor predicting repeat prostate biopsy outcome [11]

This work describes the development and the application of a lateral flow biosensor for the detection of the prostate specific antigen in urine (uPSA). The biosensor allowed uPSA detection in 10 minutes with a limit of detection and a range of quantification respectively of 20 ng mL⁻¹ and 37 – 420 ng mL⁻¹, showing within and between-day coefficients of variation $\leq 13\%$. It showed 92% of accuracy and an almost perfect concordance with the reference electrochemiluminescence immunoassay method. The biosensor design provides the disappearance of the Test line signal at the cut-off concentration. This was achieved with a double layer sensing strategy, in which gold nanoparticles were functionalized with Staphylococcal protein A – a mediator – instead of anti-PSA antibody. This strategy allow making a fine-tune on the concentration of the specific antibody, obtaining an on/ off switch of the Test line at the cut-off value. The cut-off value was also established in this work, based on the distribution of uPSA levels from 140 patients, who were suspected of prostate cancer and who underwent to first biopsy. The clinical application of the biosensor to predict repeat biopsy outcome in 28 patients showed sensitivity, specificity, positive and negative predictive values of 100%, 64%, 74% and 100%, respectively.

Monoclonal antibodies with subnanomolar affinity to tenofovir for monitoring adherence to antiretroviral therapies: From hapten synthesis to prototype development [12]

Approximately 32 million people have died of HIV infection since the beginning of the outbreak, and 38 million are currently infected. Among strategies adopted by the Joint United Nations Program on HIV/AIDS to end the AIDS global epidemic, the treatment, diagnosis, and viral suppression of the infected subjects are considered crucial for HIV prevention and transmission. Although several antiretroviral (ARV) drugs are successfully used to manage HIV infection, their efficacy strictly relies on perfect adherence to the therapy, which is seldom achieved. Patient supervision, especially in HIV-endemic, low-resource settings, requires rapid, easy-to-use, and affordable analytical tools, such as the enzyme-linked immunosorbent assay (ELISA) and especially the lateral flow immunoassay (LFIA). In this work, high-affinity monoclonal antibodies were generated to develop ELISA and LFIA prototypes for monitoring tenofovir (TFV), an ARV drug present in several HIV treatments. TFV was functionalized by inserting a carboxylated C5-linker at the phosphonic group of the molecule, and the synthetic derivative was conjugated to proteins for mice immunization. Through a rigorous screening strategy of hybridoma supernatants, a panel of monoclonal antibodies strongly binding to TFV was obtained. Following antibody characterization for affinity and selectivity by competitive ELISA, a LFIA prototype was developed and tentatively applied to determine TFV in simulated urine. The point-of-care test showed ultra-high detectability (the visual limit of detection was 2.5 nM, 1.4 ng

mL⁻¹), excellent selectivity, and limited proneness to matrix interference, thus potentially making this rapid method a valuable tool for the on-site assessment of patient adherence to ARV therapy.

Ten years of lateral flow immunoassay technique applications: Trends, challenges and future perspectives [8]

The Lateral Flow Immunoassay (LFIA) is by far one of the most successful analytical platforms to perform the on-site detection of target substances. LFIA can be considered as a sort of lab- in-a-hand and, together with other point-of-need tests, has represented a paradigm shift from sample-to-lab to lab-to-sample aiming to improve decision making and turnaround time. The features of LFIAs made them a very attractive tool in clinical diagnostic where they can improve patient care by enabling more prompt diagnosis and treatment decisions. The rapidity, simplicity, relative cost- effectiveness, and the possibility to be used by nonskilled personnel contributed to the wide acceptance of LFIAs. As a consequence, from the detection of molecules, organisms, and (bio)markers for clinical purposes, the LFIA application has been rapidly extended to other fields, including food and feed safety, veterinary medicine, environmental control, and many others. This review aims to provide readers with a 10-years overview of applications, outlining the trends for the main application fields and the relative compounded annual growth rates. Moreover, future perspectives and challenges are discussed.

Design of multiplexing lateral flow immunoassay for detection and typing of foot-and-mouth disease virus using pan-reactive and serotype-specific monoclonal antibodies: Evidence of a new hook effect [4]

The foot-and-mouth disease (FMD) is the most important transboundary viral disease of livestock in the international context, because of its extreme contagiousness, widespread diffusion, and severe impact on animal trade and animal productions. The rapid and on-field detection of the virus responsible for the FMD represents an urgent demand to efficiently control the diffusion of the infection, especially in low resource setting where the FMD is endemic. Colorimetric lateral flow immunoassay (LFIA) is largely used for the development of rapid tests, due to the extreme simplicity, cost-effectiveness, and on-field operation. In this work, two multiplex LFIA devices were designed for the diagnosis of FMD and the simultaneous identification of major circulating serotypes of the FMD virus. The LFIAs relied on the sandwich-type immunoassay and combined a set of well-characterized monoclonal antibodies (mAb) pairs. One LFIA aimed at detecting and identifying O, A and Asia-1 serotypes, the second device enabled the detection and differentiation of the SAT 1 and SAT 2 serotypes. Both devices also incorporated a broad-specific test line reporting on infection from FMDV, regardless the strain and the serotype involved. Accordingly, five and

four reactive zones were arranged in the two devices to achieve a total of six simultaneous analyses. The development of the two multiplex systems highlighted for the first time the relevance of the mAb positioning along the LFIA strip in connection with the use of the same or different mAb as capture and detector ligands. In fact, the excess of detector mAb typically employed for increasing the sensitivity of sandwich immunoassay induced a new type of hook effect when combined with the same ligand used as the capture. This effect strongly impacted assay sensitivity, which could be improved by an intelligent alignment of the mAb pairs along the LFIA strip. The analytical and diagnostic performances of the two LFIAs were studied by testing reference FMDV strains grown in cell cultures and some representative field samples (epithelium homogenates). Almost equivalent sensitivity and specificity to those of a reference Ag-ELISA kit were shown, except for the serotype SAT 2. These simple devices are suitable in endemic regions for in-field diagnosis of FMD accompanied by virus serotyping and, moreover, could be deployed and used for rapid confirmation of secondary outbreaks after FMD incursions in free-areas, thus contributing to promptly implement control measures.

Bacterial ligands as flexible and sensitive detectors in rapid tests for antibodies to SARS-CoV-2 [3]

Lateral flow immunoassay (LFIA) is widely employed as point-of-care tests (POCT) for the diagnosis of infectious diseases. The accuracy of LFIA largely depends on the quality of the immunoreagents used. Typical LFIAs to reveal the immune response to severe acute respiratory syndrome coronavirus-2 (SARS-CoV-2) employ anti-human immunoglobulin (hIg) antibodies and recombinant viral antigens, which usually are unstable and poorly soluble. Broad selective bacterial proteins, such as Staphylococcal protein A (SpA) and Streptococcal protein G (SpG) can be considered alternatives to anti-hIg to increase versatility and sensitivity of serological LFIAs because of their high binding capacity, interspecies reactivity, and robustness. We developed two colorimetric LFA devices including SpA and SpG linked to gold nanoparticles (GNP) as detectors and explored the use of a specific, stable, and soluble immunodominant fraction of the nucleocapsid protein from SARS-CoV-2 as the capturing agent. The optimal amount of SpA-GNP and SpG-GNP conjugates and the protein-to-GNP ratios were defined through a full factorial experimental design to maximize the diagnostic sensitivity of the LFIAs. The new LFA devices were applied to analyze 105 human serum samples (69 positive and 36 negatives according to reference molecular diagnostic methods). The results showed higher sensitivity (89.9%, 95% CI 82.7–97.0) and selectivity (91.7%, 82.6–100) for the SpA-based compared to the SpG-based LFA. In addition, 18 serum samples from cats and dogs living with COVID-19 patients were analyzed and 14 showed detectable levels of anti-SARS-CoV-2 antibodies, thus illustrating the flexibility of the SpA- and SpG-based LFAs

Investigation of the "Antigen Hook Effect" in Lateral Flow Sandwich Immunoassay: The Case of Lumpy Skin Disease Virus Detection [2]

Lumpy skin disease (LSD) is an infectious disease affecting bovine with severe symptomatology. The implementation of effective control strategies to prevent infection outbreak requires rapid diagnostic tools. Two monoclonal antibodies (mAbs), targeting different epitopes of the LSDV structural protein p32, and gold nanoparticles (AuNPs) were used to set up a colorimetric sandwich-type lateral flow immunoassay (LFIA). Combinations including one or two mAbs, used either as the capture or detection reagent, were explored to investigate the hook effect due to antigen saturation by the detector antibody. The mAb-AuNP preparations were optimized by a full-factorial design of experiment to achieve maximum sensitivity. Opposite optimal conditions were selected when one Mab was used for capture and detection instead of two mAbs; thus, two rational routes for developing a highly sensitive LFIA according to Mab availability were outlined. The optimal LFIA for LSDV showed a low limit of detection (103.4 TCID₅₀/mL), high inter- and intra-assay repeatability (CV% < 5.3%), and specificity (no cross-reaction towards 12 other viruses was observed), thus proving to be a good candidate as a useful tool for the point-of-need diagnosis of LSD

Development of molecular and antigenic-based rapid tests for the identification of African swine fever virus in different tissues [16]

African swine fever (ASF) is a severe haemorrhagic infectious disease affecting suids, thus representing a great economic concern. Considering the importance of the early diagnosis, rapid point of care testing (POCT) for ASF is highly demanded. In this work, we developed two strategies for the rapid onsite diagnosis of ASF, based on Lateral Flow Immunoassay (LFIA) and Recombinase Polymerase Amplification (RPA) techniques. The LFIA was a sandwich-type immunoassay exploiting a monoclonal antibody directed towards the p30 protein of the virus (Mab). The Mab was anchored onto the LFIA membrane to capture the ASFV and was also labelled with gold nanoparticles for staining the antibody-p30 complex. However, the use of the same antibody for capturing and as detector ligand showed a significant competitive effect for antigen binding, so required an experimental design to minimize reciprocal interference and maximize the response. The RPA assay, employing primers to the capsid protein p72 gene and an exonuclease III probe, was performed at 39 °C. The limit of detection of the method was assessed using a plasmid encoding the target gene and resulted in 5 copy/μL. The new LFIA and RPA were applied for ASFV detection in the animal tissues usually analysed by conventional assays (i.e., real-time PCR), such as kidney, spleen, and lymph nodes. A simple and universal virus extraction protocol was applied for sample preparation, followed by DNA extraction and purification for the RPA. The LFIA only required the addition of 3% H₂O₂ to limit matrix interference and prevent false positive results. The two rapid methods (25 min and 15 min were needed to

complete the analysis for RPA and LFIA, respectively) showed high diagnostic specificity (100%) and sensitivity (93% and 87% for LFIA and RPA, respectively) for samples with high viral load ($Ct < 27$). False negative results were observed for samples with low viral load ($Ct > 28$) and/or also containing specific antibodies to ASFV, which decreased antigen availability and were indicative of a chronic, poorly transmissible infection. The simple and rapid sample preparation and the diagnostic performance of the LFIA suggested its large practical applicability for POC diagnosis of ASF.

10.2 PUBLICATIONS

- [1] V. Testa, L. Anfossi, S. Cavalera, M. Chiarello, F. Di Nardo, T. Serra, C. Baggiani. Effect of surfactants on the binding properties of a molecularly imprinted polymer. *Polymers*, **2022**, *14*, 5210, doi: 10.3390/polym14235210.
- [2] S. Cavalera, G. Pezzoni, S. Grazioli, E. Brocchi, S. Baselli, D. Lelli, B. Colitti, T. Serra, F. Di Nardo, M. Chiarello, V. Testa, S. Rosati, C. Baggiani, L. Anfossi. Investigation of the “antigen hook effect” in lateral flow sandwich immunoassay: the case of lumpy skin disease virus detection. *Biosensors*, **2022**, *12*, 739, doi: 10.3390/bios12090739.
- [3] S. Cavalera, F. Di Nardo, M. Chiarello, T. Serra, B. Colitti, C. Guiotto, F. Fagioli, C. Cagnazzo, M. Denina, A. Palazzo, F. Artusio, R. Pisano, S. Rosati, C. Baggiani, L. Anfossi. Bacterial ligands as flexible and sensitive detectors in rapid tests for antibodies to SARS-CoV-2. *Analytical and Bioanalytical Chemistry*, **2022**, *414*, 5473-5482, doi: 10.1007/s00216-022-03939-2.
- [4] S. Cavalera, A. Russo, E.A. Foglia, S. Grazioli, B. Colitti, S. Rosati, C. Nogarol, F. Di Nardo, T. Serra, M. Chiarello, C. Baggiani, G. Pezzoni, E. Brocchi, L. Anfossi. Design of multiplexing lateral flow immunoassay for detection and typing of foot-and-mouth disease virus using pan-reactive and serotype-specific monoclonal antibodies: evidence of a new hook effect. *Talanta*, **2022**, *240*, 123155, doi: 10.1016/j.talanta.2021.123155.
- [5] M. Chiarello, L. Anfossi, S. Cavalera, F. Di Nardo, T. Serra, F. Sordello, C. Baggiani. Rabbit IgG-imprinted nanoMIPs by solid phase synthesis: the effect of cross-linkers on their affinity and selectivity. *Journal of Materials Chemistry B*, **2022**, *10*, 6724-6731, doi: 10.1039/d2tb00245k.
- [6] M. Chiarello, L. Anfossi, S. Cavalera, F. Di Nardo, T. Serra, C. Baggiani. Nanomip-based solid phase extraction of fluoroquinolones from human urine: a proof-of-concept study. *Separations*, **2021**, *8*, 226, doi: 10.3390/separations8110226.
- [7] M. Chiarello, L. Anfossi, S. Cavalera, F. Di Nardo, T. Serra, F. Artusio, R. Pisano, C. Baggiani. Effect of polymerization time on the binding properties of ciprofloxacin-imprinted nanomips prepared by solid-phase synthesis. *Polymers*, **2021**, *13*, 2656, doi: 10.3390/polym13162656.
- [8] F. Di Nardo, M. Chiarello, S. Cavalera, C. Baggiani, L. Anfossi. Ten years of lateral flow immunoassay technique applications: trends, challenges and future perspectives. *Sensors*, **2021**, *21*, 5185, doi: 10.3390/s21155185.

- [9] S. Cavalera, M. Chiarello, F. Di Nardo, L. Anfossi, C. Baggiani. Effect of experimental conditions on the binding abilities of ciprofloxacin-imprinted nanoparticles prepared by solid-phase synthesis. *Reactive and Functional Polymers*, **2021**, *163*, 104893, doi: 10.1016/j.reactfunctpolym.2021.104893.
- [10] S. Cavalera, B. Colitti, S. Rosati, G. Ferrara, L. Bertolotti, C. Nogarol, C. Guiotto, C. Cagnazzo, M. Denina, F. Fagioli, F. Di Nardo, M. Chiarello, C. Baggiani, L. Anfossi. A multi-target lateral flow immunoassay enabling the specific and sensitive detection of total antibodies to SARS COV-2. *Talanta*, **2021**, *223*, 121737, doi: 10.1016/j.talanta.2020.121737.
- [11] F. Di Nardo, S. Occhipinti, P. Gontero, S. Cavalera, M. Chiarello, C. Baggiani, L. Anfossi. Detection of urinary prostate specific antigen by a lateral flow biosensor predicting repeat prostate biopsy outcome. *Sensors and Actuators, B: Chemical*, **2020**, *325*, 128812, doi: 10.1016/j.snb.2020.128812.
- [12] S. Cavalera, C. Agulló, J.V. Mercader, F. Di Nardo, M. Chiarello, L. Anfossi, C. Baggiani, A. D'Avolio, A. Abad-Somovilla, A. Abad-Fuentes. Monoclonal antibodies with subnanomolar affinity to tenofovir for monitoring adherence to antiretroviral therapies: From hapten synthesis to prototype development. *Journal of Materials Chemistry B*, **2020**, *8*, 10439-10449, doi: 10.1039/d0tb01791d.
- [13] S. Cavalera, F. Di Nardo, L. Forte, F. Marinoni, M. Chiarello, C. Baggiani, L. Anfossi. Switching from multiplex to multimodal colorimetric lateral flow immunosensor. *Sensors (Switzerland)*, **2020**, *20*, 6609, pp. 1-14,. doi: 10.3390/s20226609.
- [14] L. Anfossi, C. Giovannoli, F. Di Nardo, S. Cavalera, M. Chiarello, F. Trotta, C. Baggiani. Selective enrichment of ailanthone from leaves of ailanthus altissima by tandem reverse phase/molecularly imprinted solid phase extraction. *Microchemical Journal*, **2020**, *158*, 105198, doi: 10.1016/j.microc.2020.105198.
- [15] F. Di Nardo, S. Cavalera, C. Baggiani, M. Chiarello, M. Pazzi, L. Anfossi. Enzyme immunoassay for measuring aflatoxin B1 in legal cannabis. *Toxins*, **2020**, *12*, 265, doi: 10.3390/toxins12040265.
- [16] S. Cavalera, B. Colitti, G.M. De Mia, F. Feliziani, S. Dei Giudici, P.P. Angioi, F. D'Errico, D. Scalas, A. Scollo, T. Serra, M. Chiarello, V. Testa, F. Di Nardo, C. Baggiani, A. Oggiano, S. Rosati, L. Anfossi. Development of molecular and antigenic-based rapid tests for the identification of African swine fever virus in different tissues. *Talanta*, **2023**, *258*, 124443, doi: 10.1016/j.talanta.2023.124443.

10.3 ACTIVITY DURING THE PHD

Courses

- Ion Beam Techniques for Materials Science, Università di Torino, 2020
- Academic English for PhD students of scientific and mathematical disciplines, Università di Torino, 2020
- Carbanion Chemistry in Organic Synthesis, Università di Torino, 2020
- Chemical Sensors for Scientific Research and Everyday Life, Università di Torino, 2020
- Advances in Phytochemistry, Università di Torino, 2020
- Organic Chemistry for Chemical Biology and Biomedical Applications, Università di Torino, 2021

Schools and workshops

- Machine learning meets chemistry, Università di Torino, 17-18 February 2020
- Raman days, Università di Torino, 2021
- Chemometric School - experimental design Module, Università di Genova, 24-28 May 2021
- Advances in Biotechnology and New Horizons for Industry, Saint-Pierré d'Oleron, France, organized by University of Leicester, 13-17 June 2022

Conferences I attended

- Bioanalytical day, Società chimica italiana, online, 13 July 2021
- XXVII Congresso Nazionale della Società Chimica Italiana, Società chimica italiana, poster, 14-23 September 2021

Posters and oral presentations

- NanoMIPs by solid phase polymerization synthesis: optimization and analytical applications of a new technique. Oral presentation. Bioanalytical day 2021
- Matteo Chiarello, Simone Cavalera, Fabio Di Nardo, Thea Serra, Laura Anfossi, Claudio Baggiani. Effect of polymerization time on the binding properties of imprinted nanoparticles (nanoMIPs) obtained by solid phase synthesis. Poster, XXVII Congresso Nazionale della Società Chimica Italiana, 2021

Teaching

- Laboratory of analytical chemistry, Bachelor's degree in Chemistry and chemical technologies, Università di Torino, aa. 2020/2021, 2021/2022 and 2022/2023, Prof. Marco Minella and Debora Fabbri, 40 hours per year

Public engagement

- Tecnologie per la salute pubblica: test diagnostici e Ingegneria dei tessuti. Cervelli in città. Associazione dottorandi e dottori di ricerca in Italia, Biblioteche civiche torinesi, Città di Torino. Biblioteca civica centrale, Torino. 9 March 2022
- Tecnologie per la salute pubblica: test diagnostici. Biennale tecnologia per le scuole. Politecnico di Torino. IIS Ettore Majorana, Torino. 20 October 2022

10.4 ABBREVIATION USED IN THE TEXT

9-BBN	Borabicyclo[3.3.1]nonane
AA	Acrylic acid
AEMA	2-aminoethylmethacrylate hydrochloride
AFM	Atomic force microscopy
AIBN	Azo-bis-isobutyronitrile
APS	Ammonium persulphate
APTMS	3-(aminopropyl)trimethoxysilane
BIgG	Bovine immunoglobuline G
BIS	N,N'-methylen-bis-acrylamide
BSA	Bovine serum albumin
CHNA-Phe	N-(4- chloro-1-hydroxy-2-naphthoylamido)-(L)-phenylalanine
CME	Carboxymethoxy-
CPX	Ciprofloxacin
CTX	Chlorotetracycline
DAN	Danofloxacin
DIC	N,N'-diisopropylcarbodiimide
DMAP	4-(N,N-dimethylamino)pyridine
dT₃	dTriiodothyronine
dT₄	Dextrothyroxine
EDAM	N,N'-ethylene dimethacrylamide
EDC	1-ethyl-3-(3-dimethylaminopropyl)carbodiimide
EDMA	Ethylene glycol dimethacrylate
EGMP	Ethylenglycole methacrylate phosphate
ENR	Enrofloxacin
ESI	Electrospray ionization
GDMA	Glycerol dimethacrylate
HMDS	Hhexamethyldisilazane
IF	Imprinting factor
IgG	Immunoglobuline G
LC	Long chain
LOM	Lomefloxacin
L₃T₂	3',5'-diiodo-L-thyronine
L₃T₃	L ₃ Triiodothyronine
L₃T₄	Levothyroxine
L₄T₄	Levothiroyne
LVX	Levofloxacin
LZM	Hen egg lysozyme

MAA	Methacrylic acid
MES	Morpholinethansulphonic acid
MIP	Molecularly imprinted polymer
MISPE	Molecularly imprinted solid phase extraction
MOX	Moxifloxacin
nanoMIP	Molecularly imprinted polymer with nanodimensions
nanoNIP	Non-imprinted polymer with nanodimensions
NHS	N-hydroxysuccinimide
NIP	Non-imprinted polymer
NIPAm	N-isopropylacrylamide
NOBE	N,O-bis-methacryloylethanolamine
NOR	Norfloxacin
NTA	Nanoparticles tracking analysis
OTA	Ochratoxin A
RIgG	Rabbit immunoglobuline G
SAR	Sarafloxacin
SC	Short chain
SPPS	Solid phase polymerization synthesis
TBA_m	N-tert-butylacrylamide
TEMED	N,N,N',N'-tetramethylethylenediamine
TRIM	Trimethylolpropane trimethacrylate

10.5 BUFFERS PREPARATION

Below are reported the recipes used for the preparation of all the buffers. The quantities refer to a final volume of 1 L. All the buffers were prepared by dissolving the salts water ultra-purified in Purelab Prima System from Elga (Marlow, UK). The pH values of all buffers were adjusted using 1 M NaOH or 1 M HCl solutions. All the buffers were filtered through a 0.45 μm recycled cellulose filter before used, and stored a 4°C.

Phosphate buffer 20 mM pH 6

- Disodium hydrogen phosphate $\text{Na}_2\text{HPO}_4 \cdot 2 \text{H}_2\text{O}$ 0.3320 g
- Sodium dihydrogen phosphate $\text{NaH}_2\text{PO}_4 \cdot \text{H}_2\text{O}$ 2.5030 g

Phosphate buffer 20 mM pH 7.4

- Disodium hydrogen phosphate $\text{Na}_2\text{HPO}_4 \cdot 2 \text{H}_2\text{O}$ 2.8840 g
- Sodium dihydrogen phosphate $\text{NaH}_2\text{PO}_4 \cdot \text{H}_2\text{O}$ 0.5240 g

MES buffer 50 mM pH 4.7

- Morpholinethansulphonic acid (sodium salt) 10.861 g

MES buffer 10 mM pH 4.7

- Morpholinethansulphonic acid (sodium salt) 2.1722 g

Synthetic urine pH 6.5

- Calcium chloride $\text{CaCl}_2 \cdot 2\text{H}_2\text{O}$ 0.65 g
- Magnesium chloride $\text{MgCl}_2 \cdot 6\text{H}_2\text{O}$ 1.17 g
- Sodium chloride NaCl 4.6 g
- Sodium sulphate Na_2SO_4 2.3 g
- Sodium citrate $\text{Na}_3 \text{ citrate} \cdot 2\text{H}_2\text{O}$ 0.65 g
- Potassium dihydrogen phosphate KH_2PO_4 2.8 g
- Potassium chloride KCl 1.6 g
- Ammonium chloride NH_4Cl 1.0 g
- Urea 25 g
- Creatinine creatinine·HCl 1.46 g

11 RINGRAZIAMENTI

“Viaggiano i perdenti. Viaggiano perché i vincenti non hanno bisogno di andarsene. Viaggiano i perdenti più adatti ai mutamenti. Viaggia chi non ha speranza. Viaggia la polvere. Viaggia quello che può essere spazzato via senza stabilità. Viaggia chi le ha provate tutte e ha trovato solo terra bruciata attorno a sé. Viaggia Ahmed che se ne va. Viaggia perché Falchera non gli ha mai offerto nulla. Il sogno successivo era Torino, ma quello che gli aveva da offrirgli è stata solo una sequenza di contratti di poche settimane da pochi soldi per volta, spesso in nero. E si ritrova a quasi trent'anni senza nulla nel presente e ancora meno del domani. E allora viaggia, prima di essere spazzato via come la polvere. Ahmed spiega che ha trovato questo lavoro in Germania. È duro, sarà dura, ma almeno ha un contratto di un anno per partire. È una fabbrica, di quelle che schiantano e uccidono, e sarà su turni. Lo ascoltiamo tra un piatto e un bicchiere, tra una risata e una uscita più seria, sapendo che anche se fingiamo che nulla cambierà, il nostro gruppo - o almeno il gruppo che abbiamo vissuto fino in questo momento - muore quella sera e che sarà sempre più difficile organizzarsi come il solito.

- Ma non è già cambiato? - mi fa da contraltare Amedeo all'espone i miei pensieri indicando la sedia vuota che sarebbe di Simone. - Il futuro lo abbiamo già superato e non ce ne siamo accorti - conclude.

- Sto pensando di andare a convivere con Camilla - rispondo io.

- Ecco il futuro che abbiamo superato - dice Amedeo alzando il calice di vino.

- Ma quando è che siamo diventati vecchi? - si chiede Francesco.

- Da quando ci siamo resi conto di non avere una direzione- dice Amedeo, -ma guardiamo Lorenzo: quasi laureato, un'offerta di una borsa in università, anche nel caso sicuramente un bel lavoro. Ma è messo come noi. Ma non dovrebbe essere lui il fortunato? -

Ahmed chiede perché dovrei essere il fortunato.

- Perché sono l'unico che è riuscito ad andare all'università, che non ha mai avuto i vostri problemi economici, che nei fatti non dovrei lamentarmi rispetto a voi - rispondo io.

- Però ognuno ha i propri problemi, e ci troviamo sulla stessa barca- conclude Amedeo.

- Tu zitto, che hai l'alpeggio - dice ridendo Ahmed.

Francesco chiede sorpreso che cosa è questa storia dell'alpeggio, e Amedeo inizia a spiegare che lui e Marta sono in trattativa per ristrutturarne uno su in Val Grande, che anche per loro qua si trova nulla di importante e allora meglio andarsene dalla città. Solo chi è cresciuto fuori dalla città può sognare di venire a viverci sostiene: chi ci ha vissuto vuol fare il contrario. E allora se devi resistere a questo mondo cosa fai? Non ti resta che salire in montagna. Ripenso alle nostre camminate e dormite in tenda che sembra siano passati mille anni da quando si facevano tutti insieme, là sull'Assietta o in val Tronca. E ora Amedeo ci va a vivere su quelle montagne. Dieci pecore, del latte, produrre formaggio. La neve, il freddo, la legna da tagliare. Una donna insieme, tante difficoltà, ma la volontà di fare qualcosa di estraneo a quello che ci impone l'esterno. E perché dovremo criticarlo nel suo coraggio?”

Da “I ragazzi di Falchera sognano Torino ma vanno a Berlino”, tratto da un qualcosa che prima o poi sarà, scritto da me

Sono stato io il fortunato? Guardando gli amici attorno a me, in quasi tutti i casi posso rispondere di sì, che lo sono stato. Concludo questo percorso di studi durato 24 anni con poca certezza nel futuro, ma con molte certezze nel presente e nel passato, con certezze che molti miei amici non hanno potuto avere. Con certezze costruite grazie al contributo di molte persone. Dovrei fare un elenco? Non lo ho fatto per la tesi magistrale e dovrei farlo ora? Massì, facciamolo. Però rapido:

Partiamo col ringraziare il mio professore, Claudio Baggiani, e quella domanda secca: - Vuoi fare un dottorato? Devi darmi una risposta subito -. Domanda dalla quale è partito tutto, e tutto è stato.

Ringrazio poi Marco Ghibaudi, unico mio antico amico che ha affrontato lo stesso viaggio sulla barca del dottorato. E lo ringrazio soprattutto per quella telefonata, con me nel panico, seguita immediatamente alla domanda di cui sopra.

Ringrazio chi ho incrociato nel laboratorio tra una tesi e l'altra, prima come insegnanti poi come colleghi e ogni tanto ancora insegnanti: Fabio, Simone, Thea, Alida, Laura, Marco, Alberto.

Ringrazio soprattutto i miei tesisti, i tesisti a cui ho insegnato e ho gestito in questi anni, i cui lavori hanno contribuito ad arrivare alla mole di dati presentati in questa tesi: Lucia, Simona, Lorenzo, Katuscia, Sofia, Mario, Melissa, Federica. Ringrazio anche dell'amicizia che alcuni di loro mi hanno poi concesso.

Ringrazio da sola Valentina, solo perché altrimenti la dovrei mettere due volte, sia come collega che come tesista e amica.

Ringrazio gli amici di sempre che mi hanno sopportato. Quelli esterni all'università. Tanto sapete di chi parlo.

Ringrazio gli amici di ADI Torino, quelli vecchi però, con i quali ho condiviso battaglie e mi hanno insegnato molto, e con i quali ogni tanto ho anche condiviso la gioia delle vittorie (poche). Grazie anche a loro che ora sono espertissimo di regolamenti e procedure. Cosa me ne farò di tali conoscenze adesso è un mistero.

Ringrazio Simone e Federica, che mi hanno corretto l'inglese di questa tesi.

Federica la ringrazio anche per condividere con me la vita e tutto quello che ne consegue, di cui questo dottorato è stato solo una piccola parte.

Ringrazio i miei genitori, che capiscono poco del mio lavoro ma non per questo non capiscono dove sia arrivato, e per farmici arrivarci hanno fatto tutto per me.

In ultimo ringrazio chi non può essere qui a vedermi oggi: mio nonno, che sarebbe orgoglioso; Giovannoli, che mai sono riuscito a chiamare per nome e a cui spesso in questi anni ho pensato, pensando a come sarebbe stato il mio dottorato se...; e Garbero, all'occasione che lui non ha potuto avere.